



The
University
Of
Sheffield.

Access to Electronic Thesis

Author: Olalekan Adeniyi
Thesis title: The Use of Biomass in Molten Carbonate and Solid Oxide Fuel Cells
Qualification: PhD

This electronic thesis is protected by the Copyright, Designs and Patents Act 1988. No reproduction is permitted without consent of the author. It is also protected by the Creative Commons Licence allowing Attributions-Non-commercial-No derivatives.

This thesis was embargoed until September 2014.

If this electronic thesis has been edited by the author it will be indicated as such on the title page and in the text.

THE USE OF BIOMASS IN MOLTEN CARBONATE AND SOLID OXIDE DIRECT CARBON FUEL CELLS



Olalekan David Adeniyi

B.Eng., M.Eng., GradEI, AMIChemE

Department of Chemical and Biological Engineering

The University of Sheffield

Supervised by

Dr. Bruce C.R. Ewan

A thesis submitted to the University of Sheffield for the degree of Doctor of Philosophy.

September 2011

Acknowledgment

I would like to thank my supervisor, Dr. Bruce C.R. Ewan, for always having the time for me. His critical assessments of issues as they arise and how he tackles them have always impressed me. I would like to thank the departmental staff of Chemical and Biological Engineering both academic and non academic. The technical team of the department have been so wonderful, they are always ready to help out when called upon. I also appreciate Dr. Nik Reeves of the department of Materials Science and Engineering for putting me through the X-ray diffraction procedure. I would like to appreciate all the supports I received from my late brother and his wife, Prof. & Dr. (Mrs.) J.O. Adeniyi. A special thank to a special uncle and his wife, Mr. & Mrs. Olusegun Adeniyi. Big thanks to Chris Hill of the Biomedical Sciences for helping me through the protocol and application of the SEM. I am grateful to Dr. R. I. Ristic for his help and advice in some aspect of this work.

The Petroleum Technology Development Fund Abuja, Nigeria has supported my research work through their scholarship scheme, this I owe them a million thanks. I also appreciate the Federal University of Technology, Minna for their support. I would like to thank Pastor & Pastor (Mrs.) Musa Bako and the entire members of Victory Assembly for their love and support. I also appreciate Pastor & Mrs. Andrew Nkemchor for their love, supports and sacrifices for my family, you are truly a rare gem, God bless you tremendously. I sincerely thank Deacon & Mrs. Benson Ikini for all their understanding and help all through the years. A big thanks to Dr. & Mrs. Adegbola Ojo for the many invaluable discussions over the years, thanks for being there for us. A big thank you to all the companies who have supplied me with the various biomasses used in this research, they include; BICAL (Swindon), Keighley Tree Services (Bradford), Coppice Resources Ltd (Retford), BBSRC (Swindon) and Manco Energy Ltd (North Newbald). And finally a big kudos to my family for their understanding and support during this research programme.

Dedication

The research work is dedicated to God Almighty through our Lord and Saviour Jesus Christ. Also to Mary, Samuel and Ruth my wonderful family, the melodies of my life.

Summary

A direct carbon fuel cell (DCFC) is a special type of high temperature fuel cell that uses solid carbon as fuel and air as oxidant. Researches in the area of the DCFC have focused on using fuel derived from petroleum products, coal and activated carbon but this current research investigates the use of biomass carbon fuel in a single cell DCFC. Six different biomasses were investigated (miscanthus, switchgrass, wheat, spruce, poplar and willow). The biomasses were subjected to pyrolysis reaction at 800°C, 7°C/min with particle sizes of 0.50 mm to 1.00 mm, yielding 25 wt.% biomass carbon. The two electrolyte systems investigated were; molten carbonate electrolyte direct carbon fuel cell (MCDCFC) and solid oxide electrolyte direct carbon fuel cell (SODCFC) and these were tested using hand and ball milled biomass carbon fuels (HM and BM).

The overall electrochemical reactions of the biomass carbon fuels in the SODCFC were better than those of the MCDCFC. The BM biomass fuels performed better in the SODCFC while the HM biomass fuels performed better in the MCDCFC. In terms of the open circuit voltage, miscanthus fuel (1.24 V) had the best value for SODCFC while willow fuel (0.83 V) for MCDCFC. The best peak power density was recorded for miscanthus fuel (77.41 mW/cm²) in the SODCFC and willow fuel (18.48 mW/cm²) in the MCDCFC. Miscanthus fuel (180.52 mA/cm²) gave the maximum current density for the SODCFC while spruce fuel (73.02 mA/cm²) for the MCDCFC. For the current density at 80% voltage efficiency miscanthus fuel (100 mA/cm²) was superior for the SODCFC and willow fuel (6.67 mA/cm²) for MCDCFC. Miscanthus fuel (0.66 V) showed the highest voltage at peak power for the SODCFC and willow fuel (0.48 V) for the MCDCFC. The overall energy strategy considering two major routes of electricity generation from biomass were investigated. The first route is the burning of biomass in a power plant to generate 6.5 MJ of electricity and the second is the DCFC integrated route using biomass to generate 12.8 MJ of electricity. The DCFC integrated route gave superior outputs of energy generation with an overall conversion efficiency of 70% when compared with the 35% of the first route.

Table of Contents

Acknowledgment	ii
Dedication	iii
Summary	iv
Table of content	v
List of Tables	x
List of Figures	xii
Nomenclature	xvii
Acronyms and Abbreviations	xix
1.0 Introduction	2
1.1 Renewable energy	2
1.2 Sustainability and fuel cell technology	5
1.2.1 Sustainable hydrogen from water electrolysis	6
1.2.2 Fuel cell powered by biomass	6
1.3 Carnot efficiency and fuel cell efficiency	11
1.4 Fuel cell voltage and efficiency	13
1.5 Research aims and objectives	14
1.6 Outline of thesis	16
2.0 Literature review	17
2.1 Introduction	18
2.2 Biomass energy content and composition	18
2.2.1 Heating values, ultimate and proximate analysis	18
2.2.2 Relationship between carbon and energy content of biomass	19
2.2.3 Enthalpies of formation	25
2.2.4 Chemical structures of biomass	27
2.3 Energy production using virgin biomass	30
2.3.1 Forest biomass	30
2.3.2 Grasses	31
2.3.3 Cultivated crops	32
2.4 Disordered carbon structures	33
2.5 Amorphous (disordered) materials	34
2.6 Preparation of disordered carbon	34
2.6.1 Pyrolysis of organic materials	35
2.6.2 Irradiation of graphitic structure	36
2.6.3 Cracking of hydrocarbons	36
2.6.4 Sputtering and evaporation	36
2.7 Method of characterisation	37
2.7.1 Optical microscopy	37

2.7.2	Raman spectroscopy	37
2.7.3	X-ray diffraction	38
2.7.4	Electron microscopy	39
2.8	Summary	40
3.0	Theory of biomass and fuel cell	41
3.1	Introduction	42
3.2	Conversion route for energy crop	42
3.3	Biomass pyrolysis	43
3.3.1	Conventional and fast pyrolysis	43
3.3.2	Mechanism of biomass pyrolysis	44
3.3.3	Kinetics of biomass pyrolysis	45
3.3.4	Thermodynamics of biomass pyrolysis	47
3.3.5	Products and yields of biomass pyrolysis	48
3.3.5.1	Conventional slow biomass pyrolysis	49
3.3.5.2	Fast biomass pyrolysis	50
3.4	Gasification	52
3.5	Mechanical treatment of biomass	54
3.5.1	Size reduction of biomass	54
3.5.2	Machines for biomass size reduction	54
3.5.3	Mechanical milling of carbon materials	55
3.6	Classification of fuel cells	55
3.7	Historical background of fuel cells	56
3.8	Molten carbonate fuel cell (MCFC)	60
3.9	Solid oxide fuel cell (SOFC)	68
3.10	Direct carbon fuel cell (DCFC)	70
3.10.1	Advantages of DCFC	73
3.10.2	Electrochemical oxidation of carbon	75
3.10.2.1	Mechanism	76
3.10.3	Molten carbonate electrolyte in DCFC	77
3.10.4	Molten hydroxide electrolyte in DCFC	80
3.10.5	Yttria Stabilised Zirconia solid electrolyte in DCFC	86
3.10.6	DCFC with mass and heat integration systems	88
3.11	The process of fuelling fuel cells	90
3.11.1	Hydrogen	90
3.11.2	Petroleum	91
3.11.3	Coal and coal gas	92
3.11.4	Natural gases	92
3.11.5	Bio-fuels	92
3.12	Energy and the EMF of the hydrogen fuel cell	93
3.12.1	Zero energy reference point	93

3.12.2	Mechanical potential energy	94
3.13	Fuel cell irreversibilities	95
3.13.1	Activation losses	97
3.13.2	Fuel crossover and internal currents	97
3.13.3	Ohmic losses	98
3.13.4	Concentration losses (Mass transport)	98
3.14	Summary	99
4.0	Experimental	100
4.1	Introduction	101
4.2	Biomass preparation and analysis	101
4.2.1	Proximate analysis of biomass	101
4.2.1.1	Moisture content analysis of biomass	102
4.2.1.2	Ash content analysis of biomass	104
4.2.1.3	Volatiles content analysis of biomass	105
4.2.1.4	Fixed carbon analysis of biomass	105
4.2.2	Ultimate analysis of biomass	106
4.2.2.1	Carbon and hydrogen contents	106
4.2.3	Calorific value determination of biomass	108
4.3	Pyrolysis of biomass	109
4.4	X-ray diffraction analysis	113
4.5	Particle analysis with Malvern mastersizer	113
4.6	Ball milling of biomass carbon	113
4.7	Design and assembling of the DCFC	114
4.7.1	Preparation of carbonate electrolyte using ZrO ₂ cloth	114
4.7.2	Preparation of carbon fuel particles	115
4.7.3	Behaviour of carbon fuel particles	116
4.7.4	Assembling of the DCFC	116
4.7.5	Preparation of the SODCFC button cells	121
4.7.6	Performance testing setup for the DCFC	122
5.0	Pyrolysis, XRD, SEM results and discussions	125
5.1	Introduction	126
5.2	Lenton cylindrical furnace for pyrolysis	126
5.2.1	Lenton cylindrical furnace temperature profile	126
5.2.2	Design modification for Lenton cylindrical furnace	128
5.3	Biomass analyses	131
5.4	Pyrolysis and carbon analyses	135
5.4.1	Pyrolysis results from the old Lenton furnace	135
5.4.2	Pyrolysis results from the modified Lenton furnace	137
5.4.3	Carbon analyses	141

5.5	Hand and ball milling of biomass carbon	145
5.6	X-ray diffraction pattern	146
5.7	Scanning electron microscope of biomass carbons	154
6.0	MCDCFC single cell performances	161
6.1	Introduction	162
6.2	MCDCFC electrochemical design and development	162
6.3	Voltages from MCDCFC operation	167
6.3.1	Voltages from MCDCFC using carbon black and porous nickel	167
6.3.2	Voltages from MCDCFC using biomass and gold mesh	170
6.4	MCDCFC performance with porous nickel-ZrO ₂ -gold mesh electrolyte	171
6.4.1	MCDCFC performance using carbon black	171
6.4.2	MCDCFC performance using miscanthus with porous nickel	175
6.4.3	MCDCFC performance using willow carbon	177
6.5	MCDCFC performance with gold mesh-ZrO ₂ -gold mesh electrolyte	180
6.5.1	First day performances of the MCDCFC using HM carbon	180
6.5.2	Temperature effects on MCDCFC performances on HM fuel	187
6.5.3	MCDCFC power efficiency and ASR for HM biomass carbon fuels	189
6.6	MCDCFC performances with BM biomass carbon fuels	190
6.6.1	First day performances of the MCDCFC using BM carbon fuels	190
6.6.2	Temperature effects on MCDCFC performances with BM Fuel	196
6.6.3	MCDCFC performance efficiency using BM biomass carbon fuels	197
6.7	Comparison of MCDCFC performances for HM and BM carbon fuels	198
6.7.1	Miscanthus (<i>Miscanthus x giganteus</i>) carbon fuel	198
6.7.2	Switchgrass (<i>Panicum virgatum</i>) carbon fuel	202
6.8	Summary	205
7.0	SODCFC single cell performances	207
7.1	Introduction	208
7.2	SODCFC electrochemical design and development	208
7.3	SODCFC performance with BM biomass carbon fuel	212
7.3.1	First day performances of the SODCFC	212
7.3.2	Temperature effects on SODCFC performances with BM fuel	217
7.3.3	SODCFC performance efficiency using BM biomass carbon fuel	219
7.4	SODCFC performance with HM biomass carbon fuel	220
7.4.1	First day performances of the SODCFC	220
7.4.2	Temperature effects on SODCFC performances with HM fuel	226
7.4.3	SODCFC performance efficiency using HM biomass carbon fuel	227
7.5	Comparison of MCDCFC performances for HM and BM carbon fuels	229
7.5.1	Miscanthus carbon fuel	229
7.5.2	Switchgrass carbon fuel	231

7.6	Comparison of SODCFC and MDCFC performances for BM fuels	233
	7.6.1 Miscanthus carbon fuel	233
	7.6.2 Switchgrass carbon fuel	235
7.7	Energy strategy of electricity generation from biomass	237
7.8	Summary	239
8.0	Conclusions and recommendations	241
8.1	Conclusions	242
8.2	Recommendations for future work	246
	References	248
	Appendix A Malvern biomass carbon particle analysis	263
	Appendix B Information dissemination	270
	Appendix B1 Departmental seminar	271
	Appendix B2 Conference presentation	271
	Appendix B3 Conference proceeding	271
	Appendix B4 Journal publication	271
	Appendix C Graphs of DCFC performances	272
	Appendix D Tables of DCFC performances	288

List of Tables

Table	page
1.1 Different sources of energy	3
1.2 More different sources of energy	4
1.3 Typical gas composition of biogas from organic household waste	10
1.4 Hydrogen fuel cell , maximum EMF and efficiency limit	12
2.1 Typical proximate analysis and HHV for biomass, coal and peat	20
2.2 Typical compositions and HHV of virgin, waste biomass, peat & coal	21
2.3 Typical composition of biomass feedstock-bone dry material basis	22
2.4 Analysis of ash from Hybrid poplar, pine and switchgrass	23
2.5 Typical carbon content and heating value of biomass component	24
2.6 Typical lower heating value of biomass and fossil materials	25
2.7 Measured and calculated HHVs comparison for biomass, coal & peat	26
3.1 Composition of gases evolved from slow dry distillation of wood	45
3.2 Exothermic reactions on cellulose pyrolysis	48
3.3 Product yield from thermal decomposition of biomass over 8 hr & 400°C	50
3.4 Product yields from various biomasses at different pyrolysis temp.	51
3.5 Fuel cells classification, characteristics and applicability	57
3.6 Values of E and Δ for H ₂ and CO at 650 °C	64
3.7 Tolerable Impurity levels for MCFC and SOFC	66
3.8 Operating characteristics of DCFC and other conventional fuel cells	71
3.9 Hydrogen and other fuels properties for fuel cell systems	91
3.10 The Δ for the reaction $H_2 + \frac{1}{2}O_2 \rightarrow H_2O$ at different temperature	95
5.1 Proximate, ultimate & calorific value analyses for ground miscanthus	131
5.2 Proximate, ultimate & calorific value analyses for ground Switchgrass	132
5.3 Proximate, ultimate & calorific value analyses for ground wheat straw	132
5.4 Proximate, ultimate & calorific value analyses for ground willow wood	133
5.5 Proximate, ultimate & calorific value analyses for ground spruce wood	133
5.6 Proximate, ultimate & calorific value analyses for ground poplar wood	134
5.7 Comparison of ground biomass analyses	134
5.8 Industrial graphite under same pyrolysis condition	137
5.9 Pyrolysis of miscanthus at 800°C	137
5.10 Miscanthus pyrolysis using modified Lenton furnace	138
5.11 Switchgrass pyrolysis using modified Lenton furnace	138
5.12 Wheat straw pyrolysis using modified Lenton furnace	139
5.13 Willow wood chip pyrolysis using modified Lenton furnace	139
5.14 Spruce wood chip pyrolysis using modified Lenton furnace	140
5.15 Poplar wood chip pyrolysis using modified Lenton furnace	140
5.16 Moisture, calorific value & ultimate analyses for miscanthus carbon	141
5.17 Moisture, calorific value & ultimate analyses for switchgrass carbon	142

Table	page	
5.18	Moisture, calorific value & ultimate analyses for wheat carbon	142
5.19	Moisture, calorific value & ultimate analyses for willow carbon	142
5.20	Moisture, calorific value & ultimate analyses for spruce carbon	143
5.21	Moisture, calorific value & ultimate analyses for poplar carbon	143
5.22	Moisture, calorific value and ultimate analyses for carbon black	144
5.23	Moisture, calorific value and ultimate analyses for graphite	144
5.24	Comparison of the pyrolysed biomass carbons and industrial carbons	144
5.25	Hand milled particle size analysis of biomass carbon	145
5.26	Ball milled particle size analysis of biomass carbon	145
6.1	MCDCFC Electrochemical data for miscanthus and willow (HM)	189
6.2	MCDCFC Electrochemical data for miscanthus and willow (BM)	197
6.3	MCDCFC Electrochemical performance at 800°C (HM and BM)	206
7.1	SODCFC Electrochemical data for miscanthus and willow (BM)	219
7.2	SODCFC Electrochemical data for miscanthus and willow (HM)	228
7.3	Mass and percentage of biomass fractions	238
7.4	Heating values of biomass fractions	239
7.5	SODCFC and MCDRFC electrochemical performance at 800°C (BM)	240

List of Figures

Figure	Page	
1.1	Illustrative lifecycle of forest biomass	5
1.2	Renewable fuel for fuel cells from biomass process routes	7
1.3	Fuel cells technology for biogas processing and clean up	9
1.4	Maximum H ₂ fuel cell efficiency at standard pressure	13
2.1	Hypothetical network of lignin and polysaccharides in wood	28
2.2	Pyrolysis of lignin model in the presence of formic acid giving demethoxylated products	28
2.3	Chemical structures of lignin in biomass	29
2.4	Chemical structures of triglyceride in biomass	29
2.5	Various types of disordered carbon	35
2.6	Carbon modes of vibration	38
3.1	Thermochemical conversion route for energy crops	44
3.2	β-glucosan formation on pyrolysis	46
3.3	Cellulose pyrolysis pathways	46
3.4	Fuel cell technology in automobile	59
3.5	Motorbike powered by fuel cell technology	59
3.6	Light aircraft powered by fuel cell technology	60
3.7	MCFC anode and cathode reaction for hydrogen fuel	62
3.8	Addition of carbon dioxide to the cathode gas stream	62
3.9	The anode and cathode reaction for MCFC using CO as fuel	63
3.10	MCFC 250 kW MTU stack construction	67
3.11	MCFC 250 kW MTU early demonstration under construction	67
3.12	Tubular SOFC end view	69
3.13	Tubular SOFC in 24 stacks	69
3.14	Larger stack of tubular SOFC consisting of 1152 cells	70
3.15	Configuration of the DCFC	72
3.16	Carbon electrochemical oxidation description	77
3.17	LLNL tilted direct carbon fuel cell with carbon particle anode	79
3.18	Performance of the LLNL tilted direct carbon fuel cell	80
3.19	SARA direct carbon fuel cell with a carbon rod anode	83
3.20	Performance profile of the SARA direct carbon fuel cell	83
3.21	Cell configuration of the SRI direct carbon fuel cell	85
3.22	Flowing liquid anode of the SRI direct carbon fuel cell	85
3.23	Performance of the SRI direct carbon fuel cell liquid anode	86
3.24	CCE Proposed DCFC combining SOFC and fluidized-bed technologies	87
3.25	Highly integrated DCFC, pyrolyser and dryer for maximum efficiency	89
3.26	Integrated DCFC and pyrolyser for high efficiency	89
3.27	Non-integrated DCFC and pyrolyser with maximum flexibility	90
3.28	The voltage for a typical low temperature, air pressure fuel cell	96

3.29	The voltage for a typical air pressure fuel cell operating at about 800°C	97
4.1	Miscanthus straws and ground	102
4.2	Spruce wood chips and ground	103
4.3	Poplar wood chips and ground	103
4.4	Switchgrass straws and ground	103
4.5	Wheat straws and ground	104
4.6	Willow wood chips and ground	104
4.7	Lenton cylindrical furnace used for pyrolysis	110
4.8	Modified Lenton cylindrical furnace used for pyrolysis	111
4.9	More modification to Lenton furnace incorporating a condenser	112
4.10	Components of the condenser	112
4.11	Malvern mastersizer used for particle size analysis	114
4.12	Experimental setup for saturation of ZrO ₂ cloth	115
4.13	Components of the DCFC	117
4.14	Initial and modified DCFC design	117
4.15	Schematic of the DCFC with overall height of 280 mm	118
4.16	Dimensions in mm of the DCFC	119
4.17	DCFC appearance after initial performance in furnace	120
4.18	Experimental setup for the DCFC	123
4.19	DCFC in operation	123
4.20	Resistor and voltmeter connected to the DCFC	124
4.21	Internal section of the resistor box	124
5.1	Lenton furnace temperature profile at set point of 100 - 450°C	127
5.2	Lenton furnace temperature profile at set point of 500 - 600°C	127
5.3	Dimensions and components of the Lenton furnace	128
5.4	Modified Lenton furnace temperature profile at set point of 200-600°C	129
5.5	Modified furnace temperature profile at set point of 800-1000°C	129
5.6	Dimensions and components of the modified Lenton furnace	130
5.7	Powder X-ray diffraction pattern for industrial carbon black	146
5.8	X-ray diffraction (XRD) pattern on Graphite	147
5.9	X-ray diffraction (XRD) pattern for miscanthus pyrolysed at 400°C	148
5.10	X-ray diffraction (XRD) pattern for miscanthus pyrolysed at 800 °C	150
5.11	X-ray diffraction (XRD) pattern for Switchgrass carbon	151
5.12	X-ray diffraction (XRD) pattern for Wheat carbon	151
5.13	X-ray diffraction (XRD) pattern for willow carbon	152
5.14	X-ray diffraction (XRD) pattern for Spruce carbon	153
5.15	X-ray diffraction (XRD) pattern for poplar carbon	153
5.16	SEM of hand milled poplar carbon particles at magnification of 500x	154
5.17	SEM of ball milled poplar carbon particles at magnification of 500x	155
5.18	SEM of hand milled spruce carbon particles at magnification of 800x	156
5.19	SEM of ball milled spruce carbon particles at magnification of 800x	156

5.20	SEM of HM switchgrass carbon particles at magnification of 500x	157
5.21	SEM of ball milled switchgrass carbon particles at magnification of 500x	157
5.22	SEM of hand milled wheat carbon particles at magnification of 500x	158
5.23	SEM of ball milled wheat carbon particles at magnification of 500x	158
5.24	SEM of hand milled willow carbon particles at magnification of 500x	159
5.25	SEM of ball milled willow carbon particles at magnification of 500x	159
5.26	SEM of HM miscanthus carbon particles at magnification of 500x	160
5.27	SEM of ball milled miscanthus carbon particles at magnification of 500x	160
6.1	Gold mesh, porous alumina, gold mesh electrolyte cell unit	163
6.2	Porous nickel, zirconia, gold mesh electrolyte cell unit	163
6.3	Porous nickel, zirconia, gold mesh electrolyte cell unit with ceramic disc	164
6.4	Gold mesh, zirconia, gold mesh electrolyte cell unit	164
6.5	Gold mesh, zirconia, gold mesh electrolyte cell unit with ceramic disc	165
6.6	Saturate zirconia electrolyte for MCDCFC	165
6.7	Saturated zirconia and porous nickel electrolyte	166
6.8	Ceramic disc, gold mesh, zirconia and gold wire electrolyte	166
6.9	Mica seals used as protection for DCFC casing	166
6.10	MCDCFC OCV at varying temperature with CO ₂ flow at 140 cm ³ /min	168
6.11	MCDCFC OCV at varying temperature with CO ₂ flow at 250 cm ³ /min	168
6.12	MCDCFC voltage at varying temperature using carbon black	169
6.13	MCDCFC OCV for the six biomass carbon fuels at different temperature	170
6.14	Voltage, current density using carbon black at different temperature	172
6.15	Power, current density using carbon black at different temperature	173
6.16	Voltage, power & current density using carbon black at different temp.	174
6.17	Voltage, current density using miscanthus at different temperature	175
6.18	Power, current densities using miscanthus at different temperature	176
6.19	Voltage, power and current densities using miscanthus Fuel	177
6.20	Voltage versus current density using willow at different temperature	178
6.21	Power versus current density using willow at different temperature	179
6.22	Voltage, power, current density using willow at different temperature	179
6.23	Voltage, current density for the 6 biomass fuels at 600°C (HM-Day 1)	180
6.24	Voltage, current density for the 6 biomass fuels at 700°C (HM-Day 1)	181
6.25	Voltage, current density for the 6 biomass fuels at 800°C (HM-Day 1)	182
6.26	Voltage, Power & current density with curving back phenomena at 700°C (Jia <i>et al.</i> , 2010)	183
6.27	Power, current density for the 6 biomass fuels at 600°C (HM-Day 1)	184
6.28	Power, current density for the 6 biomass fuels at 700°C (HM-Day 1)	184
6.29	Power, current density for the 6 biomass fuels at 800°C (HM-Day 1)	185
6.30	Overall performances for the 6 biomass fuels at 600°C (HM-Day 1)	186
6.31	Overall performances for the 6 biomass fuels at 700°C (HM-Day 1)	186
6.32	Overall performances for the 6 biomass fuels at 800°C (HM-Day 1)	187

6.33	MDCFC voltages for the 6 biomass fuels at different temp. (HM-Day 1)	188
6.34	Voltage, current density for the 6 biomass fuels at 600°C (BM-Day 1)	191
6.35	Voltage, current density for the 6 biomass fuels at 700°C (BM-Day 1)	191
6.36	Voltage, current density for the 6 biomass fuels at 800°C (BM-Day 1)	192
6.37	Power vs current density for the 6 biomass fuels at 600°C (BM-Day 1)	193
6.38	Power vs current density for the 6 biomass fuels at 700°C (BM-Day 1)	193
6.39	Power vs current density for the 6 biomass fuels at 800°C (BM-Day 1)	194
6.40	Overall performances for the 6 biomass fuels at 600°C (BM-Day 1)	194
6.41	Overall performances for the 6 biomass fuels at 700°C (BM-Day 1)	195
6.42	Overall performances for the 6 biomass fuels at 800°C (BM-Day 1)	195
6.43	MDCFC OCV for the 6 biomass fuels at different temp. (BM-Day 1)	196
6.44	Miscanthus performances for hand and ball milled fuels at 600°C	199
6.45	Miscanthus performances for hand and ball milled fuels at 700°C	199
6.46	Miscanthus performances for hand and ball milled fuels at 800°C	200
6.47	SEM micrograph of hand milled miscanthus carbon particles (800x)	201
6.48	SEM micrograph of ball milled miscanthus carbon particles (800x)	201
6.49	Switchgrass performances for hand and ball milled fuels at 600°C	202
6.50	Switchgrass performances for hand and ball milled fuels at 700°C	203
6.51	Switchgrass performances for hand and ball milled fuels at 800°C	203
6.52	SEM micrograph of hand milled switchgrass carbon particles (800x)	204
6.53	SEM micrograph of ball milled switchgrass carbon particles (800x)	205
7.1	SODCFC Button cell, Gold mesh, Ni/YSZ, LSM/ScSZ, gold mesh cell unit	209
7.2	Button cell for the SODCFC, cathode (black-LSM), anode (green-NiO ₂)	209
7.3	Button cell bond with gold mesh on each side as the electrolyte	210
7.4	Assembled SODCFC ready for high temperature operation	210
7.5	SODCFC during high temperature operation	211
7.6	Resistor box and voltmeter connected to SODCFC	211
7.7	SODCFC voltage, current density for the 6 biomass fuels at 600°C	212
7.8	SODCFC voltage, current density for the 6 biomass fuels at 700°C	213
7.9	SODCFC voltage, current density for the 6 biomass fuels at 800°C	213
7.10	SODCFC power versus current density for the 6 biomass fuels at 600°C	214
7.11	SODCFC power versus current density for the 6 biomass fuels at 700°C	215
7.12	SODCFC power versus current density for the 6 biomass fuels at 800°C	215
7.13	SODCFC overall performances for the 6 biomass fuels at 600°C	216
7.14	SODCFC overall performances for the 6 biomass fuels at 700°C	216
7.15	SODCFC overall performances for the 6 biomass fuels at 800°C	217
7.16	SODCFC OCV for the 6 biomass fuels at different temp. (Ball milled)	218
7.17	SODCFC voltage, current density for the 6 biomass fuels at 600°C (HM)	221
7.18	SODCFC voltage, current density for the 6 biomass fuels at 700°C (HM)	221
7.19	SODCFC voltage, current density for the 6 biomass fuels at 800°C (HM)	222
7.20	SODCFC power vs current density for the 6 biomass fuels at 600°C (HM)	223

7.21	SODCFC power vs current density for the 6 biomass fuels at 700°C (HM)	223
7.22	SODCFC power vs current density for the 6 biomass fuels at 800°C (HM)	224
7.23	SODCFC overall performances for the 6 biomass fuels at 600°C (HM)	224
7.24	SODCFC overall performances for the 6 biomass fuels at 700°C (HM)	225
7.25	SODCFC overall performances for the 6 biomass fuels at 800°C (HM)	225
7.26	SODCFC OCV for the 6 biomass fuels at different temp. (HM)	227
7.27	SODCFC miscanthus performances for HM and BM fuels at 600°C	229
7.28	SODCFC miscanthus performances for HM and BM fuels at 700°C	230
7.29	SODCFC miscanthus performances for HM and BM fuels at 800°C	230
7.30	SODCFC switchgrass performances for HM and BM fuels at 600°C	231
7.31	SODCFC switchgrass performances for HM and BM fuels at 700°C	232
7.32	SODCFC switchgrass performances for HM and BM fuels at 800°C	232
7.33	BM Miscanthus performances for SODCFC and MCDCFC at 600°C	233
7.34	BM Miscanthus performances for SODCFC and MCDCFC at 700°C	234
7.35	BM Miscanthus performances for SODCFC and MCDCFC at 800°C	234
7.36	BM Switchgrass performances for SODCFC and MCDCFC at 600°C	235
7.37	BM Switchgrass performances for SODCFC and MCDCFC at 700°C	236
7.38	BM Switchgrass performances for SODCFC and MCDCFC at 800°C	236
7.39	Routes of electricity generation from biomass	238

Nomenclature

Symbol	Description	Unit
ΔG_c	Change in Gibbs free energy of combustion	kJ
ΔG_f	Change in Gibbs free energy of formation	kJ
ΔS	Change in entropy	JK^{-1}mol
Δ	Change in molar specific Gibbs free energy of combustion	kJ mol^{-1}
Δ	Change in molar specific Gibbs free energy of formation	kJ mol^{-1}
	Activation Overvoltage	V
ΔH	Change in enthalpy	kJ
	Change in molar specific enthalpy of combustion	kJ mol^{-1}
ΔH_f	Enthalpy of formation	kJ
ΔV_{ohm}	Voltage Drop	V
ΔV_{trans}	Voltage Change due to Mass Transport	V
A	Tafel Equation Constant	-
A	Pre-exponential factor	time^{-1}
A	Surface area	m^2
A, a	Constant	-
B	Constant	-
$B_{(hk)}$	Breadth for a two-dimensional lattice reflection in XRD	mm
C	Capacitance	μF
d	Separation of the plates in fuel cell	nm
d	Layer spacing for carbon/crystal structure	Å
D1	Dwell time 1 in Lenton furnace	min
D2	Dwell time 2 in Lenton furnace	min
E	Electromotive force of fuel cell at a given state	V
E	Apparent activation energy	Jmol^{-1}
E_o	Electromotive force of fuel cell at standard state	V
E_{ocv}	Reversible open circuit voltage	V
F	Faraday constant	C
FR	Nitrogen gas flow rate	cm^3/min
i	Current Density	mAcm^{-2}
i_o	Exchange Current Density	mAcm^{-2}
k	Wave vector	-
L1	Target set point 1 in Lenton furnace	$^{\circ}\text{C}$
L2	Target set point 2 in Lenton furnace	$^{\circ}\text{C}$
L_a	Mean layer length for a 2-D lattice reflection in XRD	mm
L_c	Height of crystallite	mm
m	Fraction of Volatiles Produced	-
m	Constant in mass transfer overvoltage equation	V
M_1	Mass of empty crucible	g
M_2	Mass of crucible plus sample before heating	g

Symbol	Description	Unit
M_3	Mass of crucible plus residue after heating and	g
M_4	Final mass of soda asbestos absorber	g
M_5	Initial mass of water absorber	g
M_6	Final mass of water absorber	g
M_{Al}	Mass of moisture in the aluminium oxide	g
M_c	Percentage of moisture content	%
n	Constant in mass transfer overvoltage equation	mA^{-1}
p	Vapour pressure	kPa
P	Pressure	kPa
r	Area-Specific Resistance	$\text{k}\Omega\text{cm}^2$
R	Universal gas constant	$\text{JK}^{-1}\text{mol}^{-1}$
R_1	Ramp rate 1 in Lenton furnace	$^{\circ}\text{C}/\text{min}$
R_2	Ramp rate 2 in Lenton furnace	$^{\circ}\text{C}/\text{min}$
RT	Drop in Nernst voltage	V
T	Temperature	$^{\circ}\text{C}$
V	Voltage	V
V_c	Voltage of the fuel cell	V
Wt.%	Weight percentage on dry basis	%
z	Number of electrons transferred	-

Greek Symbols

μ_f	Fuel utilization coefficient	-
θ	Bragg scattering angle	$^{\circ}$
α	Charge Transfer Coefficient	-
ϵ	Electrical permittivity	Fm^{-1}
η	Efficiency	%
λ	Wavelength of the x-ray	m

Subscripts

hk	Two-dimensional lattice peak in carbon
hkl	Three-dimensional lattice peak in carbon
a	Anode compartment
c	Cathode gas compartment
rs	Carbon reactive surface site

Acronyms and Abbreviations

AFC	Alkaline Fuel Cell
APUs	Auxiliary Power Units
ASR	Area Specific Resistance
ASTM	American Society of Testing and Materials
BET	Brunauer-Emmett-Teller
BM	Ball milled biomass carbon fuel
BSU	Basic Structural Unit
CCE	Clean Coal Energy
CCS	Carbon Capture and Storage
CHP	Combine Heat and Power
C _{RS}	Reactive Carbon Surface Sites
CV	Calorific Value
DCFC	Direct Carbon Fuel Cell
DIR	Direct Internal Reforming
DMFC	Direct Methanol Fuel Cell
EMF	Electromotive force
EXAFS	Extended X-ray Absorption Fine Structure
FC	Fuel Cell
FCVs	Fuel cell vehicles
HCs	Hydrocarbons
HDS	Hydrodesulphurisation
HHV	Higher Heating Value
HM	Hand milled biomass carbon fuel
HR	Heating Rate
ICE	Internal Combustion Engine
IIR	Indirect Internal Reforming
Lha ⁻¹	Litres per Hectare Annual Yield
LHV	Lower Heating Value
LLNL	Lawrence Livermore National Laboratory
LSM	Lanthanum Strontium Manganate
maf	Moisture and Ash-Free Material
MCDCFC	Molten Carbonate Electrolyte Direct carbon Fuel Cell
MCDCFCP	Molten Carbonate Electrolyte Direct carbon Fuel Cell Power Density
MCDCFCV	Molten Carbonate Electrolyte Direct carbon Fuel Cell Voltage
MCFC	Molten Carbonate Fuel Cell
Mf	Moisture Free Material
MH	Molten Hydroxide Electrolyte
Mis	Miscanthus carbon fuel
MisP	Miscanthus carbon fuel power density
MisV	Miscanthus carbon fuel voltage

MSW	Municipal Solid Waste
NMR	Nuclear Magnetic Resonance
NTEL	National Energy Technology Laboratory
OCV	Open Circuit Voltage
OTEC	Ocean Thermal Energy Conversion
PAFC	Phosphoric Acid Fuel Cell
PEMFC	Proton Exchange Membrane Fuel Cell
Pop	Poplar carbon fuel
PopP	Poplar carbon fuel power density
PopV	Poplar carbon fuel voltage
RDF	Refused-Derived Fuel
SARA	Scientific Application and Research Associates
ScSZ	Scandium-Stabilised Zirconium
SEM	Scanning Electron Microscope
SODCFC	Solid Oxide Electrolyte Direct Carbon Fuel Cell
SODFCFP	Solid Oxide Electrolyte Direct Carbon Fuel Cell Power Density
SODFCFV	Solid Oxide Electrolyte Direct Carbon Fuel Cell Voltage
SOFC	Solid Oxide Fuel Cell
Spr	Spruce carbon fuel
SprP	Spruce carbon fuel power density
SprV	Spruce carbon fuel voltage
STP	Standard Temperature and Pressure
Swi	Switchgrass carbon fuel
SwiP	Switchgrass carbon fuel power density
SwiV	Switchgrass carbon fuel voltage
t ha ⁻¹	Tonnes per Hectare Annual Yield
TCD	Thermal Conductivity Detector
THT	Tetrahydrothiophene
Whe	Wheat carbon fuel
WheP	Wheat carbon fuel power density
WheV	Wheat carbon fuel voltage
Wil	Willow carbon fuel
WilP	Willow carbon fuel power density
WilV	Willow carbon fuel voltage
wt.	Weight
XANES	X-Ray Near Edge Structure
XRD	X-Ray Diffraction
YSZ	Yttria Stabilised Zirconia

Chapter One

Introduction

1.0 Introduction

Renewable energy sources are derived primarily from the enormous power of the sun's radiation and are the most ancient as well as the most modern forms of energy used by humanity. Renewable energy from biomass or bioenergy is our emphasis in this research. The main fossil fuel energy sources continue to present challenges for CO₂ emission reduction, and carbon neutral biomass options like miscanthus will make an increasing contribution to the energy mix in decades ahead. The use of carbons for electricity production in carbon fuel cells have been shown to provide conversion efficiencies up to 80%. The direct carbon fuel cell (DCFC) is a special kind of high temperature fuel cell that directly uses carbon as anode and fuel. The DCFC has a higher achievable efficiency (80%) as an electrical power generator than other fuel cells. The raw material for powering DCFC is solid carbon-rich fuels, such as biomass, coal, and organic waste, which are abundant in nature (Adeniyi and Ewan, 2011; Desclaux *et al.*, 2010; Cao *et al.*, 2007; Boyle, 2004; Boyle *et al.*, 2003; Sorensen, 2000; Twidell and Weir, 1986).

This chapter introduces renewable energy and gives the different sources of it. It also talks about the sustainability of fuel cell technology using biomass. The Carnot efficiency as it relates to heat engines and the fuel cell efficiency limits are discussed along with the fuel cell voltage and its efficiency. The research aims and objectives are given and the thesis outline is also discussed.

1.1 Renewable Energy

The energy that exists in the world can be stored, converted or amplified in different ways. Thus these energy resources can be classified as either finite or perpetual. The finite resources include both organic and inorganic based substances (e.g. coal, crude oil, natural gas, oil shale natural bitumen, extra heavy oil, uranium and thorium). The principal perpetual resources are solar energy, wind power and bioenergy; all these depend on the extra-terrestrial source which is the sun. Other sources such as marine energy (tidal energy), wave power and ocean thermal energy conversion (OTEC) also exists. Bioenergy are renewable energy resources, because each crop harvested

represent a partial renewal of its resource base, which on its own is subject to depletion as a result of being used as feedstock or fuel. Tables 1.1 and 1.2 give a comparison on the various energy sources (Babu, 2008; Lauzon *et al.*, 2007).

Table 1.1: Different sources of energy (Babu, 2008)

Source	Features	Disadvantages	Reserves
Nuclear power	<ul style="list-style-type: none"> a. Generated using Uranium. b. Nuclear fission of Uranium produces heat and energy. c. No smoke or CO₂ produced. d. Huge amounts of energy from small amounts of fuel with small amounts of waste. 	<ul style="list-style-type: none"> a. Highly dangerous waste product. b. Waste must be sealed up and buried for several years to allow the radioactivity to die away. c. Lot of investment on safety. A nuclear accident can be a major disaster. 	<ul style="list-style-type: none"> a. Not renewable, once all the earth's Uranium is dug up and used, there is no other.
Coal	<ul style="list-style-type: none"> a. Finite energy source. b. The most rapidly growing fuel on global basis. 	<ul style="list-style-type: none"> a. Burning produces dust, smoke and oxides of impurities, leading to environmental pollution. b. Burning fossil fuel produces carbon dioxide leading to greenhouse effect. c. Burning also produces photochemical pollution from nitrous oxide and acid rain from sulphur dioxide. 	<ul style="list-style-type: none"> a. 850 billion tonnes of coal currently recoverable. b. Globally available in more than 70 countries.
Oil	<ul style="list-style-type: none"> a. Finite in nature. b. Different types of oil, different costs, characteristic and having depleting profiles. c. Most important primary fuel globally (36.4% of global energy consumption, without biomass). 	<ul style="list-style-type: none"> a. Burning produces carbon dioxide leading to greenhouse effect. b. Burning also produces photochemical pollution from nitrous oxide and acid rain from sulphur dioxide. 	<ul style="list-style-type: none"> a. Expected resources of 82 billion tonnes. b. 47% of total reserves of conventional oil discovered have been consumed. c. Cumulative crude oil production reached 143 billion tonnes in 2005. Half was produced within the last 23 years.

Biomass describes all biologically produced matter and it is the name given to all earth's living matter. Biomass represents the general term for materials derived from growing plants or from animal manure. The solar energy drives the photosynthesis process in all the plant matter. The chemical energy contained in biomass is derived from the solar energy using the process of photosynthesis. In this process, plants take up carbon dioxide, water and using solar energy, convert them into sugars, starches, cellulose, lignin etc., which make up carbohydrate (Babu, 2008).

Material such as wood from natural forests, waste from agricultural and forestry processes, industrial, human and animal waste are the basic sources for biomass energy. Naturally, all biomass ultimately decomposes to its molecules with the release of heat. Biomass combustion is a replicate of the natural processes. Thus the energy from biomass is a form of renewable energy, which does not add CO₂ to the environment in contrast to fossil fuel (Babu, 2008; Twidell, 1998).

Table 1.2: More different sources of energy (Babu, 2008)

Source	Features	Disadvantages	Reserves
Solar energy	a. The sun is the most abundant permanent source of energy. b. The annual solar radiation reaching earth is over 7500 times the world's annual primary energy consumption of 450 Exajoules.	Large investment cost for solar photovoltaic collectors.	-
Geothermal energy	The natural heat of the earth.	-	Not a clear cut example of a perpetual source of energy like solar, wind and marine energy.
Hydro-electric	The largest of the perpetual or renewable energy resources.	-	Total world hydro capacity is about 778 GW.
Wind energy	Wind generation occurs by complex mechanisms involving the rotation of the earth, heat energy from the sun, the cooling effects of the oceans and polar ice caps, temperature gradients between land and sea and the physical effects of mountains and other obstacles.	This usually involves large investment cost for windmills.	a. The world's windiest regions are in the coastal regions of the America, Europe, Asia and Australasia. b. The world wind resources are vast: it has been estimated that if only 1% of the land area were utilized and allowance made for wind's relatively low capacity factors, wind power potential would roughly equate to the current level of worldwide generating capacity.

This makes biomass unique in that it effectively stores solar energy and it is the only renewable energy source of carbon which is able to convert conveniently into solid, liquid and gaseous fuels (Kwapinski *et al.*, 2010; Babu, 2008; Demirbas, 2001; Twidell,

1998). Bioenergy are renewable and carbon neutral. The CO_2 released during the energy conversion of biomass (e.g. combustion, gasification, pyrolysis, anaerobic digestion or fermentation) circulates through the biosphere, and is reabsorbed in equivalent stores of biomass through photosynthesis. Figure 1.1 shows the combustion of wood and the generation of CO_2 , this also depicts that the net CO_2 generation is zero as new biomass is developed photosynthetically (Babu, 2008).

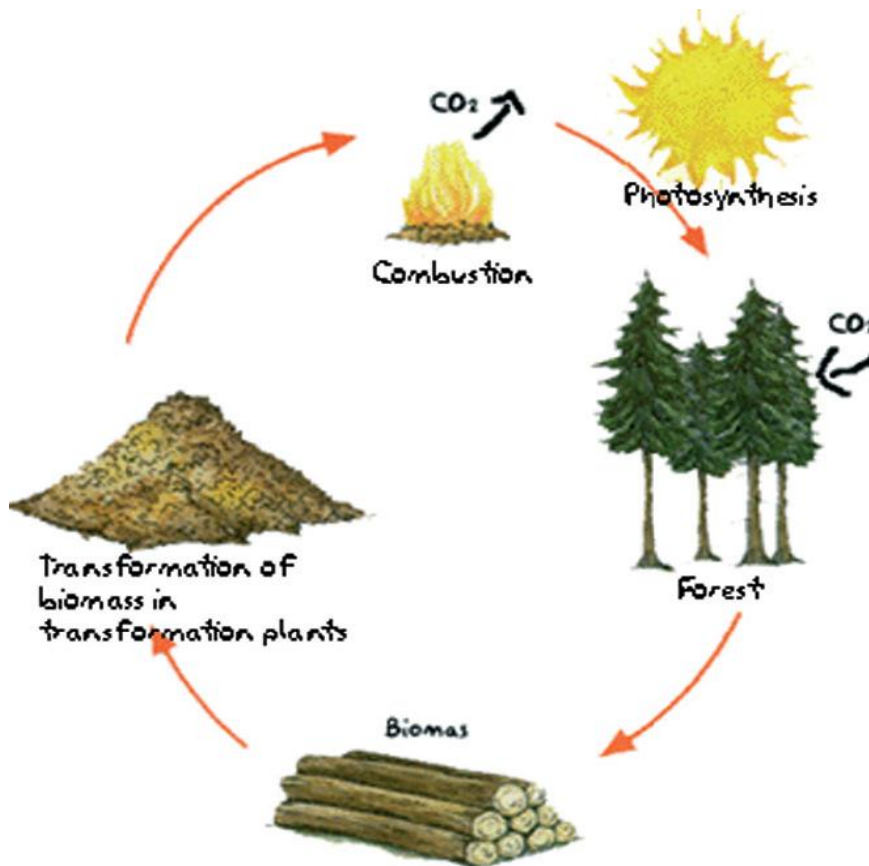


Figure 1.1: Illustrative lifecycle of forest biomass (Babu, 2008)

1.2 Sustainability and Fuel Cell Technology

Regardless of all the benefits of fuel cells (FCs) in terms of reduced emission, higher fuel efficiencies, there is a need for FC sustainability through the use of renewable sources of energies, that is, non-fossil sources of energy that do not diminish on a human time scale or that is continuously regenerated by some natural processes (Desclaux *et al.*, 2010; Hoogers, 2003 cited Hoogers and Potter, 1999). All other known renewables can be traced back to the main sources, with solar energy exceeding the

others by many orders of magnitude. Plant and algae harness the use of solar energy, by evaporation of water giving it an increased potential energy, and by the pressure differentials on the surface of the planet which together with the earth's rotations to give wind (Hoogers, 2003). Geothermal energy is currently applied in various geographic locations that allow easy access to high temperature reservoirs (150-200°C), for power generation through steam processes or in locations with low grade thermal water for heating purposes (e.g. as applied in Iceland, Japan, Los Alamos in United States). Tidal energy on the other hand can only be used in very few special geographical locations where differences in tidal sea levels of many meters exist within large estuaries. Sources of renewable and sustainable energy using fuel cell technology could be applied in two main routes as follow (Hoogers, 2003):

- i. The generation of hydrogen by water electrolysis with electricity based on renewable.
- ii. The use of biomass to generate carbon, biogas, syngas (CO and H₂), methanol or hydrogen.

1.2.1 Sustainable Hydrogen from Water Electrolysis

Clean supplies of hydrogen to industries have been achieved through electrolyzers. They have recently been used as an option for generating CO₂-neutral hydrogen in conjunction with electrical energy made from renewables. Hydrogen fuelling stations are being set up in Sacramento, Las Vegas, Michigan, Vancouver, Hamburg, Munich, Milan, Osaka and other places (Hoogers, 2003 cited Dunn, 2001). Many researches in the area of hydrogen fuel cell have been carried out and many are still going on (Dikwal *et al.*, 2008; Bujalski *et al.*, 2007; Chan *et al.*, 2002).

1.2.2 Fuel Cell Powered by Biomass

The possibility of sustainable and renewable solutions to fuel problems comes from biomass. As shown in Figure 1.2, the potential process routes from biomass to powering FCs are schematically presented. Biomass can be burned to generate steam

for driving steam turbines (or steam engine) to make electric power. The most interesting things are the chemical routes i.e., anaerobic digestion of “soft” biomass and thermal processing of “hard” biomass to make syngas, a mixture of carbon monoxide and hydrogen. The thermal process can also be applied in conjunction with almost any carbon-containing material. Typical fuels are wood, straw, fast growing reeds (miscanthus) and trees harvested green (Klass, 1998).

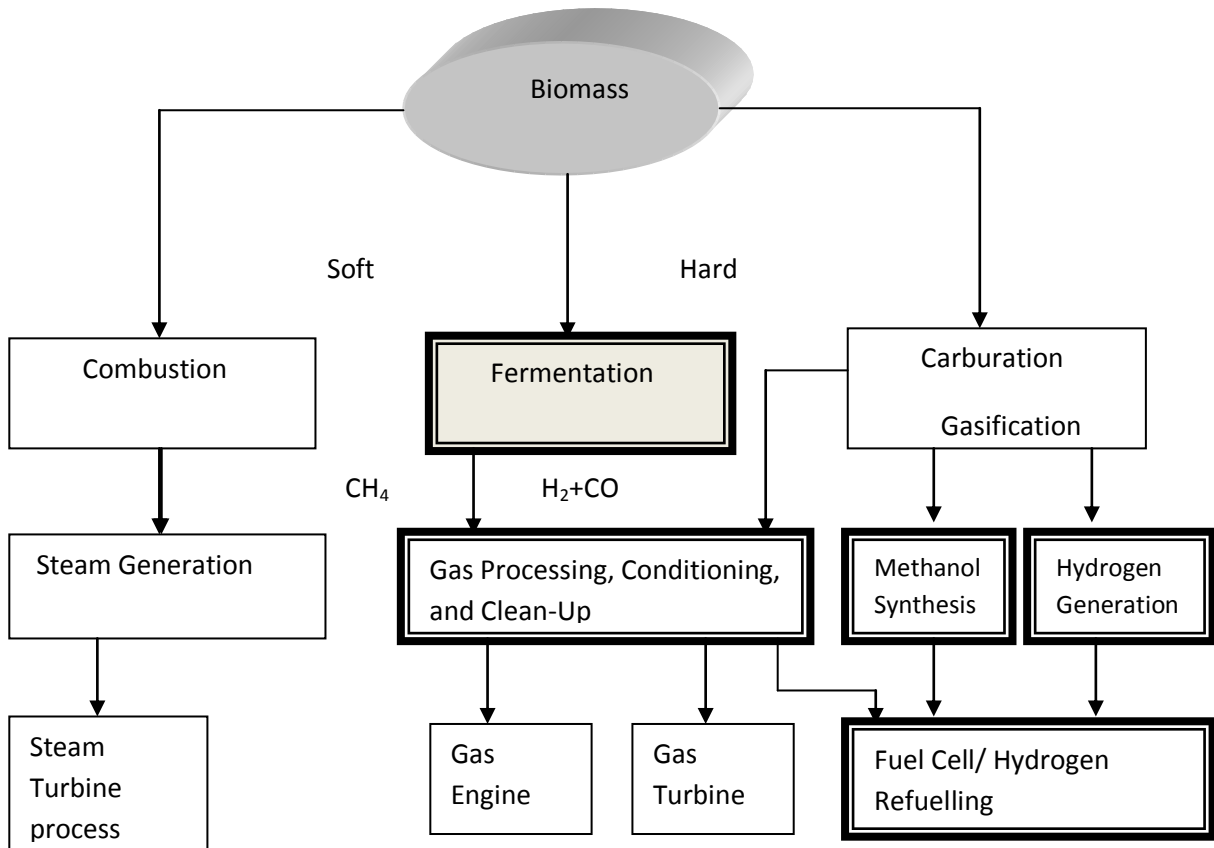
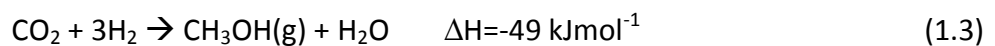
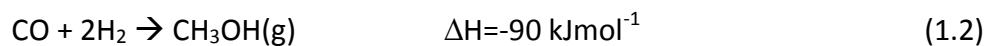
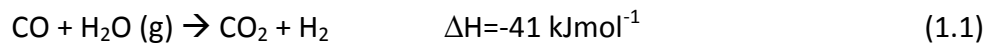


Figure 1.2: Renewable fuel for fuel cells from biomass process routes (Hoogers, 2003).

For farming that involves the cultivation of energy crops, it is important to use primary fuels that requires neither the use of extensive machinery for planting and harvesting nor artificial fertilizers. This would counteract the concept of CO_2 neutrality. For the same reason, liquid biofuels such as plant oils are less suitable. They often require high (fossil) energy returns which varies from one country to the other, depending on climatic and agricultural conditions (Hoogers, 2003 cited Koßmehl and Heinrich, 1998).

Waste material processing is currently of keen interest all over the world. In Germany, an automated process to separate and dry household waste to a so-called dry stabilate has been developed by Herhof (Hoogers, 2003 cited Kern and Sprick, 2001). Their technique is a good comparison between the consideration of the use of resources and excessive recycling. The process gives a result of clean iron and non-ferrous metals, ceramics and stone, glass and batteries. The other materials (dry stabilates) are burnt in power plants or in the cement industry, having a heating value similar to lignite. It was observed by Witzenhausen Institute, that 60 wt.% of the dry stabilate consists of organic matters (Hoogers, 2003; Kern and Sprick, 2001). Also currently available are energy efficient processes to generate syngas from dry organic materials (Hoogers, 2003 cited Kwant, 2001). Biomass is available in large quantities all over the world. In terms of FC technology, syngas from biomass gasification can be further converted into more hydrogen and methanol by the following processes:

- a. Water-gas shift reaction as shown in Equation 1.1
- b. The use of methanol synthesis (Equation 1.2 and Equation 1.3)
- c. Fed directly into high temperature stationary fuel cell system of the molten carbonate fuel cell (MCFC) or solid oxide fuel cell (SOFC) type (Figure 1.3).



The ability to make hydrogen and methanol is noteworthy because these chemicals can be stored as automotive fuels (Adeniyi, 2008; Hoogers, 2003).

The product of anaerobic digestion in biogas is illustrated in Figure 1.3. The feed stock for Figure 1.3 is normally softer organic matter such as organic household waste, grass cuttings, manure, canteen and industrial food offal among others (Hoogers, 2003 cited Köttner, 2001). Table 1.3 gives the typical composition of biogas from household waste without additional meat and food offal co-fermentation, this composition can vary

greatly depending upon the feed. Methane is observed to be the major component in the gas, ranging between 50% and 75% by volume (Hoogers, 2003).

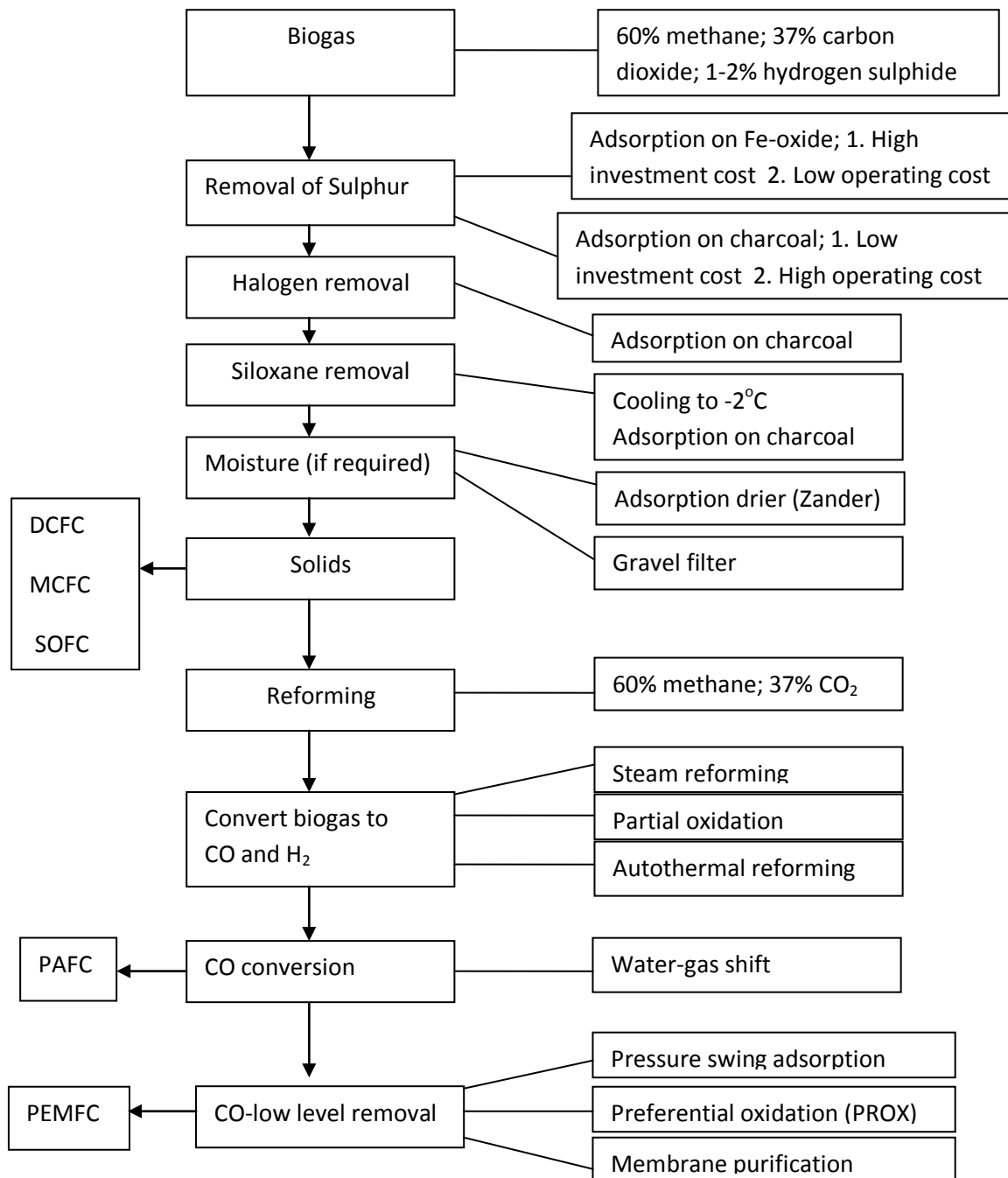


Figure 1.3: Fuel cells technology for biogas processing and clean up (Hoogers, 2003).

Table 1.3: Typical gas composition of biogas from organic household waste (Hoogers, 2003).

Component	Concentration (Wet gas)
Methane	60-75 %
Carbon dioxide	< 35%
Water vapour	0-10%
Nitrogen	<5 %
Oxygen	<1%
Carbon monoxide	0.2%
Siloxanes	< 10 mg per m ³ CH ₄
Hydrogen sulphide	150 ppm

A well known fact is that the biogas having similar compositions to natural gas makes use of the benefits ranging from direct use in high temperature fuel cells (Molten carbonate fuel cell (MCFC) and Solid oxide fuel cell (SOFC)) to further reforming to syngas or hydrogen, to meet the requirements for low temperature fuel cells (Adeniyi, 2008; Hoogers, 2003).

A flow chart for using biogas in conjunction with fuel cells is shown in Figure 1.3. Biogas is known to contain a wide range of contaminants, some of which are also found in natural gas, but there are cleanup technologies as shown in the same Figure 1.3. This flow chart also gives alternatives to activated charcoal, iron oxide filters (biological filters). The latter are believed to be maintenance-free and would increase the useful lifetime of the subsequent activated charcoal stage (Hoogers, 2003 cited Lehmann *et al.*, 2001). The use of biogas in high temperature FCs would require fewer processing steps than alternative FCs, with the DCFC and MCFC being particularly attractive due to their inherent affinity to CO₂. Both solid biomass and biogas represent viable and cost effective routes to powering FCs, even from waste materials. These options are going to become important points in the integrated management of effluent and fresh materials flow (Hoogers, 2003 cited Lehmann *et al.*, 2001).

1.3 Carnot Efficiency and Fuel Cell Efficiency

The Carnot efficiency limit for heat engines (like steam and gas turbines) is well known. The Carnot maximum efficiency possible for heat engines is given by Equation 1.4 (Larminie and Dicks, 2003).

(1.4)

T_1 is the maximum temperature of the heat engine, T_2 is the temperature of the heated fluid release, where temperatures are given in Kelvin. Consider a steam turbine operating at 400°C (673 K), with the exhaust water from the condenser at 50°C (323 K), then by Equation 1.4, the Carnot efficiency limit is 52%. For the heat engines there are inevitably some heat energy (proportional to T_2) that is wasted (Larminie and Dicks, 2003).

With the fuel cells the situations are much different, and are not subject to the Carnot efficiency limit. Where there is no irreversibility then the efficiency could be 100%. It is the Gibbs free energy that is converted to electrical energy. If it were not for the irreversibility, all this energy would be converted to electrical energy giving 100% efficiency (this is discussed in greater details in chapter four). Materials are usually burnt in a fuel cell to release energy, thus the comparison is made in the electrical energy produced with the heat that would be released by the fuel burning. This is known as the calorific value but more precisely the enthalpy of combustion (). The is negative when energy is released, so that Equation 1.5 gives the efficiency limit (Larminie and Dicks, 2003).

(1.5)

The maximum electrical energy possible is equal to the change in Gibbs free energy, so that we have Equation 1.6 (Larminie and Dicks, 2003).

(1.6)

The fundamental equation for the electromotive force (EMF) or reversible open circuit voltage of the hydrogen fuel cells is given by Equations 1.7 (Larminie and Dicks, 2003).

(1.7)

Where F is the faraday constant or the charge on one mole of electron and ΔG is the Gibb free energy released. These are further discussed in more details in Chapter 4. Table 1.4 gives the values of the efficiency limit, relative to the higher heating value (HHV), for a hydrogen fuel cell and the maximum voltage. Figure 1.4 shows the maximum H_2 fuel cell efficiency at standard pressure with reference to HHV (higher heating value), the Carnot limit in the figure is shown for comparison with a 50°C exhaust temperature (Larminie and Dicks, 2003).

Table 1.4: Hydrogen fuel cell ΔG , maximum EMF and efficiency limit (Larminie and Dicks, 2003).

Form of water product	Temperature ($^\circ\text{C}$)	ΔG (kJ mol^{-1})	Maximum EMF (V)	Efficiency limit (%)
Liquid	25	-237.2	1.23	83
Liquid	80	-228.2	1.18	80
Gas	100	-225.2	1.17	79
Gas	200	-220.4	1.14	77
Gas	400	-210.3	1.09	74
Gas	600	-199.6	1.04	70
Gas	800	-188.6	0.98	66
Gas	1000	-177.4	0.92	62

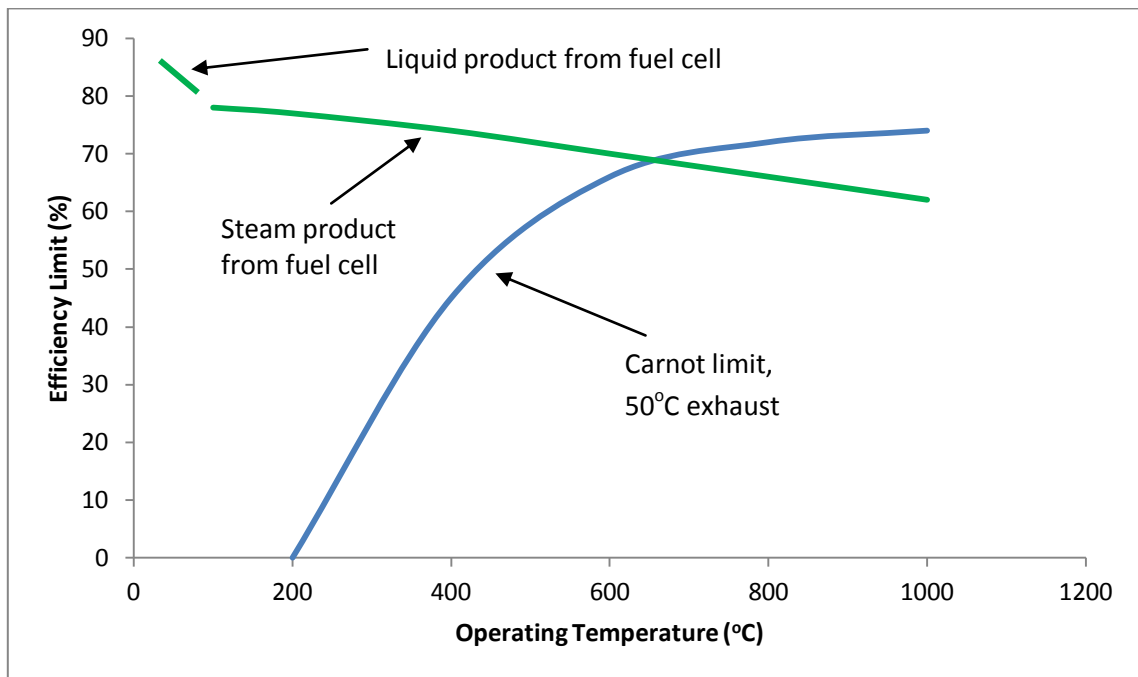


Figure 1.4: Maximum H₂ fuel cell efficiency at standard pressure (Larminie and Dicks, 2003)

1.4 Fuel Cell Voltage and Efficiency

There is a relation between the maximum EMF and the maximum efficiency of a fuel cell. If all the energy from the fuel cell were converted to electrical energy, then the EMF is given by Equation 1.8 (Larminie and Dicks, 2003).

(1.8)

This gives 1.48 V for HHV and 1.25 V for LHV (lower heating value) and represents the maximum voltages obtainable under standard conditions. The efficiency is the actual voltage (V_c) divided by the maximum voltage to give Equation 1.9 (Larminie and Dicks, 2003).

(1.9)

Where V_c is the fuel cell voltage. There are other definitions of efficiency which put into consideration the fuel cell design and fuel utilisation. Under experimental condition, it is not all the fuel put inside the fuel cell that is used, some passes through unreacted. This requires the use of a fuel utilization coefficient (μ_f) given by Equation 1.10 (Larminie and Dicks, 2003).

(1.10)

This gives the ratio of the fuel cell current and the current obtained when all the fuel is reacted. The cell efficiency is then given by Equation 1.11 (Larminie and Dicks, 2003).

(1.11)

In cases involving the use of LHV, then 1.25 instead of 1.48 will be applied in Equation 1.11. A good estimation value for μ_f which will allow the efficiency of a fuel cell being accurately estimated from voltage is 0.95 (Larminie and Dicks, 2003).

1.5 Research Aims and Objectives

This research project explores the use of biomass materials in fuel cells. The aim is to take advantage of the higher efficiencies available for electricity production through the direct carbon fuel cells (DCFCs) when compared with those from thermal cycles. The form of carbon required for direct carbon fuel cells is disordered carbon (amorphous) and this research concentrates on the most effective and energy efficient methods of producing carbons from a range of biomass source materials including miscanthus, switchgrass, wheat, spruce, willow and poplar. These were produced using thermochemical and mechanical routes and tested by means of available structural

measurement techniques and fuel cell devices. Thus the objectives of this research are;

1. To complete a broad literature search involving;

- ❖ Biomass as a renewable source of energy for fuel cell technology.
- ❖ Thermochemical and mechanical conversion of biomass.
- ❖ The technologies behind fuel cells, molten carbonate electrolyte direct carbon fuel cells (MDCFCs) and solid oxide electrolyte direct carbon fuel cells (SODCFCs).

2. To investigate thoroughly different theoretical aspect involving;

- ❖ Thermochemical and mechanical conversion of biomass.
- ❖ The technologies and operations behind molten carbonate electrolyte DCFCs and solid oxide electrolyte DCFCs.

3. To outline and execute experimental methodologies involving;

- ❖ Conceptualisation and development of a pyrolyser. Conversion of biomass using slow/conventional pyrolysis and the testing of different designs parameters for the pyrolysis of biomass.
- ❖ Testing carbon particles produces by proximate and ultimate, calorific value, carbon and hydrogen contents, Malvern particle sizer, scanning electron microscope (SEM) and X-ray diffraction (XRD) analyses.
- ❖ Conceptualisation, design and construction of a single cell direct carbon fuel cell, development of molten carbonate electrode assembly and testing different design options for the electrode assembly components of the MDCFC and SODCFC.
- ❖ Preparation of the electrolytes, electrode, biomass carbon fuel with molten carbonate mixtures, testing and performance investigations of the direct carbon fuel cell using carbon black fuel with molten carbonate mixture in the MDCFC.

- ❖ Testing and performance investigations of the MDCFC and SDCFC using hand and ball milled biomass carbon fuels from miscanthus, switchgrass, wheat, spruce, willow and poplar.

4. To present and discuss the results obtained including;

- ❖ Results from mechanical, thermochemical treatment of biomass and biomass carbon, particle size, SEM and XRD analyses.
- ❖ Performance investigations from a single cell MDCFC and SDCFC using hand and ball milled biomass carbon fuels from miscanthus, switchgrass, wheat, spruce, willow and poplar.

1.6 Outline of Thesis

This thesis report consists of eight chapters. Chapter one gives an overview and introduction to this research. Chapter two talks about biomass energy content, composition and the relationship between carbon, energy content, enthalpies of formations, and chemical structures of some biomasses. Chapter three discusses the various thermochemical and mechanical processes involved in the conversion of biomass into energy with emphasis placed on pyrolysis. It also presents the technologies behind fuel cells, its classification, history, current applications and fuel processing. Chapter three also discusses the history, descriptions and advantages of the DCFC. Chapter four gives a description of the various experimental works carried out during this research. Chapter five gives the various results obtained from pyrolysis, XRD, SEM and others during this research work. Chapters six and seven present the performances of a single cell MDCFC and SDCFC respectively. Chapter eight gives the conclusions and recommendations for future work within this field.

Chapter Two

Literature Review

2.1 Introduction

Renewable energy as defined by Twidell and Weir (1986) is energy obtained from the continuous or repetitive current of energy recurring in the natural environment. Another definition by Sorensen (2000) is the energy flows which are replenished at the same rate as they are used. One clear point is that renewable energy sources are derived primarily from the enormous power of the sun's radiation (Boyle, 2004; Boyle *et al.*, 2003). Our emphasis in this research is on bioenergy and it considers biomass as a form of renewable energy. This chapter talks about biomass energy content and composition giving some heating, ultimate and proximate values for various types of biomass products. It also discusses the relationship between carbon, energy content, enthalpies of formations, and chemical structures of some biomasses. Energy production from biomass using virgin, forest, grasses and cultivated crops are also considered. Disordered or amorphous carbon structure, its preparations and the methods of characterisation are discussed.

2.2 Biomass Energy Content and Composition

2.2.1 Heating Values, Ultimate and Proximate Analysis

Experimental determination of the physical moisture contents of biomass are done by drying a given sample at 100 to 105°C at atmospheric pressure or at lower temperature and reduced pressure. Some organic compounds may be lost by these procedures because of volatilization and/or steam distillation, but in most cases the results are suitable for the characterization of biomass. Typical proximate analyses and higher heating value (HHV- product water in liquid state) of many biomass types and species illustrate a wide range of some parameters such as moisture content and ash content and a relatively limited range of heating values (Table 2.1). The moisture contents shown in Table 2.1 varies from 2 to 3 wt.% for the char and paper biomass to a higher value of 98 wt.% for primary biosolids (primary sewage sludge). In the field, greenwood usually contains 50 wt.% moisture before drying, whereas primary biosolids contain only a few percent suspended and dissolved solids in water (Klass,

1998). The total organic matter is estimated by difference between 100 and the ash percentage that is experimentally determined by ashing the biomass samples at elevated temperature using standard methods (like ASTM standard, American Society of Testing and Materials; Methods for the Examination of Water and Wastewater). The chemical analysis of the components in the ash from woody and herbaceous biomass samples are given in Table 2.2, which shows that metal oxides are present, but the distribution of the metallic elements are different in the various samples. The distribution of metals in biomass and the compositions of the ash are important in the development of certain types of biomass conversion processes because they can affect the process performance (Klass, 1998).

It is observable from Tables 2.1 to 2.4 that the organic matter content and the HHV are affected by the ash, which in almost all cases has no energy value. The higher the ash value, the lower the organic matter and the HHV. The elemental compositions shown in Table 2.2 vary over a wide range because there are so many different types and species. Table 2.2 shows typical proximate and ultimate analyses and the HHVs of land and water-based biomass and waste biomass, these are compared with those of cellulose, peat and bituminous coal (Klass, 1998). Table 2.3 gives the typical percentage composition of biomass feedstock on bone dry material basis (Montross and Crofcheck, 2010).

2.2.2 Relationship between Carbon and Energy Content of Biomass

The energy content of biomass is a crucial factor to be considered when converting biomass for energy, syngases and fuel cell applications. Different components of biomass have different heat of combustion simply because of the difference in chemical structures and carbon content. The higher the state of carbon in a given biomass the higher the energy content, this is illustrated in Tables 2.2 to 2.5. Monosaccharides have the lowest carbon content, highest degree of oxygenation, and lowest heating values.

Table 2.1: Typical proximate analysis and high heating value (HHV) for biomass, coal and peat (Klass, 1998)

Category	Name	Type	Moisture range (wt.%)	Organic matter (dry wt.%)	Ash (dry wt.%)	HHV (MJ/dry kg)
Wastes	Cattle manure	Feedlot	20-70	76.5	23.5	13.4
	Activated biosolids	Sewage	90-97	76.5	23.5	18.3
	Primary biosolids	Sewage	90-98	73.5	26.5	19.9
	Refuse-derived fuel (RDF)	Municipal	15-30	86.1	13.9	12.7
	Sawdust	Woody	15-60	99.0	1.0	20.5
Herbaceous	Cassava	Tropical	20-60	96.1	3.9	17.5
	<i>Euphorbia lathyris</i>	Warm season	20-60	92.7	7.3	19.0
	Kentucky bluegrass	Cool season	10-70	86.5	13.5	18.7
	Sweet sorghum	Warm season	20-70	91.0	9.0	17.6
	Switchgrass	Warm season	30-70	89.9	10.1	18.0
Aquatic	Giant brown kelp	Marine	85-97	54.2	45.8	10.3
	Water hyacinth	Fresh water	85-97	77.3	22.7	16.0
Woody	Black alder	Hardwood	30-60	99.0	1.0	20.1
	Cottonwood	Hardwood	30-60	98.9	1.1	19.5
	Eucalyptus	Hardwood	30-60	97.6	2.4	18.7
	Hybrid poplar	Hardwood	30-60	99.0	1.0	19.5
	Loblolly pine	Softwood	30-60	99.5	0.5	20.3
	Redwood	Hardwood	30-60	99.8	0.2	21.0
	Sycamore	Hardwood	30-60	98.9	1.1	19.4
Coal	Illinois bituminous	Soft	5-10	91.3	8.7	28.3
	North Dakota lignite	Soft	5-15	89.6	10.4	14.0
Peat	Reed sedge	Young coal	70-90	92.3	7.7	20.8

Table 2.2: Typical compositions and heating values of virgin and waste biomass, peat and coal (Klass, 1998)

Test	Pure cellulose	Pine wood	Kentucky bluegrass	Giant brown kelp	Water hyacinth	Feedlot manure	RDF	Primary biosolids	Reed sedge peat	Bituminous coal
Ultimate analysis (wt.%)										
C	44.44	51.8	45.8	27.65	41.1	35.1	41.2	43.75	52.8	69.0
H	6.22	6.3	5.9	3.73	5.29	5.3	5.5	6.24	5.45	5.4
O	49.34	41.3	29.6	28.16	28.84	33.2	38.7	19.35	31.24	14.3
N		0.1	4.8	1.22	1.96	2.5	0.5	3.16	2.54	1.6
S		0	0.4	0.34	0.41	0.4	0.2	0.97	0.23	1.0
Ash		0.5	13.5	38.9	22.4	23.5	13.9	26.53	7.74	8.7
C (maf)	44.44	52.1	52.9	45.3	52.9	45.9	47.9	59.5	57.2	75.6
Proximate analysis (wt.%)										
Moisture		5-50	10-70	85-95	85-95	20-70	18.4	90-98	84.0	7.3
Organic matter		99.5	86.5	61.1	77.7	76.5	86.1	73.47	92.26	91.3
Ash		0.5	13.5	38.9	22.4	23.5	13.9	26.53	7.74	8.7
Higher Heating values										
MJ/dry kg	17.51	21.24	18.73	10.01	16.00	13.37	12.67	19.86	20.79	28.28
MJ/kg (maf)	17.51	21.35	21.65	16.38	20.59	17.48		27.03	22.53	30.97
MJ/kg carbon	39.40	41.00	40.90	36.20	38.93	38.09		45.39	39.38	40.99

maf - moisture and ash-free material, RDF- Refused-Derived Fuel

Table 2.3: Typical composition of biomass feedstock - bone dry material basis (Montross and Crofcheck, 2010)

Biomass	Extractives (wt.%)	Cellulose (wt.%)	Hemicellulose (wt.%)	Lignin (wt.%)	Ash (wt.%)	HHV (MJ/kg)
<i>Agricultural Residues</i>						
Maize stover	5.9	35.5	22.8	18.7	11.6	18.3
Sugarcane bagasse	4.5	39.1	22.6	24.3	5.2	19.1
Wheat straw	13.0	32.6	22.6	16.9	10.2	17.4
<i>Forestry Products</i>						
American sycamore	3.0	39.7	18.5	25.8	1.2	19.6
Black locust	4.7	40.8	18.1	26.2	1.6	19.7
Eucalyptus	1.9	46.3	14.9	27.2	1.1	19.6
Hybrid Poplar	4.2	41.5	17.9	25.7	1.8	19.6
Spruce (pine)	2.7	41.7	20.5	25.9	0.3	19.6
Willow	NE	48.5	13.9	19.7	1.7	20.0
<i>Herbaceous Crops</i>						
Switchgrass Alamo	11.1	33.1	26.3	18.0	5.4	18.9
Miscanthus x giganteus	NE	45.0	30.0	21.0	2.3	17.7
Sericea Lespedeza	7.7	36.6	16.9	26.2	3.0	19.4
Reed canary grass	NE	42.6	29.7	7.6	NE	17.9
Timothy grass	NE	28.8	27.2	4.8	NE	NE
Alfalfa	NE	27.4	11.7	4.8	NE	18.5
Tall fescue	20.3	24.5	19.5	14.7	11.8	NE

NE-Not evaluated

Table 2.4: Analysis of ash from Hybrid poplar, pine and switchgrass (Klass, 1998)

Component	Hybrid poplar (dry wt.%)	Pine (dry wt.%)	Switchgrass (dry wt.%)
CaO	47.20	49.20	4.80
K ₂ O	20.00	2.55	15.00
P ₂ O ₅	5.00	0.31	2.60
MgO	4.40	0.44	2.60
SiO ₂	2.59	32.46	69.92
Al ₂ O ₃	0.94	4.50	0.45
BaO	0.70		0.22
Fe ₂ O ₃	0.50	3.53	0.45
TiO ₂	0.26	0.40	0.12
Na ₂ O	0.18	0.44	0.10
Mn ₂ O ₄	0.14		0.15
SrO	0.13		0.04
CO ₂ ^a	14.00		
SO ₃ ^a	2.74	2.47	1.90
Total	98.78	96.30	98.35

^aThe presence of carbon and sulphur in the ash is that the ashing procedure was probably performed at an insufficient temperature and/or for an insufficient time to volatilize all non-mineral components (Klass, 1998).

With increase in carbon content, the degree of oxygenation is reduced and the structures become more hydrocarbon-like and thus the heating value increases. The dominant component in most biomass is usually cellulose with a high heating value of 17.51 MJ/kg (Klass, 1998).

Table 2.5: Typical carbon content and heating value of biomass component

(Klass, 1998)

Component	Carbon (wt.%) ^a	HHV (MJ/kg) ^a
Monosaccharides	40	15.6
Disaccharides	42	16.7
Polysaccharides	44	17.5
Crude protein	53	24.0
Lignins	63	25.1
Lipids	76-77	39.8
Tarpenes	88	45.2
Crude carbohydrates	41-44	16.7-17.7
Crude fibres ^b	47-50	18.8-19.8
Crude triglycerides	74-78	36.5-40.0

^aApproximate values for dry mixtures, ^bContains 15-30% lignins

The lower heating values (LHV, product water in vapour state) of some biomass are given in Table 2.6. It is observed that woody and fibrous materials have energy contents between 19 and 21 MJ/kg, whereas the water-based algae *Chlorella* has a higher value, this is attributed to the high lipid or protein contents. Also oils derived from plant seeds have higher energy content and approach the heating value of paraffinic hydrocarbons. High concentrations of inorganic components in a given biomass species can greatly affect its energy content because inorganic materials do not contribute to heat of combustion (Klass, 1998). The energy value of the total material can be estimated from the carbon analysis and moisture determinations without actual measurement using a calorimeter. Data manipulation of Table 2.2 led to a simple equation for calculating the HHV of biomass and also coal and peat with reasonable accuracy as given by Equation 2.1 (Klass, 1998).

$$\text{HHV (MJ/dry kg)} = 0.4571 (\%C \text{ on dry basis}) - 2.70 \quad (2.1)$$

Table 2.6: Typical lower heating value of biomass and fossil materials (Klass, 1998)

Material	Lower Heating Value (LHV) (MJ/dry kg)
Trees	
Oak	19.20
Bamboo	19.23
Birch	20.03
Beech	20.07
Oak bark	20.36
Pine	21.03
Fibre	
Bagasse	19.25
Buckwheat hulls	19.63
Coconut shells	20.21
Green algae	
Chlorella	26.98
Seed oils	
Linseed	39.50
Rape	39.77
Cottonseed	39.77
Amorphous carbon	33.80
Paraffinic hydrocarbon	43.30
Crude oil	48.20

Experimental HHVs and the calculated HHVs using Equation 2.1 for the biomass, coal and peat (applying carbon analysis of Table 2.2) were compared and this is given in Table 2.7, giving a reasonably small variation (Klass, 1998).

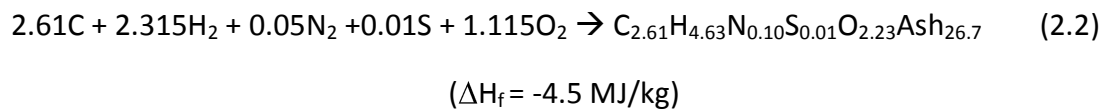
2.2.3 Enthalpies of Formation

Biomass enthalpies of formation are very important in their thermodynamic calculations. The standard enthalpies of formation at 298 K of the combustion products in MJ/kg are: CO₂, -3.94; liquid H₂O, -2.86; NO₂, 0.34; SO₂, -2.97, the elemental analysis and the HHV of the biomass can be used to estimate its heats of specific reactions.

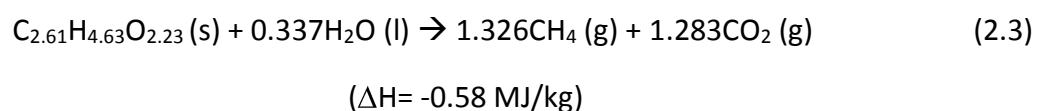
Table 2.7: Measured and calculated HHVs comparison for biomass, coal and peat
(Klass, 1998)

Material	Measured HHV (MJ/dry kg)	Calculated HHV (MJ/dry kg)	Error (%)
Giant brown kelp	10.01	9.94	-0.70
Cattle feedlot manure	13.37	13.34	-0.19
Water hyacinth	16.00	16.09	+0.54
Pure cellulose	17.51	17.61	+0.59
Kentucky bluegrass	18.73	18.24	-2.64
Primary biosolids	19.86	17.30	-12.90
Reed sedge peat	20.79	21.43	+3.10
Pine wood	21.24	20.98	-1.23
Illinois bituminous coal	28.28	28.84	+1.98

The enthalpy of formation of a given biomass sample is equal to the weighted sum of the heats of formation of the products of combustion minus the HHV. It is mostly assumed that the ash is inert. Taking a giant brown kelp as an example, with empirical formula $C_{2.61}H_{4.63}N_{0.10}S_{0.01}O_{2.23}$ (dry basis), derived from the elemental analysis, and a HHV of 12.39 MJ/kg, at an assumed molecular weight of 100 (including the ash). The enthalpy of formation stoichiometry calculation is given by Equation 2.2 (Klass, 1998);



The enthalpy of formation is -4.50 MJ/kg with the ash for the biomass inclusive. Application of this information to a biological gasification process under anaerobic conditions, with a process stoichiometry is given in Equation 2.3 (Klass, 1998):



The process enthalpy is calculated to be -0.58 MJ/kg of the kelp reacted (Klass, 1998 cited Klass and Ghosh, 1977). A basic assumption made by the authors is that the inorganic components are carried through the process unchanged, and the sulphur and nitrogen was ignored because of their small concentration (Klass, 1998).

2.2.4 Chemical Structures of Biomass

In order to develop processes for producing derived fuels and chemicals from biomass the knowledge of the major organic components are essential as this can lead to the improvement of existing processes, development of other advanced conversion techniques and a better understanding of fuel cell performances using different type of biomass carbon (Adeniyi, 2008; Klass, 1998). Polysaccharides such as alpha cellulose have a general formula $(C_6H_{10}O_5)_n$ with an average molecular weight in the range of 300,000-500,000. Complete hydrolysis shows that the polymer consists of D-glucose units. Partial hydrolysis yields cellobiose (glucose- β -glucoside), cellotriose and cellotetrose (Klass, 1998). Wood cellulose, the raw material for pulp and paper industry, always occurs in association with hemicelluloses and lignins whereas cotton is almost pure α -cellulose. Cellulose is insoluble in water, forms the skeletal structure of most terrestrial biomass and constitutes approximately 50% of the cell wall material (Klass, 1998). Figures 2.1 and 2.2 show some hypothetical organisation of lignin and polysaccharides in wood and the pyrolysis product of lignin model (Henriksson *et al.*, 2010).

The general formula of starches, which is a polysaccharide, is $(C_6H_{10}O_5)_n$. They are normally reserve sources of carbohydrate in some biomass and are made up of D-glucose, in contrast to the structure of cellulose, the hexose units are linked as in maltose or glucose- α -glucoside. Another major difference between cellulose and starch is that starch can be separated into two fractions by treatment with hot water: amylose (10-20%), which is a soluble component and amylopectin (80-90%), which is

insoluble. Amylose and amylopectin have molecular weights in the ranges of 10,000-50,000 and 50,000-1,000,000 respectively (Klass, 1998).

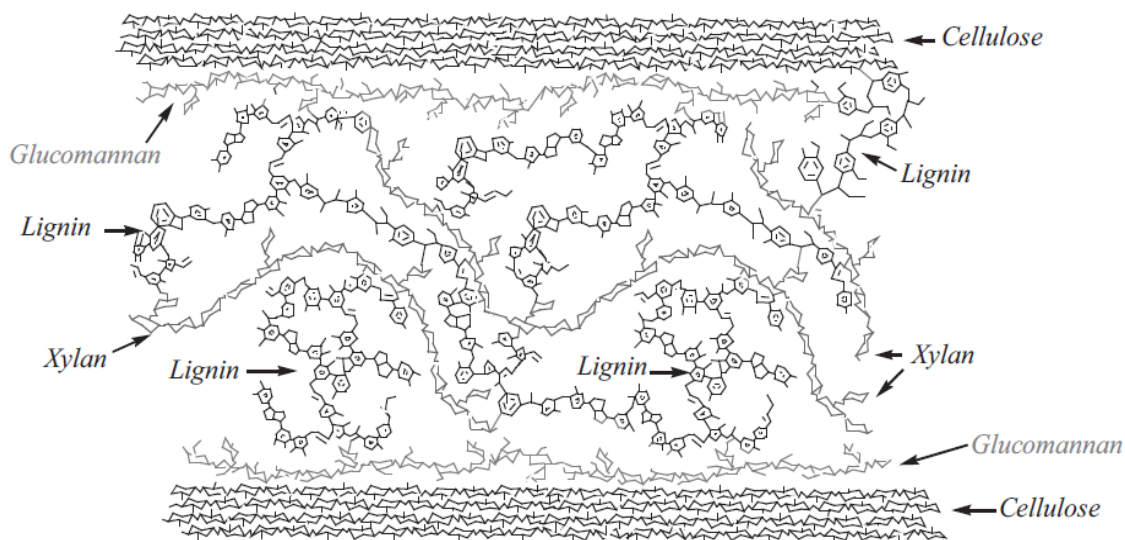


Figure 2.1: Hypothetical network of lignin and polysaccharides in wood (Henriksson *et al.*, 2010).

Hemicelluloses occur in association with cellulose in the cell walls and are complex polysaccharides. Hemicelluloses are soluble in dilute alkali and consist of branched structures, which can vary among different species of herbaceous and woody biomass. They have the generic formula $(C_5H_8O_4)_n$. Hemicelluloses consist of 50-200 monomeric units and a few simple sugar residues. Xylan is the most abundant type of hemicelluloses, and consists of D-xylose units linked in the 1- and 4-positions (Klass, 1998).

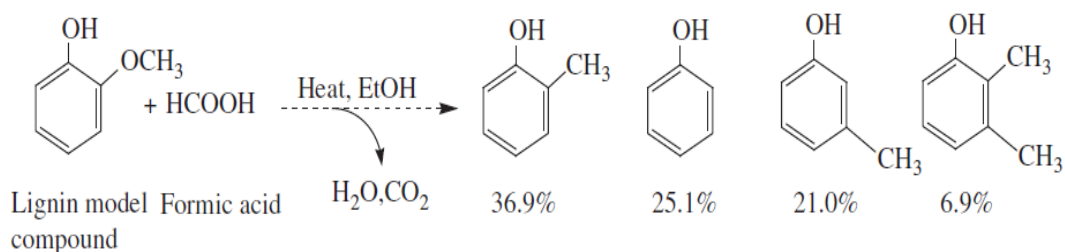


Figure 2.2: Pyrolysis of lignin model in the presence of formic acid giving demethoxylated product (Henriksson *et al.*, 2010)

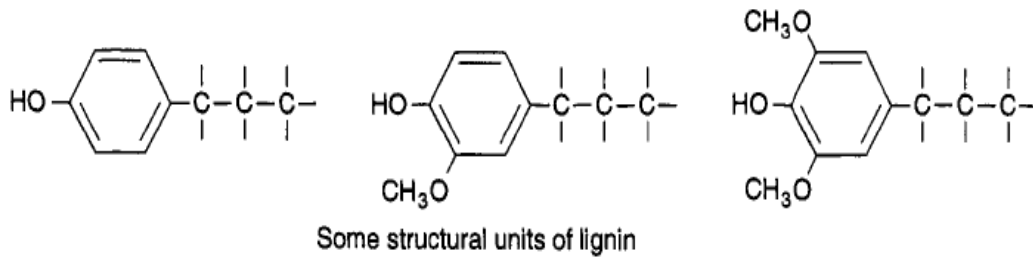


Figure 2.3: Chemical structures of lignin in biomass (Klass, 1998)

Lignins are highly branched, substituted, mononuclear aromatic polymers in the cell walls of most biomass, like woody species, and are bound to adjacent cellulose fibres to form a lignocellulosic complex. The complex and lignins are very resistant to conversion by microbial systems and many chemical agents. This complex can be broken and the lignin fraction separated by treatment with strong sulphuric acid (in which lignins are insoluble). The monomeric units which are dominant in the polymers are benzene rings bearing methoxyl, hydroxyl, and propyl groups which are attachable to other groups (Figure 2.3). The lignin contents on dry basis in softwoods and hardwoods range from 20-40% by weight, and from 10-40% by weight in other herbaceous species such as bagasse, corncobs, peanut shells, rice hulls and straws (Klass, 1998).

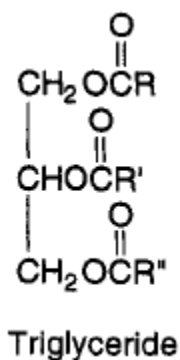


Figure 2.4: Chemical structures of triglyceride in biomass (Klass, 1998)

The triglycerides found in biomass are esters of triol, glycerol and fatty acids (Figure 2.4). They are water-insoluble, oil-soluble esters and are found in many biomass species, especially the oilseed crops in minute concentration. Most lipids in biomass are esters of two or three fatty acids; the most common are lauric (C₁₂), myristic (C₁₄), palmitic (C₁₆), oleic (C₁₈) and linoleic (C₁₈) acids. The fatty acid of palm oil is palmitic (35-45%). Palm-kernel oil (52%), coconut oil (48%) and babassu nut oil (46%) are lauric acid. The monounsaturated oleic acid and polyunsaturated linoleic acid are about 90% of sunflower oil fatty acid. Linoleic acid greatly dominate the fatty acid found in corn oil (55%), soybean oil (53%) and safflower oil (75%) (Klass, 1998).

2.3 Energy Production Using Virgin Biomass

Energy products manufacture from virgin biomass requires that suitable quantities of biomass chosen for use as energy crops be grown, harvested and transported to the conversion plant. For a continuous, integrated biomass production and conversion, it is necessary to have sufficient supply of the feedstock to sustain the operation of various conversion plants. In comparison to the total known botanical species (250,000 of which only 300 are cash crops), a relatively small number are suitable for the manufacture of synfuels and energy products. Most of the virgin biomass which could be used for the production of energy are terrestrial and they include; forest, grasses and cultivated crops (Klass, 1998).

2.3.1 Forest Biomass

It is stated that about one-third of the world's land area is forestland (Klass, 1998). The dominant species in tropical rain forest near the equator are broad-leaved evergreen trees (Klass, 1998). The coniferous softwood trees such as spruce, fir, and larch are dominant in the boreal forests at the higher latitudes in the Northern hemisphere, while the broad-leaved deciduous hardwoods such as oak, beach and maple and the conifers such as pine and fir are found in the middle latitudes. Trees are pertinent resources which still and will serve as major energy resources in developing countries.

About 1.5 billion people derive at least 90% of their energy requirement from wood and charcoal in developing countries, and another billion people meet at least 50% of their energy needs this way. Many species such as *Acacia*, *Casuarina*, *Eucalyptus*, *Pinus*, *Prosopis* and *Trema* are used as fuelwood in developing countries. Eucalyptus is one tree species that has been studied as a renewable energy resource. It is an evergreen hardwood tree belonging to the myrtle family, Myrtaceae, and the genus *Eucalyptus*, with about 450 to 700 identifiable species in the genus (Klass, 1998).

2.3.2 Grasses

The most abundant form of biomass is grass, with about 400 genera and 6000 species distributed all over the world. Grass, as a family (Gramineae), includes the great fruit crops, sugarcane, wheat, rice, corn, sorghum, millet, barley and oats. The many species of sod crops that provide forage or pasturage for all farm animals are also grasses. Grass also includes legumes family of the clovers, and alfalfas. Another successful feedstock for conversion to synfuels are perennial grasses. Most of these grasses can be grown vegetatively, and they re-establish themselves rapidly after harvesting. Again more than one harvest can usually be obtained from these grasses annually. The warm-season grasses are preferred over the cool-season grasses because their growth increases rather than decline as the temperature rises to maximum in summer time. Some tropical and semitropical grasses are very productive with a yield of about 50–60 t/ha-year on good sites. *Digitaria decumbens* is a tropical fodder grass, has a yield of organic matter of 85 t/ha-year (Klass, 1998).

Sugarcane (*Saccharum* spp.) is a tropical grass that is grown commercially as a combination foodstuff and fuel crop. Sugarcane grows rapidly and produces high yield, the fibrous bagasse is used as boiler fuel for the generation of electric power, and sugar derived ethanol is used as a motor fuel in gasoline blends (gasohol). About half of the organic material in sugarcane is sugar and the other half is fibre. The total cane biomass yield has been reported in the range of 80-85 dry t/ha-year (Klass, 1998).

Miscanthus and switchgrass (*Panicum virgatum*) are other promising biomass energy crop, which has a high yield potential, adaptation to marginal sites, and tolerant to water and nutrient limitation. The perennials reed canary grass, tall fescue, crested wheatgrass, weeping lovegrass, Bermuda grass, the annual sorghum and its hybrids are other productive grasses being considered as raw materials for production of energy (Klass, 1998).

2.3.3 Cultivated Crops

Other terrestrial biomass species have been proposed as renewable energy resources for their high-energy components that can be used as fuels, or their components being capable of conversion to biofuels and chemicals. Among this group are the like of kenaf (*Hibiscus cannabinus*), an annual plant reproducing by seed only; sunflower (*Helianthus annuus* L.), an annual oil seed crop; *Eurphorbia lathyris*, a sesquiterpene-containing plant species that grows in the semiarid climates; Buffalo gourd (*Curcubita foetidissima*), a perennial root crop native to arid and semiarid regions; Jerusalem artichoke (*Helianthus tuberosus*), fodder beet (*Beta vulgaris*), and cassava (*Manihot esculenta*); alfalfa (*Medicago sativa*), a perennial legume that grows well on good sites; soybean (*Glycine max*) and rapeseed (*Brassica campestris*), oilseed crops that produce high-quality oil and protein (Klass, 1998).

Sunflower is a good candidate for biomass energy application because of its rapid growth, wide adaptability, drought tolerance, short growing season, massive vegetative production, and adaptability to root harvesting. The dry yield is projected as high as 34 t/ha per growing season. Rapeseed is another good example, yielding 38-44 wt.% high quality protein and over 40 wt.% of oil from the seeds. The oil offer high quality biodiesel fuel at the rate of 750 to 900 L/ha-year on extraction and transesterification. Alfalfa is another good example, it is a widely planted herbaceous crop that offers environmental and soil conversation advantages when grown as a 4-year segment in a 7-year rotation with corn and soybeans. The yield is about 9 dry

t/ha-year, the leaf fraction is sold as a high-value animal feed, the remaining alfalfa stem fraction is normally used as feedstock for power generation (Klass, 1998).

2.4 Disordered Carbon Structures

Carbon materials have a large range of properties and structures. Generally there are the crystalline (ordered) carbon forms and the amorphous (disordered) carbon forms. The bondings between the neighbouring atoms of carbon based materials make them unique in nature. Graphite and diamonds are crystalline polymorphs having hexagonal structure layer and ABAB-stacking for graphite. The cubic structure with tetragonal bonded carbon atoms are found in diamond. Fullerenes and carbon nanotubes are currently being researched for their industrial applications. Carbon nanotubes are mono or multilayered tubes produced by graphene sheets wrapping, fullerene on the other hand are closed shell structure. The many potential application of carbon nanotubes are in the drug delivery system, hydrogen storage, electronic and display devices, composite fibres etc. Fullerene potential applications are in the optics, superconductivity, and drug delivery system (Popov and Lambin, 2006; Reich *et al.*, 2004; Dasgupta and Sathiyamoorthy, 2003; Holliday *et al.*, 1973).

Disordered carbons are becoming more important for industrial and research purposes. In the industries carbon black and glassy carbon are widely employed for their disordered carbon nature and there are growing potential applications in the area of fuel cells, low temperature thermal nuclear reactors and other area. Depending on the structure of the precursor materials and the processing conditions the carbon obtained from the pyrolysis of organic material could be ordered or disordered (Dasgupta and Sathiyamoorthy, 2003; Franklin and Watt, 1957; Franklin, 1950). Carbonaceous substances like the petroleum coke at lower temperature (1000°C) could possess ordered or disordered structure and when exposed to higher temperature could form graphite structure. These are known as soft or graphitisable

carbons. Hard carbons do not graphitise even at higher temperatures of 3000°C (Dasgupta and Sathiyamoorthy, 2003).

2.5 Amorphous (Disordered) Materials

Disordered materials have many properties which are unique to them and which are not shared by crystalline materials. They possess a degree of randomness which could be topological, spin, substitutional and vibrational disorder (Elliot, 1990). The form of randomness in which there is no translational periodicity is known as the topological or geometric disorder. In spin or magnetic disorder an underlying perfect crystalline lattice is available with each atomic site possessing a spin or magnetic moment which is oriented randomly. In substitutional disorder there is also an underlying crystalline lattice which is available, the material is an alloy (Cu-Au) with one type of atom randomly substituting for the other in the lattice. In vibrational disorder the atoms are vibrating about their equilibrium crystalline positions (Elliot, 1990; Holliday *et al.*, 1973). These types of disorder are schematically representing in Figure 2.5.

2.6 Preparation of Disordered Carbon

There are different routes in which disordered carbon can be prepared. Some of them are pyrolysis of organic materials, irradiation of graphitic structure, cracking of hydrocarbons, sputtering and evaporation (Dasgupta and Sathiyamoorthy, 2003). Other techniques include the glow-discharge decomposition, chemical vapour deposition, melt quenching, gel desiccation, electrolytic decomposition, reaction amorphisation, pressure-induced amorphisation, solid-state diffusional amorphisation among others (Elliot, 1990). Few of these are briefly described here.

2.6.1 Pyrolysis of Organic Materials

During pyrolysis organic substances are heated in a controlled manner in the absence of oxygen/air to produce solid, liquid and gaseous products. During the pyrolysis process polymerisation and cross-linking will take place and non-carbon materials are volatilized (Dasgupta and Sathiyamoorthy, 2003). Pyrolysis of biomass to produce disordered carbon materials is of great importance to this research work because it is the main route used in the production of carbon from the various biomasses for the direct carbon fuel cell. Pyrolysis processes are fully described in chapter three and other chapters of this thesis.

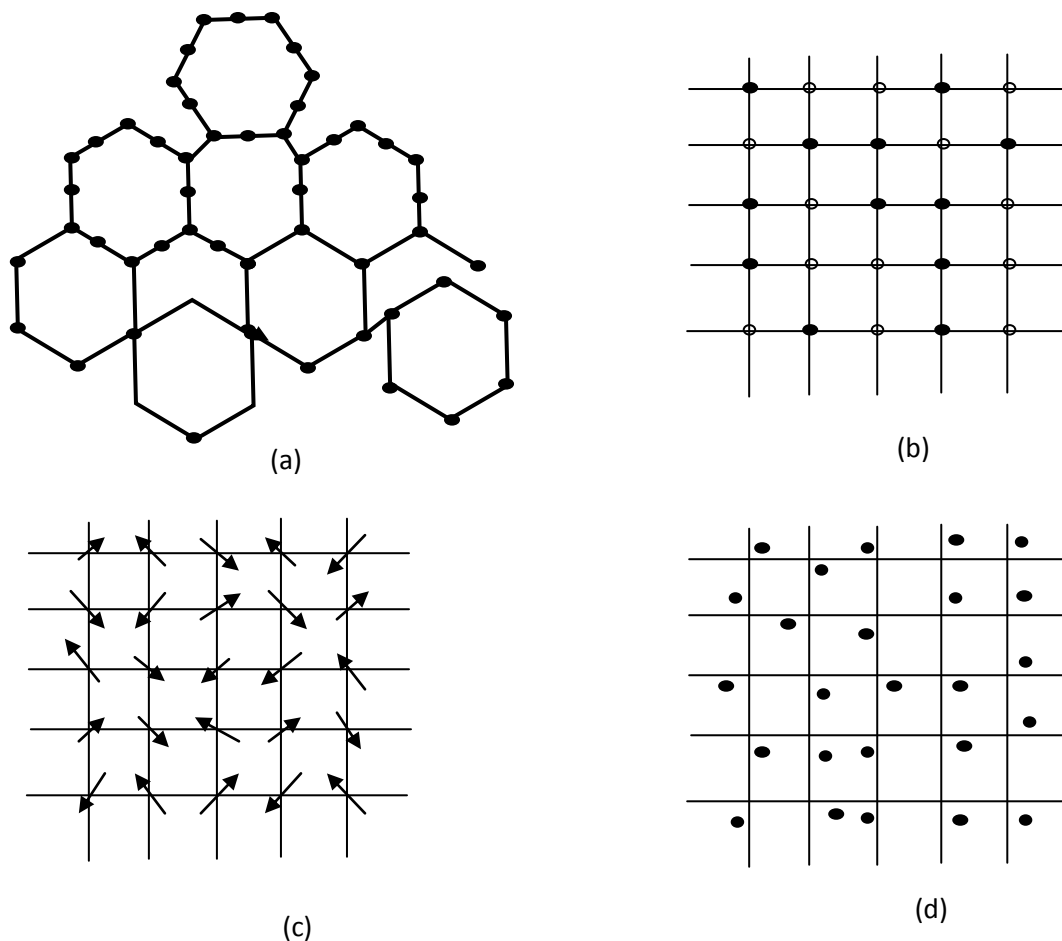


Figure 2.5: Various type of disorder (a) topological (no long range order) (b) substitutional (no regular lattice), (c) spin (on regular lattice), (d) vibrational (equilibrium positions of a regular lattice) (Elliot, 1990).

2.6.2 Irradiation of Graphitic Structure

Amorphisation of graphitic structure is brought about by the irradiation with ions or neutrons where energy is provided to break the crystalline structure through irradiation (Dasgupta and Sathiyamoorthy, 2003). The bombardment of crystalline solids by ions produces amorphous surface layers which could be hundreds of angstroms in thickness. The interaction between high energy ionizing particles and the crystalline solids usually produces enough structural damage to amorphise the material (Elliot, 1990).

2.6.3 Cracking of Hydrocarbons

Using fluidised or static bed hydrocarbons can be cracked. The properties and structure of the carbon produced will depend on the hydrocarbon used, the cracking temperature, concentration, residence time and the geometry of the reactor used (Dasgupta and Sathiyamoorthy, 2003).

2.6.4 Sputtering and Evaporation

Sputtering and evaporation can be achieved with the aid of plasma or by the arcing method where carbon atoms are evaporated and deposited to form disordered (amorphous) structure (Dasgupta and Sathiyamoorthy, 2003). Sputtering involves the bombardment of materials with energetic ions from low pressure plasma, bringing about the erosion of the material atom by atom or as clusters of atoms and the deposition of a film on the substrate. In thermal evaporation the starting materials is vaporised and the product material is collected on a substrate (Elliot, 1990).

2.7 Method of Characterisation

2.7.1 Optical Microscopy

Reflection microscopy is used on polished carbon because of their high absorption properties. The understanding of their anisotropy properties are done by polarised and cross-polarisers where the optical anisotropy is expressed by the phase shift produced by the object using Newton chart. For disordered carbons, the elemental aromatic layers stacks are usually smaller than the microscopic resolution, this gives rise to averaging the data relative to the basic structural unit (BSU, proposed by Franklin, 1957) which is known as the nanocrystal of graphite. The data generated are highly sensitive to the textures, that is, to the three dimensional BSUs arrangement, to its perfection and to the occurrence which is of no preferred orientation but not sensitive to the crystalline order. A carbon material become optically isotropic where there is no local molecular orientation or where it is largely below the resolution of the microscope (Dasgupta and Sathiyamoorthy, 2003 cited Oberlin *et al.*, 1998).

2.7.2 Raman Spectroscopy

The structural information on a given disordered carbon can be obtained using the Raman spectroscopy which involves the illumination of a given sample with monochromatic light and the investigation of the light scattered by the sample using the spectrometer. The scattering process could be elastic (known as the Rayleigh scattering) or inelastic (known as the Raman scattering). The excitations to a virtual state occur when the electric field component of the scattering photon perturbs the electron cloud of the carbon molecules. When the system exchanges energy with the photon whereby the system decays to vibrational energy levels below or above that of its initial state, then Raman scattering has occurred. Raman shift describes the frequency shift that corresponds to the energy difference between the scattered photon and the incident. In disordered carbon two broad peaks are usually generated (Dasgupta and Sathiyamoorthy, 2003). Figure 2.6 shows the mode of vibration in carbons.

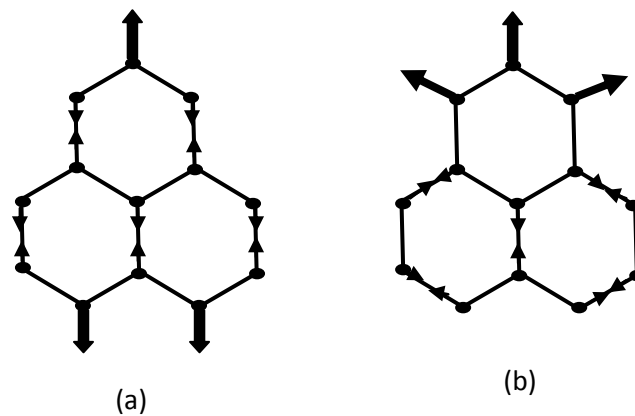


Figure 2.6: Carbon modes of vibration (a) E_{2g} mode-stretching (b) A_{1g} disordered mode-breathing (Dasgupta and Sathiyamoorthy, 2003)

Due to the loss of long range order there is no k (wave vector) conservation for amorphous or disordered carbon but all modes are allowed. The D mode corresponds to a peak in photon density of state of graphite due to the A_{1g} mode or the breathing mode. This mode develops a strong Raman activity when k is no longer conserved and inactive for an infinite layer (Dasgupta and Sathiyamoorthy, 2003; Tuinstra and Koenig, 1970).

2.7.3 X-Ray Diffraction

The powder diffraction pattern of amorphous carbon shows two-dimensional (hk) and three-dimensional (001) peaks. Equation 2.4 gives the mean layer length (L_a) in terms of the breadth ($B_{(hk)}$) for a two-dimensional lattice reflection (Dasgupta and Sathiyamoorthy, 2003 cited Warren, 1941).

$$L_a = 1.84\lambda / [B_{(hk)} \cos \theta] \quad (2.4)$$

Where 2θ is the Bragg angle and λ is the wavelength of the x-ray. This was further modified to give Equation 2.5 (Dasgupta and Sathiyamoorthy, 2003 cited Warren and Bodestein, 1966).

$$L_a = 1.77\lambda / [B_{(hk)} \cos \theta] \quad (2.5)$$

L_c gives the height of the crystallite as given by Equation 2.6:

$$L_c = 0.94\lambda / [B_{(001)} \cos \theta] \quad (2.6)$$

The layer spacing for pure graphite structure is 3.354 Å (26.56°) and for turbostratic is 3.44 Å (25.88°). Franklin (1951) suggested a relation for the mean interlayer spacing as given by Equation 2.7 which relates the fraction of layers that are disordered (p) and mean layer spacing (d) for partially graphitised carbons (Dasgupta and Sathiyamoorthy, 2003).

$$d = 3.44 - 0.086(1-p^2) \quad (2.7)$$

2.7.4 Electron Microscopy

A good technique for measuring the direct images of the carbon structure is the high resolution electron microscopy. Better information about the movement of the building blocks are obtained from images of disordered carbon treated at different temperature. Electron micrographs interpretation is very important. The folded film gives (001) reflections in the region where the aromatic layers are almost parallel to the incident beam, which can reflect 10 to 11 beams when the layers are perpendicular to the incident beam. In graphitised carbon micrographs only the (002) fringes are resolved which are visible only when they are approximately parallel to the electron beam (Dasgupta and Sathiyamoorthy, 2003). Other techniques which could be used include nuclear magnetic resonance (NMR), extended X-ray absorption fine structure (EXAFS) and X-ray near edge structure (XANES) (Dasgupta and Sathiyamoorthy, 2003).

2.8 Summary

The chemical energy stored in biomass materials can be effectively utilised to generate electricity and heat for the growing world population through electrochemical reaction in a direct carbon fuel cell. Typical proximate analyses and higher heating value of many biomass species illustrate a wide range of parameters and heating values. The chemical analysis of the components in biomass shows that metal oxides are also present. The energy content of biomass is a crucial factor to be considered when converting biomass for energy, synfuels and fuel cell application. Different chemical structures and carbon content of biomass brings about different heat of combustion, the higher the state of carbon in a given biomass the higher the energy content. Disordered carbon structures are known to be good for direct carbon fuel cell operation which is achieved by pyrolysis and other methods. Six biomasses (miscanthus, switchgrass, wheat, spruce, poplar and willow) are investigated in this research with a view to producing disordered carbon fuel for their electrochemical application in the direct carbon fuel cell.

Chapter Three

Theory of Biomass and Fuel Cell

3.1 Introduction

The major conventional energy resources are at the verge of extinction, these include petroleum, coal and natural gas. More promising environmentally friendly options are the biomasses. Turning these biomasses into energy form can be achieved by a range of thermochemical processes that include combustion, gasification, liquefaction, hydrogenation and pyrolysis. Pyrolysis has received a lot of attention in the current energy scenario because it can convert biomass directly into solid, liquid and gaseous products by the thermal decomposition of the biomass in the absence of oxygen (Goyal *et al.*, 2008). This chapter discusses the various thermochemical processes involved in the conversion of biomass into energy with greater emphasis placed on pyrolysis. It also reports on the mechanism, kinetic, thermodynamics, products and yields of biomass pyrolysis. Size reduction in biomass, machines involved and the millings of carbon materials are some of the mechanical processes discussed. It also talks about the technology behind fuel cells, its classification, history, current applications and fuel processing. It takes a look at the energy and the electromotive force (EMF), fuel cell irreversibilities and concentration losses. Brief discussion on the history and advantages of the DCFC are presented. The electrochemical oxidations of carbon are covered including the mechanism, molten carbonate electrolyte, molten hydroxide electrolyte and the YSZ-based solid electrolyte in DCFC. Mass and heat integration systems for DCFC are also discussed.

3.2 Conversion Route for Energy Crop

Energy crops can be converted into electricity, heat and into transportation fuels. Heuvel (1994) suggested a conversion route for energy crops to electricity and heat as presented in Figure 3.1. For energy crops with high cellulose content, like miscanthus, switch grass, sugar cane and wheat straws, thermochemical conversion routes are most suitable.

3.3 Biomass Pyrolysis

Biomass pyrolysis is the direct thermal decomposition of the organic components in biomass in the absence of oxygen to yield an array of useful products, such as liquid and solid derivatives and fuel gases. The knowledge of the effects of various independent parameters of biomass has led to the development of advanced biomass pyrolysis processes. Some of these parameters are feedstock type and composition, product yield, product selectivities and catalysts on reaction rates. The accumulation of considerable experimental data on these parameters has resulted in advanced pyrolysis methods for the direct thermal conversion of biomass to liquid fuels and other chemicals in higher yields (Klass, 1998).

3.3.1 Conventional and Fast Pyrolysis

Conventional (or slow) pyrolysis involves carbonisation, destructive distillation, dry distillation, and retorting which normally consist of slow, irreversible, thermal degradation of the organic components in biomass, most of which are lignocellulosic polymers, in the absence of oxygen. Slow pyrolysis is the traditional method used in the production of charcoal. A comprehensive study of biomass pyrolysis began in the 1970s, which has led to the methods of controlling the selectivities and yields of the gaseous, liquid and solid products, by controlling the pyrolysis temperature and heating rate. Today, researches in the area of pyrolysis are generating considerable interest and are yielding good and important results in the development of methodologies. Flash, rapid and ultra pyrolysis are short-residence-time pyrolysis, which occur at moderate temperature and can be used to provide high yield of gas, liquid and char products (Klass, 1998).

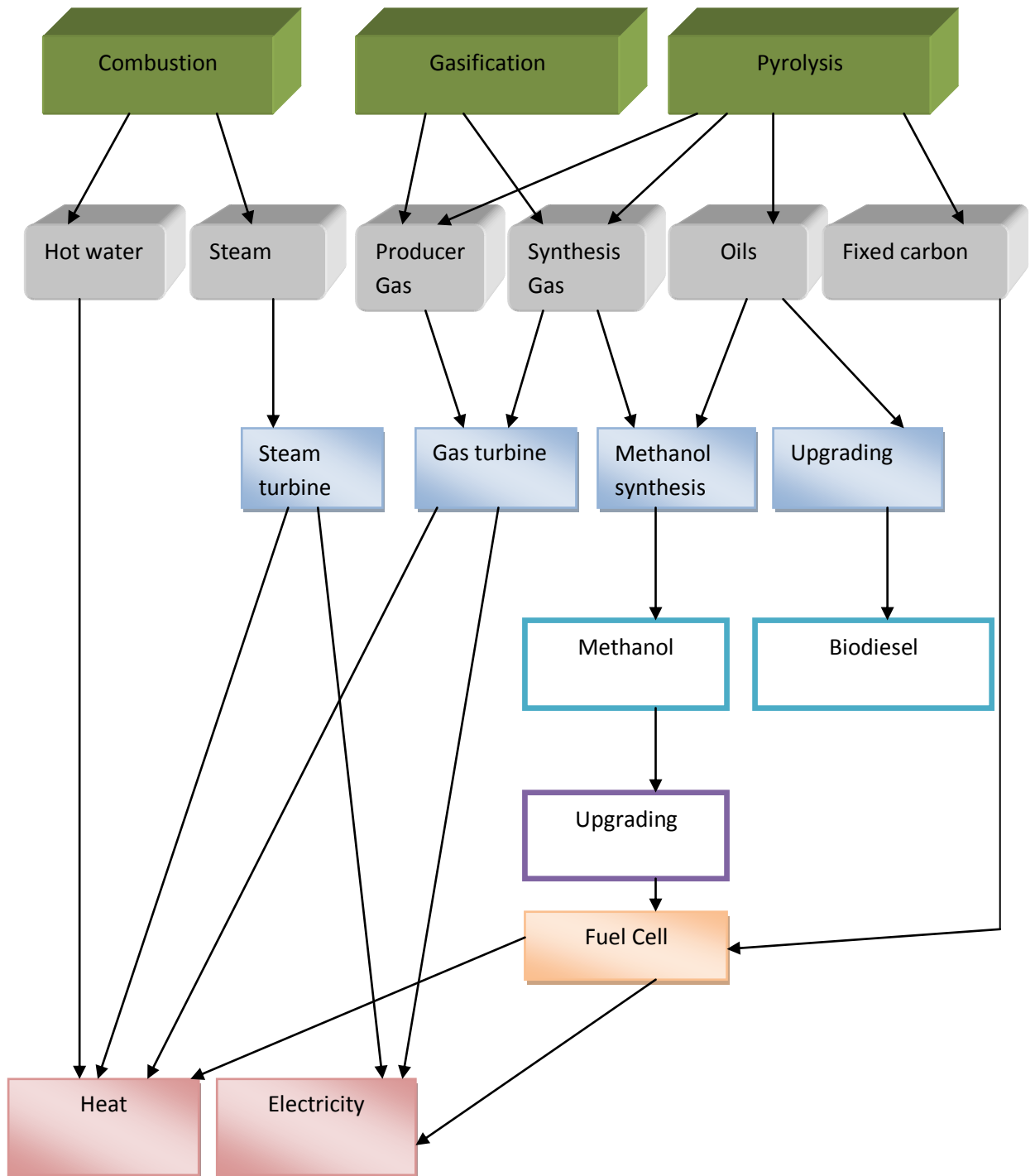


Figure 3.1: Thermochemical conversion route for energy crops (Heuvel, 1994)

3.3.2 Mechanisms of Biomass Pyrolysis

During pyrolysis many processes take place such as, cracking, dehydration, isomerisation, dehydrogenation, aromatisation, coking, condensation reactions and

rearrangements. The products are water, carbon oxides, other gases, charcoal, organic compounds (having lower average molecular weights than their immediate precursors), tars and polymers. Table 3.1 shows the mechanism of the slow, dry distillation of wood (Klass, 1998). The pyrolysis of cellulose yields 1, 6-anhydrohexoses, β -glucosan or levoglucosan in good yield (Figure 3.2). Levoglucosan is a primary product of the pyrolysis of pure cellulose. The yield of levoglucosan on pyrolysis of most biomass is low even though the cellulose content is about 50 wt.%. When pure cellulose is treated with only a small amount of alkali, levoglucosan formation is inhibited and a different product state composed of furan derivative is produced (Klass, 1998).

Table 3.1: Composition of gases evolved from slow dry distillation of wood
(Klass, 1998)

Process	Temperature ($^{\circ}$ C)	H ₂ (mol.%)	CO (mol.%)	CO ₂ (mol.%)	HCS ^a (mol.%)
Elimination of water	155-200	0	30.5	68.0	2.0
Evolution of carbon oxides	200-280	0.2	30.5	66.5	3.3
Hydrocarbon evolution starts	280-380	5.5	20.5	35.5	36.6
Evolution of hydrocarbons	380-500	7.5	12.3	31.5	48.7
Dissociation	500-700	48.7	24.5	12.2	20.4
Evolution of hydrogen	700-900	80.7	9.6	0.4	8.7

^aHydrocarbons

3.3.3 Kinetics of Biomass Pyrolysis

Most kinetic studies on cellulose pyrolysis have been built on the multistep model proposed in the early work with cellulose and described the evolution of volatiles by a single, pseudo-first-order reaction type, as represented by Figure 3.3 and Equation 3.1 (Klass, 1998).

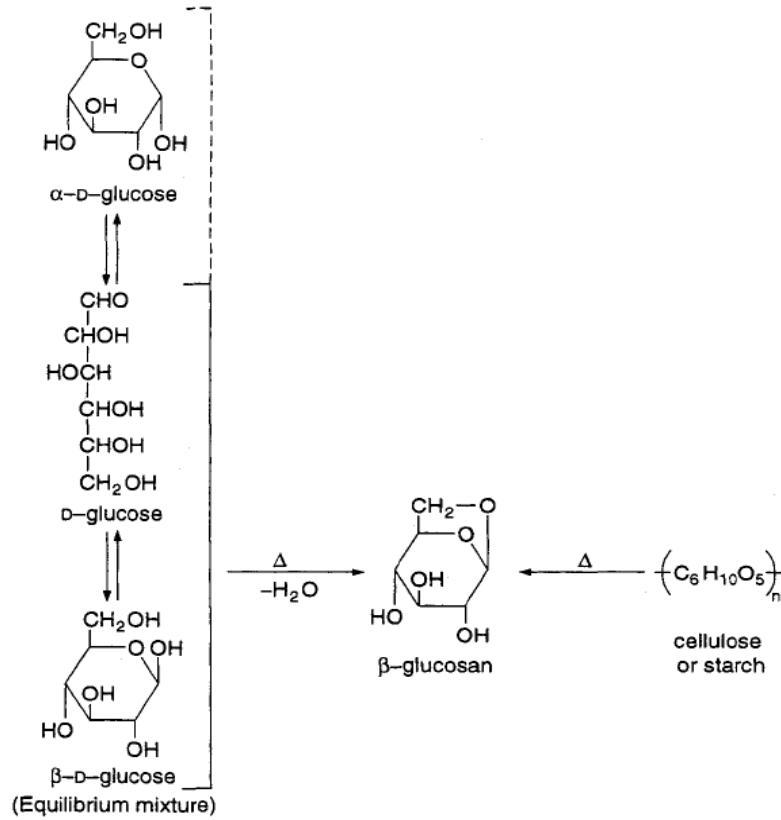


Figure 3.2: β -glucosan formation on pyrolysis (Klass, 1998).

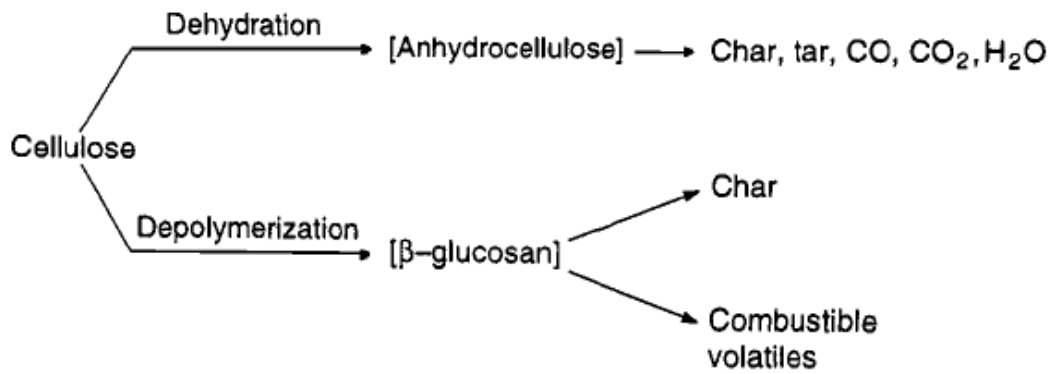


Figure 3.3: Cellulose pyrolysis pathways (Klass, 1998)

(3.1)

From Equation 3.1, A is the pre-exponential factor (time^{-1}), E is the apparent activation energy (J/mol), R is the ideal gas constant (J/mol-K), T is the absolute temperature (K),

and m is the fraction of volatiles produced at time t (Klass, 1998). Currently there are many experimental studies on plasma pyrolysis using agricultural waste, waste tyre, municipal solid waste and other (Babu, 2008 cited Babu, 2007; Huang and Tang, 2007; Huang *et al.*, 2003; Nema and Ganesh, 2002; Guddeti *et al.*, 2000). Thermal plasma pyrolysis is the process of reacting carbonaceous solid with limited amounts of oxygen at very high temperature to produce gas and solid products. In the highly reactive plasma zone, there is a large fraction of electrons, ions and excited molecules together with the high energy radiation. When carbonaceous particles are injected into plasma, they are heated very rapidly by the plasma and the volatile matter is released and cracked giving rise to hydrogen and light hydrocarbons such as methane and acetylene (Babu, 2008 cited Babu, 2007).

3.3.4 Thermodynamics of Biomass Pyrolysis

Depending on the temperature of the reactants, the pyrolysis of biomass feedstocks may be endothermic or exothermic. For most biomass containing highly oxygenated hemicellulosics and celluloses as the main components, pyrolysis is endothermic at temperatures below 400 to 450°C and exothermic at temperatures higher than that. In a properly designed system, little or no external heat is needed to sustain the process once the necessary temperature has been reached. The principal exothermic reaction occurring during biomass pyrolysis are the reduction of carbon oxides to methane and methanol, water gas shift reaction, and carbonisation of celluloses as shown in Table 3.2 (Klass, 1998).

A reasonable amount of hydrogen is required for the reduction of carbon oxides to methane and methanol, but hydrogen is not required for the water gas shift reaction, which produces hydrogen and the char formation reaction (Table 3.2). The pyrolysis temperature should be high enough to generate the requisite hydrogen for reduction of the carbon oxides. The water formed on pyrolysis and the vaporisation of the

physically contained moisture in the fresh feed can participate in the water gas shift reaction.

Table 3.2: Exothermic reactions on cellulose pyrolysis (Klass, 1998)

Process	Reaction	Enthalpy (kJ/g-mol)	
		Carbon converted at ^a	
		300 K	1000 K
Methanation	$\text{CO} + 3\text{H}_2 \rightarrow \text{CH}_4 + \text{H}_2\text{O}$	-205	-226
	$\text{CO}_2 + 4\text{H}_2 \rightarrow \text{CH}_4 + 2\text{H}_2\text{O}$	-167	-192
Methanol formation	$\text{CO} + 2\text{H}_2 \rightarrow \text{CH}_3\text{OH}$	-92	-105
	$\text{CO}_2 + 3\text{H}_2 \rightarrow \text{CH}_3\text{OH} + \text{H}_2\text{O}$	-50	-71
Char formation	$0.17\text{C}_6\text{H}_{10}\text{O}_5 \rightarrow \text{C} + 0.85\text{H}_2\text{O}$	-81	-80
Water gas shift	$\text{CO} + \text{H}_2\text{O} \rightarrow \text{CO}_2 + \text{H}_2$	-42	-33

^aThe standard enthalpy of formation of cellulose was calculated from its heat of combustion

The exothermicity of cellulose carbonisation is high per monomeric unit ($\text{C}_6\text{H}_{10}\text{O}_5$). Char formation is the dominant driving force for biomass pyrolysis at lower temperature at which autogenous pyrolysis begins but generates low hydrogen. At these temperatures, pyrolysis is normally reaction-rate controlled, and at higher temperatures, the process is mass-transfer controlled (Klass, 1998).

3.3.5 Products and Yields of Biomass Pyrolysis

Based on the pyrolysis temperature, the char fraction contains inorganic materials ashed to varying degrees, any unconverted organic solids, and carbonaceous residues produced on thermal decomposition of the organic components. The liquid fraction is usually a complex mixture of water and organic chemicals having lower average molecular weights than the feedstock components. In highly cellulosic biomass feedstocks, the liquid fraction normally contains acids, alcohols, aldehydes, ketones, esters, heterocyclic derivatives and phenolic compounds. The tars contain native

resins, intermediate carbohydrates, phenols, aromatics, aldehydes, their condensation products and other derivatives. The pyrolysis gas contains carbon dioxide, carbon monoxide, methane, hydrogen, ethane, ethylene, minor amounts of higher gaseous organics and water vapour. The pyrolysis gas is usually a low-to medium energy gas having a heating value of about 3.9 to 15.7 MJ/m³ (n) (Klass, 1998).

3.3.5.1 Conventional Slow Biomass Pyrolysis

The pyrolysis of biomass gives rise to chars, gases, light and heavy liquids and water in varying amounts. The yields depend on the feed composition, dimensions of the feed particles, heating rate, reaction time and temperature. Heating hardwoods in the absence of air produces charcoal and a volatile fraction that partly condenses on cooling to a liquor known as pyroligneous acid, separating into a dark heavy oil as the lower layer in about 10 wt.% yields, and an upper aqueous layer. Pine, which is a softwood, can be dry distillate to give similar product in equivalent amounts as well as a lighter pine oils and terpene liquid such as turpentine. The contents of the supernatant layer are methanol, acetic acid, allyl alcohol, traces of acetone and other water-soluble compounds. The wood tars and pitches are complex mixtures, while the heavy oil contains tars, higher viscosity pitches and some char. Methanol is formed from the lignin components bearing methoxyl groups (Ioannidou *et al.*, 2011; Neves *et al.*, 2011; Kwapinski *et al.*, 2010; He *et al.*, 2009; Garcia-Perez *et al.*, 2007; McKendry 2002; Klass, 1998; Raveendran *et al.*, 1996, 1995). During conventional pyrolysis, extensive depolymerisation of the cellulose begins at about 300°C and usable charcoal formation, with carbon content of about 75 wt.%, begins at about 350°C. The higher the temperature with long residence times, there is a promotion of gas production but higher char yields are obtained at lower temperature and slow heating rate. Tables 3.3 and 3.4 give result of the long-term pyrolysis of some biomass. In Table 3.4 the balance of the yield for the feedstock is water (Klass, 1998 cited Zaror and Pyle, 1982; Epstein *et al.*, 1978).

Table 3.3: Product yields from thermal decomposition of biomass over 8 hours and 400°C (Klass, 1998)

Products	Birch (wt.%)	Pine (wt.%)	Spruce (wt.%)
Gases			
H ₂	0.03	0.03	0.03
CO	4.12	4.10	4.07
CO ₂	11.19	11.17	10.95
CH ₄	1.51	1.49	1.59
C ₂ H ₄	0.21	0.14	0.15
Subtotal	17.06	16.93	16.79
Charcoal			
	33.66	36.40	37.43
Pyroligneous oil			
Water	21.42	22.61	23.44
Settled tar	3.75	10.81	10.19
Soluble tar	10.42	5.90	5.13
Volatile acids	7.66	3.70	3.95
Alcohols	1.83	0.89	0.88
Aldehydes	0.50	0.19	0.22
Esters	1.63	1.22	1.30
Ketones	1.13	0.26	0.29
Subtotal	48.34	45.58	45.40
Losses			
	0.94	1.09	0.38

3.3.5.2 Fast Biomass Pyrolysis

Fast pyrolysis of biomass is usually continuously operated at temperatures within the range of 400 to 650°C and residence times of a few seconds to a fraction of a second. The control of these parameters permits the bulk product yields to be changed from those of conventional pyrolysis systems within a wide range, but the products are still chars, liquids, gases and water. Notable characteristics about fast pyrolysis are that it has high heating rates and rapid quenching of the liquid products to terminate additional conversion of the products downstream of the pyrolysis reactor. The fragmentation of the polymeric components of biomass is brought about by high heating rate, to give 60 to 70 wt.% primary vapour products composed of oxygenated monomers and polymer fragments.

Table 3.4: Product yields from various biomasses at different pyrolysis temperature (Klass, 1998 cited Epstein *et al.*, 1978)

Feedstock	Charcoal (wt.% at °C)			Pyrolytic oil (wt.% at °C)			Low-energy gas (wt.% at °C)		
	500°C	700°C	900°C	500°C	700°C	900°C	500°C	700°C	900°C
Biosolids	12	11		10	2		10	26	
Corncoobs	26	14	17	22	7	3	17	65	52
Manure	28	14	11	18	7	2	20	30	42
MSW- Municipal solid wastes		24	13	11	6	3	23	36	50
Paper	10	6	4	47	8	3	16	45	70
Wood chip	27	20	22	19	6	2	23	35	53

The moisture content of the feedstock is not given. The balance in the yield for the feedstock is water.

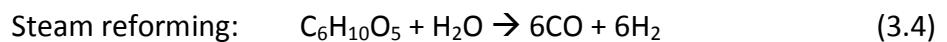
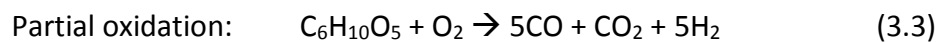
Rapid efficient quenching of the product streams and short residence time tend to “freeze” the product compositions so that they correspond more closely with the chemicals formed initially on the biomass pyrolysis (Klass, 1998). Pyrolysis of biomass is used in the production of solid (charcoal), liquid (tar and other organics) and gas products. Research in the area of pyrolysis is becoming more and more important, because it is not only an independent process, it is also a first step in the gasification and combustion processes and has many advantages as shown by the several researches carried out on biomass pyrolysis (Razuan *et al.*, 2010; Goyal *et al.*, 2008; Onay and Kockar, 2004; Yaman, 2004; Şensöz, 2003; Onay *et al.*, 2001; Zanzi *et al.*, 2001; Putun *et al.*, 2001; Şensöz *et al.*, 2000; Minkova *et al.*, 2000; Di Blasi *et al.*, 1999; Xia *et al.*, 1999; Encinar *et al.*, 1998; Lanzetta and Di Blasi, 1998; Drummond and Drummond, 1996).

3.4 Gasification

There are three types of biomass gasification processes namely pyrolysis, partial oxidation and reforming. In sufficiently high temperature the primary products from the pyrolysis of biomass is gases, charcoal and liquids are either minor products or not present in the product mixture. Partial oxidation processes (direct oxidation, starved-air or starved-oxygen combustion) utilises less than the stoichiometric amounts of oxygen needed for complete combustion, so that partially oxidised products are formed. Reforming was originally used to describe the thermal conversion of petroleum fractions to more volatile products of higher octane number, and represented the total effect of other simultaneous reactions, like cracking, isomerisation and dehydrogenation. Reforming could also refer to the conversion of hydrocarbon gases and vaporised organic compounds to hydrogen-containing gases such as synthesis gas, mixture of carbon monoxide and hydrogen. Synthesis gas can be produced from natural gas by reforming it in the presence of steam (steam reforming). In the case of biomass, reforming is the gasification of the biomass in the presence of another reactant. Examples of biomass gasification are steam reforming (steam gasification, steam pyrolysis), and steam-oxygen and steam-air reforming. Steam

reforming processes involves reactions of biomass and steam and of the secondary products formed from biomass and steam. Steam-oxygen or steam-air gasification of biomass often includes combustion of residual char from the gasifier, of a portion of the product gas, or of a portion of the biomass feedstock to supply heat (Klass, 1998).

The primary products of biomass gasification under idealised conditions are virtually the same, with carbon oxides and hydrogen being formed. Methane and light hydrocarbons could also be formed. Equations 3.2, 3.3 and 3.4 give the stoichiometries of cellulose gasification (Klass, 1998).



Biomass gasification yield varying energy content of the product gas. When there is a direct contact of biomass feedstocks and air low-energy gases are usually formed (3.92 to 11.78 MJ/m³ (n) or 100 to 300 Btu/SCF). This is because of the dilution of the product gases with nitrogen from air during the process of gasification. Medium-energy gases (11.78 to 27.48 MJ/m³ (n) or 300 to 700 Btu/SCF) usually is obtained from direct heating of biomass gasifier with oxygen and also from indirect heating of biomass gasifier in air with heat transfer occurring through an inert solid medium. Indirect heating of the gasifier eliminates dilution of the product gas with nitrogen in air and keeps it separated from the gasification products. High-energy product gases (27.48 to 39.26 MJ/m³ (n) or 700 to 1000 Btu/SCF) is usually obtained when the gasification conditions promote the formation of methane and other light hydrocarbons, or processing subsequent to gasification is carried out to increase the concentration of these fuel components in the product gas (Klass, 1998).

3.5 Mechanical Treatment of Biomass

3.5.1 Size Reduction of Biomass

Before biomass can be used as a fuel in a fuel cell or even as a feedstock there is a need for a physical size reduction. Biomass storage volumes are greatly enhanced with smaller particles, which also facilitate the transportation of the material as slurry, the solid state handling of materials, and enable the easy separation of the bark and whitewood. During drying the exposed surface area is important as well as the particle size because they determines the drying time, conditions and techniques needed in moisture removal (Klass, 1998). The conversion technique applied to biomass is related to the physical dimensions, because there is a need for the particle size to satisfy the required specifications of the conversion process and reactor. The optimum size characteristics of biomass fuel are determined by the combustion chamber and heat exchanger design, technique of delivering the solid fuel, operating conditions and ash removal. In thermal liquefaction and gasification processes the rate of conversion are influenced by the particle size, size distribution, operating conditions and the product yields and distributions. In biological processes they are influenced by the size of the feedstock. Reaction rates are higher in smaller particles because more surface areas are exposed to chemical and biological reactions. For many biomasses the size of the feed are reduced by cutting, grinding and impact mechanism (Klass, 1998).

3.5.2 Machines for Biomass Size Reduction

Commercially available for the reduction of biomass sizes are the dry shredders and the common types are the horizontal and vertical shaft hammer mills. They are metallic hammers on rotating shafts which reduce the biomass by impacting the feed materials until they are small enough to pass through the grate opening. For Municipal Solid waste (MSW), hammer mills are usually employed before separating the refuses-derived fuel (RDF) and other components. As tree chippers and agricultural choppers hammer mills are also employed. Wet shredders such as hydropulpers are employed on wet biomass to produce wood pulp. They consist of high-speed cutting blades which pulverises a water suspension of the feed over perforated plate allowing

the pulped materials to pass through the plate and the nonpulp materials are expelled. Hydropulpers are also applied in the simultaneous size reduction and separation of combustible component of MSW from inorganic materials and also RDF for microbial conversion (Klass, 1998).

In the field, agricultural chopper in addition to the harvester are employed to chop crop during harvesting to prepare into hay as commonly applied on wheat and other food crops. Forage choppers normally produce materials of 25 mm or less in length. Chipping is a popular mechanical size reduction method used to prepare wood fuels for direct combustion which could be disc chipping or hogging. Hammer hogs consists of free-swing hammers which breaks the feed into smaller pieces, while the knife hogs cut the feed with blades into smaller pieces (Klass, 1998).

3.5.3 Mechanical Milling of Carbon Materials

The high electrochemical capacities of disordered carbons have given them prominent place in fuel cell and batteries technologies, they are used as anode in direct carbon fuel cell and lithium-ion rechargeable battery. Pyrolysis of biomass yield different types of the carbon. The use of mechanical shock or shear milling produces carbon powders with well defined interlayer spacing, surface area, morphology, and crystallite size without the production of heteroatoms such as O, H, S, N, etc. Salver-Disma *et al.* (1999) reported that mechanical grinding gave an increasing amount of disordered carbon at rate depending on the grinding mode of shear-and shock-grinding (Salver-Disma *et al.*, 1999). Many researchers have shown the effect that mechanical ball milling have in generating disordered (amorphous) carbon structures from given precursor (Salver-Disma *et al.*, 1999; Fukunaga *et al.*, 1998; Zhou *et al.*, 1995).

3.6 Classification of Fuel Cells

The classification of fuel cells (FCs) is based on the electrolyte used. But it is noteworthy to say their functions are basically the same as shown in Table 3.5. For the operations at the anode, a fuel (hydrogen, carbon, etc.) is oxidized into electrons and

proton, and at the cathode, oxygen is reduced to oxide species. Depending on the electrolyte, either protons or oxide ions are transported through the ion conducting but electrically insulating electrolyte to combine with oxide or protons to generate water and electric power (Hoogers, 2003).

3.7 Historical Background of Fuel Cells

The historical background of various researches into fuel cells began in the early nineteenth century with the use of hydrogen and oxygen as reactants. This further developed after 1950 when the technology was applied in space mission (Hoogers, 2003 cited Cohen, 1966, 1956; Grove, 1839). Grove and Schoenbein studied the first FCs in which they called it “gaseous voltaic batteries.” They demonstrated the electrochemical reaction of hydrogen and oxygen where chemical reactions took place on platinum (Hoogers, 2003; Grove, 1845, 1843, 1842, 1839). The design of Grove was improved by increasing the surface area of the platinum electrode and Lord Rayleigh used platinum sponge (Hoogers, 2003 cited Rayleigh, 1882). Because of the problem of the catalyst flooding, Mond and Langer (1889) used a diaphragm to contain the sulphuric acid electrolyte. This was a self-contained battery of cell but was modified by Alder Wright and Thompson (1889) and they called it double-aeration plate cells (Hoogers, 2003). Fuel cell classification and application are shown in Table 3.5.

The success of using hydrogen as fuel in FC prompted research work using carbon and coal as fuel, in which they were used to produce electricity directly in a more efficient and cleaner process (Liu *et al.*, 2010; Li *et al.*, 2009; Li *et al.*, 2008; Antal and Nihous, 2008; McPhee and Tao, 2008; Hackett *et al.*, 2005; Balachov *et al.*, 2005; Berkovich, 2003; Hemmes, 2003; Weston, 1963). Jacques (1896) was one of the earlier pioneers in direct coal FC which he called “carbon electric generator”. Haber and Bruner (1904) explained that the reaction was between the coal and the electrolyte rather than between the coal and the oxidant making it an indirect FC.

Table 3.5: Fuel cells classification, characteristic and applicability (Li *et al.*, 2011; Jia *et al.*, 2010; Wolk *et al.*, 2007; Hoogers, 2003).

Fuel Cell Type	Electrolyte	Charge Carrier	Operating Temp.	Fuel	Electrical Efficiency (system)	Power Range / Application
Alkaline FC (AFC)	KOH	OH ⁻	60-120°C	Pure H ₂	35-55%	<5 kW, niche market (military, space)
Proton Exchange Membrane FC (PEMFC)	Solid Polymer (e.g. Nafion)	H ⁺	50-100°C	Pure H ₂ (tolerate CO ₂)	35-45%	Automotive CHP (5-250 kW), portable
Phosphoric Acid FC (PAFC)	Phosphoric Acid	H ⁺	~ 220°C	Pure H ₂ (tolerate CO ₂ , approx. 1% CO)	40%	CHP (200 kW)
Molten Carbonate FC (MCFC)	Lithium & Potassium Carbonate	CO ₃ ²⁻	~ 650°C	H ₂ , CO, CH ₄ , hydrocarbons (tolerate CO ₂)	>50%	200 kW-MW range, CHP and stand alone
Direct Carbon FC (DCFC)	MH/MC/SO	OH ⁻ / CO ₃ ²⁻ / O ²⁻	~700°C	Solid carbon	>70%	2 kW-MW range, CHP and stand alone
Solid Oxide FC (SOFC)	Solid Oxide Electrolyte	O ²⁻	~1000°C	H ₂ , CO, CH ₄ , hydrocarbons (tolerate CO ₂)	>50%	2 kW-MW range, CHP and stand alone

MH-molten hydroxide, MC-molten carbonate, SO- Solid oxide, FC-fuel cell

The problem of the FC which was the degrading of the alkaline electrolyte as a result of CO₂ in the product of the oxidation reaction was tackled by Baur and Ehrenberg (1912) by the use of hydroxide, carbonate, silicate and borate as electrolyte. Further modifications were made by Baur and Brunner (1937) in reducing the concentration polarization. As a continuation of the work, Baur and Preis (1937) developed a fuel cell with a solid electrolyte using “Nerst-Mass” containing a mixture of Zirconia and yttria compounds (Andujar and Segura, 2009; Hooger, 2003).

The alkaline fuel cells were developed by Bacon (1969, 1979) which was further modified by Pratt and Whitney Aircraft for use in the Apollo space mission to produce on-board electricity (Hooger, 2003). Davtyan influenced the modern development of the molten carbonate FC electrolyte which was further improved by Broers and

Ketelaar (1960a, b) where they chose carbonate over other compounds because of their compatibility with the products of the reaction of hydrocarbon fuel. The research was continued by the Institute of Gas Technology and the General Electric Company (Hooger, 2003 cited Bacon, 1954, 1969).

The hope of oxidizing fuel directly was rekindled in the development of the direct methanol fuel cell in which sulphuric acid was used as electrolyte. Sulphuric acid was selected over phosphoric acid because, at low operating temperatures (60-70°C), sulphuric acid had higher conductivity, and the oxygen electrodes used in the test performed better in the acid. Further development enabled solid polymer membranes to be used as electrolyte and revived the prospect of developing a practical direct methanol fuel cell (Hoogers, 2003 cited William *et al.*, 1965; Tarmy and Ciprios, 1965; Murray and Grimes, 1963). The first solid polymer fuel cell developed by General Electric had problems with the membrane and an improvement was made by the use of nafion catalyst and electrolyte, as well as increases in the catalyst surface area of the electrode (Hoogers, 2003 cited Grubb and Niedrach, 1960). The solid polymer FC was deemed the most appropriate type for use in road vehicle because of its compatibility with the reaction products of hydrocarbon fuels (Hoogers, 2003).

The applicability of modern fuel cells is in transportation, stationary power and portable application (Table 3.5). In the transport sector, fuel cells (FCs) are seriously competing with the internal combustion engines (ICEs). FCs are highly efficient because they are electrochemical rather than thermal engine and they can help to reduce the consumption of primary energy and the emission of CO₂. Stationary power generation is viewed as the leading market for FC technology other than buses. The reduction of CO₂ emission is an important argument for the use of FCs in small stationary power systems especially in combined heat and power (CHP) generation. In fact, FCs are currently the only practical engines for micro-CHP systems in the domestic environment (5 – 10 kW). The portable market is less well defined, but a potential for quiet fuel cell power generation is seen in 1 kW portable range and possibly as

ancillary supply in cars, the so called auxiliary power units (APUs). Portable FC often includes grid-dependent applications such as camping, yachting and traffic monitoring (Hoogers, 2003). The development in the technology of fuel cells has made it more feasible in its application in airplanes, motorbikes, cars and other areas. Figure 3.4 to Figure 3.6 shows some current innovations in fuel cell technology and their applications (Strahan, 2009; Moore, 2009).



Figure 3.4: Fuel cell technology in automobile (Strahan, 2009)



Figure 3.5: Motorbike powered by fuel cell technology (Moore, 2009)



Figure 3.6: Light aircraft powered by fuel cell technology (Moore, 2009)

3.8 Molten Carbonate Fuel Cell (MCFC)

The molten carbonate fuel cells electrolyte is a mixture of alkali carbonates, mostly Li_2CO_3 and K_2CO_3 , sometimes with additions of alkaline earth carbonates, above their melting point at operating temperatures of around 650°C . The charge carrier ion in MCFC is a carbonate ion, CO_3^{2-} , moving from cathode to anode. An interesting feature of MCFC is that the depletion of carbonate ion from the cathode makes it necessary to recycle CO_2 from anode to cathode, or less commonly, to supply CO_2 from some alternative source. A typical cathode gas is composed of 12.6% O_2 , 18.4% CO_2 and 69% N_2 . The anode and cathode reactions in MCFC are given by Equations 3.5 and 3.6 (Hoogers, 2003; EG&G, 2000):



The formation of water from hydrogen and oxygen with the CO_2 undergoing no net reaction gives the overall cell reaction. The standard reversible potential is therefore the same as for other fuel cells, although different partial pressure of CO_2 at the anode

and cathode will lead to an offset due to a concentration cell effect. It is also noteworthy that the product water is generated at the anode (Hoogers, 2003). The overall reaction of the MCFC is given by Equation 3.7 (Adeniyi, 2008; Larminie and Dicks, 2003).



The Nernst reversible potential for the MCFC, taking into account the transfer of CO_2 , is given by Equation 3.8 (Larminie and Dicks, 2003).

(3.8)

Where E , E° are the voltages of the fuel cell (EMF), F is the Faraday constant, p the vapour pressures, RT signify that the drop in Nernst voltage due to fuel utilization will be greater in high temperature FC. Subscript a and c refer to the anode and cathode gas compartments respectively. When the partial pressure of CO_2 are identical at the cathode and anode, and the electrolyte is invariant, the cell potential depends only on the partial pressures of H_2 , O_2 , and H_2O (Larminie and Dicks, 2003). At high operating temperature (600-700°C), the alkaline carbonate in MCFC form a highly conductive molten salt, with carbonate, CO_3^{2-} , ions providing ionic conduction as shown in Figure 3.7 (Adeniyi, 2008; Larminie and Dicks, 2003).

The CO_2 generated at the anodes of MCFC system is recycled externally to the cathode where it is consumed. This can be achieved by feeding the anode exhaust gas to a combustor (burner), which converts any unused hydrogen or fuel gas into water and CO_2 . The exhaust gas from the combustor is then mixed with fresh air and fed to the cathode inlet as shown in Figure 3.8 (Adeniyi, 2008; Larminie and Dicks, 2003).

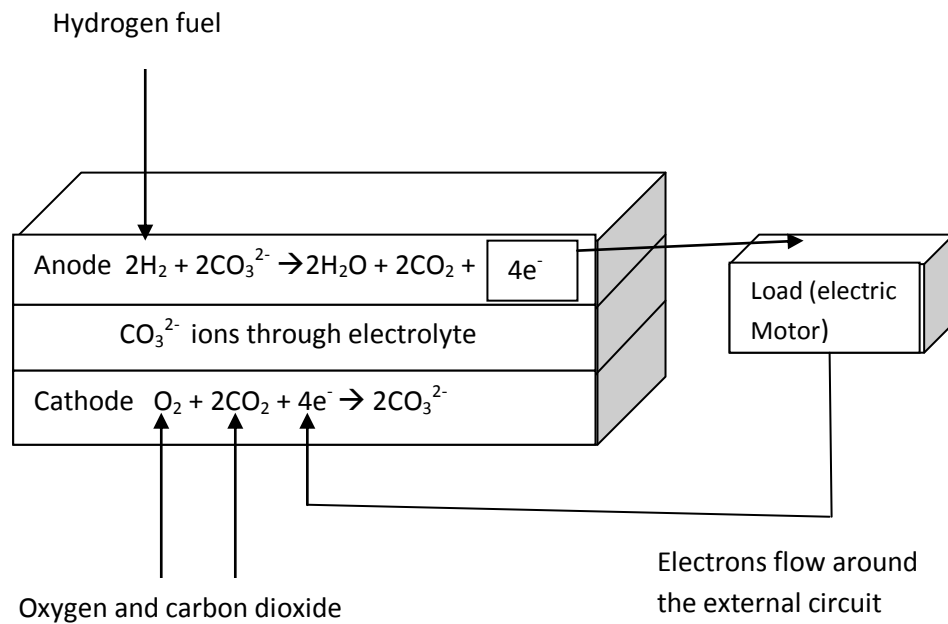


Figure 3.7: MCFC anode and cathode reaction for hydrogen fuel (Larminie and Dicks, 2003).

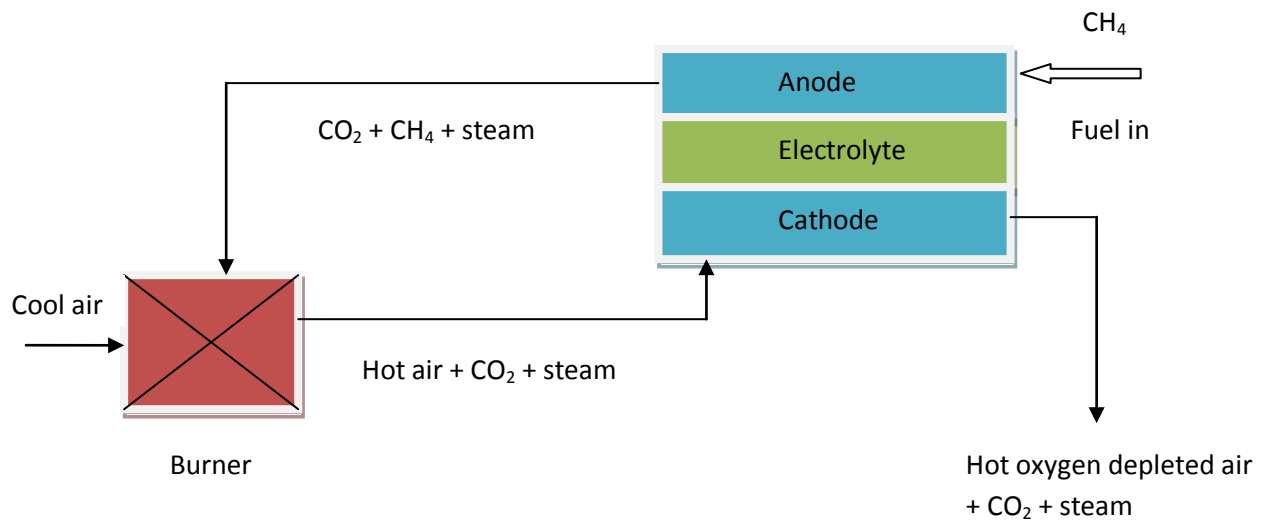


Figure 3.8: Addition of carbon dioxide to the cathode gas stream (Larminie and Dicks, 2003)

Nickel (anode) and nickel oxide (cathode) are adequate catalysts to promote the two electrochemical reactions at the operating temperature of MCFC. Unlike PAFC and PEMFC, noble metals are not required. Another important advantage of MCFC is the ability to electrochemically convert carbon monoxide directly and to internally reform

hydrocarbon fuels. If carbon monoxide was fed inside the MCFC as fuel, the reactions at each electrode shown in Figure 3.9 would occur (Larminie and Dicks, 2003).

The electromotive force (EMF) of the carbon monoxide fuel cell is calculated in exactly the same way as for the hydrogen fuel cell. Two electrons are released for each molecule of CO, just as two electrons are released for each molecule of H₂. Thus the formula for the “no loss”, reversible Open Circuit Voltage (OCV) is identical and given by Equation 3.9.

(3.9)

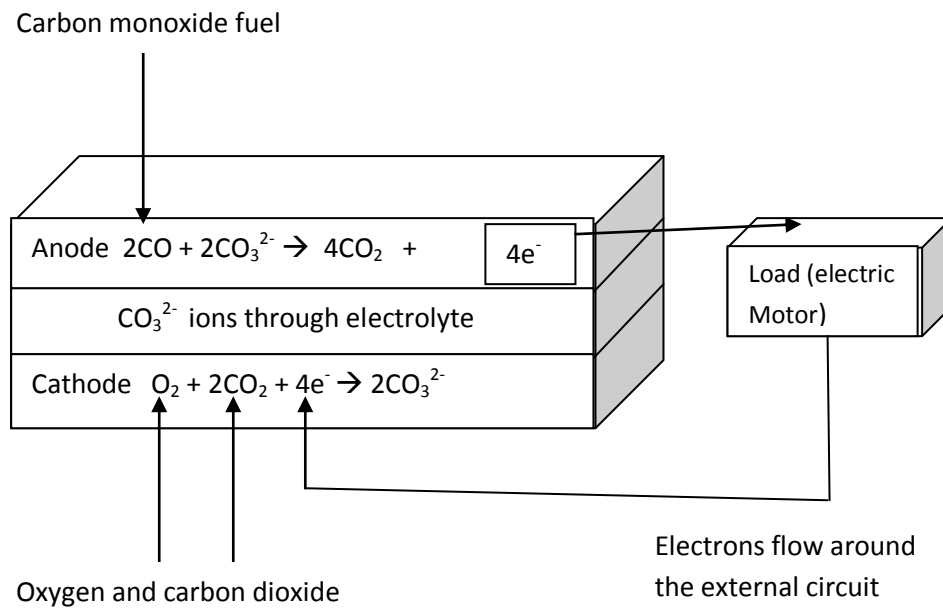


Figure 3.9: The anode and cathode reaction for MCFC using CO as fuel (Larminie and Dicks, 2003).

The values of E and Δ for both hydrogen and carbon monoxide at 650°C are similar as shown in Table 3.6 (Larminie and Dicks, 2003).

Table 3.6: Values of E and Δ for H₂ and CO at 650°C

Fuel	Δ (kJ mol ⁻¹)	E (V)
Hydrogen (H ₂)	-197	1.02
Carbon monoxide (CO)	-201	1.04

MCFCs achieve power densities in excess of 100 mWcm⁻², with performance mainly limited by ohmic losses. MCFC has the same stack building blocks as the PEMFC and the PAFC i.e. bipolar plates, electrodes and electrolyte layer, but of higher advantage including high operating temperature and the corrosivity of molten carbonate salts require radically different materials and design features. A much higher operating temperature is a clear advantage with MCFC, in which the reaction kinetics is drastically improved to such a degree that noble metal catalysts are no longer required. Most MCFC cathodes are made up of lithiated NiO and the anodes are made up of Ni alloys (e.g. NiCr and NiAl). The order of the thickness of the electrodes and electrolyte layer are usually 1 mm (Larminie and Dicks, 2003).

MCFCs can operate on CO as a fuel, in this case, CO is not directly electro-oxidized but is converted to hydrogen by rapid water-gas shift reaction inside the electrode. So the problem of anode poisoning by CO and to a certain extent, by other reformer gas impurities is not an issue of concern. MCFCs can even operate on natural gas and some other hydrocarbons when some pre-reforming is applied (Hoogers, 2003; EG&G, 2000). High temperature corrosion is a major problem in MCFC technology and requires the use of expensive materials and protective layers. Again sealing and water proofing can no longer rely on polymer materials.

The two gas compartments sealing from each other is achieved by using an ingenious combination of material porosities, more specifically well chosen pore size distributions. Capillary forces hold the electrolytes in a nano-porous matrix of LiAlO₂ and thus make the gas tight. The two electrodes are micro-porous and enable reactant

diffusion to the reactive interfaces, at the same time allowing some electrolyte penetration into the open pores. The size of the reactive interface, mostly the electrolyte-wetted parts of the porous electrodes, depends on a fine porosity/pressure balance and good electrolyte management (Hoogers, 2003 cited Kunz, 1987). The bipolar plates are made from high grade stainless steels and protected from corrosive attack by additional coatings of metals such as Ni for the anode or Cr for the cathode (Hoogers, 2003 cited Kunz, 1987). Most of these effects are now controlled reasonably well enough to achieve practical lifetimes for the MCFC. The process that still limits its lifetime is nickel dissolution from the NiO cathode. The leaching of Ni leads to a coarsening of the cathode pore structure, deposition of Ni at the anode and growth of Ni dendrites through the electrolyte layer, ultimately resulting in electric shortening and system failure. This is still one of the major challenges facing MCFC most especially for high pressure operation (Hoogers, 2003; EG&G, 2000).

Table 3.7 gives the effect of fuel gas impurities and it is noteworthy to say that due to the recycling anode gas to cathode (for CO₂ supply) practice, some contaminants may also harm the cathode electrode (Hoogers, 2003). Elevated temperature operation offers a lot of options for fuel processing. The nickel based anode catalyst, or more commonly, oxide supported Ni catalysts added to the anode compartment show sufficient (gas phase) catalytic activity to enable internal reforming (steam reforming) of fuels such as methane inside the anode compartment. The endothermic steam reforming reaction (as shown in Equation 3.10) is driven by the exothermic fuel cell reaction and is conveniently controlled by the rate at which hydrogen generated is electro-oxidized at the fuel cell anode.



In contrast with this direct internal reforming (DIR), other designs employ indirect internal reforming (IIR) within a gas phase reactor separated from but in thermal contact with the anode or the two. The possibility of internal reforming simplifies the overall system for MCFC (Hoogers, 2003).

Figures 3.10 and 3.11 show practical examples of a 250 kW system of MCFC called the hot module (MTU Friedrichshafen). Figure 3.10 show the stack construction and Figure 3.11 show an early demonstration unit under construction (Larminie and Dicks, 2003).

Table 3.7: Tolerable Impurity levels for MCFC and SOFC

(Hoogers, 2003; EG&G, 2000)

Fuel Impurity	Molten Carbonate Fuel Cell (MCFC)		Solid Oxide Fuel Cell (SOFC)	
	Effect	Level	Effect	Level
CO	Fuel	-	Fuel	-
CO ₂	Diluent, @Cathode	18.4% in air 67% in O ₂	Diluent	-
H ₂ S	Poison	<1 ppm	Poison	<1 ppm
NH ₃	Relatively Harmless	1%	Relatively Harmless	0.5%
HCl, other halides	Poison	0.1 ppm	Poison	0.1 ppm
Si	Probably Poison	?	Anode poison	?
Other	Poison	0.2 ppm H ₂ Se 0.1 ppm As	-	-

The properties of the MCFC 250 kW MTU presented in Figures 3.10 and 3.11 show that it has a power rating of 279 kW (250 kW net AC) with 292 cells and efficiency of 49% LHV, the temperature of available heat is at 450°C, and a stack degradation of 1%/1000 hour of operation (Larminie and Dicks, 2003).

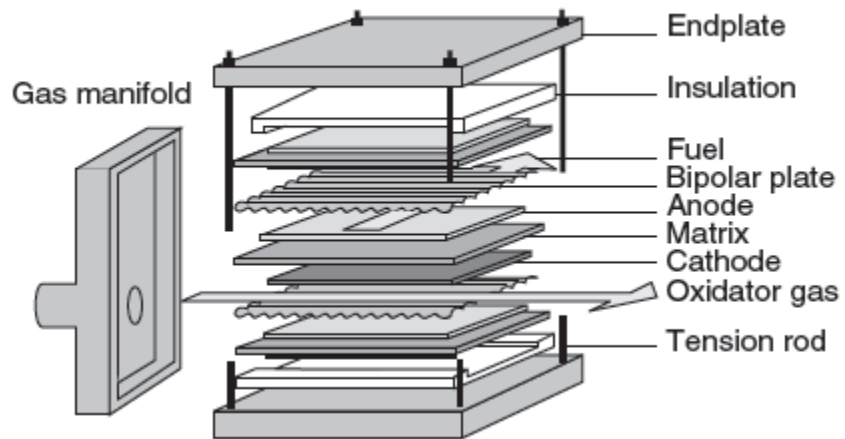


Figure 3.10: MCFC 250 kW MTU stack construction (Larminie and Dicks, 2003).



Figure 3.11: MCFC 250 kW MTU early demonstration under construction (Larminie and Dicks, 2003).

3.9 Solid Oxide Fuel Cell (SOFC)

The operation of solid oxide fuel cell is at a temperature at which certain oxidic electrolytes become oxygen ion, O^{2-} , conducting. It is the same effect that is experienced in the Lambda sensor supplied with three-way catalytic converters in spark ignition automobiles, and lambda sensor are used as convenient lab models for SOFCs. The oxides normally employed are mixture of yttria and zirconia. The electrode reactions are given by Equations 3.11 and 3.12 (Hooger, 2003).



The overall cell reaction is similar to those of MCFC with standard reversible potential and water is generated at the anode. The SOFC benefits from excellent kinetics at the anode and cathode. For thermodynamics reasons, the reversible potential at the operating temperature is lower in SOFC than for low temperature fuel cells. The inherent advantages of the SOFC are the solid-state design with no water management problems. The main problems encountered with SOFC are materials problems relating to sealing and thermal cycling. The searches for the right stack design for SOFC are still a focal point of current research work. The tolerance impurities levels for SOFCs are given in Table 3.7. The SOFC technology uses two major designs, which are the planar and tube bundles designs (Hooger, 2003).

Figure 3.12 show the end view of tubular type of the SOFC with the electrolyte and anode built onto the air cathode. Figure 3.12 show a small stack of 24 tubular SOFCs, each tube is 150 cm long and 2.2 cm in diameter. Figure 3.13 show a larger stack from bundles of 24 SOFC tubes consisting of 1152 cells and a power output of 200 kW (Larminie and Dicks, 2003).

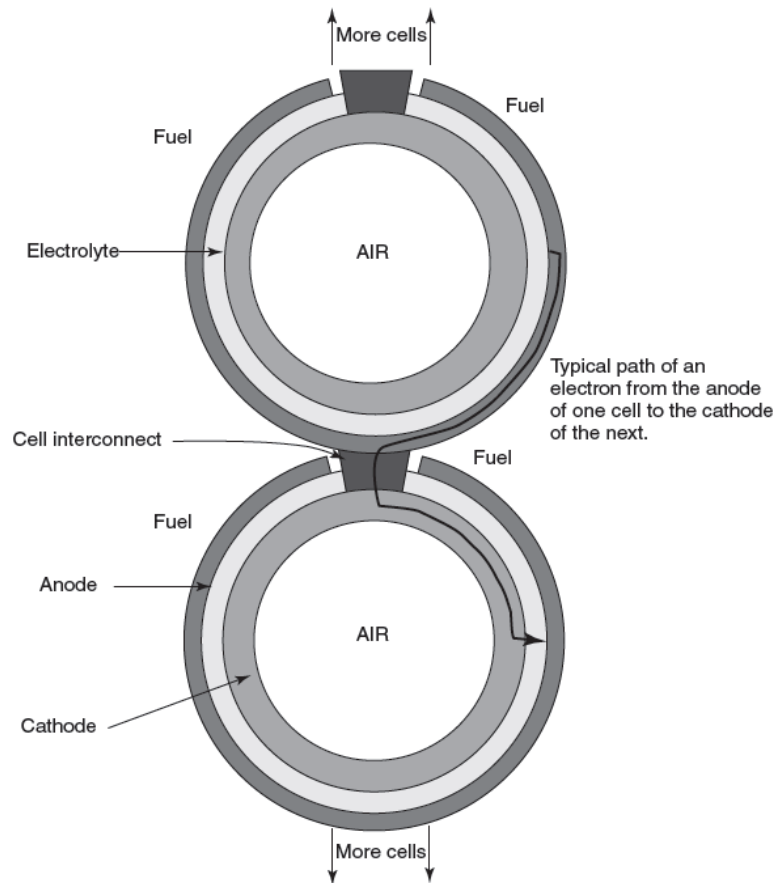


Figure 3.12: Tubular SOFC end view (Larminie and Dicks, 2003).

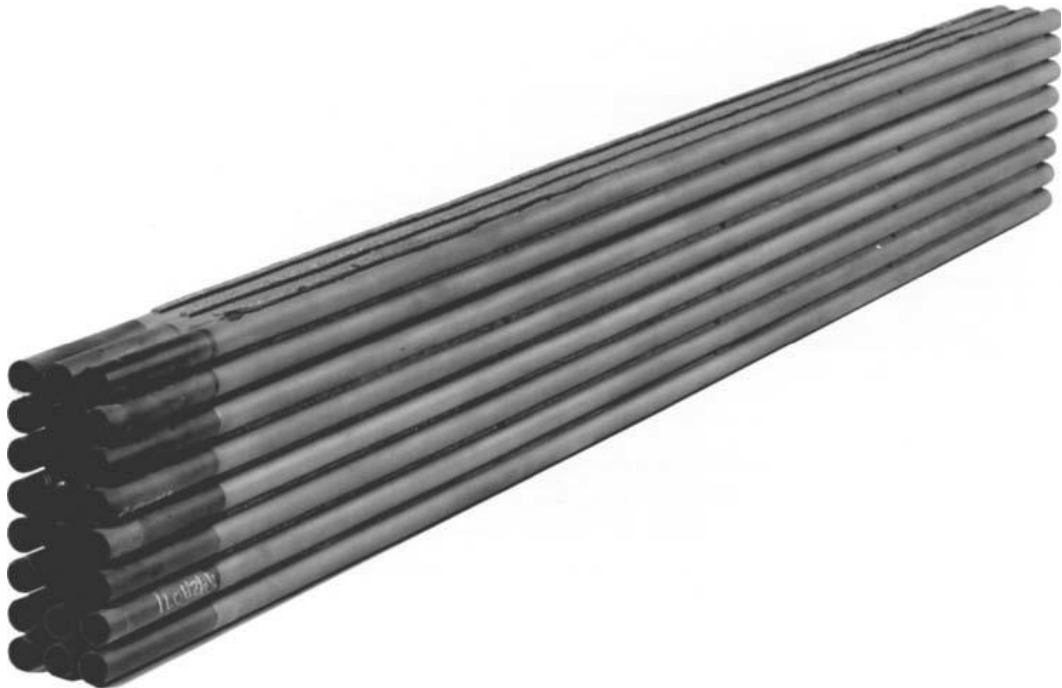


Figure 3.13: Tubular SOFC in 24 stacks (Larminie and Dicks, 2003).

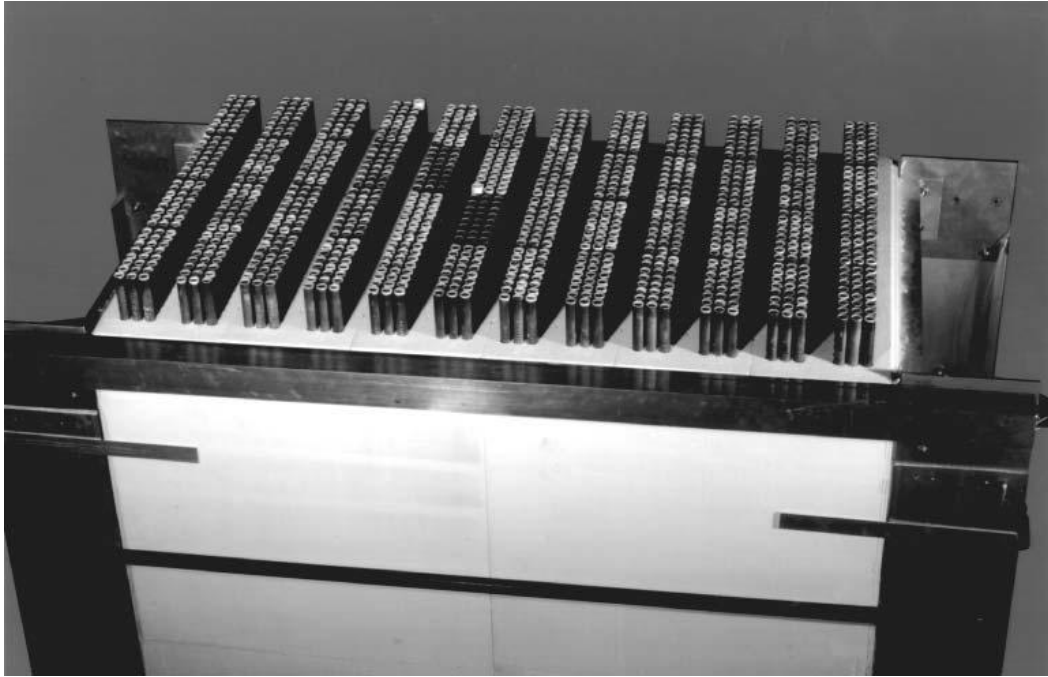


Figure 3.14: Larger stack of tubular SOFC consisting of 1152 cells (Larminie and Dicks, 2003).

3.10 Direct Carbon Fuel Cell (DCFC)

The DCFC technology has a long history dated to mid-nineteenth century. The theoretical principles and configuration of the DCFC are similar to those of the high temperature fuel cells (SOFC and MCFC). Usually the DCFC have three main components: the anode, the cathode and the electrolyte. Its difference from the MCFC and the SOFC is that instead of operating on gaseous fuels it uses solid carbon as fuel (Cao *et al.*, 2007; Wolk *et al.*, 2007). A comparison of the DCFC to other fuel cells is given in Table 3.8.

Table 3.8: Operating characteristics of DCFC and other conventional fuel cells
(Li *et al.*, 2011; Jia *et al.*, 2010; Wolk *et al.*, 2007)

Type	Electrolyte	Operating Temp.	Fuel	Reforming	Oxidant	Efficiency (HHV)
DCFC	MH/MC /SO	700°C (1110°F)	Solid carbon	Not needed	Humidified Air	80%
MCFC	Molten carbonate	650°C (1200°F)	H ₂ /CO ₂ /reformate	External/ Internal	CO ₂ /O ₂ /air	50-60%
SOFC	SO/ Ceramic	1000°C (1830°F)	H ₂ /CO ₂ /CH ₄ / Reformate	External/ Internal	O ₂ /air	45-55%
PAFC	Phosphoric acid	190°C (375°F)	H ₂ reformate	External	O ₂ /air	40-50%
PEMFC	Polymer	80°C (175°F)	H ₂ reformate	External	O ₂ /air	30-35%

MH-molten hydroxide, MC-molten carbonate, SO- Solid oxide

Solid carbon is directly introduced into the anode compartment and electro-oxidised to CO₂ at high temperature generating electricity as shown in Figure 3.15. The overall cell reaction is given by Equation 3.13 (Cao *et al.*, 2007).



The first literature record of the DCFC may be traced back to the mid of 19 century. Bacquerelle in 1885 and Jablochhoff in 1877 built electrochemical devices using electrode-grade carbon as anode, Pt/Fe as cathode, and fused KNO₃ as electrolyte. The devices though unstable due to electrolyte degradation still produce electricity. In 1896, a large assembly of cells consisting of 100 single cells with rods of baked coal as anode, iron pots as cathode and molten sodium hydroxide as electrolyte were demonstrated by Dr William Jacques. By heating the iron pot containing the electrolyte to 400-500°C in a furnace and blowing air through it, a current density of about 100 mA cm⁻² and an electric power of 1.5 kW were obtained from the system. This could be considered the first DCFC (Cao *et al.*, 2007).

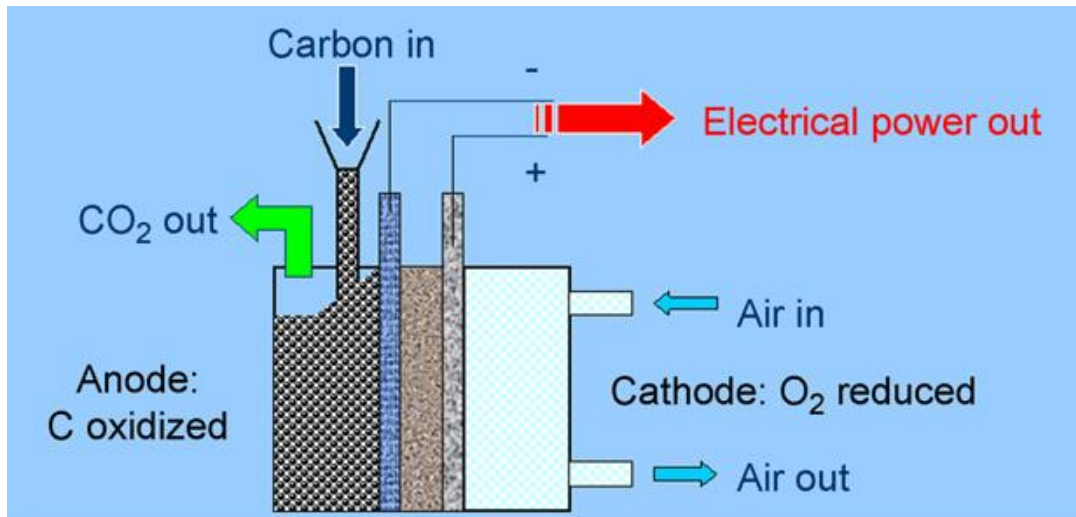
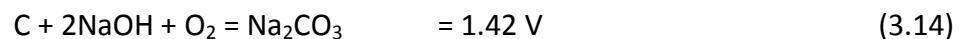


Figure 3.15: Configuration of the DCFC (Cao *et al.*, 2007).

Jacques's DCFC gave rise to many speculations over the actual performance and debates about the electrical power generation mechanism. For example the cell reaction was believed to be given by Equation 3.14 (Cao *et al.*, 2007).



Because the electrolyte was consumed by an irreversible reaction as given by Equation 3.15, the device was regarded as not a fuel cell but rather a battery (Cao *et al.*, 2007).



The cell stack was suspected to generate electricity not by electrochemical reaction but by a thermoelectrical effect. These doubts and the inability of reproducing Jacques's results by others and also the reducing incentive for seeking electrochemical conversion of coal as a result of the improved efficiency of the steam-driven generator in the early 20th century pushed aside the development in the technology of DCFC for about two-third of a century until the 1970s, when a series of studies at SRI International (Menlo Park, CA, a National Energy Technology Laboratory (NETL, Morgantown, WV) contractor) verified the practicability of completely electro-oxidising carbon to generate electricity (Cao *et al.*, 2007 cited Weaver *et al.*, 1981; Weaver *et al.*, 1979; Weaver *et al.*, 1975). Studies on the DCFC in the last few years

have clarified the earlier misunderstanding of the DCFC and have confirmed the electrochemical foundation of the direct conversion of carbon to electricity and also demonstrated the feasibility of the DCFC (Cao *et al.*, 2007). Currently with the significant development of fuel cell technology and the need for a cleaner environment, the fuel cell research community regained the interest of developing DCFC with this research being part of that development.

3.10.1 Advantages of DCFC

The direct carbon fuel cell has many unique attractive features. DCFC offers great thermodynamic advantages over other fuel cell types, such as MCFC and SOFC operated on hydrogen fuel (Cao *et al.*, 2007; Cherepy *et al.*, 2005; Cooper, 2004; Zecevic *et al.*, 2004). Its theoretical electrochemical conversion efficiency based on Equation 3.13 slightly exceeds 100%. This is because the entropy change for the cell reaction is positive ($\Delta S = 1.6 \text{ JK}^{-1} \text{ mol}$ at 600°C), which results in a slightly larger standard Gibbs free energy change ($\Delta G = -395.4 \text{ kJ mol}^{-1}$ at 600°C) than the standard enthalpy change ($\Delta H = -394.0 \text{ kJ mol}^{-1}$ at 600°C). The product, CO_2 , and the reactant, C (carbon), exist as pure substance in separate phases, thus their chemical potentials (activities) are fixed and independent of the extent of conversion of the fuel or position within the cell. This may allow a full conversion of the carbon fuel in a single pass with the theoretical voltage of DCFC remaining nearly constant at $\sim 1.02 \text{ V}$ during the operation (minimal Nernst loss). The fuel utilisation efficiency could reach 100%, giving a practical typical coal to electricity efficiency of around 80%. This value is higher than MCFC or SOFC running on hydrogen or natural gas (nominal efficiency of 50-60%, Table 3.8). Thus one can say that the DCFC is one of the potentially efficient electrochemical power generation systems available for our time (Desclaux *et al.*, 2010; Nürnberger *et al.*, 2010; Cao *et al.*, 2007; Wolk *et al.*, 2007; Dicks, 2006; Cooper, 2003b).

Again the DCFC releases lower emissions than coal-firing power plant, it is estimated that DCFC can cut carbon emissions from coal by 50% and reduce off-gas volume by 10 times when compared to conventional coal-burning power plants (Cao *et al.*, 2007; Cooper and Berner, 2005; Cooper, 2003a,b). This reason may be attributed to the fact that the oxidation of carbon in a DCFC occurs electrochemically at the anode compartment without the direct mixing with air, and thus the CO₂ produced is not mixed with other gases. The major components in the off-gas is carbon dioxide, which can be injected into an oilfield to enhance oil recovery and at the same time used as carbon capture storage (CCS) beneath the earth, further reducing the release of CO₂ into the atmosphere. DCFC also releases no particulates (fly ash). A major significance of using DCFC to produce electricity is a major consideration for regions heavily dependent on coal, like China, in which, around 80% of the electricity power is from burning coal, releasing 70% of its total CO₂ emissions (ranked 2nd in the world), 90% of its SO₂ emission (ranked 1st in the world), 70% of its total particles and 67% of its total NO_x. In the United States coal-fired plants produces 55% of their electricity and large amount of pollutants (Cao *et al.*, 2007; Schneider, 2005).

Most solid carbon fuel can easily be produced from many different resources, such as coal, biomass (miscanthus straw, wheat straw, grass, wood chips, sugarcane bagasse, etc.), petroleum coke and organic waste. Coal is known to be the earth's most abundant fossil resources and accounts for 60% of the world's fossil fuel resources with 80% of the world's coal belonging to the United States, Canada, former Soviet Union and China. DCFC uses pyrolysed tiny carbon particles which consumes less energy and requires less capital than the production of hydrogen-rich fuels for MCFC or SOFC by steam reforming processes. Carbon releases a very high energy per unit volume on oxidation with oxygen (20.0 kWh L⁻¹) exceeding many other fuel cells, in case of hydrogen (2.4 kWh L⁻¹), methane (4.0 kWh L⁻¹), gasoline (9.0 kWh L⁻¹), and diesel (9.8 kWh L⁻¹). Since no reformers or heat engines is required for a DCFC system it is therefore mechanically simple. It can be built on the site of coal mine and biomass plantation, thus eliminating transportation, saving energy and reducing environmental pollution caused by shipping and handling (Cao *et al.*, 2007).

3.10.2 Electrochemical Oxidation of Carbon

Carbon electrochemical oxidation requires high temperature because of its sluggish kinetics and is therefore generally performed in molten salt electrolytes (such as molten carbonates, molten hydroxides and cryolites)(Cao *et al.*, 2007; Cherepy *et al.*, 2005; Cooper, 2003; Selman, 2003). Experimental works have been carried out in the area of anodic oxidation and their findings are summarised below (Cao *et al.*, 2007):

[A] The predominant product is CO₂ at polarisations greater than around 0.1 V at temperature above 700°C. In 1935 Tamaru and co-workers found by analysing the off-gas composition that CO₂ is dominant and concluded that the overall electrochemical oxidation of carbon was the same as its complete combustion (Cao *et al.*, 2007 cited Tamaru and Kamada, 1935). This result was further confirmed by Hauser using gas evolved from graphite anode (Cao *et al.*, 2007 cited Hauser, 1964). Over the temperature range of 650-800°C, he found the current efficiency based on four electron processes was more than 99% at applied current densities between 20 and 120 mA cm⁻². Weaver and co-workers also found that more than 90% of the anode gas was CO₂ at high current density (Cao *et al.*, 2007 cited Weaver *et al.*, 1981; Weaver *et al.*, 1979). Vutetakis and co-workers reported that the anodic product was CO₂ and the CO/CO₂ ratio increases as current density decreases (Cao *et al.*, 2007 cited Vutetakis *et al.*, 1987; Vutetakis, 1985). These findings overturned the assumption that the anodic oxidation of carbon would produce CO as the dominant species at temperature above 750°C according to Boudouard reaction equilibrium. These observations proved that complete electro-oxidation of carbon to CO₂ (a four-electron process) is feasible, and the formation of CO (a two-electron process) could be avoided at high current density (polarized condition) and thus built the sound foundation for the DCFC (Cao *et al.*, 2007).

[B] The reactivity of carbon reaction is affected by its properties, such as, electrical conductivity, crystallisation, particle size and surface area. The poor crystallised, highly lattice disordered carbons are more reactive probably due to their surface defects (edges, steps), which acts as active sites. Carbons with good electrical conductivity would lower the ohmic polarisation and benefit the carbon electrochemical reaction

(Cooper, 2008; Cao *et al.*, 2007; Cherepy *et al.*, 2005). Weaver and co-workers concluded that the devolatilised coal is more reactive than spectroscopic carbon and pyrolytic graphite and attributed the high reactivity to large surface area and poor crystallisation (Cao *et al.*, 2007 cited Weaver *et al.*, 1979). But the work by Cooper and co-workers found that surface area has no strong effects on carbon discharge rate (Cherepy *et al.*, 2005).

3.10.2.1 Mechanism

Carbon electrochemical oxidation mechanism is difficult because of lack of techniques to detect the reaction intermediates in molten salts at high temperature (> 600°C). Through some indirect evidence Haupin and co-workers have proposed a mechanism for the anodic oxidation of carbon in molten cryolite/alumina electrolyte (acidic melts-Hall process) as given by Equations 3.16 – 3.22 (Cao *et al.*, 2007; Cherepy *et al.*, 2005; Frank and Haupin, 1985; Haupin and Frank, 1981):



The source of the O^{2-} is the melt, the dissociation of a complex fluoaluminate ion generates a free oxide ion, which adsorbs on the reactive carbon surface sites, C_{RS} (edges or steps). The adsorbed oxygen undergoes discharge in two, single-electron steps to form a C-O-C (C_2O) bridge between reactive carbon atoms on the exposed carbon structure as shown in Figure 3.16A. The second oxygen ion adsorbs right next to the C_2O site to extend the surface species to a C-O|C-O-C (C_3O) bridge as shown in

Figure 3.16B. This adsorption is kinetically hindered and requires considerable over potential, and thus constitutes the rate-determining step. The C_3O_2 is discharged in two, one-electron steps to form an unstable group and readily releases CO_2 by cutting of edge C-O bonds (Cao *et al.*, 2007).

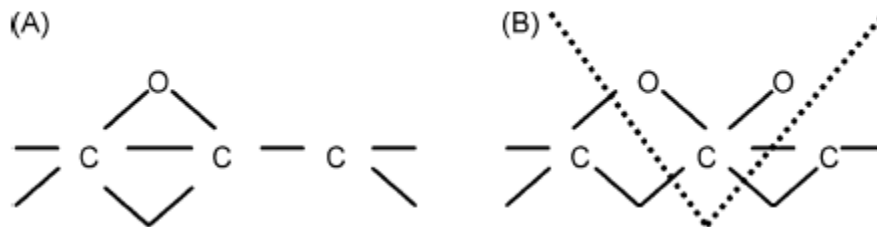


Figure 3.16: Carbon electrochemical oxidation description. (A) The first oxygen ion adsorption and (B) the second oxygen ion adsorption and CO_2 formation (Cao *et al.*, 2007; Cherepy *et al.*, 2005).

Cooper and co-workers suggested that the anodic oxidation of carbon in molten carbonates (basic melts) might follow a similar mechanism to the Hall process with the exception of the oxygen ion formation step (Cao *et al.*, 2007; Cherepy *et al.*, 2005). Molten carbonates easily dissociate into CO_2 and O^{2-} at DCFC operation temperature, Cooper and co-worker proposed that carbonates decompose at a high temperature to form oxygen ions as shown in Equation 3.23, and this initiates the carbon oxidation reactions given in Equations 3.17 to 3.22. For molten hydroxides, the mechanism for anodic oxidation of carbon is unknown (Cao *et al.*, 2007).



3.10.3 Molten Carbonate Electrolyte in DCFC

The use of mixed molten carbonates (Li_2CO_3/K_2CO_3) for DCFC is recommended because of their high conductivity, good stability in the presence of CO_2 (carbon electro-oxidation product) and suitable melting temperature (Cao *et al.*, 2007; Cherepy *et al.*,

2005). Equations 3.24 and 3.25 represent the anode and cathode reaction in molten carbonate electrolytes. Equation 3.25 gives the cell voltage. CO₂ is formed at the anode side and consumed at the cathode side, therefore, its partial pressure has an influence on the cell voltage (Cao *et al.*, 2007).



$$E_{\text{cell}} = E^0 - (RT/4F)\ln[\text{CO}_2]_{\text{anode}}^3 + (RT/4F)\ln([\text{O}_2][\text{CO}_2]_{\text{cathode}}^2) \quad (3.26)$$

Cooper and co-worker at the Lawrence Livermore National Laboratory (LLNL, Livermore, CA) constructed a DCFC with a tilted orientation design as shown in Figure 3.17 (Cherepy *et al.*, 2005; Cooper and Berner, 2005; Cooper *et al.*, 2004; Cooper, 2003a). They used 32% Li₂CO₃ and 68% K₂CO₃ melt as the electrolyte. The anode was a paste of carbon particles (<100 μm) in the melt with open-foam nickel as the current collector. The cathode consists of a sintered frit of fine nickel particles (compressed foam nickel). Between the anode and the cathode is a separator made of several layers of zirconia felt. The cathode catalyst was activated by thermal treatments in air to form a compact layer of NiO, which was then lithiated by exposing to lithium salts to generate the catalytic active structure. The electrode assembly was positioned at an angle of 5-45° from the horizontal. To avoid flooding of the cathode the configuration allowed excess electrolyte to drain from the cell. They tested several carbon materials with different crystallinity, particle size, surface area and surface structure at 800°C. At a cell voltage of 0.8 V (80% of the standard potential) they obtained current densities ranging from 58 to 124 mA cm⁻², as shown in Figure 3.18 (Cao *et al.*, 2007; Cooper, 2003b). They tested many carbon particles including calcined petroleum pitch, biological char, coal derived pitch, graphite, furnace and thermal black. They concluded that the carbon properties affecting DCFC performance include crystallographic disorder, electrical conductivity and number of surface reactive sites (Cao *et al.*, 2007; Dicks, 2006; Cooper and Berner, 2005).

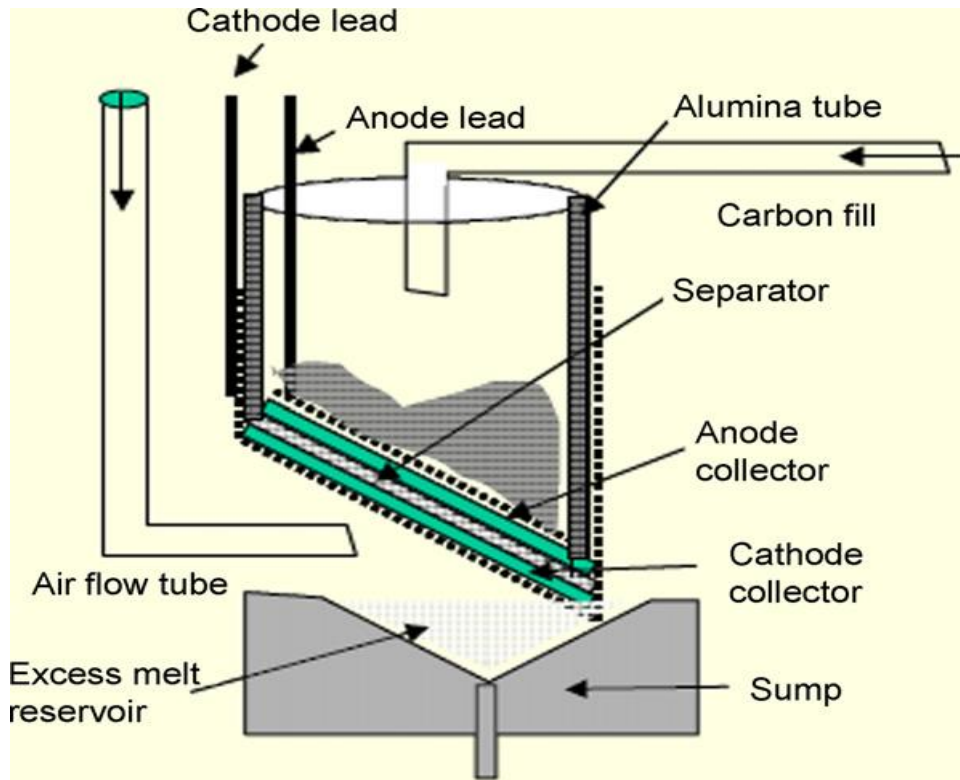


Figure 3.17: LLNL tilted direct carbon fuel cell with carbon particle anode (Cooper and Berner, 2005).

Figure 3.18 show the curve of the cell potential (voltage) versus the current density, as represented by the curve starting above 1.0 V and gradually falling, while the curve starting from the zero point on the cell voltage axis shows the power density versus the current density of the cell. The performance of the cell for furnace black fuel (having peak power density of 100 mW/cm^2) is better than that of the green needle petroleum coke fuel (with peak power density of 80 mW/cm^2). In terms of the open circuit voltage (OCV) of the cell the green needle petroleum coke fuel (1.1 V) had a higher value than that of furnace black fuel (1.02 V) as recorded for the operating temperature of 800°C . The OCV of the furnace black at 700°C was slightly higher (1.03 V) than at 800°C (1.02 V), but the overall performance of the higher temperature is better. At the cell potential of 0.8 V for 700°C we have a lower current density of 40 mA/cm^2 when compare to 120 mA/cm^2 recorded for 800°C .

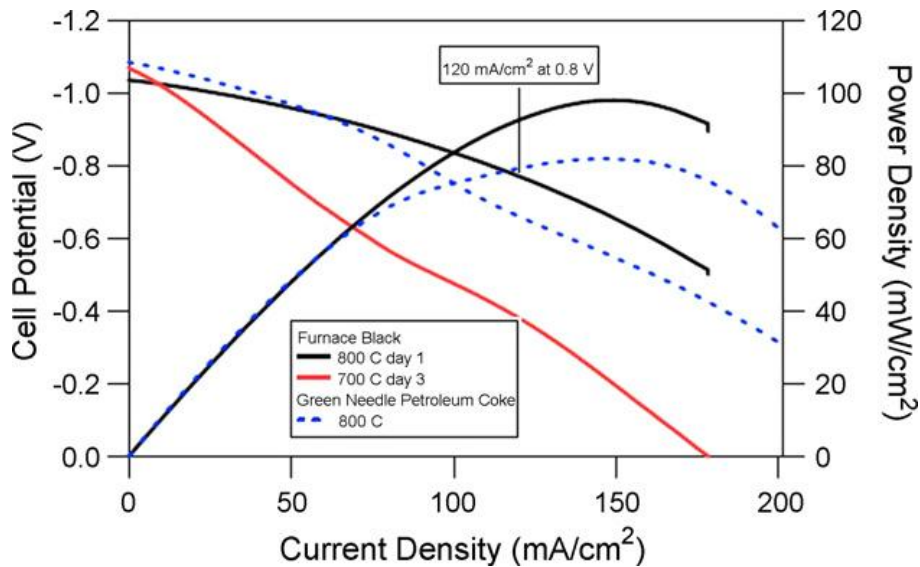


Figure 3.18: Performance of the LLNL tilted direct carbon fuel cell (Cooper and Berner, 2005).

They also studied the influence of impurities in the carbon on DCFC performance and found out that the presence of sulphur degrades the cell performance probably due to corrosion of the anode current collector Ni, leading to the formation of nickel sulphide and thus diminishing the current collection capability. They did not investigate the effect of ash (inorganic mineral containments) on anode polarisation and electrolyte properties. At LLNL they developed proprietary cathode catalyst and aerogel/carbon and xerogel/carbon composites anode for their DCFC (Cao *et al.*, 2007). Hemmes and co-worker at the Delft University of Technology developed a DCFC model based on the LLNL cell design in order to provide a theoretical base for the DCFC system. Their simulated results show that the system has a net electrical efficiency of 78% (Cao *et al.*, 2007 cited Hemmes *et al.*, 2005).

3.10.4 Molten Hydroxide Electrolyte in DCFC

William Jacques used molten hydroxide as electrolyte to test his DCFC. The criticism that followed his work led to the rejection of the DCFC because the electrolyte reacts with CO₂ produced by carbon oxidation to form carbonates. But recent researches at

the Scientific Application and Research Associates (SARA, Cypress, CA) revived and proved the feasibility of DCFC using molten hydroxide as electrolyte. When molten hydroxide is compared with molten carbonate there are certain advantages that the molten hydroxide has, like a higher ionic conductivity and a higher activity of the carbon electrochemical oxidation, meaning a higher carbon oxidation rate and a lower overpotential (Cao *et al.*, 2007 cited Zecevic *et al.*, 2005a). Using molten hydroxide as the electrolyte in DCFC permits its operation at a lower temperature of around 600°C and this in turn allows the use of less expensive materials for DCFC fabrication and thus reduces the cost of DCFC. The dominant product of carbon oxidation at low temperature (<700°C) will be CO₂ according to Boudouard equilibrium and so CO formation can be avoided. These benefits can be achieved only after the carbonate formation issue is overcome. Goret and Tremillon propose that the formation of carbonates during carbon electro-oxidation in molten hydroxides may undergo a chemical process and electrochemical process given by Equations 3.27 and 3.28. The electrochemical process consists of two steps: a fast chemical step (given by Equation 3.29) and a slow electrochemical step, which is rate-determining and given by Equation 3.30 (Cao *et al.*, 2007 cited Goret and Tremillon, 1967; Goret and Tremillon, 1966).



The concentrations of O²⁻ and water determine the rate of carbonate formation, thus increasing the water content in the hydroxide electrolyte will shift Equations 3.27 and 3.29 to the left and a significant reduction of CO₃²⁻. Zecevic and co-workers in SARA developed a DCFC with a molten hydroxide electrolyte using humidified air as the oxidant (Cao *et al.*, 2007 cited Zecevic *et al.*, 2005a). The presence of moisture (from air) in the electrolyte reduces carbonate formation and also increases the ionic conductivity of the melt. Figure 3.19 gives a description of SARA fuel cell in which a

cylindrical pure graphite rod acts as the anode and fuel that is immersed into molten sodium hydroxide contained in a cylindrical or prismatic container, which is also the cathode. Humidified air is fed into the cell from the bottom of the container via a gas distributor (Cao *et al.*, 2007; Zecevic *et al.*, 2003). They tested many materials as the cathode, such as, nickel foam lined steel and Fe₂Ti steel (Iron alloy with titanium) which showed good catalytic activity. Their cell operated between 400 and 650°C. The cell performance depends on the cathode material, air flow rate, operating temperature and fuel cell scale. They obtained an open circuit voltage between 0.75 and 0.85 V, an average power output of 40 mW/cm² at 140 mA/cm² with over 450 h running time. Their peak power output was 180 mW cm⁻² and their maximum current density greater than 250 mA/cm².

Figure 3.20 give a description of their cell performance (Cao *et al.*, 2007; Zecevic *et al.*, 2003, Patton, 2003). Figure 3.20 shows the performance of the cell at an operating temperature of 630°C and with two different surface area of the anode. The smaller surface area gave a higher value for OCV of 0.85 V than the larger surface area of 0.75 V. Also the maximum current density recorded for the smaller surface area anode (250 mA/cm²) was better than the larger one (100 mA/cm²). Their cell had no separator to prevent oxygen having direct contact with the carbon, thus giving a mixed potential as a result of oxygen reduction on carbon anode and also reducing the performance.

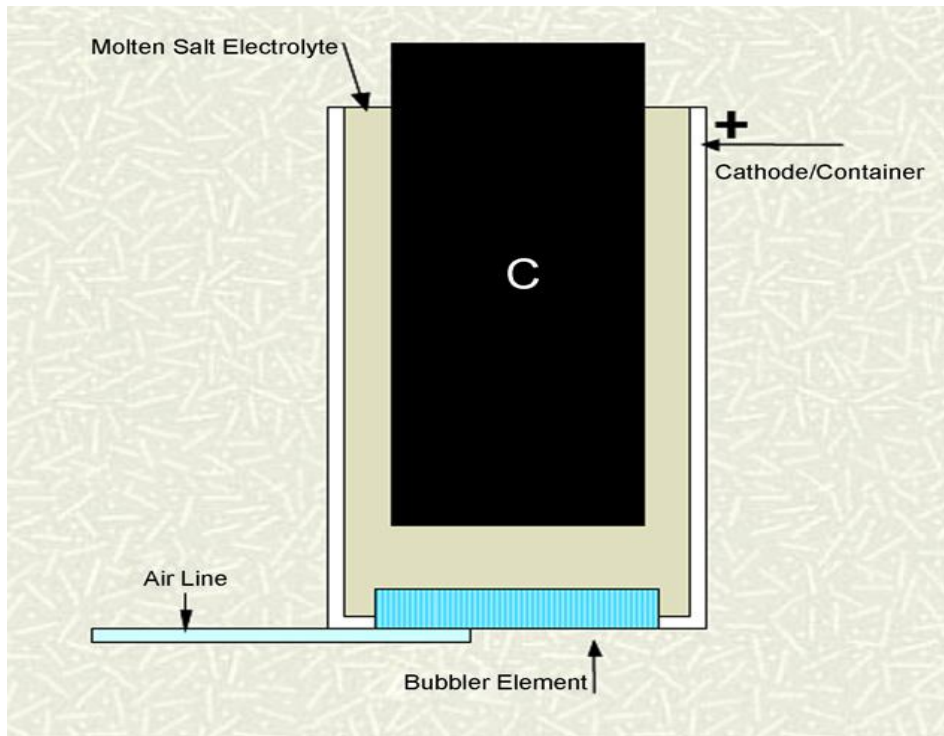


Figure 3.19: SARA direct carbon fuel cell with a carbon rod anode (Zecevic *et al.*, 2003)

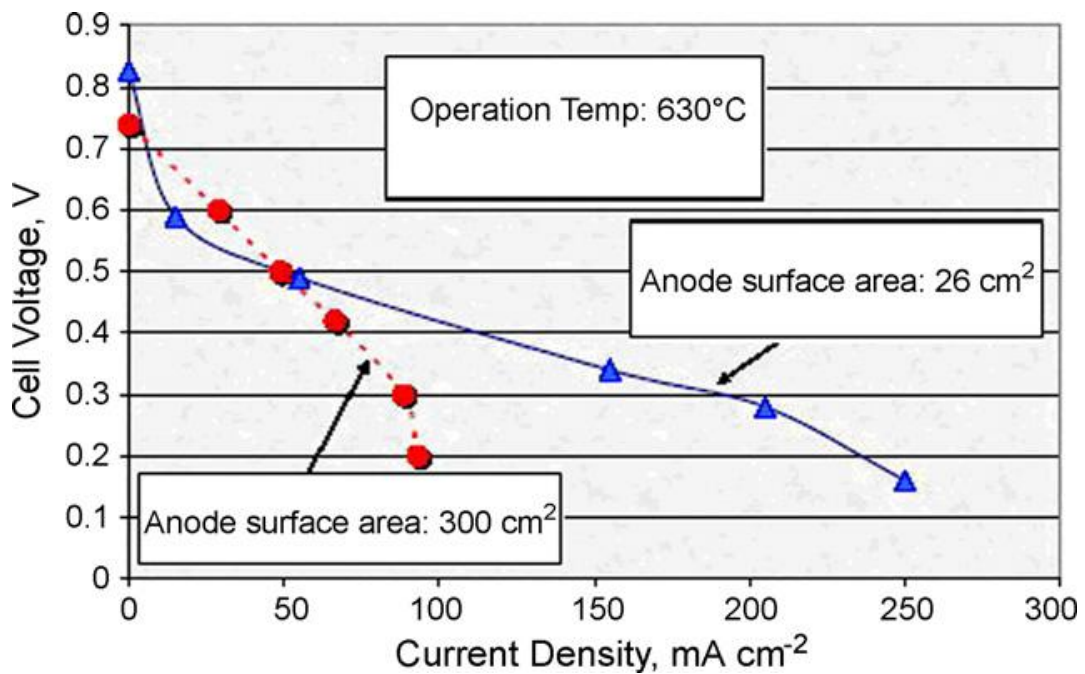


Figure 3.20: Performance profile of the SARA direct carbon fuel cell (Zecevic *et al.*, 2003)

Their cell performance can be improved upon by optimizing the cell design, the electrode material and the operation condition. Since the cell has no separator to prohibit oxygen from direct contacting with carbon, a mixed potential resulting from oxygen reduction on carbon anode might reduce the cell performance. SARA had already proposed the design of a separator cell, however, finding a suitable membrane that sustains the harsh molten hydroxide environment (corrosive, basic, high temperature) will take some great efforts (Cao *et al.*, 2007).

At the West Virginia University, Saddawi and co-workers developed a method to produce solid cylindrical carbon rods for SARA's DCFC (Cao *et al.*, 2007 cited Saddawi, 2005). Their fuel rods were made with varying amounts of petroleum coke, coal tar binder pitch, and either one or two coal-derived fuels. They tested the chemical composition, density and electrical resistivity of the carbon rods, and the results indicated that coal-derived rods perform significantly better than their graphite counterparts due to increased electrochemical activity. But the mechanisms for the electro-oxidation of carbon (anode reaction) and the electro-reduction of oxygen (cathode reaction) in molten sodium hydroxides is yet to be well understood. The overall electrode reaction is given by Equations 3.31 to 3.33, Equations 3.31 and 3.32 for the anode and Equation 3.33 for the cathode (Cao *et al.*, 2007; Zecevic *et al.*, 2005b).



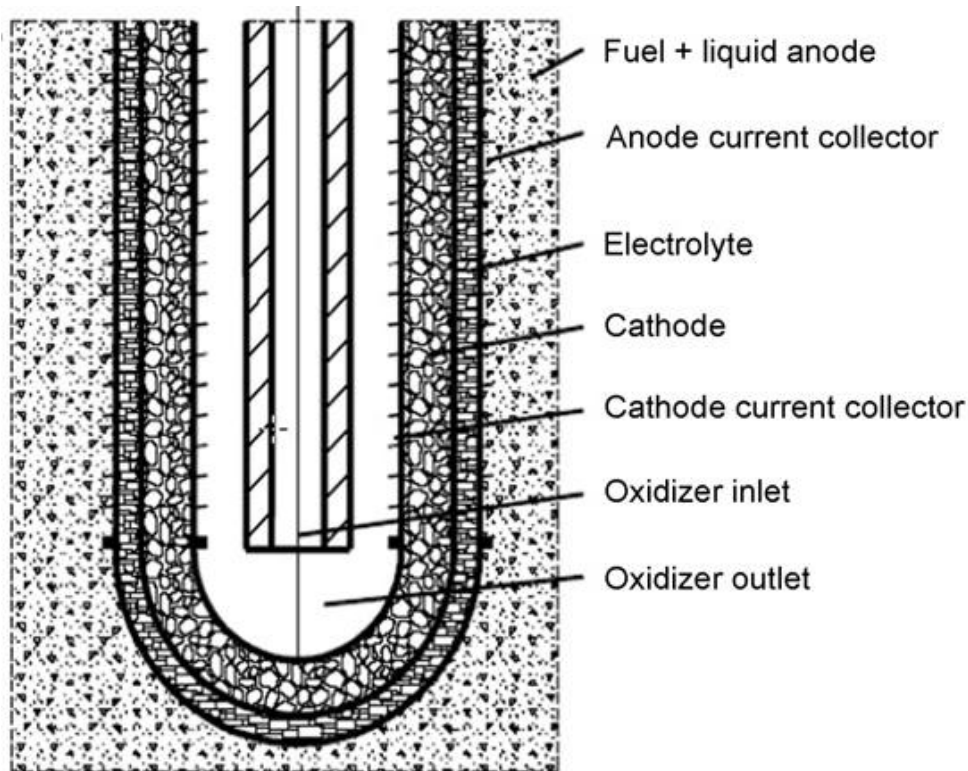


Figure 3.21: Cell configuration of the SRI direct carbon fuel cell combining advances in SOFC and MCFC technology (Cao *et al.*, 2007; Balachov *et al.*, 2005).

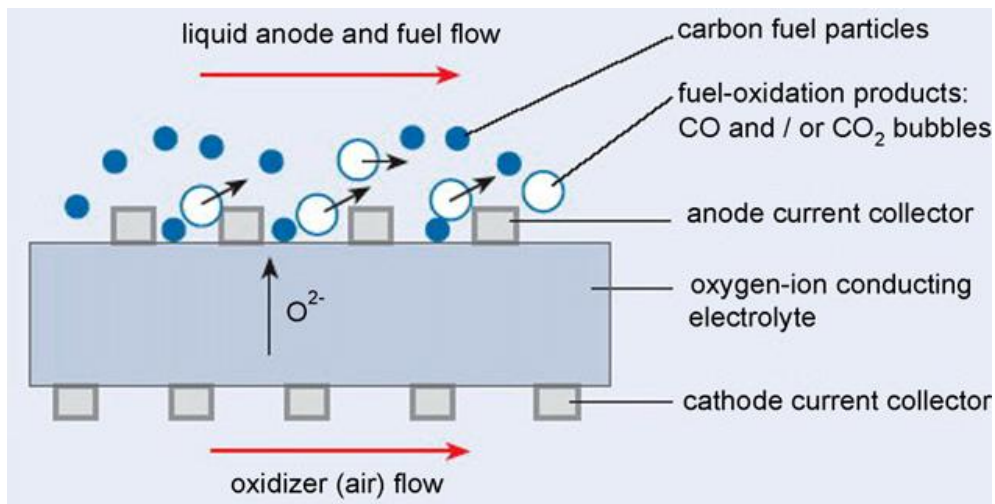


Figure 3.22: Flowing liquid anode of the SRI direct carbon fuel cell combining advances in SOFC and MCFC technology (Cao *et al.*, 2007; Balachov *et al.*, 2005).

3.10.5 YSZ (Yttria Stabilised Zirconia)-based solid electrolyte in DCFC

At SRI International, Balachov and co-workers developed a DCFC which combine the advances in SOFC and MCFC technology, this is shown in Figures 3.21 and 3.22 (Cao *et al.*, 2007; Balachov *et al.*, 2005). Their DCFC is a U-tube consisting of (from inner to outer of the tube), a metal mesh cathode current collector, a cathode layer (lanthanum strontium manganate, LSM), an electrolyte layer (Yttria Stabilised Zirconia, YSZ), and a metal mesh anode current collector. The U-tube is immersed into a liquid anode comprising a mixture of molten $\text{Li}_2\text{CO}_3 + \text{K}_2\text{CO}_3 + \text{Na}_2\text{CO}_3$ and carbon particles. Their DCFC is better operated in a flow mode (stirring) to facilitate the contact between carbon particles and anode current collector to enhance mass transport (Shown in Figure 3.22). They tested several fuels, such as, acetylene black, tar, coke, coal and mixed waste. Using conventional coal without pre-treatment they obtained power densities greater than 100 mW/cm^2 at 950°C , as shown in Figure 3.23, which is comparable to power densities achieved by commercial MCFC (Cao *et al.*, 2007; Balachov *et al.*, 2005).

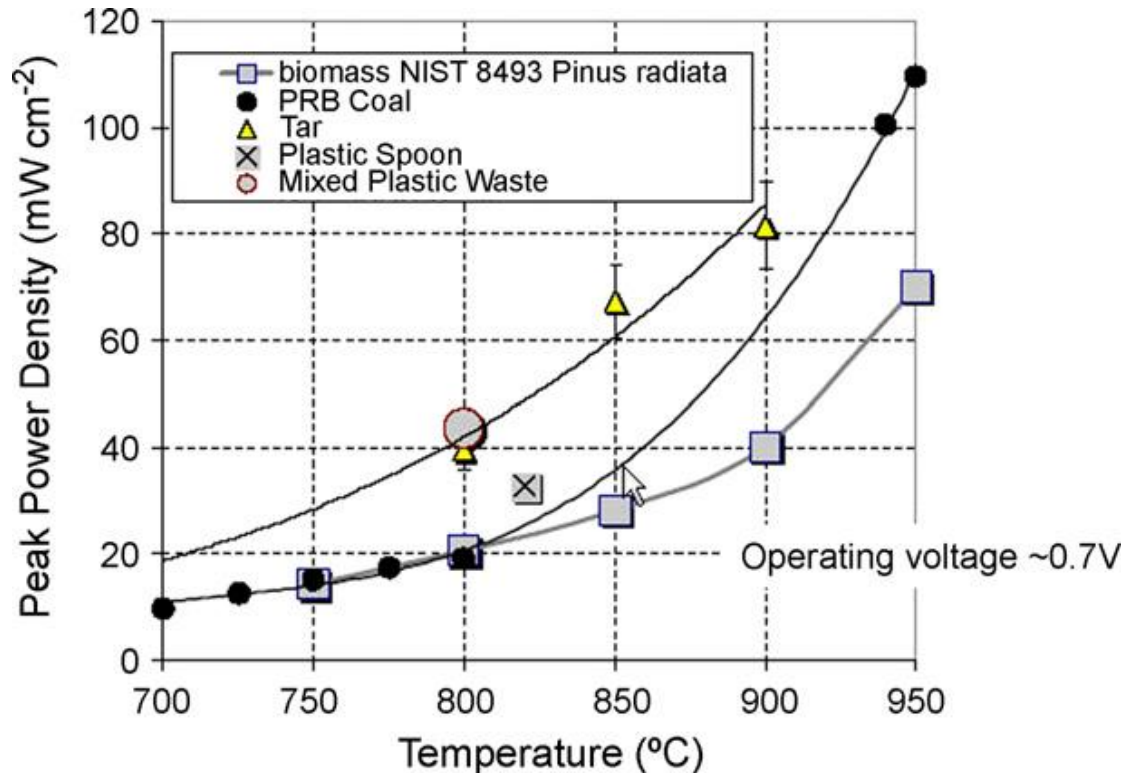


Figure 3.23: Performance of the SRI direct carbon fuel cell liquid anode (Cao *et al.*, 2007; Balachov *et al.*, 2005).

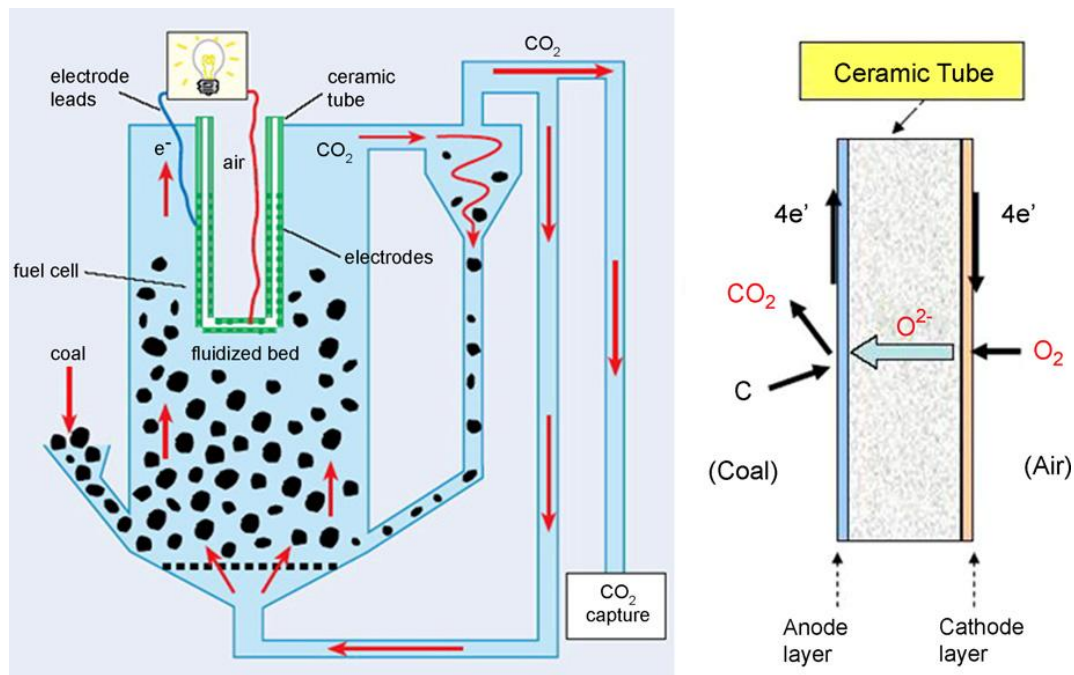


Figure 3.24: CCE Proposed DCFC combining SOFC and fluidized-bed technologies (Cao *et al.*, 2007; Duskin, 2005).

At the CellTech Power LLC (Westborough, MA), Tao and co-workers tested the direct oxidation of coal in a SOFC-like structure (Cao *et al.*, 2007; Tao, 2003; Tao, 2005). Their cathode was 0.6 mm thick $\text{La}_{0.84}\text{Sr}_{0.16}\text{MnO}_3$, the electrolyte was 0.12 mm thick $(\text{ZrO}_2)(\text{HfO}_2)_{0.02}(\text{Y}_2\text{O}_3)_{0.08}$, the anode was carbon black and platinum as the anode current collector. They obtained a power output of 10 mW/cm^2 at 0.248 V and 50 mW/cm^2 at 0.507 V at temperature of 800 and 1002°C respectively. At the University of Akron, Chuang investigated the SOFC using solid carbon fuel, their results revealed that with coke as fuel, the open circuit voltage can reach around 0.8 V at 700°C and a current density of 50 mA/cm^2 at 0.8 V can be obtained with a cell temperature of 950°C (Cao *et al.*, 2007; Chuang, 2005). Part of the problems with DCFC using electrolyte were poor contact between the carbon anode and the electrolyte and the high operation temperature, leading to the formation of CO due to Boudouard reaction (Cao *et al.*, 2007). Duskin and Gur (Clean Coal Energy, CCE, Stanford, CA) proposed a DCFC combining SOFC and fluidized-bed technologies. Figure 3.24 shows the description of their DCFC, the configuration allows continuous carbon feeding and

good contact between carbon fuel and solid electrolyte reducing mass transport limitation (Cao *et al.*, 2007; Duskin, 2005).

3.10.6 DCFC with Mass and Heat Integration Systems

For most DCFC integration system, the transportation of fuel from a central site and the transmission and distribution of the electricity from that site to the end user is a key point to put in mind. System Integration process permits maximum energy efficiency because of the integration between fuel preparation and fuel consumption and also the chance to use the waste energy (methane and thermal) in other plants or buildings that are located within the integrated system (Wolk *et al.*, 2007).

A system with highest energy efficiency potential and great energy integration opportunity and co-located facilities is represented in Figure 3.25. Under this process concept, the feed is dried at 150°C (300°F) to remove water from the wet biomass or MSW material. Then the dried feed is pyrolysed at 370°C (700°F) to remove carbon dioxide and methane and then produce char which is fed into the DCFC. The heat energy needed for the operations are provided from the hot CO₂-rich anode product gas of the DCFC which is recycled to the fuel dryer and pyrolyser. The excess energy from the pyrolyser waste gas and that from the CO₂ rich anode off-gas could be used for the generation of steam and also in some other co-located energy consuming facilities (Wolk *et al.*, 2007). An alternative and a simpler system than that of the highly integrated concept is presented in Figure 3.26. The energy to drive the pyrolysis reaction is obtained by recycling a fraction of the hot, CO₂-rich, anode product gas to the pyrolyser and the methane-rich product gas from the pyrolyser could be use as a combustion fuel for buildings and hot water heating (Wolk *et al.*, 2007).

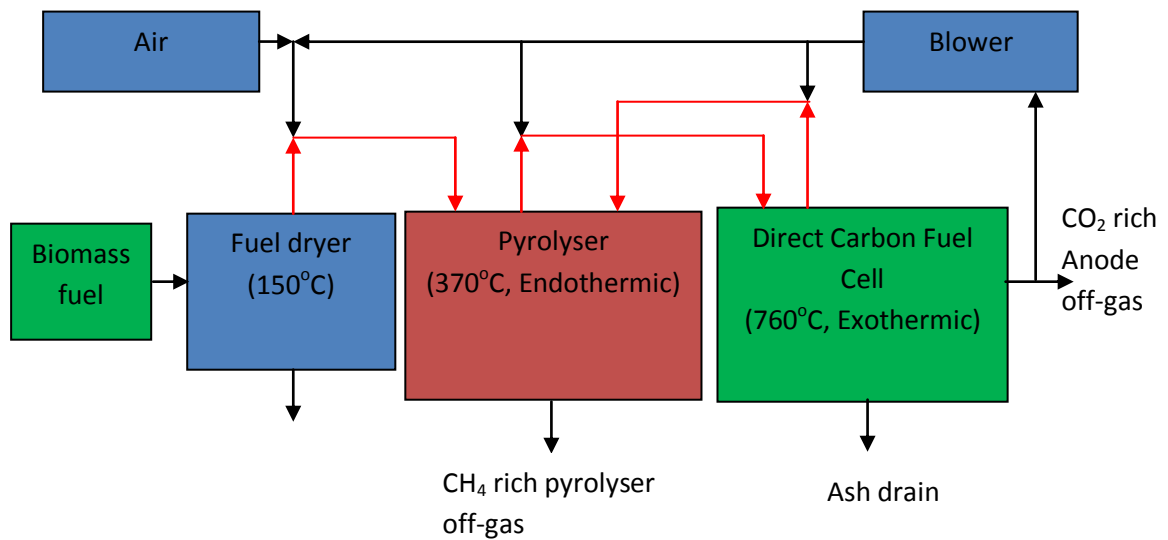


Figure 3.25: Highly integrated DCFC, pyrolyser and dryer for maximum efficiency (Wolk *et al.*, 2007)

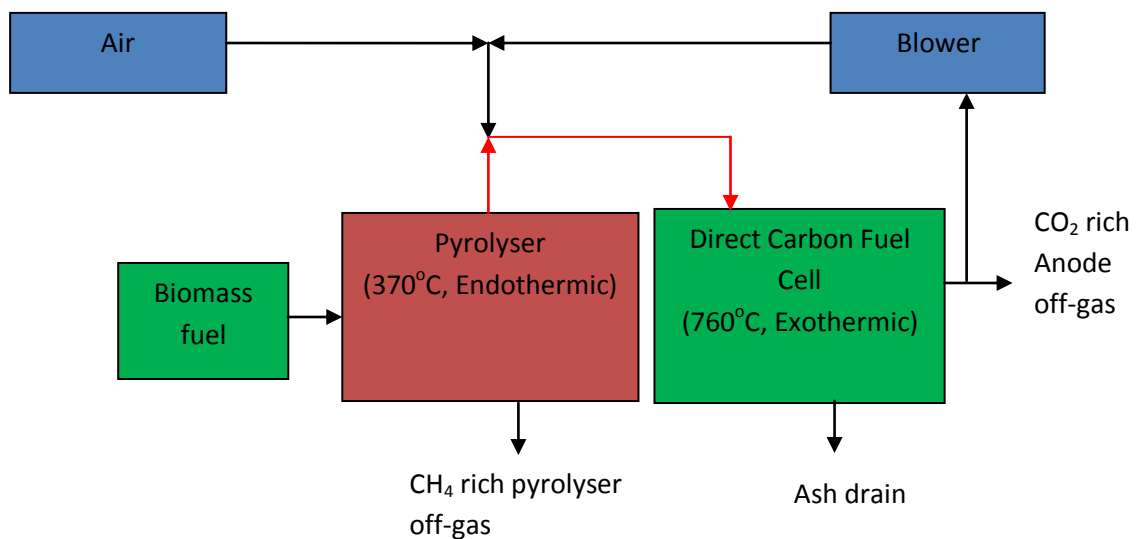


Figure 3.26: Integrated DCFC and pyrolyser for high efficiency (Wolk *et al.*, 2007)

When the biomass source is remote from the electrical demand area then the non-integration process may be more economically preferred. In such a situation, it might be cheaper to transport a lower weight particulate fuel product than the high moisture vegetation or MSW components to the generation site located near the demand centre as shown in Figure 3.27 (Wolk *et al.*, 2007).

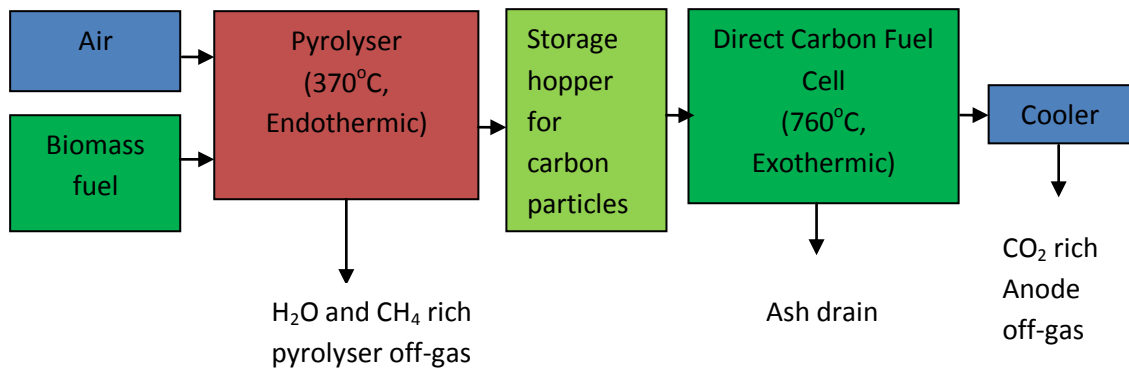


Figure 3.27: Non-integrated DCFC and pyrolyser with maximum flexibility (Wolk *et al.*, 2007)

3.11 The Process of Fuelling Fuel Cells

The type of fuelling used in fuel cells varies for different type. Traditionally hydrogen is the chosen fuel of powering fuel cells but as a result of technological advancement in various fields biomass, coal, natural gas, and municipal waste have also been found to be suitable for fuelling fuel cell systems with the added advantage of reducing environmental pollution. Below are brief discussions on the various options for fuelling the FC systems.

3.11.1 Hydrogen

Hydrogen is the preferred fuel for most fuel cells because of its high reactivity for the electrochemical anode reaction, and the oxidation of hydrogen produces water which is environmentally friendly. The only emission that vehicles running on proton exchange membrane (PEM) fuel cells is water using hydrogen and thereby called zero-emission vehicles. Hydrogen does not occur naturally as gaseous fuel, and so for practical fuel cell it has to be generated from a fuel source. Table 3.9 gives the basic chemical and physical data on hydrogen and some other fuels considered for use in fuel cells (Larminie and Dicks, 2003). There are many ways of producing hydrogen

among which are steam or methane reforming, partial oxidation, autothermal and dry reforming, water electrolysis (reverse of fuel cell operation), biological, photodissociation, direct thermal or catalytic splitting of water (Sørensen, 2005; Larminie and Dicks, 2003).

Table 3.9: Hydrogen and other fuels properties for fuel cell systems

(Larminie and Dicks, 2003)

Properties	Hydrogen	Methane	Ammonia	Methanol	Ethanol	Gasoline
	H ₂	CH ₄	NH ₃	CH ₃ OH	C ₂ H ₅ OH	C ₈ H ₁₈
Molecular weight	2.016	16.04	17.03	32.04	46.07	114.2
Freezing point (°C)	-259.2	-182.5	-77.7	-98.8	-114.1	-56.8
Boiling point (°C)	-252.77	-161.5	-33.4	64.7	78.3	125.7
Net enthalpy of combustion @ 25°C (kJ mol ⁻¹)	241.8	802.5	316.3	638.5	1275.9	5512.0
Heat of vaporisation (kJ kg ⁻¹)	445.6	510	1371	1129	839.3	368.1
Liquid density (kg m ⁻³)	77	425	674	786	789	702
Specific heat at STP (Jmol ⁻¹ K ⁻¹)	28.8	34.1	36.4	76.6	112.4	188.9
Flammability limits in air (%)	4-77	4-16	15-28	6-36	4-19	1-6
Autoignition temperature in air (°C)	571	632	651	464	423	220

3.11.2 Petroleum

This is a mixture of solid, liquid and gaseous hydrocarbon-based chemical compounds that occur in sedimentary rock deposits globally. Fuels derived from petroleum account for one half of the world's total energy supply and include gasoline, diesel fuel, aviation fuel, kerosene etc. Various components of petroleum are separated into their generic fractions by distillation (Larminie and Dicks, 2003). For fuel cell these chemical composition are very important because they determines the type of fuel processing, which could be used for generating hydrogen. Fuel converted catalytically

contains various trace compounds which could act as poisons for fuel cell stack (Larminie and Dicks, 2003).

3.11.3 Coal and Coal Gas

Coal is chemically complex and most abundant of all fossil fuels. It is formed from the compaction and indurations of many plant remains similar to those of peat. Classification of coal is based on the inherent plant material (coal type), the degree of metamorphosis (coal rank), and the degree of impurities (coal grade). Apart from combustion, further processing of coal to produce liquids, gases and coke is mainly dependent on the properties of the raw coal material. Fuel cell can be powered by the gases produced from coal gasification or from coal powder (Larminie and Dicks, 2003).

3.11.4 Natural Gases

The combustible gas that is found in the porous rocks in the earth's crust is natural gas. It is usually found with or close to crude oil reserves but can also occur alone in separate reservoirs. It mostly forms a gas cap trapped between liquid petroleum and an impervious rock layer (cap rock) in a petroleum reservoir. In high pressure, the gas will be intimately mixed with or dissolved in the crude oil. Fuel cell can also be powered by natural gas after some processing (Larminie and Dicks, 2003).

3.11.5 Bio-Fuels

These are fuel derived from biomass and all natural organic material associated with living organisms, including terrestrial and marine vegetable matter, everything from algae to trees, together with animal tissue and manure. There is a considerable attraction for using biogases in fuel cell systems. Most biogases have low heating values and high level of carbon oxides and nitrogen. Fuel cells most especially the

DCFC, MCFC and SOFC are able to handle very high concentration of carbon oxides (Larminie and Dicks, 2003).

Bio liquids are also favourites for fuel cell application, methanol and ethanol are good examples. Methanol is the proposed fuel for Fuel cell vehicles (FCVs). It can be synthesised from syngas derived from biomass or natural gas. Ethanol is produced from direct fermentation of biomass. Alcohol is also a very good choice owing to the ease of reforming it into hydrogen-rich gas (Larminie and Dicks, 2003). Solid biomasses in the form of char are also very good choice of fuel for fuel cells systems. Solid carbons are good choices for powering DCFC and MCFC (Adeniyi and Ewan 2011; Jia *et al.*, 2010; Li *et al.*, 2009; Jain *et al.*, 2008; Hackett *et al.*, 2007; Cao *et al.*, 2007; Cherepy *et al.*, 2005).

3.12 Energy and the EMF of Fuel Cell

The Gibbs free energy is very important in fuel cells. The Gibbs free energy is the energy available to do external work, neglecting any work done by changes in pressure and/or volume. In fuel cell conditions, the external work involves moving electrons round an external circuit- any work done by a change in volume between the input and output is not harnessed by the fuel cell. Exergy is all the external work that can be extracted, including that due to volume and pressure changes. The enthalpy is the Gibbs free energy plus the energy connected with the entropy. These forms of energy are all chemical energy but in resemblance to ordinary mechanical potential energy in two principal ways, the point of zero energy and the mechanical potential energy (Larminie and Dicks, 2003).

3.12.1 Zero Energy Reference Point

When working with chemical reactions, the zero energy reference point is usually define as pure elements, in the normal state, at standard temperature and pressure of

25°C and 0.1 MPa. When adopting this convention, the term Gibbs free energy of formation is usually applied instead of the Gibbs free energy, and the enthalpy of formation instead of enthalpy. Thus for an hydrogen fuel cell operating at standard temperature and pressure (STP), this means that the Gibbs free energy of formation is zero for the input, this provide a useful simplification (Larminie and Dicks, 2003).

3.12.2 Mechanical Potential Energy

The change in Gibbs free energy of formation, ΔG_f , gives the enthalpy released in fuel cell. This change is the difference between the Gibbs free energy of the products and the Gibbs free energy of the reactants or inputs as given by Equation 3.34 (Larminie and Dicks, 2003).

$$\Delta G_f = G_f(\text{products}) - G_f(\text{reactants}) \quad (3.34)$$

For simplicity it is more convenient to consider these quantities in their per mole form. This is indicated by putting a dash (-) over the lower case letter, e.g, $(\bar{g})_{\text{H}_2\text{O}}$ is the molar specific Gibbs free energy of formation for water. Equation 3.34 can be rewritten to give Equation 3.35 (Larminie and Dicks, 2003).

$$\Delta \bar{g} = \bar{g}(\text{products}) - \bar{g}(\text{reactants}) \quad (3.35)$$

Table 3.10 show the $\Delta \bar{g}$ for the basic hydrogen fuel cell reaction (Larminie and Dicks, 2003).

The electrical work done by a fuel cell is equal to the Gibb free energy and the fundamental equation that gives the electromotive force (EMF) or reversible open circuit voltage of the hydrogen fuel cell is given by Equation 3.36 (Larminie and Dicks, 2003):

$$\text{---} \quad (3.36)$$

Where E_{ocv} is the reversible open circuit voltage or electromotive force (EMF), and F is the Faradays constant. Equation 3.36 can be generalized for other fuel cells and batteries by replacing the value 2 by z in the denominator, and E_{ocv} by E , so that we have Equations 3.37 and 3.38, where z is the number of electrons transferred for each molecule of the cell (Larminie and Dicks, 2003).

$$\text{---} \quad (3.37)$$

$$\text{---} \quad (3.38)$$

Table 3.10: The Δ for the reaction $\text{H}_2 + \frac{1}{2}\text{O}_2 \rightarrow \text{H}_2\text{O}$ at different temperature (Larminie and Dicks, 2003).

Form of water product	Temperature (°C)	Δ (kJ mol ⁻¹)
Liquid	25	-237.2
Liquid	80	-228.2
Gas	80	-226.1
Gas	100	-225.2
Gas	200	-220.4
Gas	400	-210.3
Gas	600	-199.6
Gas	800	-188.6
Gas	1000	-177.4

3.13 Fuel Cell Irreversibilities

A fuel cell operated at higher temperature will give a shape similar to that of Figure 3.29, for an ideal case which involves a typical low temperature, air pressure fuel cell is depicted in Figure 3.28. Figure 3.29 represent a typical solid oxide fuel cell (SOFC) operating at about 800°C. The following points are important (Larminie and Dicks, 2003):

1. The open circuit voltage is equal to or only a little less than the theoretical value.
2. The initial fall in voltage is very small, and the graph is more linear.
3. There may be a higher current density at which the voltage falls rapidly, as with lower- temperature cells (Larminie and Dicks, 2003).

From Figures 3.28 and 3.29, it is observed that the reversible or no loss voltage is lower for the higher temperature, the operating voltage is generally higher, because the voltage drop or irreversibilities are smaller (Larminie and Dicks, 2003).

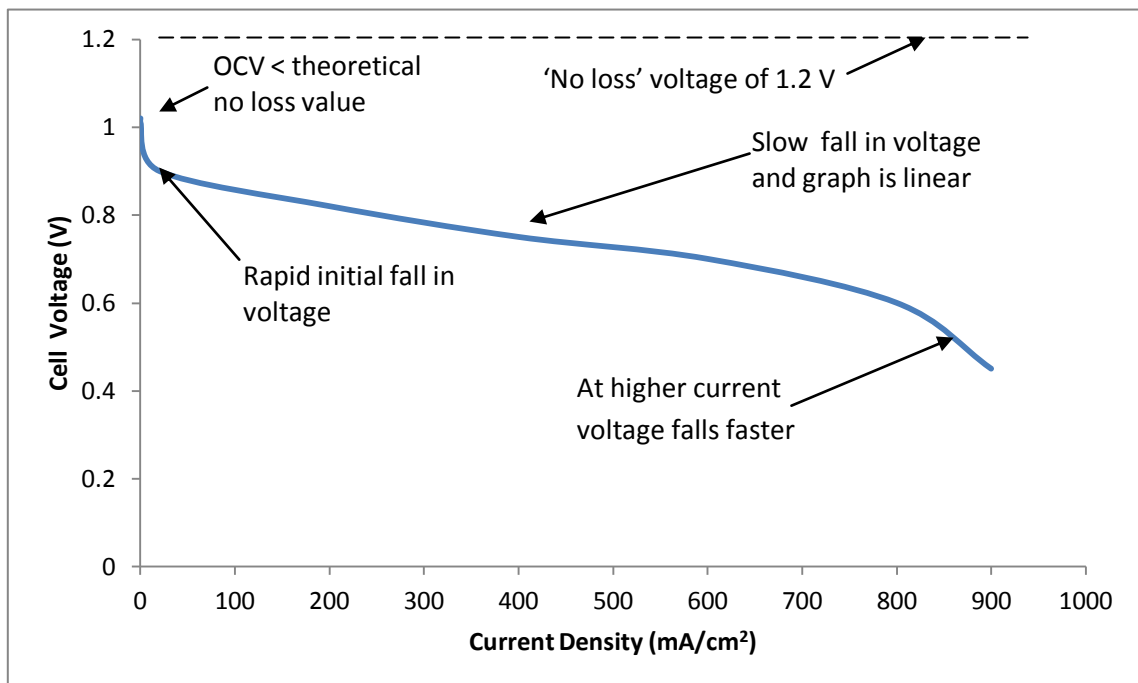


Figure 3.28: The voltage for a typical low temperature, air pressure fuel cell (Larminie and Dicks, 2003).

The voltage/current density graphs of Figures 3.28 and 3.29 characteristic shapes are as a result of four major irreversibilities, which are, activation losses, fuel crossover and internal currents, ohmic losses and mass transfer or concentration losses.

3.13.1 Activation Losses

Activation losses are caused by the slowness of the reactions taking place on the surface of the electrodes. A proportion of the voltage generated is lost in driving the chemical reaction that transfers the electrons to or from the electrode (Larminie and Dicks, 2003).

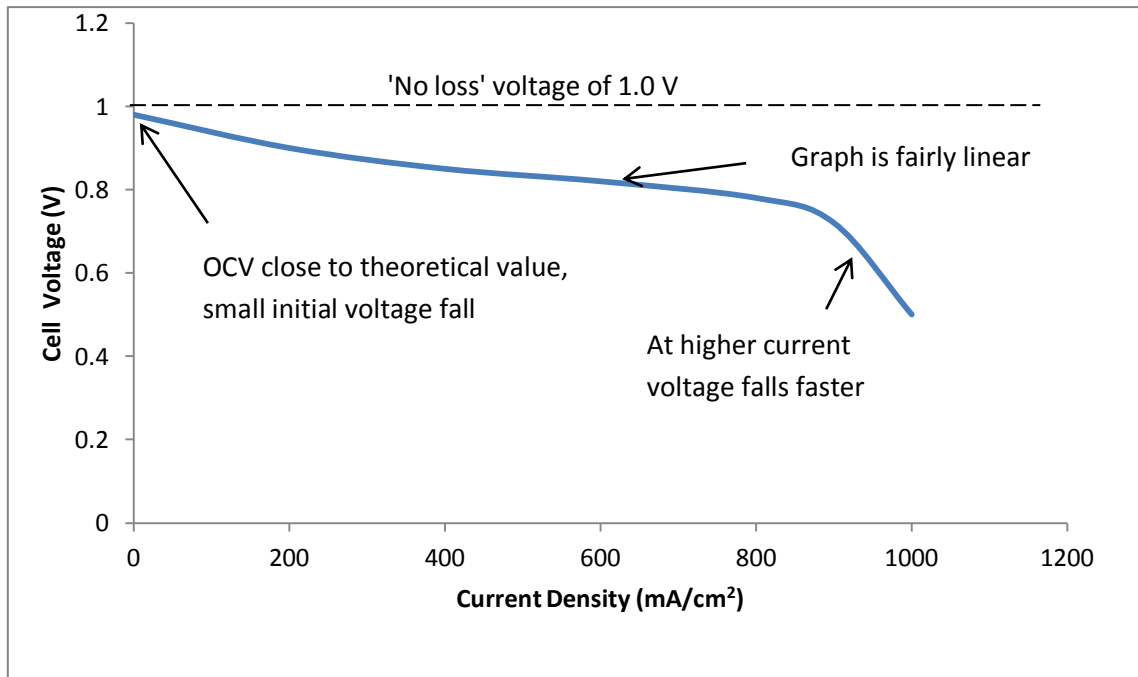


Figure 3.29: The voltage for a typical air pressure fuel cell operating at about 800°C (Larminie and Dicks, 2003).

3.13.2 Fuel Crossover and Internal Currents

In a practical fuel cell some fuel will diffuse from the anode through the electrolyte to the cathode, because of the catalyst, it will react directly with the oxygen, producing no current from the cell. Fuel crossover is the term used for that small amount of wasted fuel that migrates through the electrolyte. The crossing over of one hydrogen molecule from anode to cathode where it reacts, wasting two electrons, amounts to exactly the same as two electrons crossing from anode to cathode internally, rather than as an external current. The internal currents and the fuel crossover are essentially equivalent (Larminie and Dicks, 2003).

3.13.3 Ohmic Losses

Ohmic losses are losses due to the electrical resistance of the electrodes, and the resistance to the flow of ions in the electrolyte. The size of the voltage drop is proportional to the current, by the popular Equation 3.39.

$$V = IR \quad (3.39)$$

In fuel cells the resistance is mainly caused by the electrolyte and the cell interconnections. For fuel cell, the resistance corresponding to 1 cm² of the cell, and by using the symbol r (area-specific resistance (ASR)). The equation for the voltage drop is now given by Equation 3.40, Where i is the current density (mA cm⁻²) and r the area-specific resistance (kΩcm²).

$$\Delta V_{ohm} = ir \quad (3.40)$$

3.13.4 Concentration Losses (Mass Transport)

If at the anode of a fuel cell supplied with hydrogen and during cell operation there will be a slight drop in pressure if the hydrogen is consumed as a result of a current being drawn from the cell. This pressure reduction results from the fact that there will be a flow of hydrogen down the supply ducts and tubes, and this flow will result in a pressure drop due to their fluid resistance. This reduction in pressure will depend on the electric current from the cell (and H₂ consumption) and the physical characteristics of the hydrogen supply system (Larminie and Dicks, 2003).

In a likewise manner, if the oxygen at the cathode of a fuel cell is supplied in the form of air, during fuel cell operation there will be a slight reduction in the concentration of the oxygen in the region of the electrode as the oxygen is extracted. The extent of concentration change will depend on the current being taken from the fuel cell and on physical factors relating to how well the air around the cathode can circulate, and how quickly the oxygen can be replenished. This change in concentration will cause a

reduction in the partial pressure of the oxygen. In both cases, the reduction in gas pressure will result in a reduction in voltage. Equation 3.41 gives the change in voltage caused by a change in hydrogen pressure (Larminie and Dicks, 2003 cited Laurencelle *et al.*, 2001; Kim *et al.*, 1995).

$$\frac{dV}{dP} = \frac{RT}{2P} \quad (3.41)$$

The change in pressure caused by the use of fuel gas in terms of current density is given by Equation 3.42.

$$\frac{dP}{dI} = \frac{RT}{2P} \quad (3.42)$$

Substituting Equation 3.41 into 3.42 gives Equation 3.43.

$$\frac{dV}{dI} = \frac{RT}{2P} \quad (3.43)$$

Equation 3.43 gives the voltage change due to mass transport, for voltage drop Equation 3.44 is appropriate.

$$\frac{dV}{dI} = \frac{RT}{2P} \quad (3.44)$$

3.14 Summary

The thermochemical process of choice in this research for the production of carbon for the direct carbon fuel cell (DCFC) is the conventional slow biomass pyrolysis. The process is able to yield a high amount of chars, gases and liquids but the main focus is the char produced which is the solid carbon that can power the DCFC. The configurations of the DCFC proposed in this research consist of the molten carbonate and solid oxide fuel cell electrolyte systems. The charge carrier ions are carbonate ion, CO_3^{2-} , and oxygen ion (O^{2-}) moving from cathode to anode. An interesting feature of the configuration is that the depletion of carbonate ion and oxygen ion from the cathode makes it necessary to recycle CO_2 from anode to cathode.

Chapter Four

Experimental

4.1 Introduction

This chapter give the descriptions of the various experimental works carried out during this research. It gives the names of the apparatus and equipment used to achieve the experimental purpose and some diagrams of the equipment and setup stands. The mechanical and thermochemical preparation of the biomass are discussed. The ultimate, proximate and calorific value evaluation procedures are presented for the biomasses. X-ray diffraction and particle size analysis using Malvern mastersizer are also discussed along with the ball milling of the biomass carbons. The design and assembling of the DCFC are covered along with the preparation of the carbonate electrode assembly, carbon fuel and the solid oxide electrode assembly.

4.2 Biomass Preparation and Analysis

The biomass samples were supplied by different companies. The samples were supplied in straws and chips and these were chopped into smaller pieces before grinding. The grinding was done using the Cross Beater Mill (Model 16-150, Glen Creston Limited, England) with a sieve size of 2.0 mm. The chopped biomass was put into the mill bit by bit for effective grinding and the process was repeated three times to obtain effective particle size. Figures 4.1 to 4.6 show some of the biomass samples before and after grinding.

4.2.1 Proximate Analysis of Biomass

The proximate analysis of biomass is important because it enable us to determine the chemical composition of the various biomass used in this research and provide the key to the different combustion characteristics of the biomass. The proximate analysis of biomass composition (by mass) is given in terms of four constituents, namely: moisture content, fixed carbon, volatile matter (the gases emitted during thermal decomposition of the biomass in an inert atmosphere) and ash (inorganic matter left after combustion). The fixed carbon is estimated by difference.

4.2.1.1 Moisture Content Analysis of Biomass

The moisture content analysis was carried out on each of the biomass sample in order to know the level of moisture (water) in the sample. An empty crucible was weighed. About 1.0 g of biomass sample was added gradually to the crucible and the weight and content was measured. The crucible was tapped gently to evenly spread the sample over the bottom of the crucible. The crucible with the biomass sample was placed in a Memmert oven at a temperature of 105°C to 110°C for one hour. The crucible was cooled and reweighed. The percentage moisture was calculated using Equation 4.1.

(4.1)

Where M_1 is the mass of empty crucible, M_2 is the mass of crucible plus sample before heating and M_3 is the mass of crucible plus dried sample.



Figure 4.1: Miscanthus (a) Straws

(b) Ground



Figure 4.2: Spruce wood (a) Chips

(b) Ground



Figure 4.3: Poplar wood (a) chips

(b) Ground



Figure 4.4: Switchgrass (a) Straws

(b) Ground



Figure 4.5: Wheat (a) Straws

(b) Ground



Figure 4.6: Willow wood (a) chips

(b) Ground

4.2.1.2 Ash Content Analysis of Biomass

Ash content analysis gave an indication of the amount of inorganic matter left in the biomass sample after combustion. An empty crucible was weighed. About 1.0 g of biomass sample was added gradually to the crucible and the weight of crucible plus the content was measured. The crucible was tapped gently to evenly spread the sample over the bottom of it. The crucible was placed in a Carbolite furnace (AAF 1100). The sample was heated to a temperature of 750°C and left at that temperature for one hour so that the combustible material could be completely burnt. The crucible was removed from the furnace and allowed to cool to room temperature. The crucible was reweighed and the percentage ash was calculated using Equation 4.2.

(4.2)

Where M_1 is the mass of empty crucible, M_2 is the mass of crucible plus sample before heating and M_3 is the mass of crucible plus residue.

4.2.1.3 Volatiles Content Analysis of Biomass

Volatile content analysis gave a measure of the gas that was emitted during the thermal decomposition of the biomass in an inert atmosphere. An empty crucible was weighed. 1.0 g of biomass sample was added gradually to the crucible and the weight of crucible plus the content was measured. The crucible was tapped gently to evenly spread the sample over the bottom of it. The crucible was covered and placed in a Carbolite furnace (Eurotherm panel) which was already preheated to a temperature of 950°C and left at that temperature for seven minutes. The crucible was removed from the furnace and allowed to cool to room temperature. The crucible was reweighed and the percentage volatile was calculated using Equation 4.3.

(4.3)

Where M_1 is the mass of empty crucible, M_2 is the mass of crucible plus sample before heating, M_3 is the mass of crucible plus residue after heating and M_c is the percentage of moisture content.

4.2.1.4 Fixed Carbon Analysis of Biomass

The fixed carbon analysis gave a measure of what is left of the biomass when moisture, volatiles and ash have been removed. The fixed carbon was determined by the application of Equation 4.4.

(4.4)

4.2.2 Ultimate Analysis of Biomass

In the ultimate analysis a given biomass sample was burnt in pure oxygen in a furnace at a temperature of 1350°C. The carbon and the hydrogen in the biomass were oxidised completely to carbon dioxide and water. Any chlorine and sulphur dioxide released were retained within the apparatus by absorption onto silver gauze. The CO₂ and water pass out of the apparatus into a sequence of absorbers. Water was absorbed into magnesium perchlorate and the CO₂ by soda asbestos. The hydrogen and carbon released were determined by measuring the increase in the weight of the absorbers. The values were corrected for moisture content in the biomass sample by making separate determination of the moisture content (same as in the proximate analysis). In ultimate analysis the biomass composition (by mass) is given in term of the chemical elements that make up the biomass mainly carbon, hydrogen, nitrogen, sulphur and oxygen.

4.2.2.1 Carbon and Hydrogen Contents

The carbon and hydrogen contents of the biomass were determined to obtain the percentage weight of carbon and hydrogen present in a given sample. The Carbolite furnace was heated to and kept at a temperature of 1350°C and the silver gauze was maintained in the right position. The absorption train to the combustion tube was connected and oxygen was passed through the system at 18 litres/hour for 10 minutes. The absorption train was then disconnected from the combustion tube and connected to the air purification train. Purified air was drawn through the train at a rate of 12 litres/hour for 10 minutes. The absorption train was disconnected; each absorber was wiped with a clean dry cloth. The absorbers were allowed to cool to room temperature and then weighed.

0.5 g of the biomass sample was weighed into a clean, dry sample boat. The sample was spread evenly over the bottom of the boat and the absorption train was reconnected. The rubber stopper carrying the silica was removed and the sample boat inserted into the combustion tube to such a position that was central (240 mm) from the centre of the hottest zone (first mark on the push-rod). The silica pusher was fully withdrawn and the rubber stopper was replaced and oxygen was passed at 18 litres/hour. At the end of each four one-minute periods, the boat was pushed forward by 40 mm while withdrawing the silica pusher each time to avoid it being melted in the furnace. The boat was allowed to remain in the hottest part of the furnace tube for a further 5 minutes. The absorption train was disconnected, purge with purified air, wiped, cooled and reweighed. The percentage weight of the carbon in the biomass was evaluated using Equation 4.5.

_____ (4.5)

Where M_1 is the mass of empty boat, M_2 is the mass of boat plus sample before heating, M_3 is the initial mass of soda asbestos absorber and M_4 is the final mass of soda asbestos absorber. The percentage weight of hydrogen in the biomass was evaluated using Equation 4.6.

_____ (4.6)

Where M_5 is the initial mass of water absorber, M_6 is the final mass of water absorber, M_{Al} is the mass of moisture in the aluminium oxide and M_c is the percentage moisture content of biomass.

4.2.3 Calorific Value (CV) Determination of Biomass

The calorific value of a given biomass is the heat released by the biomass when it is completely burnt at standard pressure (1 bar) and reference temperature (298 K). The higher the calorific value of a given biomass, the greater the heat released. An empty crucible was weighed. 1.0 g of biomass sample was added gradually to the crucible and the weight of crucible plus the content was measured. The crucible was tapped gently to evenly spread the sample over the bottom of it. A 10 cm piece of nichrome wire was stretched between the electrodes of the bomb cap and the bomb cap was placed on a special stand. The crucible was placed in its holder and it was ensured that the wire nearly made contact with the sample. The bomb was assembled while making sure that the sealing ring was correctly positioned in its groove within the bomb cap and also it was ensured that both metal surfaces were cleaned and then the metal cap was tightened by hand. The F1 button on the LED display of the bomb calorimeter was pressed and 2 litres of water was decanted from the cooler circuit into the calorimeter.

The filling tube to the bomb was connected while aligning the hole in the filler cap with the hole in the bomb cap. Then the oxygen cylinder was turned on through the valves and Oxygen fill was pressed on the LED display of the calorimeter. After the display indicated that the bomb was filled with sufficient oxygen the filling was removed and a tommy-bar was used to lift the bomb into the calorimeter. The calorimeter vessel was placed inside the calorimeter in such a way that the handle was not impeding the stirrer. The bomb was then placed inside the calorimeter vessel and two black electrodes were attached to the bomb cap. The lid of the water jacket was lowered carefully. The standby light was checked to be on and then the start button was pressed on the LED display and the necessary details were entered into the system. Finally the bomb was removed from the calorimeter and examined for complete combustion. The final temperature increment was given by the calorimeter and the calorific value was computed using Equation 4.7.

(4.7)

4.3 Pyrolysis of Biomass

The pyrolysis of biomass helps to produce carbon-rich product from the various biomasses which are needed to power the direct carbon fuel cell. An empty ceramic boat was weighed, and then the biomass was put inside the boat and reweighed. The biomass sample was dried at 100°C for 1 hour before pyrolysing using Lenton cylindrical furnace (England, Figures 4.7-4.10). The pyrolysis was carried out in the furnace using a particle size range of 0.50 to 1.00 mm. In each run of the experiment 6.0 g of feed sample was fed into the reactor. The pyrolysis experiment was conducted at a temperature of 400°C with a heating rate of 7°C/min. On reaching the pyrolysis temperature of 400°C, the sample was held for 30 min at this temperature to complete the pyrolysis process (the pyrolysis process took 70 min.). After the pyrolysis and on cooling, the reactor was opened and the solid product (char) weighed. The char was finely ground by hand milling using mortar and pestle. Nitrogen gas was used to purge the system during and after the experiment using 2000 cm³/min of flow rate. The temperature profile measured for the Lenton Furnace was investigated and the results are presented in Chapter 5. The furnace was initially programmed as follows:

FR= N₂ flow rate = 2000 cm³/min

R1= Ramp rate 1 = 10°C/min

L1= Target set point 1= 100°C

D1= Dwell time 1 = 60 min

R2= Ramp rate 2 = 7°C/min

L2= Target set point 2= 400°C

D2= Dwell time 2 = 30 min

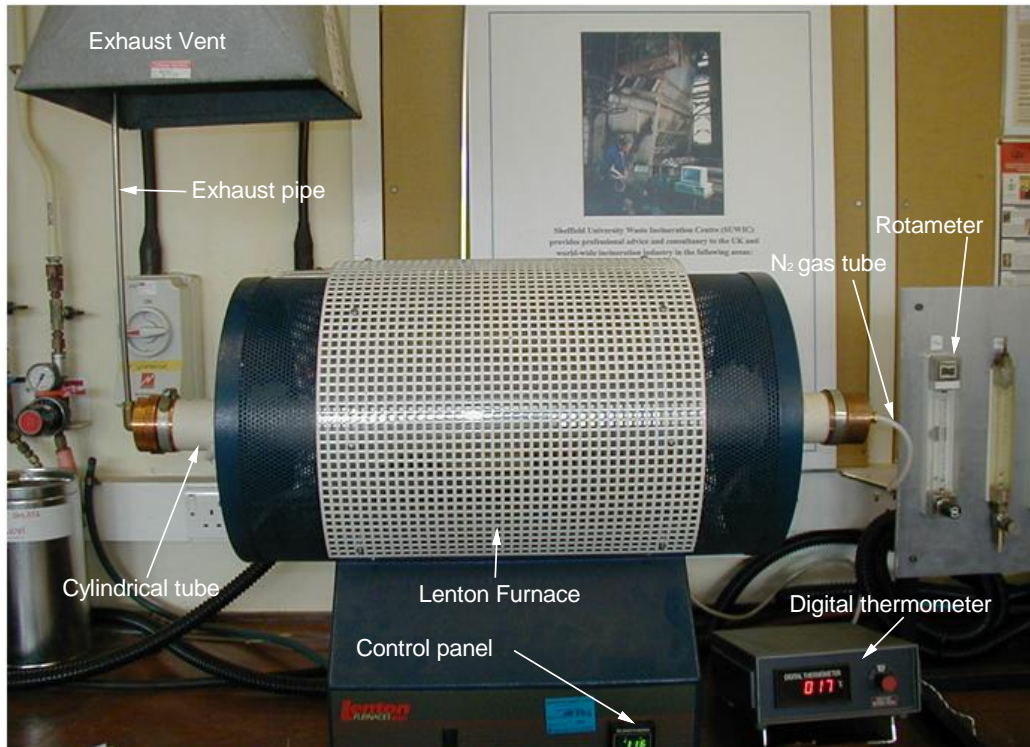


Figure 4.7: Lenton cylindrical furnace used for pyrolysis (Model LTF 16/50/180)

After the temperature profile of the furnace was taken, and on careful observations of the product of the pyrolysis process, there was a need to modify the Lenton furnace to give better temperature profile and pyrolysis product. The modified furnace is shown in Figure 4.8. The pyrolysis experiment were then repeated at a temperature of 800°C using a nitrogen flow rate of $4000\text{ cm}^3/\text{min}$ and the furnace was programmed as below:

FR= N_2 flow rate = $4000\text{ cm}^3/\text{min}$

R1= Ramp rate 1 = $10^{\circ}\text{C}/\text{min}$

L1= Target set point 1= 100°C

D1= Dwell time 1 = 60 min

R2= Ramp rate 2 = $7^{\circ}\text{C}/\text{min}$

L2= Target set point 2= 900°C

D2= Dwell time 2 = 30 min.

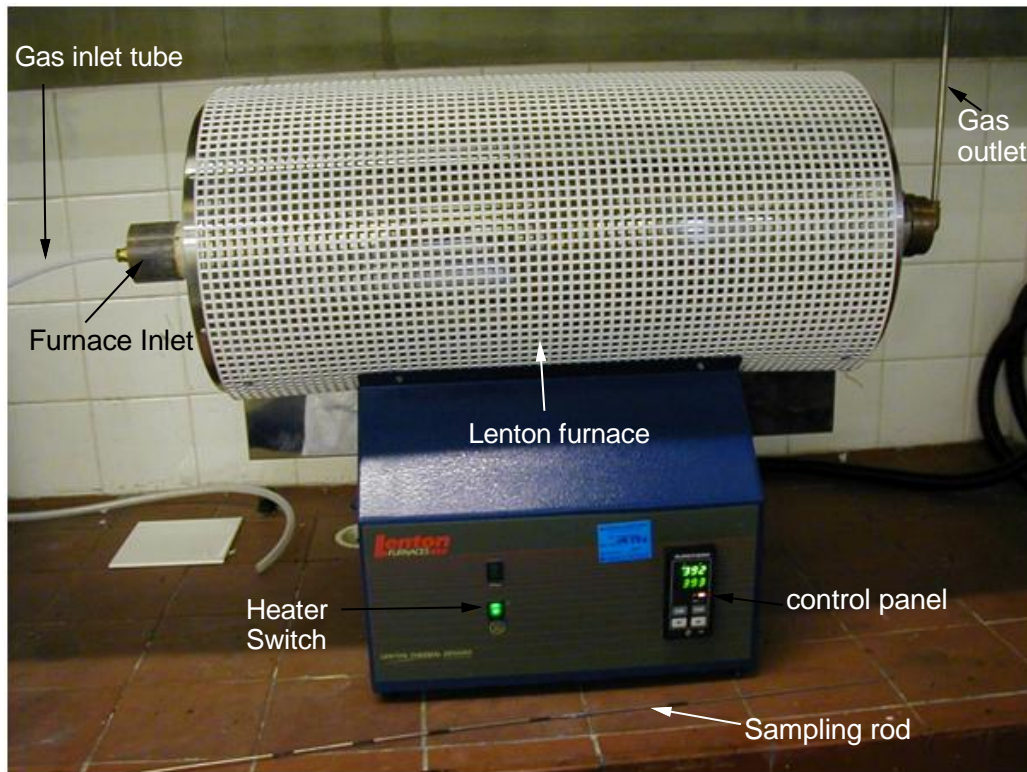


Figure 4.8: Modified Lenton cylindrical furnace used for pyrolysis (Model LTF 12/75/610)

Further modifications were needed on the cylindrical furnace to accommodate the liquid product from the biomass during the pyrolysis. A condenser was designed and connected to the furnace with an outlet at the base to collect the liquid product of the reaction. The modified furnace and condenser are shown in Figures 4.9 and 4.10.

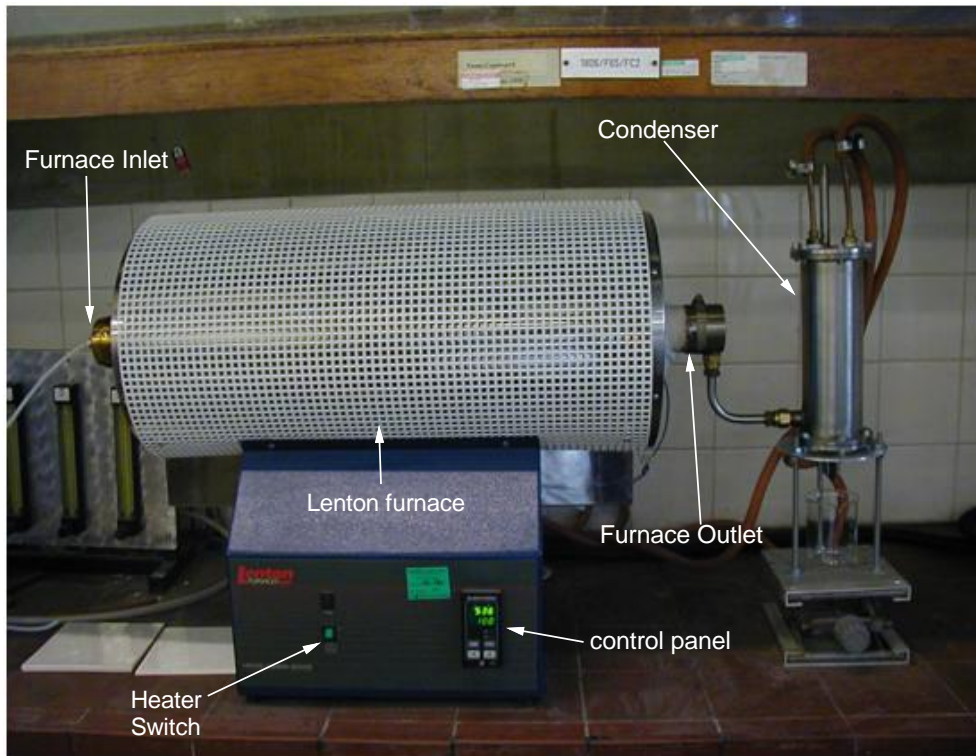


Figure 4.9: More modification to Lenton furnace incorporating a condenser

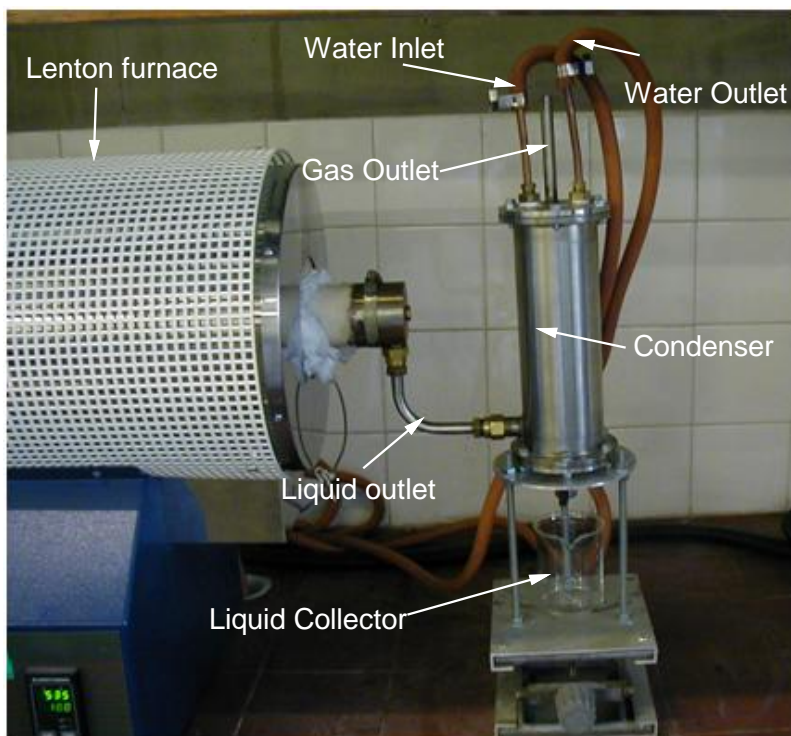


Figure 4.10: Components of the condenser

4.4 X-Ray Diffraction (XRD) Analysis

X-ray diffraction analyses carried out were important in the determination of the structure of the various biomass carbons used in this research. 1.0 g sample of the carbon was put into a circular metal disc. The disc was then placed on a spring cover which was clamped on to a bigger cylindrical disc. The mechanism was such that once the sample was clamped to the bigger disc it holds the sample firmly in place and ready for X-ray diffraction measurement. The sample was placed in the X-ray machine (Siemens D500 X-Ray Diffractometer System) and the computer linked to the X-ray machine was readjusted for fresh reading. The X-ray machine shuttle was switch on. The computer reading was adjusted between 0 and 80 degree.

4.5 Particle Analysis with Malvern Mastersizer

The biomass carbon particle sizes were measured using the Malvern Instrument (Mastersizer S standard bench MAM 5004). 0.5 g of the carbon was dispersed in distilled water and fed through the dispenser unit. The control panel was used to regulate the speed of the pump to 2610 RPM. The computer attached to the unit was used to capture the data of the dispersed solution being analysed in the Malvern Mastersizer. Figure 4.11 show the Malvern Mastersizer and some output results are presented in Appendix A.

4.6 Ball Milling of Biomass Carbon

In order to get smaller particles after the hand milling of the biomass carbon, the Fritsch Planetary mills was used. The carbons were milled in a stainless steel bowl using stainless steel balls (diameter of 1 mm and 5 mm) at 250 RPM for 40 minutes.

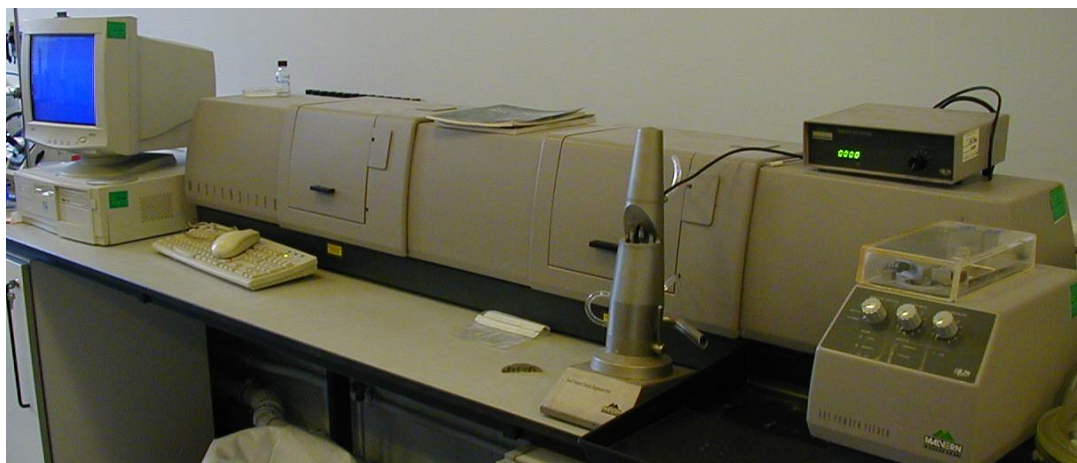


Figure 4.11: Malvern Mastersizer used for particle size analysis.

4.7 Design and Assembling of the Direct Carbon Fuel Cell (DCFC)

The design of the MDCFC followed the pattern suggested by Cooper and co-workers (Cooper *et al.*, 2004). The cathode of the DCFC was made up of nickel mesh (after several tests the nickel mesh was changed to gold mesh for better performance). The anode was made up of a porous nickel mesh with a thickness of 1.5 mm, diameter of 25 mm and 40% void, which provided the conductive surface for effective carbonate ions transportation. After several tests the porous nickel mesh was changed to gold mesh. The electrolyte was a carbonate mixture of Li_2CO_3 and K_2CO_3 , mixed in the ratio of 38 mol.% Li_2CO_3 and 62 mol.% K_2CO_3 (Cooper *et al.*, 2004). Gold wires were used as electrical contacts on the electrode (anode and cathode).

4.7.1 Preparation of Carbonate Electrolyte using ZrO_2 Cloth (ZYW-30A)

Carbonate electrolyte was prepared using zirconia cloth (ZrO_2) and molten mixture of K_2CO_3 and Li_2CO_3 to provide the medium for electrochemical reaction in the MDCFC. 12.4 g of K_2CO_3 granule was mixed with 7.6 g of Li_2CO_3 powder in a ceramic crucible making 20 g of the mixture (Cooper *et al.*, 2004). The mixture was thoroughly stirred using a stirrer. The bursen burner was prepared for melting the mixture. Bit by bit the sample was put into the stainless steel bowl on top of the burner and then stirred

continuously (Figure 4.12). The temperature of the heating was checked using a K-type Digital thermocouple inserted into the mixture from time to time. The thermocouple was connected to a reader which gave the prevailing temperatures. A melting temperature of 550°C was observed.

The ZrO₂ cloth (ZYW-30A) was cut into diameter of 25 mm. The zirconia cloth was then dipped into the melted mixture of potassium carbonate and lithium carbonate to saturate it. The saturated cloth was removed and placed on a flat surface to cool. The carbonate mixture coating on the zirconia cloth was thick, this was reduced by scrapping off the excess layer using Dremel 300 multi-tool accessories.



Figure 4.12: Experimental setup for saturation of ZrO₂ cloth (ZYW-30A).

4.7.2 Preparation of Carbon Fuel Particles

The fuel used in the DCFC was a mixture of carbon and carbonate, carbon was the actual fuel but it was mixed with carbonates which become molten at the operating temperature of the DCFC and permit the quick electrochemical reaction in the cell. The

carbon/carbonate salt mixture was prepared consisting of biomass carbon (15 wt. %), lithium carbonate (46.6 wt.%) and potassium carbonate (53.4 wt. %)(Cooper, 2008; Cooper *et al.*, 2004). 16.02 g of potassium carbonate (K_2CO_3), 13.98 g of lithium carbonate (Li_2CO_3) and 4.5 g of biomass carbon powder were measured. The carbonate mixture (Li_2CO_3/K_2CO_3) was thoroughly mixed together and dissolved in 25 ml of distilled water to ensure proper mixing. The mixture was placed in the oven at 100°C for 4 hours to dry off the moisture. The carbonate mixture was finely ground and mixed with the carbon powder to form the fuel particle for the fuel cell.

4.7.3 Behaviour of Carbon Fuel Particles (Carbon/Carbonate Mixture)

The behaviour of the carbon/carbonate mixture was tested in order to predict the behaviour of the mixture during its operation in the DCFC. 1.0 g of the carbon/carbonate mixture was weighed and placed in a crucible. This mixture was heated using a bursen burner to a temperature of 450°C. It was observed that the mixture began to melt as the temperature increases, some of the fuel particles were beginning to ignite as the temperature increased.

4.7.4 Assembling of the DCFC

The assembling of the fuel cell was done after the various preparations of the anode, cathode and electrode assembly. The electrochemical cell units were placed between the two ceramic cylindrical tubes. Gold wire contacts were used at both the anode and cathode. Figure 4.13 shows the various parts of the DCFC. Figure 4.14 show the assembled DCFC. Figures 4.15 and 4.16 give the schematic components and dimensions of the DCFC.

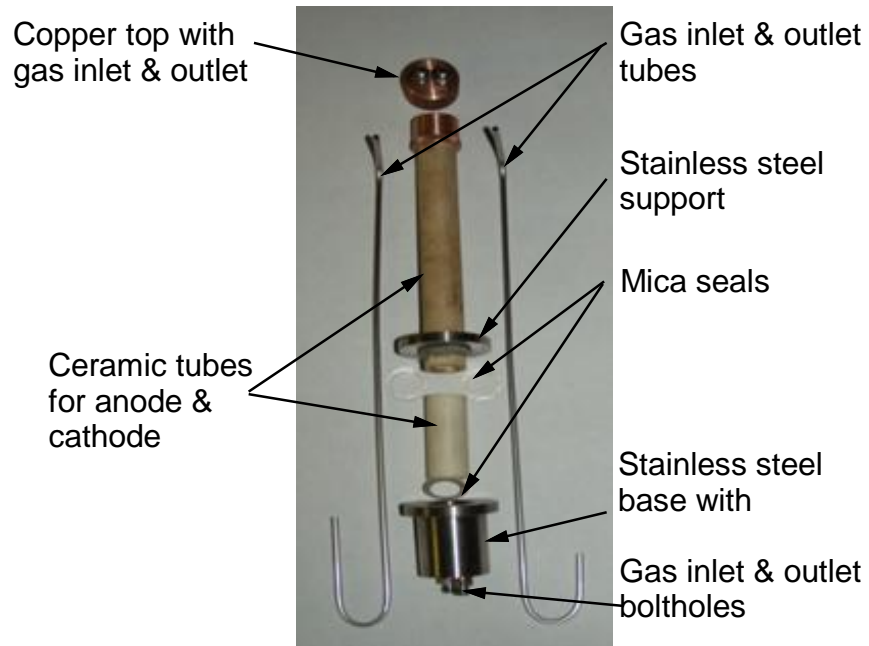


Figure 4.13: Components of the DCFC

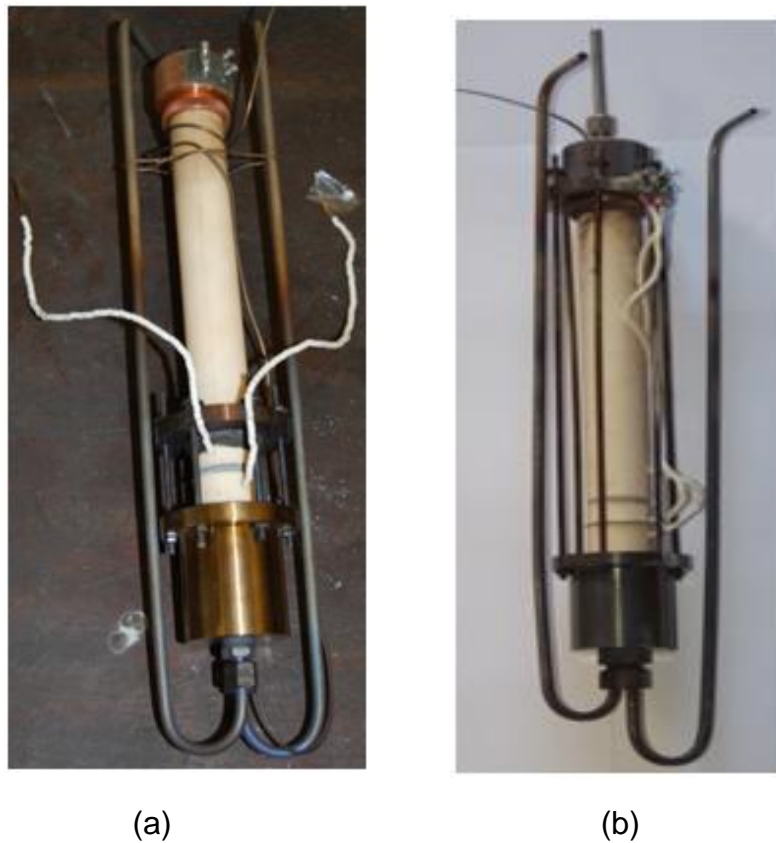


Figure 4.14: (a) Initial and (b) modified direct carbon fuel cell designs.

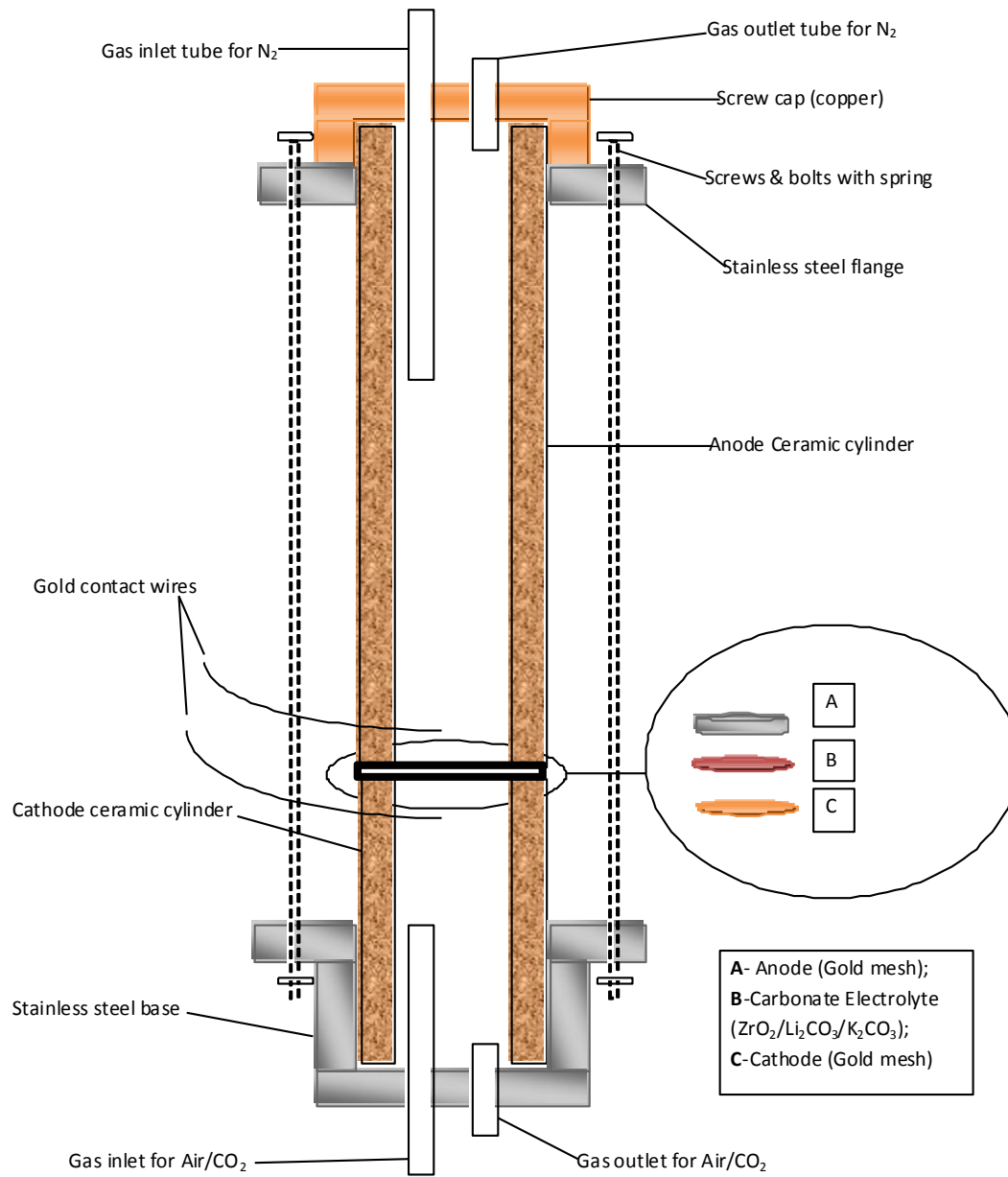


Figure 4.15: Schematic of the direct carbon fuel cell with overall height of 280 mm.

The DCFC was located between the two ceramic cylinders and mica seals were used to give a compressive hold around the DCFC, helping to prevent the leakage of gases and fuels from the system. Another mica seal was placed at the base to tolerate any expansion of material when the DCFC was placed in the furnace. Gold wire contacts were passed through the anode and the cathode as shown in Figure 4.17.

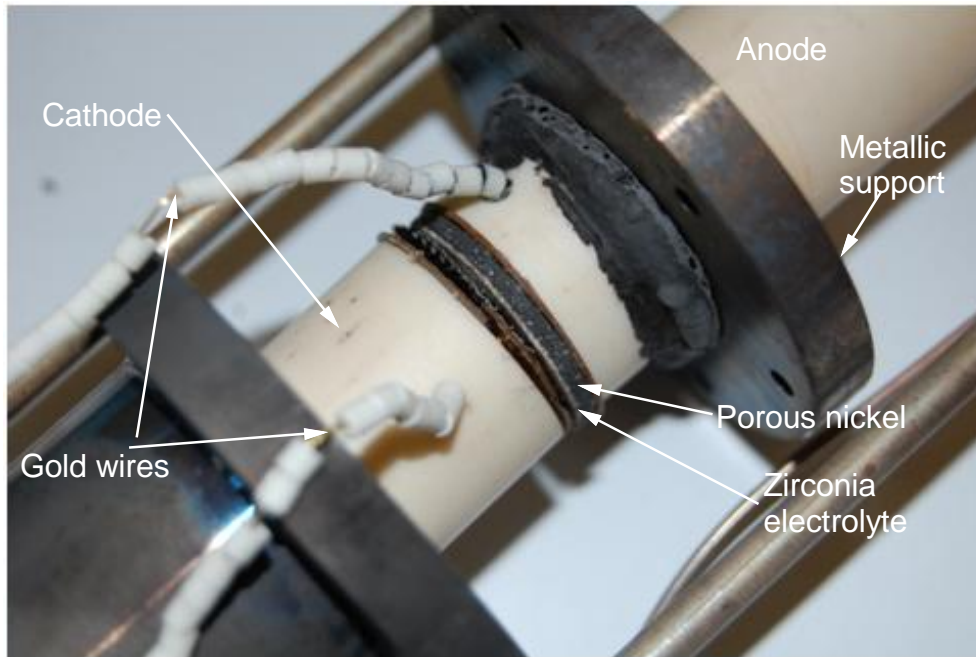


Figure 4.17: DCFC appearance after initial performance in furnace

The DCFC system was tightened and secured by using springs, nuts and bolts, these provided the tension and support needed to hold the DCFC in the furnace. The wire connectors were insulated using tiny white ceramic beads (Figure 4.17). A multimeter was used to test for electrical continuity in the anode and cathode side of the fuel cell. The connection was such that the probe was placed on the exposed side of the cathode and on the gold wire coming out of the cathode, and the same was done also on the anode side. Also the resistance between the electrodes were measured to check the electrical isolation of the two.

Figure 4.14 shows the initial and the modified design of the DCFC. The first one provided a firm compression for the electrode assembly, but on heating inside the furnace the springs lost their firmness and the contacts could not be guaranteed during fuel cell operation. Figure 4.14b gives the modification done to the DCFC in which the bolts and the steel plates were moved toward the top of the ceramic tube. In this case the electrode assembly contacts within the fuel cell could be guaranteed during operations.

2.0 g of the carbon/carbonate mixture was put through the anode side of the DCFC system. The connections of the electrical components were done by connecting the electrodes to the voltmeter. A thermocouple was connected through the cathode side in the case of the MCDCFC and anode side for SODCFC to monitor the temperature of the system. Before the fuel cell could be ready for testing, gas feeds were also connected to the system. Nitrogen gas was connected at the top inlet to the anode (to purge the system from CO₂ produced). Air/CO₂ was connected to the bottom inlet for the purpose of removing the gases produced at the surface of the cathode thereby ensuring adequate oxidant for the half-cell electrochemical reaction. For SODCFC only air was connected to the cathode.

4.7.5 Preparation of the SODCFC button cells

Button cells for the solid oxide electrolyte direct carbon fuel cell (SODCFC) were obtained from FuelCell Materials Ltd. (Ohio, USA). The button cells were 25 mm in diameter. The anode side consist of nickel oxide/ZrO₂ and the cathode consists of Lanthanum Strontium Manganese (LSM). These had to be subjected to high temperature operations to reduce the nickel oxide to nickel cermet. The furnace was set to 900°C with a heating rate of 10°C/min. Hydrogen gas (100 cm³/min, 5%) was introduced at 800°C to help in the reduction while nitrogen gas was introduced at 300°C to purge the furnace. The H₂ gas line was purged several times before connecting into the furnace to remove any air in the pipe. The button cells were left in

the furnace for one hour at 900°C, with hydrogen and nitrogen gases running, the furnace was then switch off with the gases running. Hydrogen gas was switched off at 800°C while the nitrogen was switched off at 300°C. Gold mesh was bonded on each side (to serve as the current collector) of the button cells using silver ink. It was then placed in the furnace at 900°C for 20 minutes to allow silver ink to melt and form a good bond then cooled down as before with the gases. On cooling LSM ink was spread over the cathode side to bridge the gold mesh and the LSM electrolyte side then placed in a furnace at 100°C for 20 minutes to dry. The anode side was spread with nickel ink over the gold mesh to bridge it with the anode electrolyte side and also place in the furnace for 20 minutes at 100°C. On cooling the button cells were used as the electrode assembly of the SODCFC.

4.7.6 Performance Testing Setup of the DCFC

Figures 4.18 to 4.21 show the complete DCFC stand, showing the digital thermocouple, resistor box, voltmeter, furnace in which the DCFC was heated and the various connections for the gases. With all these in their right places and in order to prevent any rapid expansion of the cell, the furnace was heated up gradually at 10 °C/min. When the MDCFC temperature was at 250°C, nitrogen gas was introduced through the anode at a rate of 200 cm³/min to purge it. At a temperature of 350°C the air/CO₂ mixture was released through the cathode at a rate of 1500 cm³/min for air, and 600 cm³/min for CO₂. For the SODCFC nitrogen was at 500 cm³/min and air at 1000 cm³/min. The DCFC was heated up to a temperature of 800°C while measuring the voltage outputs. After the measurement the furnace was shut down with nitrogen gas running till 300°C. Figures 4.20 and 4.21 show the external and internal sections of the resistor box used to apply different loads on the DCFC. Twelve different resistances were used (1.167 MΩ to 1.2 Ω), the open circuit voltage was taken at the highest resistance. The switch on the box was turned to the next resistance while allowing the voltage to settle down and the reading taken. This was repeated each time for all the resistances and the voltages taken.

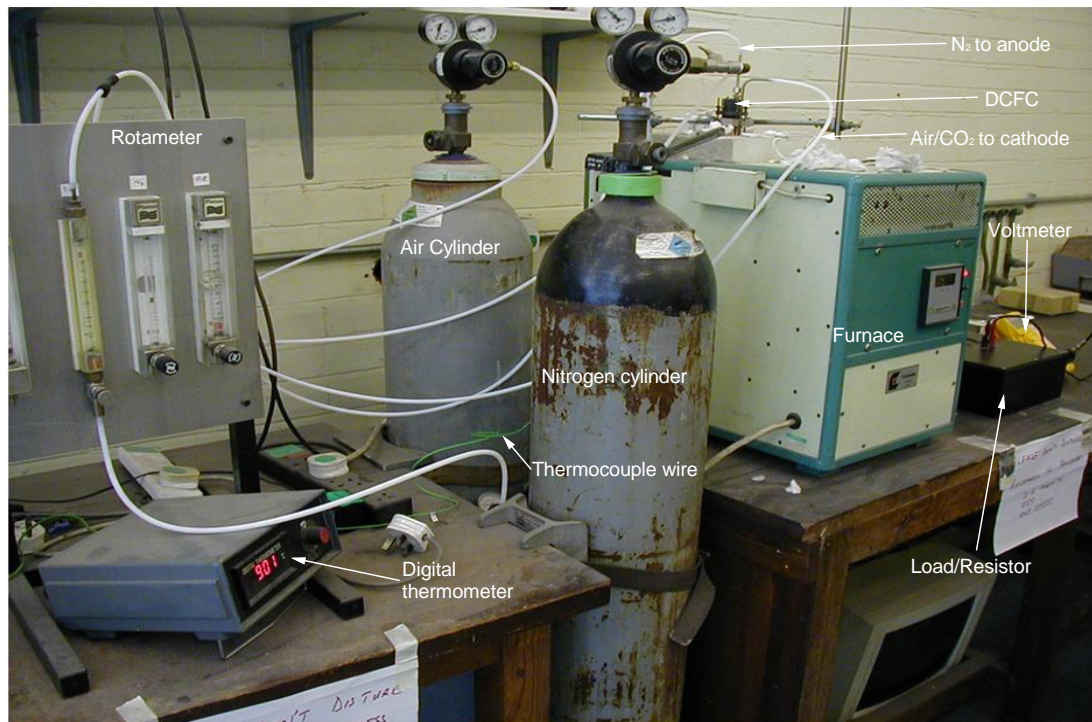


Figure 4.18: Experimental setup for the direct carbon fuel cell

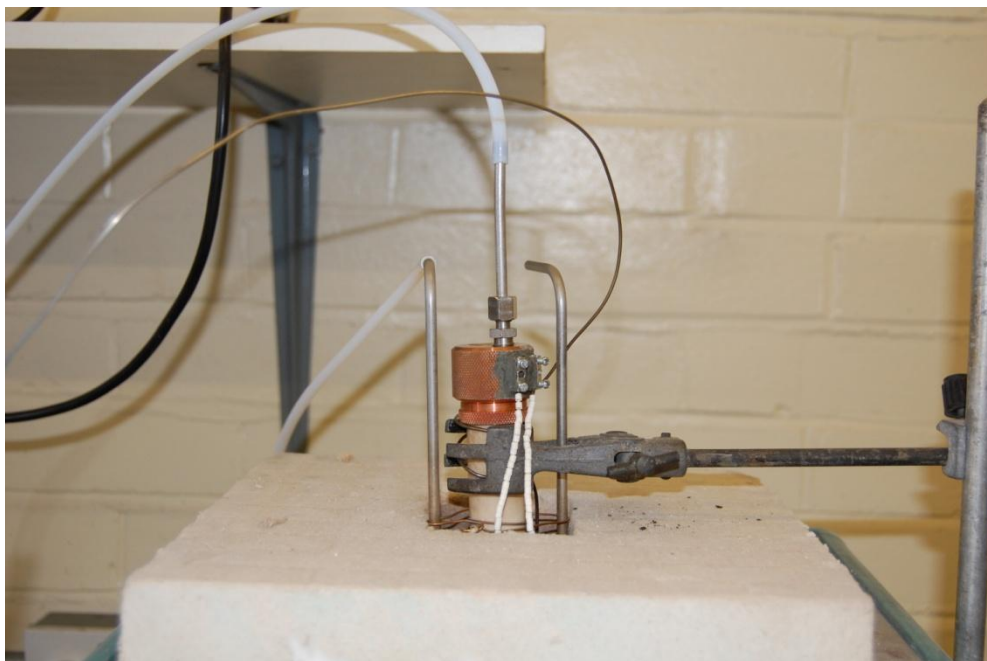


Figure 4.19: Direct carbon fuel cell in operation

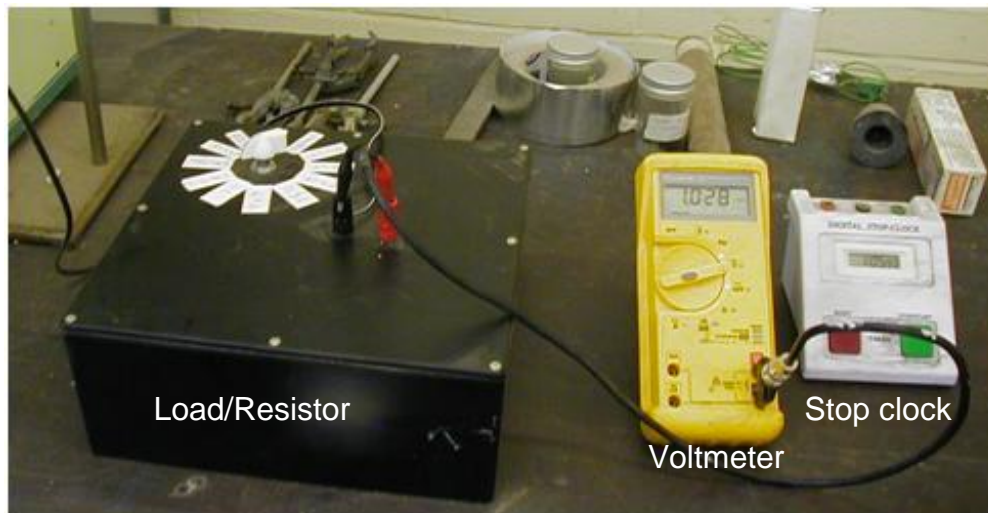


Figure 4.20: Resistor and voltmeter connected to the DCFC

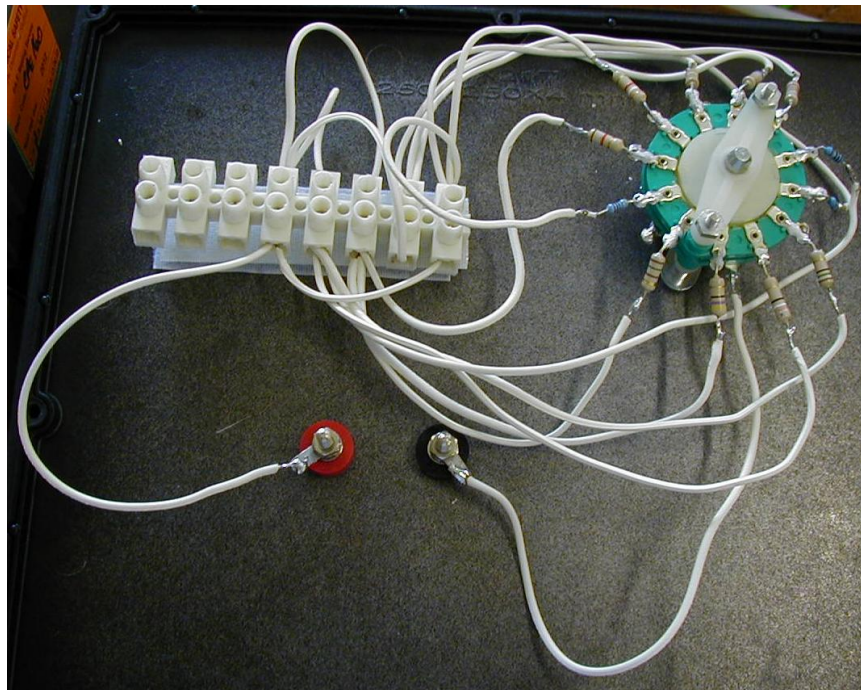


Figure 4.21: Internal section of the resistor box.

Chapter Five

Pyrolysis, XRD, SEM Results & Discussions

5.1 Introduction

This chapter give the descriptions of the various results obtained from pyrolysis, XRD, SEM and others during this research work. The temperature profiles obtained from the Lenton cylindrical furnace used for the pyrolysis of the biomass are briefly described. The proximate, ultimate and calorific values analyses of the biomass and carbon produced through the biomass pyrolysis reactions are presented. For comparison basis two industrial carbon results are also given. Both the hand and ball milled carbon particle analyses are presented here. The X-ray diffraction and scanning electron microscopy for the biomass carbons are given.

5.2 Lenton Cylindrical Furnace for pyrolysis

5.2.1 Lenton Cylindrical Furnace Temperature Profile

The temperature profiles of the Lenton cylindrical furnace (Lenton Model LTF 16/50/180, England) were measured from one end of the cylindrical ceramic tube to the other, that is, from the entrance to the exit point. This was necessary to be able to predict the prevailing furnace temperature at a given set point and position within the furnace. The first sets of profiles are presented in Figures 5.1 and 5.2 and a schematic of the furnace is in Figure 5.3. Results from this temperature profiles shows that the peak in temperature appeared toward the centre of the cylindrical tube. From Figure 5.1 the peak of the temperatures appear at 420 mm to 480 mm for the set points of 400°C and 450°C while at 100°C the peak is around 300 mm. These profiles are very important in order to determine the right positioning of the biomass during pyrolysis. For the drying process when the Lenton furnace is set at 100°C, the samples were placed at about 220 mm from the entrance of the furnace and for pyrolysis at 400°C the samples were placed at 290 mm. For pyrolysis at 800°C the samples were place at 420 mm. The outputs of the pyrolysis reactions from this furnace were not satisfactory as there were some indications that certain parts of the biomass were not well pyrolysed. This necessitated the need to modify and improve the results from the furnace, bringing about the use of the modified Lenton (Model LTF 12/75/610,

England). The temperature profiles were better distributed as shown in Figures 5.4 and 5.5. A schematic of the furnace is in Figure 5.6.

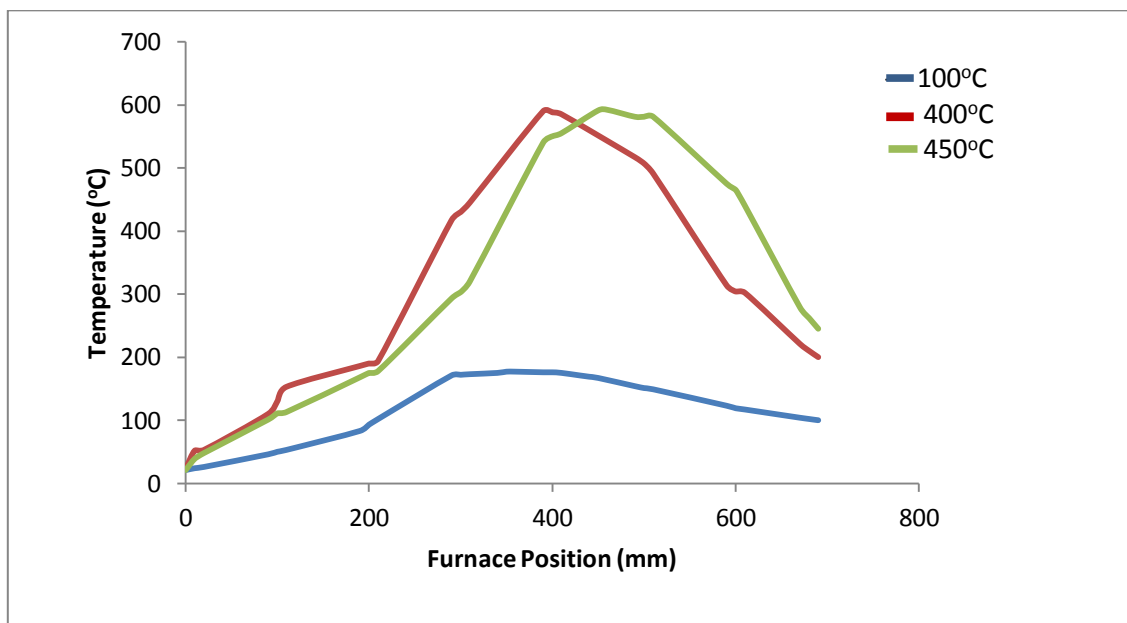


Figure 5.1: Lenton furnace temperature profile at set point of 100-450°C.

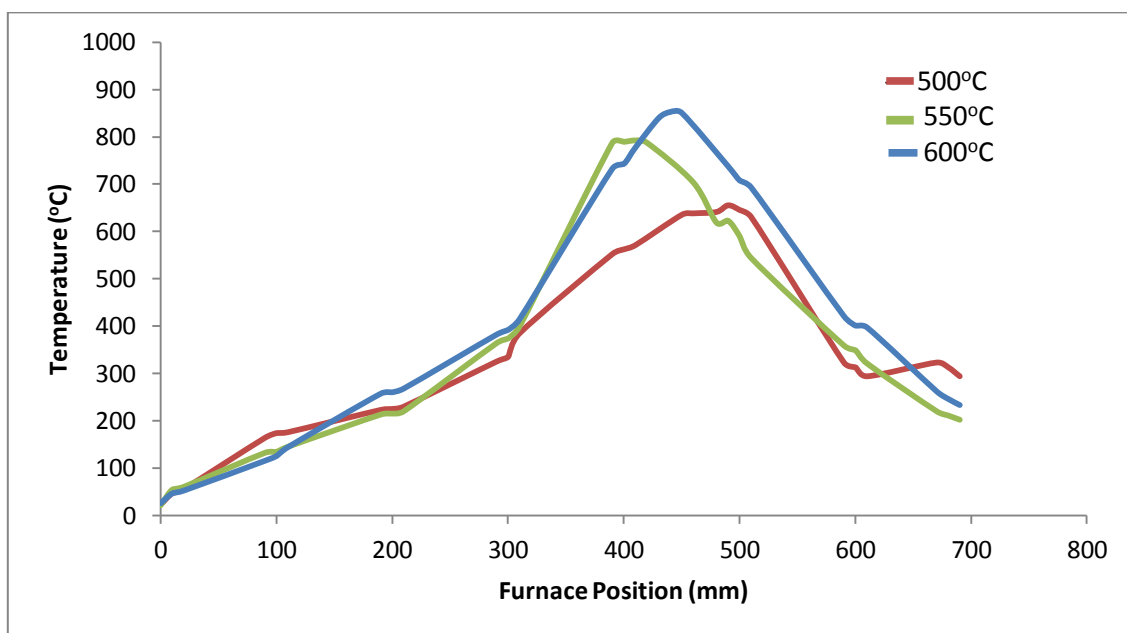


Figure 5.2: Lenton furnace temperature profile at set point of 500-600°C.

Figure 5.3 shows the dimensions and components of the Lenton cylindrical furnace, the original set-up is shown in Figure 4.7 (Chapter 4).

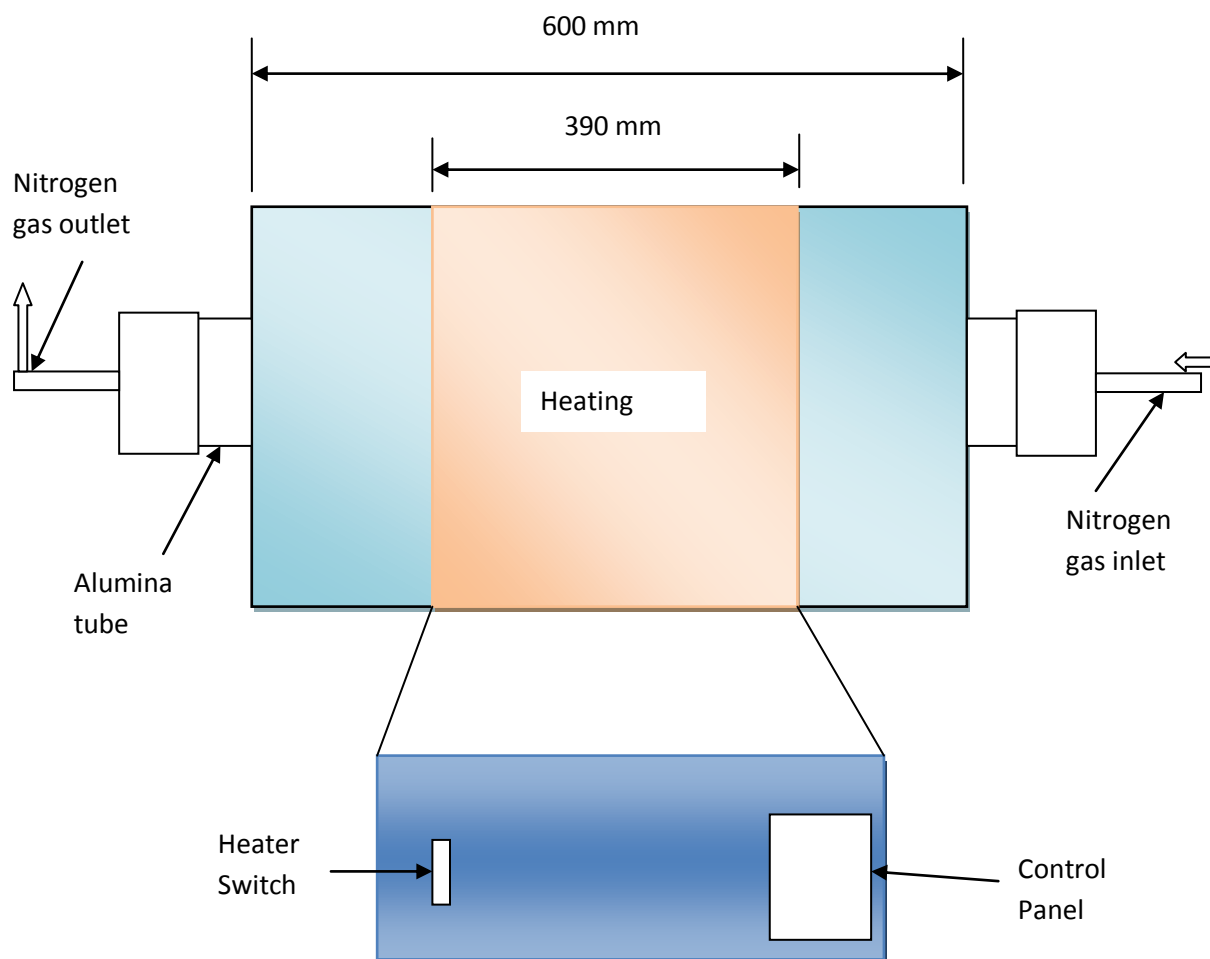


Figure 5.3: Dimensions and components of the Lenton furnace (Model LTF 16/50/180)

5.2.2 Design Modification for Lenton Cylindrical Furnace

Due to unsatisfactory temperature profiles obtained by the old Lenton cylindrical furnace where the temperatures at the peak were distributed over a narrow range, it became necessary to modify the design of the furnace to give a better temperature spread across the furnace. These modifications were carried out and a modified lenton

furnace (LTF 12/75/610) was obtained. The temperature profiles obtained are presented in Figures 5.4 to 5.5.

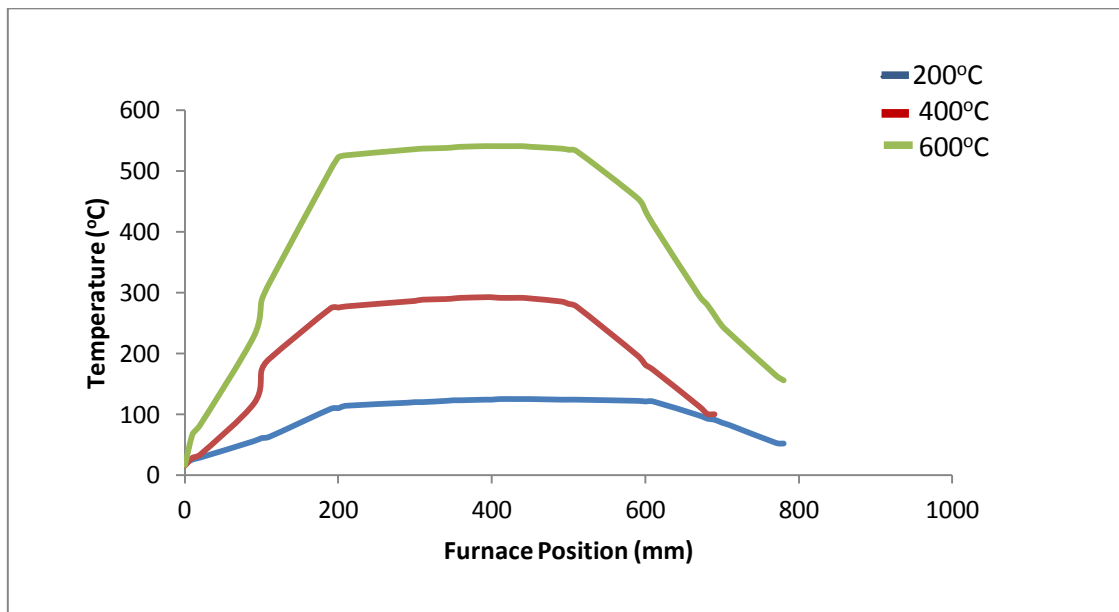


Figure 5.4: Modified Lenton furnace temperature profile at set point of 200-600°C.

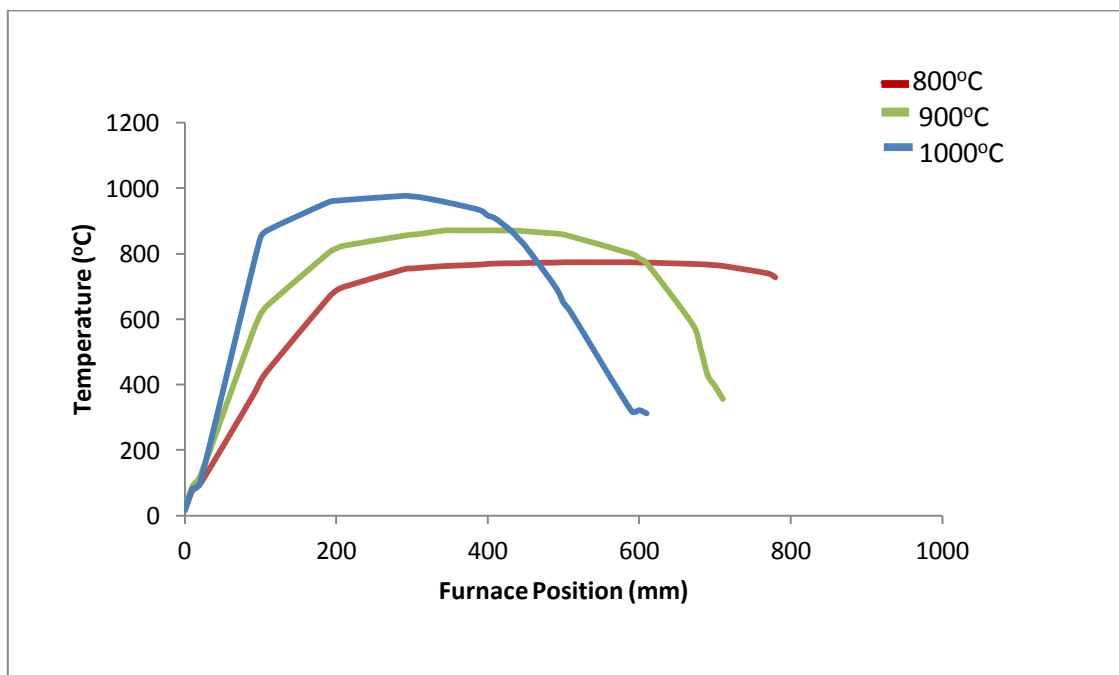


Figure 5.5: Modified Lenton furnace temperature profile at set point of 800-1000°C.

Figure 5.6 gives the dimensions and parts of the modified Lenton cylindrical furnace, the original set-up is shown in Figure 4.8 (Chapter 4).

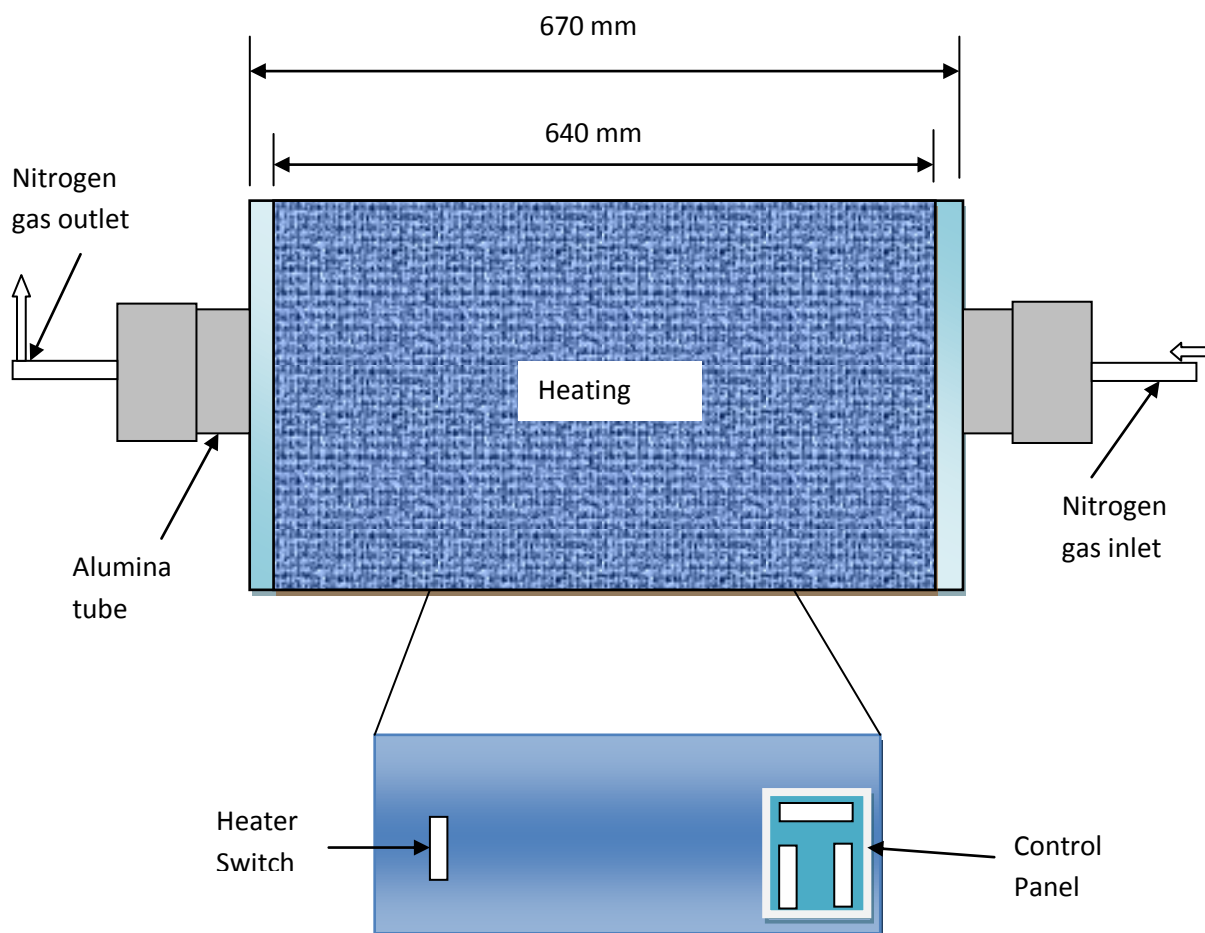


Figure 5.6: Dimensions and components of the modified Lenton furnace (Model LTF 12/75/610)

This design modification also incorporated a condenser (Figures 4.9 and 4.10, Chapter 4) and this was used for the biomass pyrolysis, which gave good results that were reproducible.

5.3 Biomass Analyses

The results of the proximate, ultimate and calorific values analyses on miscanthus straw, wheat straw, switchgrass straw, willow wood chip, spruce wood chip and poplar wood chip are given in Tables 5.1 to 5.7. Table 5.7 gives the comparison between the six biomasses. The moisture contents of the biomass vary between 5.50 wt.% and 7.38 wt.%. Miscanthus and willow wood chip samples have the highest moisture content while poplar wood chip had the lowest content (Table 5.7). The ash content analyses presented in Tables 5.1 to 5.6 show that the wood chips have lower ash contents with 1.61 wt.%, 0.30 wt.%, and 0.85 wt.% for willow, spruce and polar wood chips respectively. The ash content was higher for the energy crops with 2.00 wt.%, 7.12 wt.%, and 7.39 wt.% for miscanthus, wheat and switchgrass respectively. The volatile contents vary between 70.66 wt.% and 79.74 wt.%, with wheat straw having the lowest value at 70.66 wt.% and poplar wood chip having the highest at 79.74 wt.%. The volatile contents of the wood chips were slightly higher than those of the energy crop with the exception of miscanthus (75.84 wt.%).

Table 5.1: Proximate, ultimate and calorific value analyses for ground miscanthus

Analysis	Proximate analysis				Calorific value (CV) MJ/kg	Ultimate analysis	
	Moisture contents wt.%	Ash wt.%	Volatiles wt.%	^a Fixed carbon wt.%		Carbon (C) wt.%	Hydrogen (H ₂) wt.%
1	6.24	2.12	78.95	12.69	19.08	45.88	4.68
2	7.97	1.85	73.88	16.30	19.69	45.50	5.37
3	7.93	2.02	74.70	15.35	17.72	45.88	5.22
Average	7.38	2.00	75.84	14.78	18.83	45.75	5.09

^aby difference

Table 5.2: Proximate, ultimate and calorific value analyses for ground Switchgrass

Analysis	Proximate analysis				Calorific value (CV) MJ/kg	Ultimate analysis	
	Moisture contents wt.%	Ash wt.%	Volatiles wt.%	^a Fixed carbon wt.%		Carbon (C) wt.%	Hydrogen (H ₂) wt.%
	1	7.00	7.12	71.11		14.77	16.91
2	7.09	7.72	71.01	14.18	18.34	42.96	4.90
3	7.03	7.34	73.06	12.57	18.32	42.75	4.71
Average	7.04	7.39	71.73	13.84	17.86	41.90	4.08

^aby difference

Table 5.3: Proximate, ultimate and calorific value analyses for ground wheat straw

Analysis	Proximate analysis				Calorific value (CV) MJ/kg	Ultimate analysis	
	Moisture contents wt.%	Ash wt.%	Volatiles wt.%	^a Fixed carbon wt.%		Carbon (C) wt.%	Hydrogen (H ₂) wt.%
	1	5.93	7.77	71.04		15.26	17.40
2	5.83	7.30	71.17	15.70	18.44	38.73	4.57
3	5.54	6.29	69.78	18.39	19.18	42.36	3.35
Average	5.77	7.12	70.66	16.45	18.34	41.24	4.37

^aby difference

Table 5.4: Proximate, ultimate and calorific value analyses for ground willow wood

Analysis	Proximate analysis				Calorific value (CV) MJ/kg	Ultimate analysis	
	Moisture contents wt.%	Ash wt.%	Volatiles wt.%	^a Fixed carbon wt.%		Carbon (C) wt.%	Hydrogen (H ₂) wt.%
	1	7.30	1.63	75.10		15.97	19.47
2	7.33	1.48	75.49	15.70	19.48	43.98	3.26
3	7.36	1.72	75.31	15.61	18.91	46.21	3.90
Average	7.33	1.61	75.30	15.76	19.29	45.32	3.62

^aby difference

Table 5.5: Proximate, ultimate and calorific value analyses for ground spruce wood

Analysis	Proximate analysis				Calorific value (CV) MJ/kg	Ultimate analysis	
	Moisture contents wt.%	Ash wt.%	Volatiles wt.%	^a Fixed carbon wt.%		Carbon (C) wt.%	Hydrogen (H ₂) wt.%
	1	6.87	0.21	77.18		15.74	19.64
2	7.07	0.30	76.95	15.68	20.03	46.10	6.57
3	7.01	0.39	78.65	13.95	19.34	45.91	5.48
Average	6.98	0.30	77.59	15.12	19.67	46.23	5.43

^aby difference

Table 5.6: Proximate, ultimate and calorific value analyses for ground poplar wood

Analysis	Proximate analysis				Calorific value (CV) MJ/kg	Ultimate analysis	
	Moisture contents wt.%	Ash wt.%	Volatiles wt.%	^a Fixed carbon wt.%		Carbon (C) wt.%	Hydrogen (H ₂) wt.%
	1	5.51	0.81	78.98		14.70	20.37
2	5.56	0.83	79.74	13.87	20.24	45.93	6.05
3	5.44	0.92	80.49	13.15	20.63	45.73	4.39
Average	5.50	0.85	79.74	13.91	20.41	45.94	4.97

^aby difference

The fixed carbon contents obtained by difference were between 13.84 wt.% to 16.45 wt.%. Switchgrass has the lowest value of 13.84 wt.% and wheat straw has the highest value of 16.45 wt.%.

Table 5.7: Comparison of ground biomass analyses

Biomass	Proximate analysis				Calorific value (CV) MJ/kg	Ultimate analysis	
	Moisture contents wt.%	Ash wt.%	Volatiles wt.%	^a Fixed carbon wt.%		Carbon (C) wt.%	Hydrogen (H ₂) wt.%
	Miscanthus	7.38	2.00	75.84		14.78	18.83
Switchgrass	7.04	7.39	71.73	13.84	17.86	41.90	4.08
Wheat	5.77	7.12	70.66	16.45	18.34	41.24	4.37
Willow	7.33	1.61	75.30	15.76	19.29	45.32	3.62
Spruce	6.98	0.30	77.59	15.12	19.67	46.23	5.43
Poplar	5.50	0.85	79.74	13.91	20.41	45.94	4.97

^aby difference

The calorific value (CV) analyses presented in Tables 5.1 to 5.7 show that the wood chips have higher CV of 19.29 MJ/kg, 19.67 MJ/kg, 20.41 MJ/kg for willow, spruce and polar wood chips respectively. The CVs were lower with the energy crop with 18.83 MJ/kg, 18.34 MJ/kg, and 17.86 MJ/kg for miscanthus, wheat and switchgrass respectively. The overall assessment shows that ground poplar wood chip have the highest CV (20.41 MJ/kg) and ground switchgrass have the lowest CV (17.86 MJ/kg). Some of these results from the biomass analyses are in agreement with findings from other researchers (Ryu *et al.*, 2006; Minkova *et al.*, 2000; Jenkins *et al.*, 1998).

5.4 Pyrolysis and Carbon Analyses

5.4.1 Pyrolysis Results from the Old Lenton Furnace

Under the old Lenton furnace, 3.0 g of the biomass samples were pyrolysed at a time using ceramic boats (65 mm long and 25mm wide) at 400°C, 650°C and 800°C. Different results were obtained at 400°C, 650°C and 800°C. At a temperature of 400°C, there were fluctuations in the values obtained; this observation was as a result of placing samples at different position in the furnace. It was observed that the samples positioned at 550 mm from the entrance of the furnace were not fully pyrolysed thus giving higher percentage weight of carbon (partially pyrolysed). Sample at 290 mm from the entrance of the furnace were fully pyrolysed hence giving smaller carbon percentage weight values. The carbon percentage weights for the samples at 550 mm were high and straw like structure still observable in the sample after pyrolysis. Pyrolysis at 400°C took about 60 minute to dry the sample, 40 minutes to reach the pyrolysis temperature (400°C), and 30 minute dwelling at that temperature and took a further 120 minute to cool down to 100°C after pyrolysis reaction. Pyrolysis at 800°C took about 60 minute to dry the sample, 80 minutes to reach the pyrolysis temperature (800°C), and 30 minute dwelling at that temperature and took a further 180 minute to cool down to 100°C after the pyrolysis.

From this experiment of pyrolysis carried out, it was observed that at higher temperature (800°C) only ash content remained, signifying that the carbon present in samples were being oxidised to CO₂, possibly as a result of air getting into the furnace. This could be from these points:

1. Through the edges of the cylindrical alumina tube (mostly the entrance).
2. From the nitrogen/air cylinder

The solutions applied were to:

1. Increase the flow rate of N₂ gas from 2000 to 4000 cm³/min.
2. Use only N₂ (O₂ free) gas cylinder
3. Tighten and seal the entrance into the alumina cylindrical tube.

In order to ascertain the above observations, that is, losing carbon (by oxidising to CO₂) during the process of pyrolysis, industrial graphite was tested and exposed to the same experimental conditions of pyrolysis at 800°C. The results are presented in Table 5.8, it reveals that we lost about 23% and 39% of carbon during the process, as indicated by the first two results. A more permanent seal was now placed at the entrance using an Asbo tape, this proved to be effective as the last result shown in Table 5.8 show that 5% was lost, possibly the moisture lost from sample. The remaining miscanthus samples were now pyrolysed under the improved condition and the results are presented in Table 5.9 with carbon content of about 20%.

Table 5.8: Industrial graphite under same pyrolysis condition

Temperature (°C)	Heating rate (°C/min)	Initial mass (g)	Final mass (g)	Carbon (Wt.%)
800	7	1.8804	1.1444	60.9
800	7	2.8033	1.8894	67.4
800	7	1.6665	1.5842	95.1

Table 5.9: Pyrolysis of miscanthus at 800°C

Temperature (°C)	Heating rate (°C/min)	Biomass mass (g)	Carbon mass (g)	Carbon (wt.%)
800	7	3.5362	0.8016	22.7
800	7	3.1628	0.6396	20.2
800	7	3.4501	0.7797	22.6
800	7	3.6524	0.8654	23.7

5.4.2 Pyrolysis Results from the Modified Lenton Furnace

Tables 5.10 to 5.15 give the results obtained from the pyrolysis of the six biomasses considered. The same operating temperature (800°C) and heating rates (7°C/min) were applied to all the biomasses. For every experimental run 7.0 g of the biomass were pyrolysed in which miscanthus gave 24 wt.% carbon, switchgrass gave 25 wt.%, wheat gave 28 wt.%, willow gave 24 wt.%, spruce gave 22 wt.% and poplar gave 20 wt.% of the carbon. All these results are reproducible and they were carried out many times to produce enough carbon materials for the fuel cell operations.

Table 5.10: Miscanthus pyrolysis using modified Lenton furnace

Temperature (°C)	Heating rate (°C/min)	Moisture content (wt.%)	Biomass mass (g)	Carbon mass (g)	Percent of carbon (wt.%)
800	7	6.87	6.1723	1.4127	22.87
800	7	6.80	7.1530	1.6148	22.58
800	7	6.75	6.9467	1.5665	22.55
800	7	6.78	6.7956	1.5958	23.48
800	7	6.72	8.0341	1.8590	23.14
800	7	6.70	7.8743	1.8059	22.93
800	7	6.69	7.1094	1.7036	23.96
800	7	6.69	7.2345	1.7108	23.65
800	7	6.70	6.9378	1.6269	22.45

Table 5.11: Switchgrass pyrolysis using modified Lenton furnace

Temperature (°C)	Heating rate (°C/min)	Moisture content (wt.%)	Biomass mass (g)	Carbon mass (g)	Percent of carbon (wt.%)
800	7	7.73	5.9848	1.5538	25.96
800	7	7.42	6.2410	1.6436	26.34
800	7	7.65	6.1465	1.6137	26.25
800	7	7.62	6.6726	1.7304	25.93
800	7	7.26	6.2307	1.6185	25.98
800	7	7.38	7.1171	1.8833	26.46
800	7	7.45	6.8608	1.7592	25.64
800	7	7.23	6.5526	1.6528	25.22
800	7	7.42	7.3956	1.8479	24.99

Table 5.12: Wheat straw pyrolysis using modified Lenton furnace

Temperature (°C)	Heating rate (°C/min)	Moisture content (wt.%)	Biomass mass (g)	Carbon mass (g)	Percent of carbon (wt.%)
800	7	6.31	6.1425	1.7486	28.47
800	7	6.12	5.6371	1.5815	28.06
800	7	6.40	5.7690	1.6398	28.42
800	7	6.06	6.4061	1.7905	27.95
800	7	6.26	5.8273	1.6238	27.87
800	7	6.17	5.9584	1.6702	28.03
800	7	5.85	6.5384	1.8071	27.64
800	7	6.10	6.1719	1.7250	27.95

Table 5.13: Willow wood chip pyrolysis using modified Lenton furnace

Temperature (°C)	Heating rate (°C/min)	Moisture content (wt.%)	Biomass mass (g)	Carbon mass (g)	Percent of carbon (wt.%)
800	7	7.59	7.0610	1.7127	24.26
800	7	7.52	7.9222	1.9019	24.01
800	7	7.50	7.6216	1.8206	23.89
800	7	7.48	7.3938	1.8714	25.31
800	7	7.52	8.3241	2.0654	24.81
800	7	7.77	8.1925	2.0449	24.96
800	7	7.69	7.4495	1.8217	24.45
800	7	7.59	8.1115	1.9251	23.73
800	7	7.61	7.6714	1.8211	23.74

Table 5.14: Spruce wood chip pyrolysis using modified Lenton furnace

Temperature (°C)	Heating rate (°C/min)	Moisture content (wt.%)	Biomass mass (g)	Carbon mass (g)	Percent of carbon (wt.%)
800	7	6.85	9.2229	2.0282	21.99
800	7	6.63	8.4301	1.8253	21.65
800	7	7.07	8.9354	1.9342	21.65
800	7	7.09	8.2206	1.8597	22.62
800	7	6.83	7.7835	1.7399	22.35
800	7	7.13	8.7246	1.9632	22.50
800	7	6.45	9.6293	2.1639	22.47
800	7	6.21	8.6195	1.9216	22.29
800	7	6.40	10.4210	2.3579	22.63

Table 5.15: Poplar wood chip pyrolysis using modified Lenton furnace

Temperature (°C)	Heating rate (°C/min)	Moisture content (wt.%)	Biomass mass (g)	Carbon mass (g)	Percent of carbon (wt.%)
800	7	5.61	5.3256	1.0838	20.35
800	7	5.51	5.9827	1.1943	19.96
800	7	5.62	5.7677	1.1662	20.22
800	7	5.66	6.3072	1.2958	20.54
800	7	5.49	6.5579	1.3288	20.26
800	7	5.64	6.1136	1.2403	20.29
800	7	5.78	5.8593	1.1813	20.16
800	7	5.59	6.4064	1.2786	19.96
800	7	5.67	6.3506	1.2906	20.32

5.4.3 Carbon Analyses

The results of the analyses carried out on the six biomasses produced through the pyrolysis reactions are presented in Tables 5.16 to 5.21. Tables 5.22 and 5.23 give the results of the same analysis on industrial carbon black and industrial graphite. Table 5.24 on the other hand gives the comparison of the six biomass carbons and the industrial carbons. For miscanthus the moisture content from the ground to the carbon reduced from 7.38 wt.% to 5.61 wt.% (Tables 5.7 and 5.24). Surprisingly the biomass carbons still have high level of moisture in them. The calorific value has greatly improved from 18.83 MJ/kg to 29.11 MJ/kg (Tables 5.7 and 5.24). The carbon content almost double from 45.75 wt.% to 82.46 wt.% and the hydrogen content reduced from 5.09 wt.% to 0.97 wt.% (Tables 5.7 and 5.24). Similar patterns were observed for the other biomasses.

From Table 5.24, spruce carbon (32.53 MJ/kg) has the highest calorific value followed by poplar (30.90 MJ/kg), then willow (29.56 MJ/kg) then miscanthus (29.11 MJ/kg), switchgrass (23.82 MJ/kg) and wheat (23.36 MJ/kg). These heating values will have effects on the performance of the biomass fuel in the fuel cells. Also similar patterns were observed in the carbon contents of these carbon fuels.

Table 5.16: Moisture, calorific value and ultimate analyses for miscanthus carbon

Analysis	Moisture contents (wt.%)	Calorific value (MJ/kg)	Carbon (wt.%)	Hydrogen (wt.%)
1	5.78	28.93	83.50	1.47
2	5.50	29.27	80.39	0.71
3	5.55	29.14	83.50	0.73
Average	5.61	29.11	82.46	0.97

Table 5.17: Moisture, calorific value and ultimate analyses for switchgrass carbon

Analysis	Moisture contents (wt.%)	Calorific value (MJ/kg)	Carbon (wt.%)	Hydrogen (wt.%)
1	2.87	23.46	67.80	1.32
2	2.66	24.20	66.43	1.26
3	2.72	23.81	67.73	1.28
Average	2.75	23.82	67.32	1.29

Table 5.18: Moisture, calorific value and ultimate analyses for wheat carbon

Analysis	Moisture contents (wt.%)	Calorific value (MJ/kg)	Carbon (wt.%)	Hydrogen (wt.%)
1	5.41	23.38	65.89	0.56
2	5.73	23.40	64.72	0.48
3	6.75	23.29	65.43	0.48
Average	5.96	23.36	65.35	0.51

Table 5.19: Moisture, calorific value and ultimate analyses for willow carbon

Analysis	Moisture contents (wt.%)	Calorific value (MJ/kg)	Carbon (wt.%)	Hydrogen (wt.%)
1	4.22	29.81	75.41	1.03
2	4.21	29.44	83.60	1.65
3	4.18	29.43	83.98	1.25
Average	4.20	29.56	81.00	1.31

Table 5.20: Moisture, calorific value and ultimate analyses for spruce carbon

Analysis	Moisture contents (wt.%)	Calorific value (MJ/kg)	Carbon (wt.%)	Hydrogen (wt.%)
1	2.56	32.51	92.59	1.57
2	2.47	32.52	89.67	0.87
3	2.19	32.57	89.91	0.90
Average	2.41	32.53	90.72	1.11

Table 5.21: Moisture, calorific value and ultimate analyses for poplar carbon

Analysis	Moisture contents (wt.%)	Calorific value (MJ/kg)	Carbon (wt.%)	Hydrogen (wt.%)
1	2.64	30.91	88.26	1.31
2	2.69	30.93	85.45	2.64
3	2.59	30.84	77.50	1.16
Average	2.64	30.90	83.74	1.70

The calorific values presented in Table 5.22 shows carbon black having higher CV of 33.84 MJ/kg and graphite with 32.55 MJ/kg. These heating values are slightly higher than those obtained for the biomass carbon and are quoted for comparison purpose (Table 5.24). The carbon content is also higher in carbon black than in graphite which gives an idea on the differences in the heating values.

Table 5.22: Moisture, calorific value and ultimate analyses for carbon black

Analysis	Moisture contents (wt.%)	Calorific value (MJ/kg)	Carbon (wt.%)	Hydrogen (wt.%)
1	0.74	35.16	99.56	1.26
2	0.49	33.24	99.45	0.89
3	0.35	33.11	99.11	0.85
Average	0.53	33.84	99.37	1.00

Table 5.23: Moisture, calorific value and ultimate analyses for graphite

Analysis	Moisture contents (wt.%)	Calorific value (MJ/kg)	Carbon (wt.%)	Hydrogen (wt.%)
1	0.44	32.64	98.47	0.95
2	0.37	32.50	98.24	0.76
3	0.40	32.51	98.45	0.73
Average	0.41	32.55	98.39	0.81

Table 5.24: Comparison of the pyrolysed biomass carbons and industrial carbons

Biomass	Moisture contents (wt.%)	Calorific value (MJ/kg)	Carbon (wt.%)	Hydrogen (wt.%)
Miscanthus	5.61	29.11	82.46	0.97
Switchgrass	2.75	23.82	67.32	1.29
Wheat	5.96	23.36	65.35	0.51
Willow wood	4.20	29.56	81.00	1.31
Spruce wood	2.41	32.53	90.72	1.11
Poplar wood	2.64	30.90	83.74	1.70
Carbon black	0.53	33.84	99.37	1.00
Graphite	0.41	32.55	98.39	0.81

5.5 Hand and Ball Milling of Biomass Carbon

The pyrolysed biomass carbons were subjected to hand milling as well as ball milling before preparing them for the fuel cell operations. Tables 5.25 and 5.26 show the results of the hand and ball milled carbon particles, sampled results are given in Appendix A. The carbon were hand milled for ten minutes and ball milled for forty minute using Fritsch (Pulvirisette 6, AGAPE) and a hundred stainless steel balls each of 1 mm and 5 mm in diameter.

Table 5.25: Hand milled particle size analysis of biomass carbon

Carbon	Time (min)	Particle size (μm)				Specific Surface Area (m^2/g)	Density (g/cm^3)
		Sample	Sample	Sample	Average		
		1	2	3			
Willow	10	38.58	66.99	26.39	43.99	0.42	1.39
Switchgrass	10	59.02	6.26	23.27	29.52	0.63	1.39
Wheat	10	89.96	13.17	16.46	39.86	0.45	1.39
Poplar	10	83.48	11.27	18.73	37.83	0.53	1.39
Spruce	10	110.10	20.71	13.40	48.07	0.45	1.39
Miscanthus	10	18.52	28.12	41.04	29.23	0.57	1.39

Table 5.26: Ball milled particle size analysis of biomass carbon

Carbon	Time (min)	Particle size (μm)				Specific Surface Area (m^2/g)	Density (g/cm^3)
		Sample	Sample	Sample	Average		
		1	2	3			
Willow	40	2.78	2.56	2.56	2.63	2.23	1.39
Switchgrass	40	2.19	2.27	2.21	2.22	2.55	1.39
Wheat	40	3.15	2.55	3.35	3.02	2.07	1.39
Poplar	40	4.89	4.05	4.01	4.32	1.52	1.39
Spruce	40	8.91	9.04	6.45	8.13	0.91	1.39
Miscanthus	40	7.21	8.09	8.46	7.92	0.95	1.39

After the hand milling, miscanthus had the highest particle size of 15.09 μm , followed by spruce (13.18 μm), wheat (12.23 μm), willow (10.62 μm), poplar (10.18 μm) and switchgrass (9.18 μm). The ball milling helps to achieve a smaller particle range with the highest values recorded for spruce (4.78 μm), followed by miscanthus (4.57 μm), poplar (2.87 μm), wheat (2.10 μm), willow (1.93 μm) and switchgrass (1.70 μm).

5.6 X-ray Diffraction (XRD) Pattern

Powder X-ray diffraction (XRD) analyses were carried out on industrial carbon black (Alfa Aesar, USA), industrial graphite (Sigma-Aldrich, USA) and the six biomass carbons. The results from these XRD pattern are presented in Figures 5.7 to 5.15. The XRD from the industrial carbons are presented as a basis for comparison with the biomass carbon.

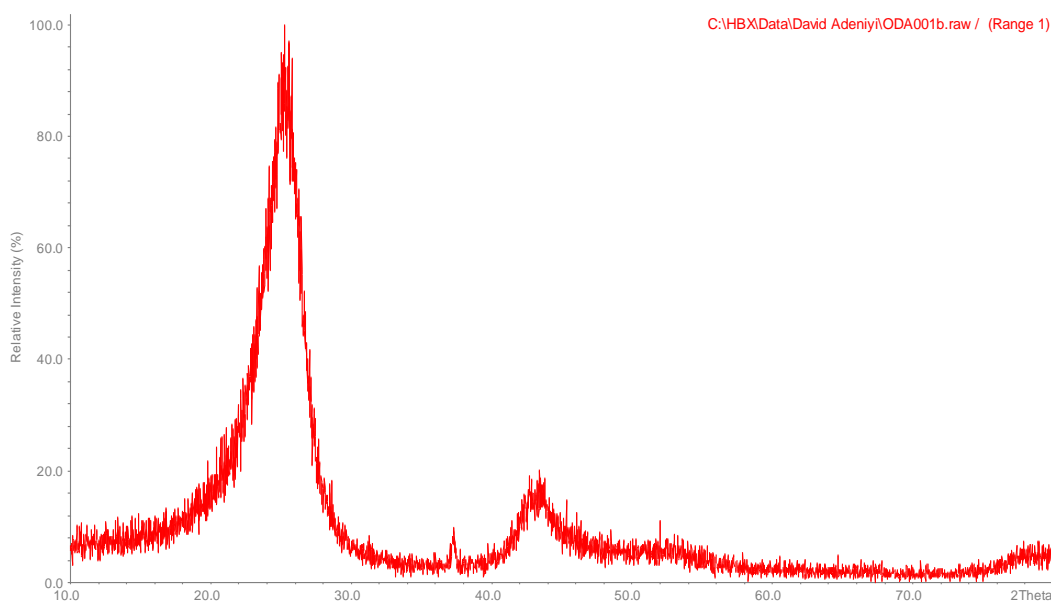


Figure 5.7: Powder X-ray diffraction pattern for industrial carbon black

Figure 5.7 gives the powder XRD of industrially supplied carbon black of 99.9% purity (metal basis), the highest peak is at an angle of 25.345° (2θ -axis), corresponding to a d-spacing of 3.5113 on a relative intensity of 100%. These figures and values were

generated using the software (STOE WinX^{POW} 2.10) that runs with the Siemens D500 X-Ray Diffractometer System.

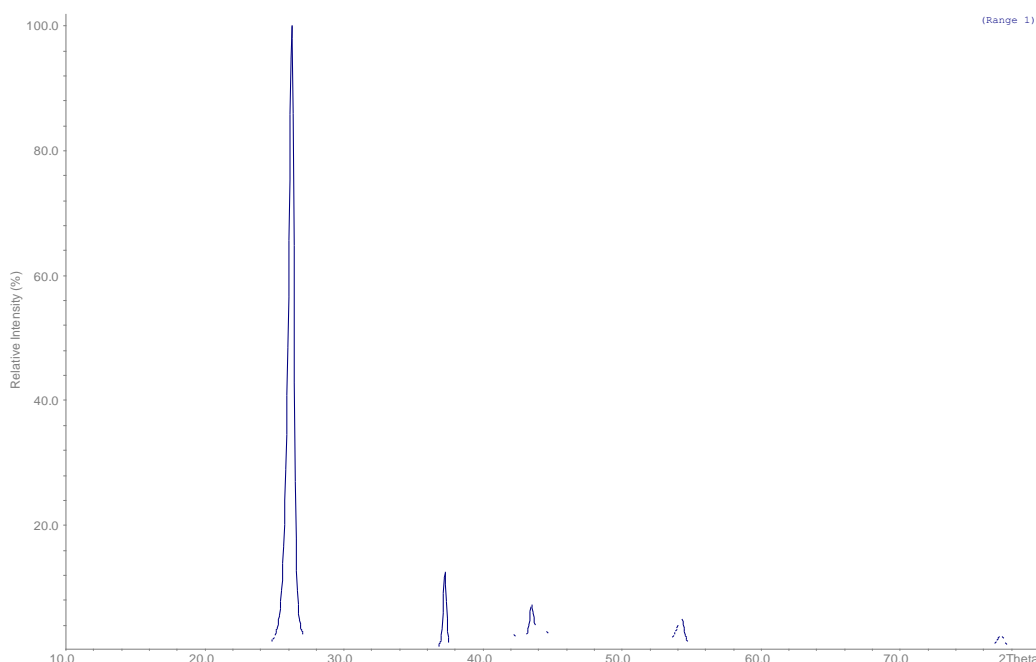


Figure 5.8: Powder X-ray diffraction (XRD) pattern on graphite

The diffraction pattern of a substance is an “almost unique” fingerprint which is defined by the reflection positions (this is measured as the d-spacing or 2θ -indicated by the x-axis of the XRD figures) and the reflection intensities (this is measured as the peak height- indicated by the y-axis of the XRD figures). The diffraction pattern of a substance may therefore allow the identification of an unknown sample, this could be achieved by comparing the diffraction pattern of the unknown with reference pattern for known pure materials (Hyatt, 2008; Cullity and Stock, 2001; Jenkins and Snyder, 1996). The underlying principle in phase identification is to match the positions and intensities of the unknown with the reference pattern of the known. This could be done using the Hanawaldt system or more recently using computer based match algorithm as presented by STOE WinX^{POW} 2.10 (Hyatt, 2008; Reeves, 2005). Computer algorithm uses sample’s chemistry to narrow down possible matches, allows background fitting and subtractions. The computer matches has a major advantage of

rapid and efficient searching of large database which is invaluable for multiphase samples with more than three components (Hyatt, 2008; Reeves, 2005).

Figure 5.8 gives the powder XRD pattern for industrially graphite. The highest peak in the figure is at an angle of 26.554° (2θ -axis), corresponding to a d-spacing of 3.3541 on a relative intensity of 100%. These figure and value were also generated using the software (STOE WinX^{POW} 2.10) that runs with the Siemens D500 X-Ray Diffractometer System. The pattern generated by the graphite sample shows a more crystalline structure unlike the disordered structure obtained from carbon black. Figures 5.9 and 5.10 show the XRD pattern for the miscanthus carbons pyrolysed at 400°C and 800°C . These show the progression in obtaining disordered carbon structure through proper pyrolysis conditions.

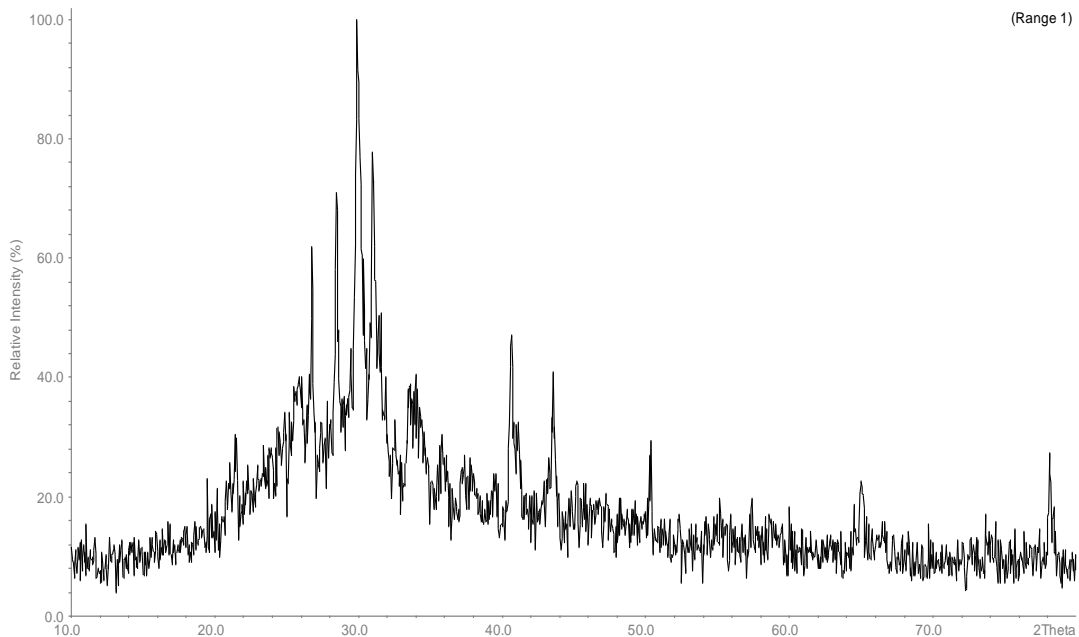


Figure 5.9: X-ray diffraction (XRD) pattern for miscanthus pyrolysed at 400°C .

Figure 5.10 gives the XRD of the miscanthus carbon sample to be used in the fuel cell, the highest peak in the figure is at an angle of 29.909° (2θ -axis), corresponding to a d-

spacing of 2.9850 and a relative intensity of 100%. It was observed that the pattern generated for the miscanthus carbon is slightly different from those of the carbon black and graphite. It was also observed from the figure that the d-spacing are different. The d-spacing is the inter-planar spacing available within the carbon structure and this gives a representation of the reactive sites within the carbon atom. The d-spacing of carbon black shows greater values which suggest a greater unit cell size and a greater possibility of reactive sites.

The peak width of the XRD pattern generated by the carbon black (Figure 5.7) suggest a disordered form of carbon, this disorder nature is what is important as fuel for the direct carbon fuel cell. The pattern generated by the graphite sample (Figure 5.8) is narrower, suggesting a form of orderliness of the carbon atom, this type of uniform pattern might perform differently in the DCFC because it has been reported that the chemical reactivity of carbons to oxidation is known to be strongly dependent on structure, particularly the extent of graphitisation (Cao *et al.*, 2007; Cherepy *et al.*, 2005). Figure 5.9 gives the miscanthus pyrolysed at 400°C, the d-spacing is much lower than the industrial carbon black and the graphite which could suggest that it has lower reactive sites. Also the peak width of the XRD pattern is not well defined, probably suggesting that further processing of the miscanthus is required at higher temperature and better pyrolysis conditions.

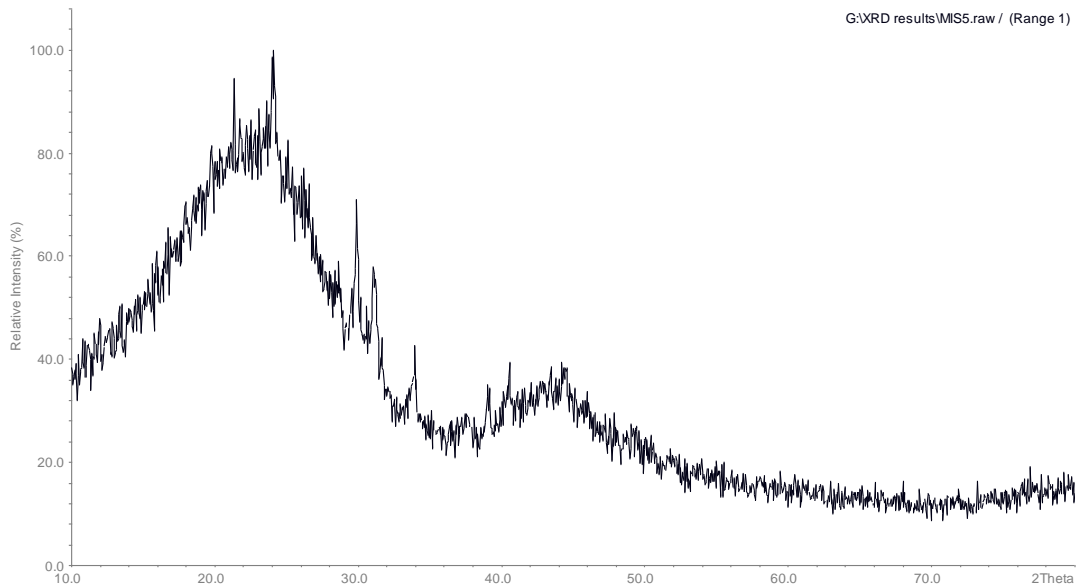


Figure 5.10: X-ray diffraction (XRD) pattern for miscanthus pyrolysed at 800 °C

Figure 5.10 gives the XRD of miscanthus pyrolysed at 800°C. The highest peak in the figure is at an angle of 24.014° (2θ -axis), corresponding to a d-spacing of 3.7029 and a relative intensity of 100%. The d-spacing is higher than the one pyrolysed at 400°C, this probably show a better carbon structure at higher temperatures. The peak width of the pattern generated by Figure 5.10 is similar to that of the carbon black, and it reveals a form of disordered carbon structure. This may be an indication that the structure of the carbons at this pyrolysed condition is suitable for use in the DCFC. Figures 5.11 to 5.15 show the powder XRD pattern for switchgrass, wheat, willow, spruce and poplar respectively. There are varying degrees of the disordered pattern presented in this XRD.

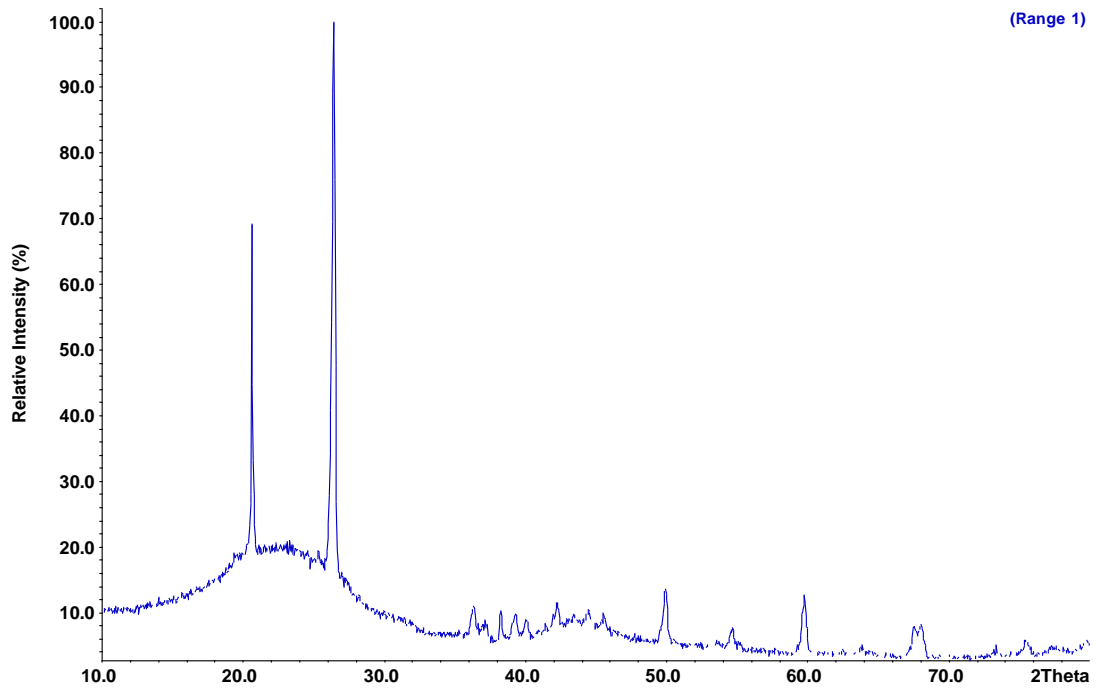


Figure 5.11: X-ray diffraction (XRD) pattern for switchgrass carbon

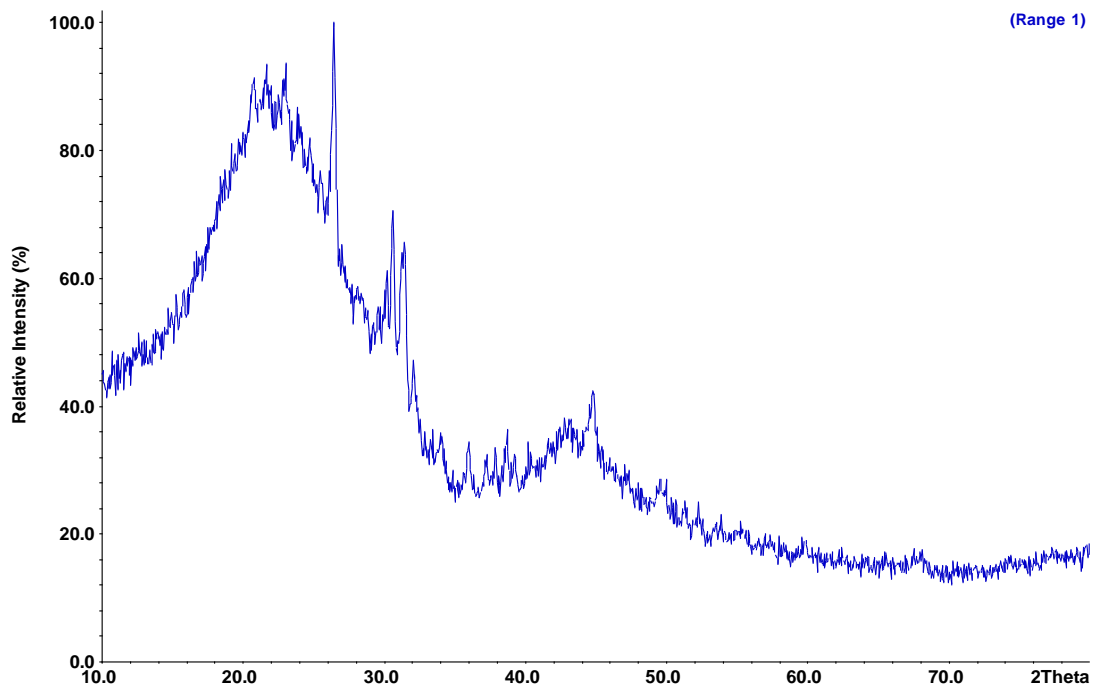


Figure 5.12: X-ray diffraction (XRD) pattern for wheat carbon

The XRD pattern for switchgrass and wheat (Figures 5.11 and 5.12) show some similarity with that of carbon black indicating that the char has a degree of disordered

graphite content. In evidence also are the sharp peaks corresponding to contributions from silica, ash and other impurities identified from the STOE databank spectra (Nowakowski *et al.*, 2007; Wornat *et al.*, 1995). Wornat and co-workers (1995) reported that the peak at 26.7° correspond to quartz (crystalline SiO_2).

Willow and spruce carbons also present different degree of disorderliness as shown by Figures 5.13 and 5.14. There are two major peaks for willow at 23° and 44° and similar to spruce carbon. The other peaks are associated with the impurities in the biomass from the field. These same patterns are similar to those generated by poplar carbon.

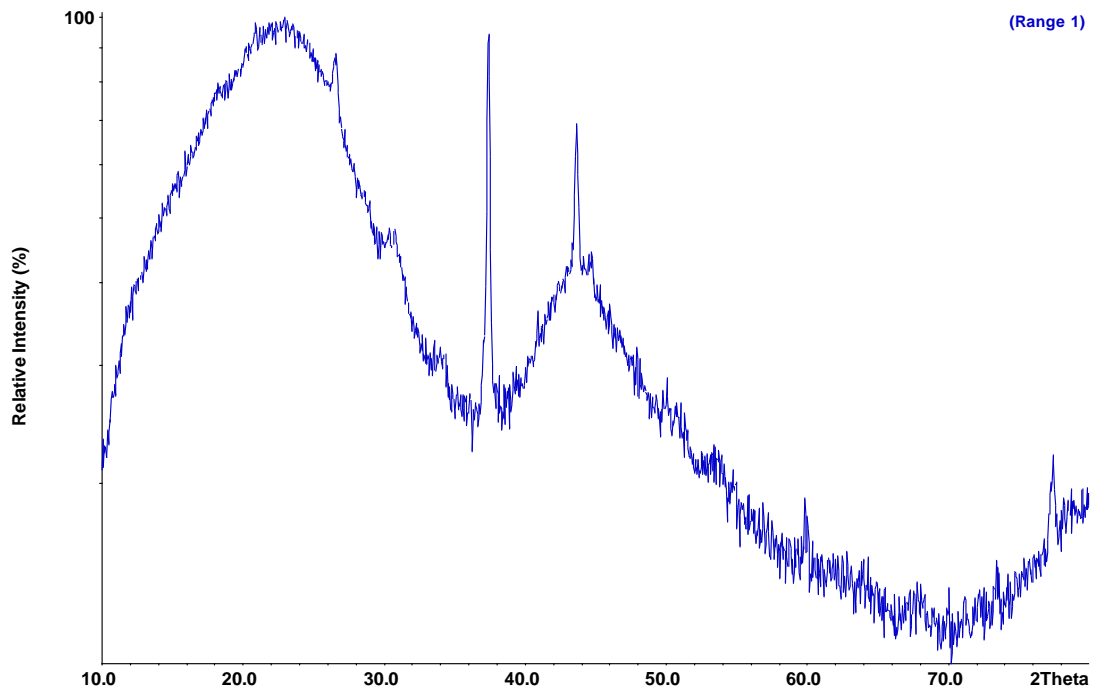


Figure 5.13: X-ray diffraction (XRD) pattern for willow carbon

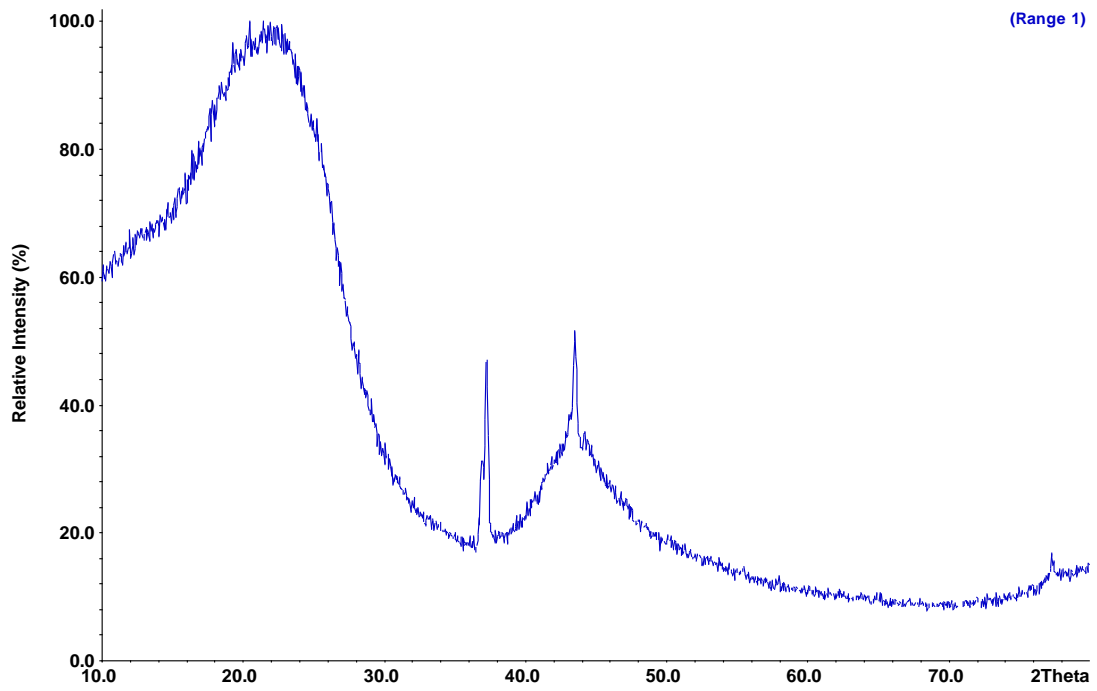


Figure 5.14: X-ray diffraction (XRD) pattern for spruce carbon

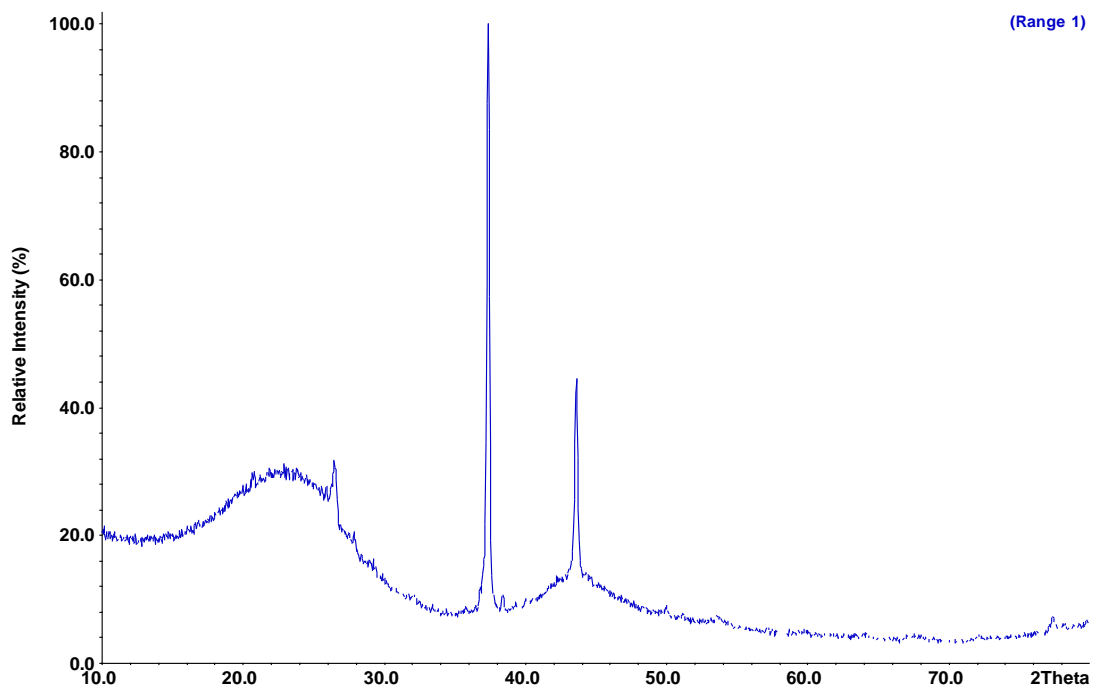


Figure 5.15: X-ray diffraction (XRD) pattern for poplar carbon

5.7 Scanning Electron Microscope (SEM) of Biomass Carbons

The six biomass carbons were subjected to scanning electron microscope (SEM) to gain further understanding on the structures and size distributions of the carbon particles. The SEMs are presented for the hand milled and the ball milled carbons, which are shown in Figures 5.16 to 5.27. Figures 5.16 and 5.17 shows the SEM magnification at 500x for both hand and ball milled poplar carbon. The hand milled shows larger particles sizes for poplar and many irregular shapes of the particles. The ball milled shows the effects that ball milling had in reducing the size and shape distributions.

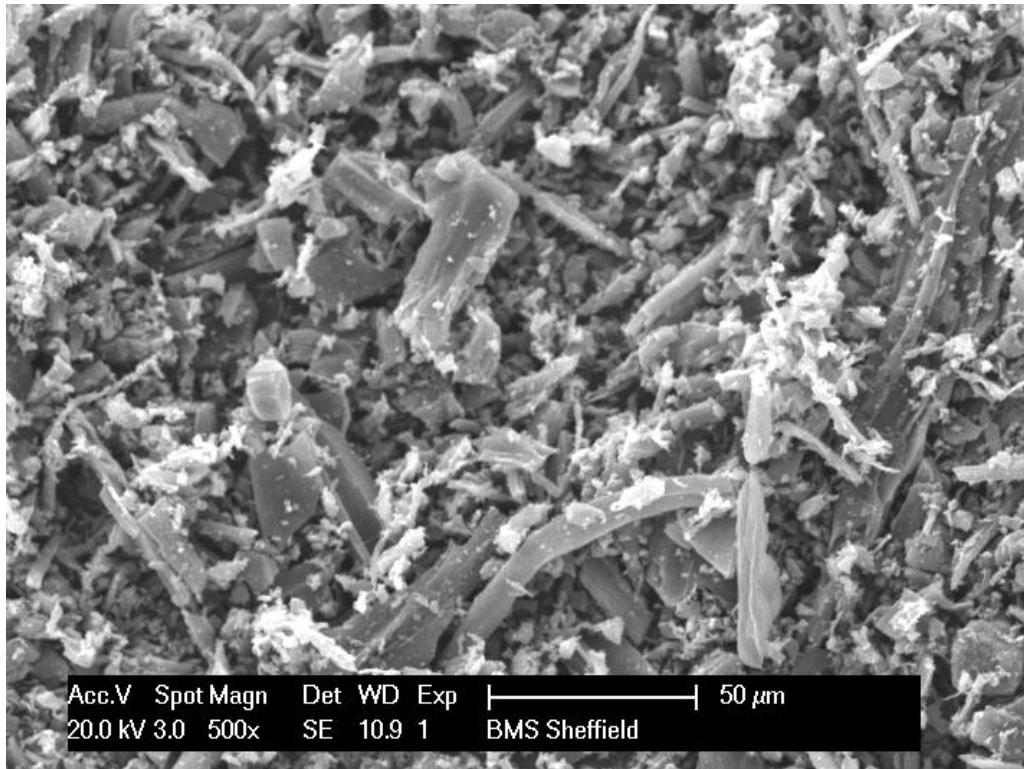


Figure 5.16: SEM of hand milled poplar carbon particles at magnification of 500x

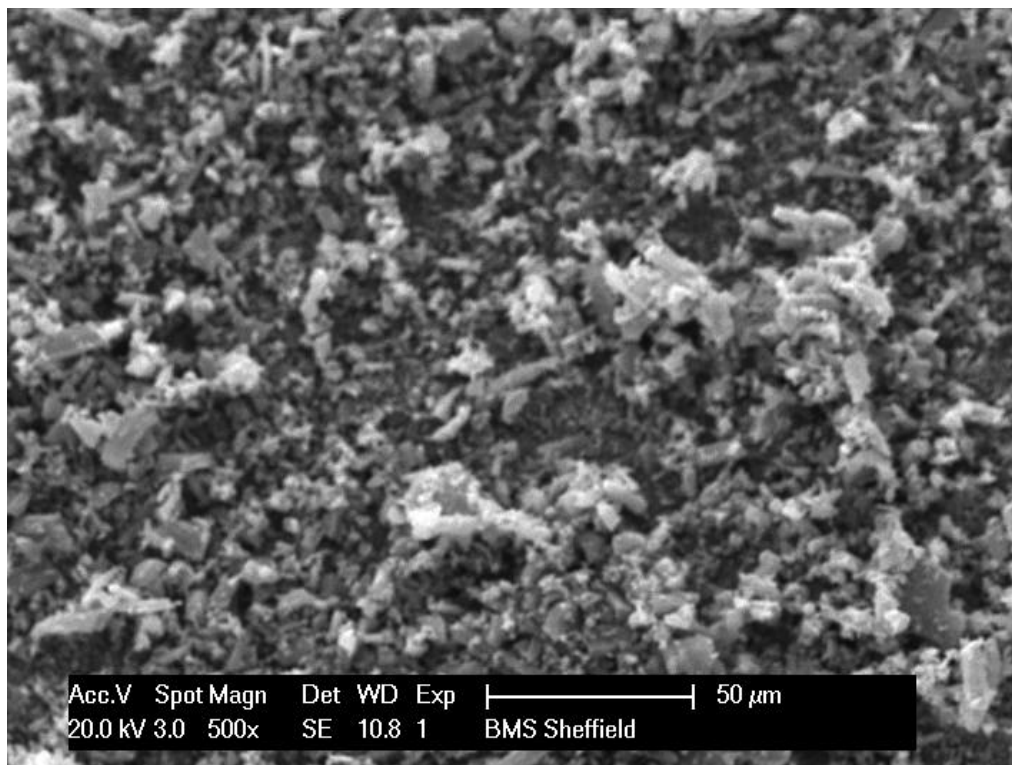


Figure 5.17: SEM of ball milled poplar carbon particles at magnification of 500x

Figures 5.17 and 5.18 show the SEM for the spruce carbon samples. There are evidences of larger particle present in the hand milled samples which were reduced by the ball milling process. The SEM results for switchgrass carbons are presented in Figures 5.20 and 5.21. The hand milled sample shows a combination of large and small particles which were further reduced by ball milling. Figures 5.22 to 5.25 show the SEM patterns for wheat and willow carbons. Figures 5.26 and 5.27 show the microscopy of miscanthus carbon. The two SEM reveals that the particle sizes and shape for the miscanthus are similar possibly suggesting that the ball and hand milled samples were within the same particle size range.

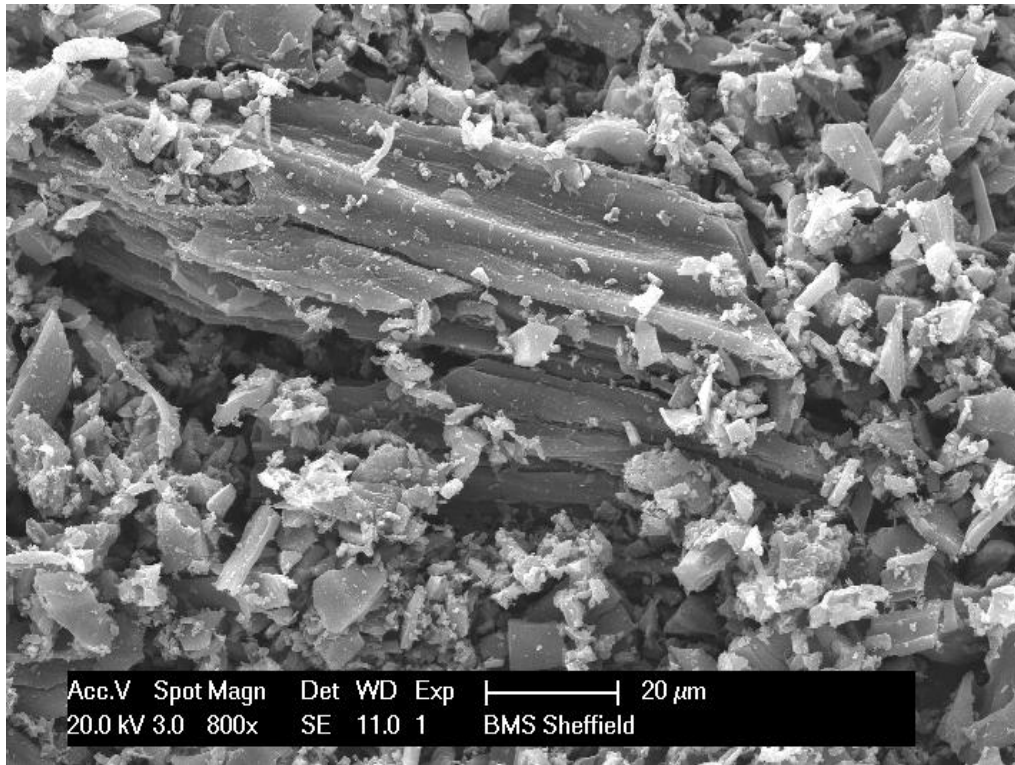


Figure 5.18: SEM of hand milled spruce carbon particles at magnification of 800x

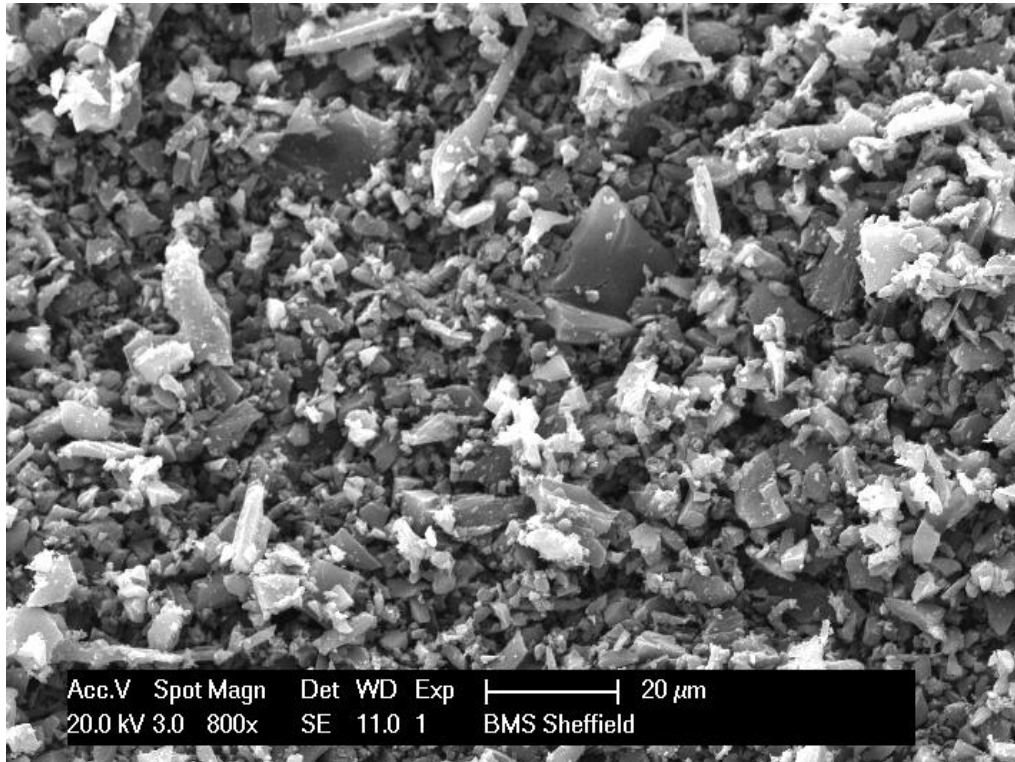


Figure 5.19: SEM of ball milled spruce carbon particles at magnification of 800x

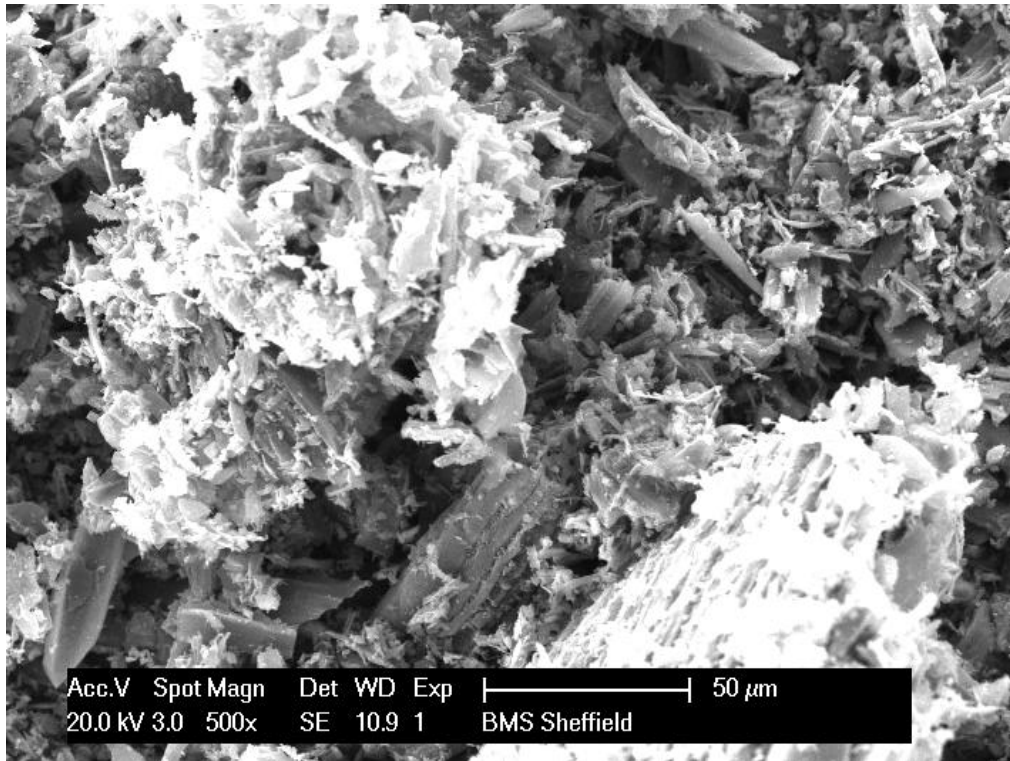


Figure 5.20: SEM of hand milled switchgrass carbon particles at magnification of 500x

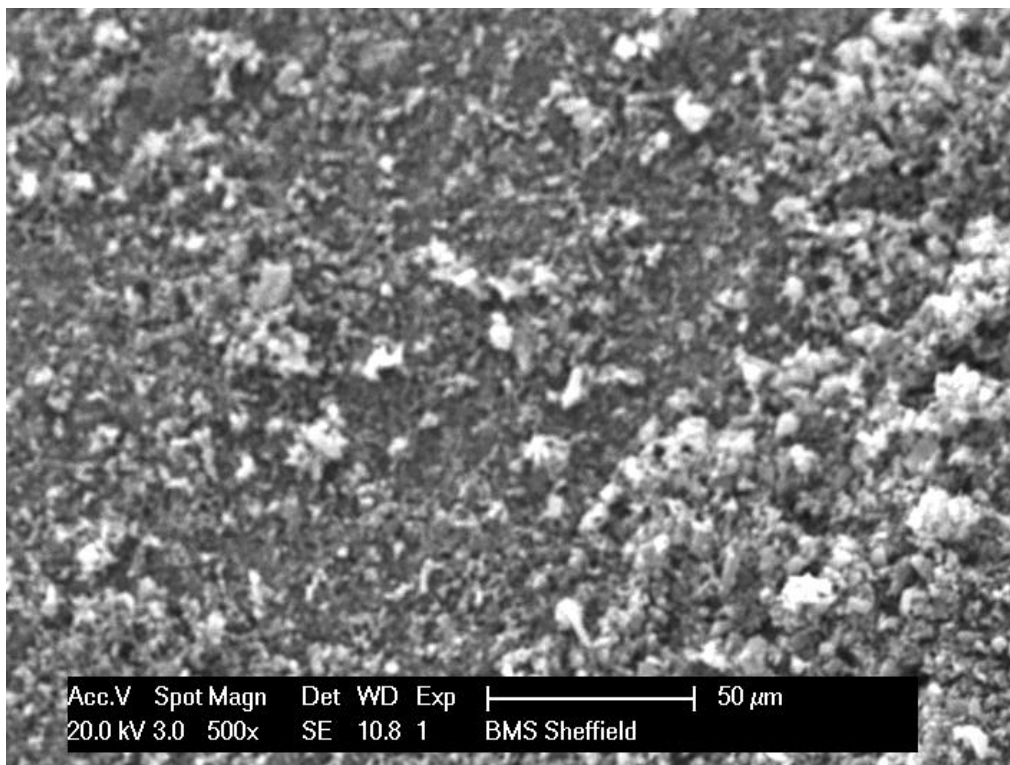


Figure 5.21: SEM of ball milled switchgrass carbon particles at magnification of 500x

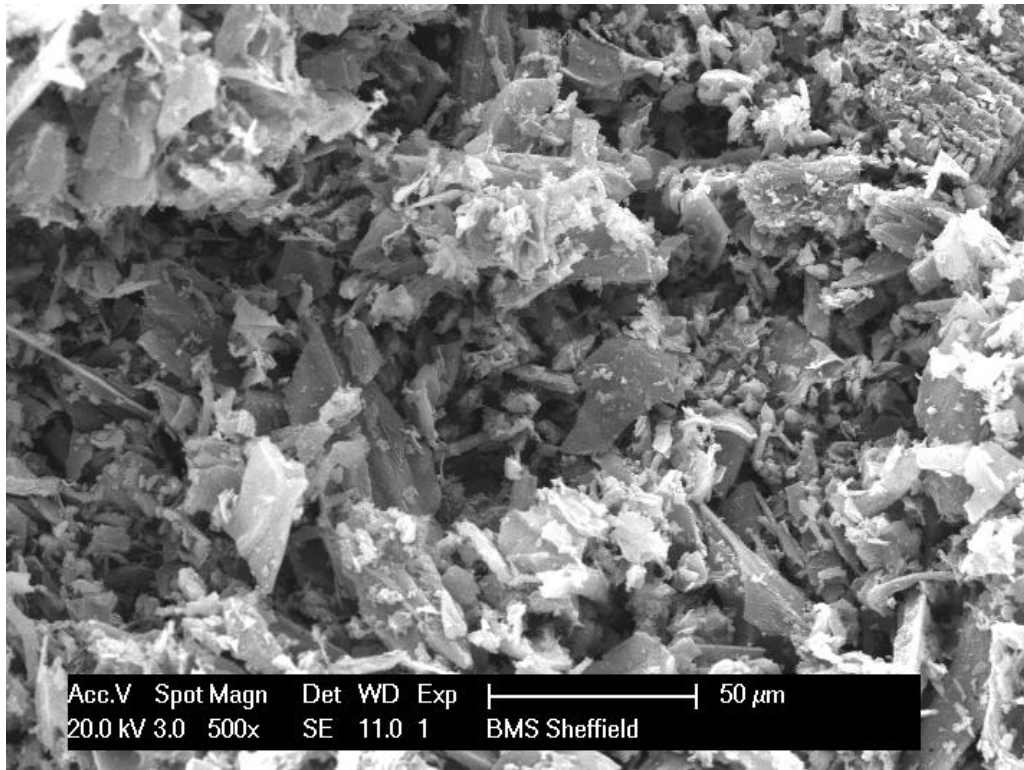


Figure 5.22: SEM of hand milled wheat carbon particles at magnification of 500x

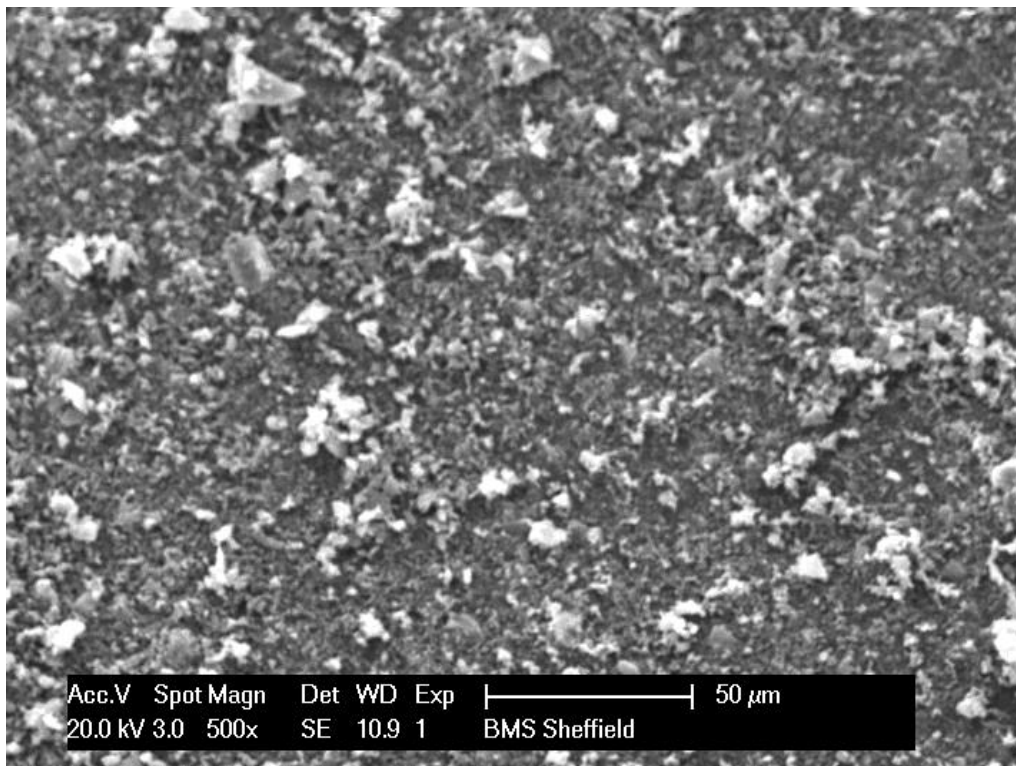


Figure 5.23: SEM of ball milled wheat carbon particles at magnification of 500x

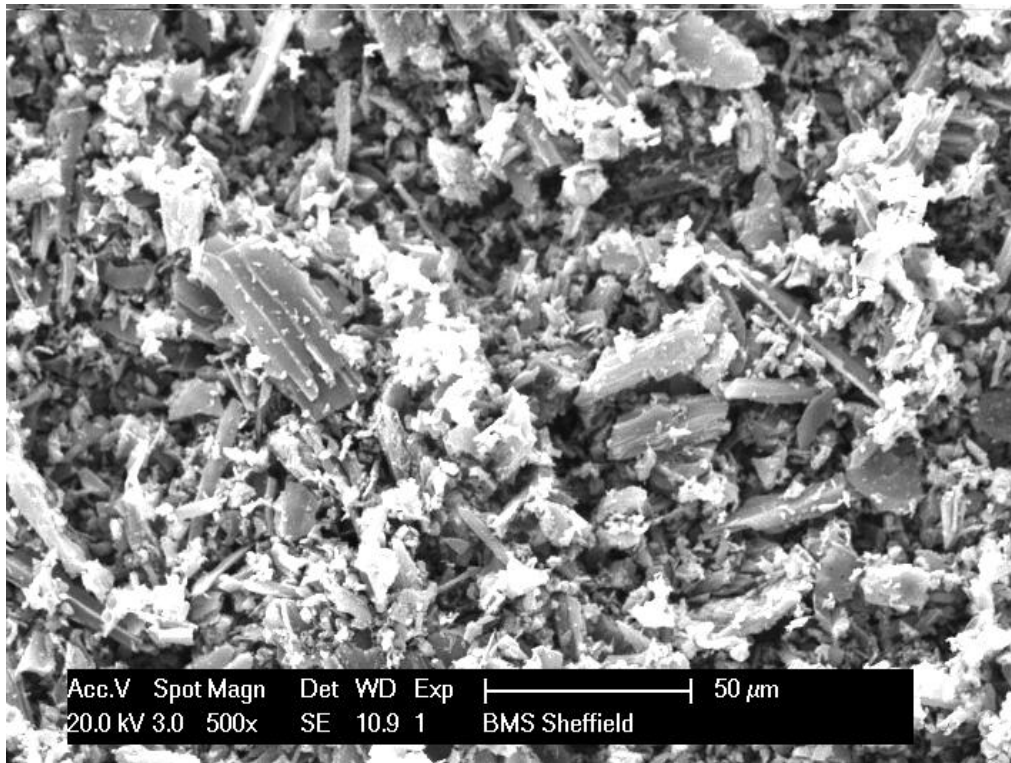


Figure 5.24: SEM of hand milled willow carbon particles at magnification of 500x

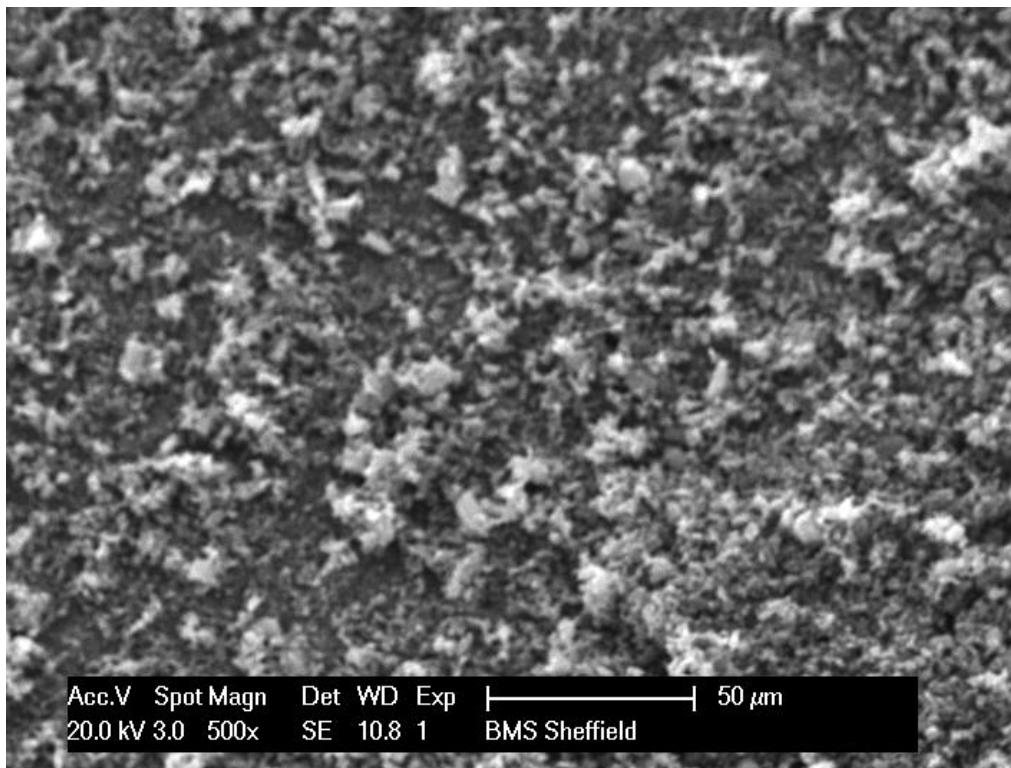


Figure 5.25: SEM of ball milled willow carbon particles at magnification of 500x

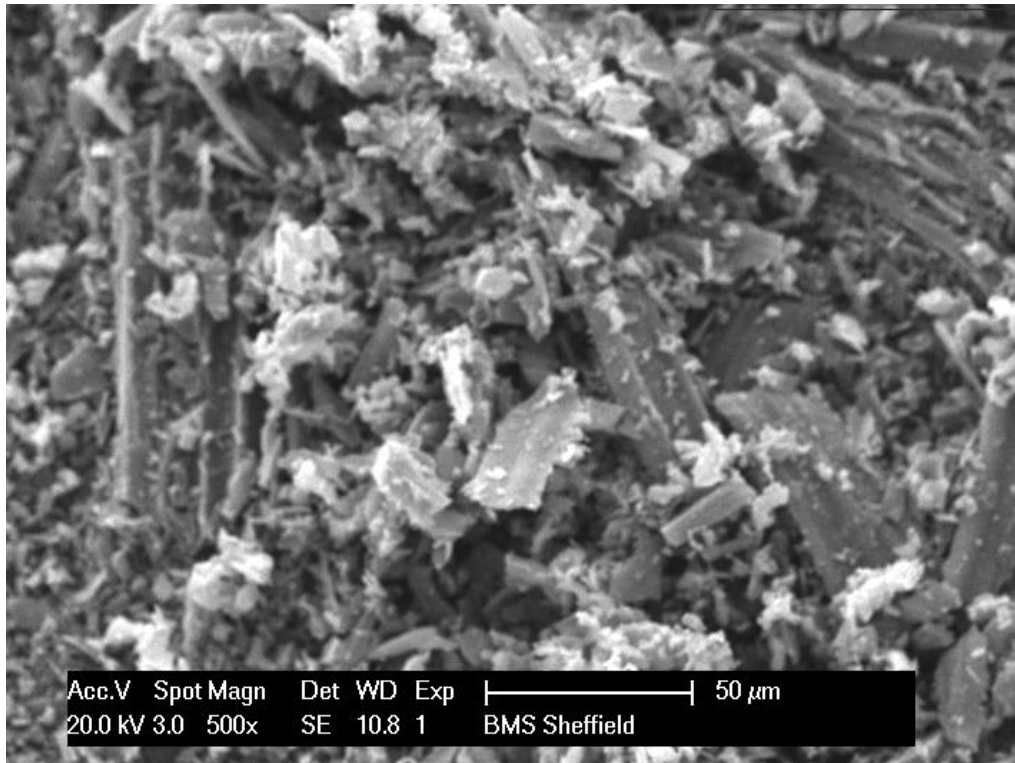


Figure 5.26: SEM of hand milled miscanthus carbon particles at magnification of 500x

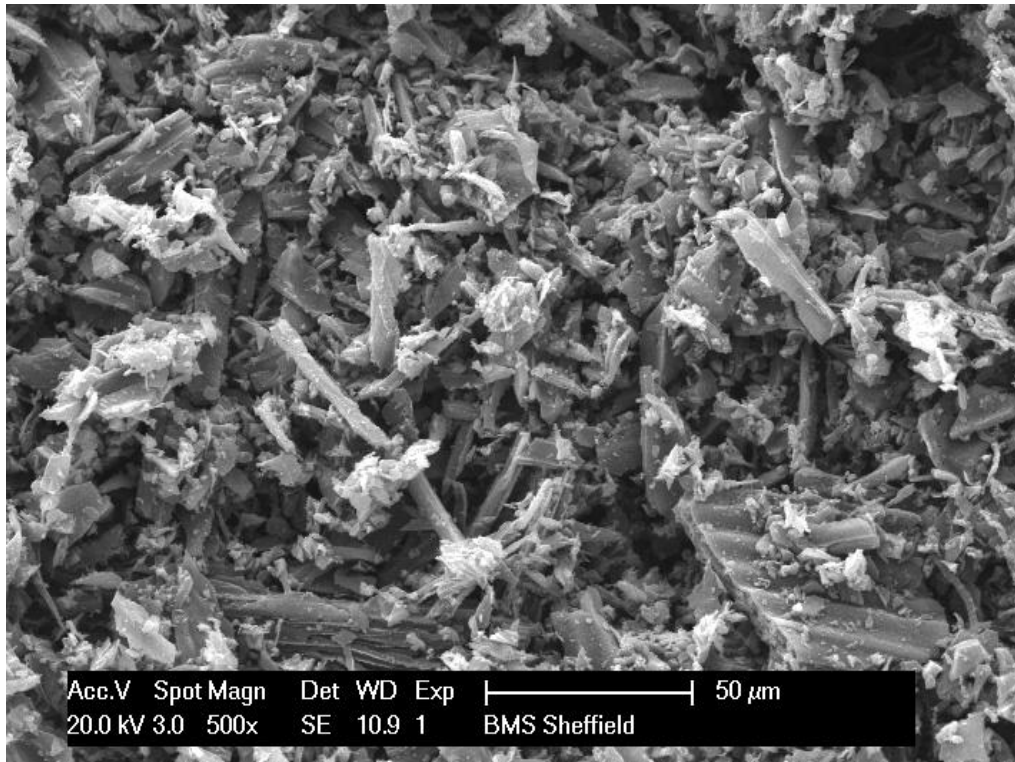


Figure 5.27: SEM of ball milled miscanthus carbon particles at magnification of 500x

Chapter Six

MCDRFC Single Cell Performances

6.1 Introduction

The performances of a single cell molten carbonate electrolyte direct carbon fuel cell (MCDRFC) with the biomass carbon fuels are presented in this chapter. The results obtained from the MCDRFC are reproducible, the variation observed in the results are due to a number of factors such as ohmic resistance, activation losses, mass transport limitation and the aging process of the electrochemical cell system. This chapter presents the MCDRFC electrochemical cell design, components and development showing the different configuration used for the DCFC. The performances recorded for the MCDRFC with industrial carbon black fuel, the biomass fuels and the various cell arrangements with the results from the hand and ball milled biomass carbon fuels are presented. The temperature effects on the performances of the MCDRFC and the tables of the summary of the electrochemical performances for the six biomass fuels are also shown. Finally a comparison between the ball and hand milled biomass carbon fuel on the MCDRFC are given.

6.2 MCDRFC Electrochemical Cell Design and Development

Several designs were explored for the electrochemical cell unit of the molten carbonate direct carbon fuel cell (MCDRFC), simply referred to as the direct carbon fuel cell (DCFC). Some of them are presented in Figures 6.1 to 6.5. Figure 6.1 shows the first cell arrangement that was developed. The electrolyte consists of porous alumina saturated in carbonated mixture (lithium carbonate and potassium carbonate). Toward the anode side is gold mesh collecting the generated electrical current and channelling it through the gold wire electrode. On top of this is a mica seal protecting the gold mesh from the anode casing. At the cathode side is also a gold mesh for current collection and mica seal for protection.

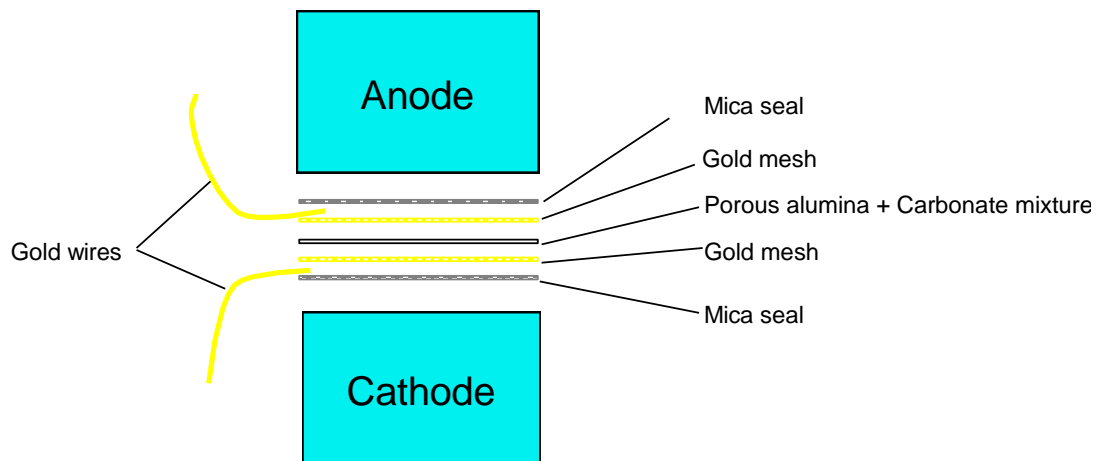


Figure 6.1: Gold mesh, porous alumina, gold mesh electrode assembly

Figure 6.2 shows the electrochemical unit cell arrangement using porous nickel, zirconia saturated in carbonated mixture (lithium carbonate and potassium carbonate) and gold mesh. The anode and cathode tube casing sides were also protected using mica seals. This design was further improved by introducing ceramic disc with holes acting as a support for the cathode side (Figure 6.3). This kept the electrolyte flat and in good contact with the electrodes.

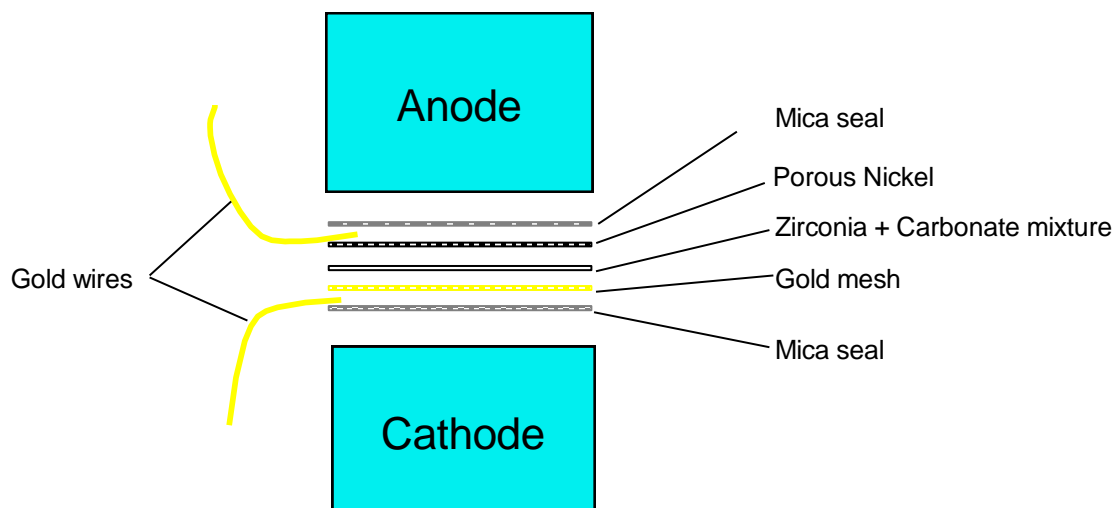


Figure 6.2: Porous nickel, zirconia, gold mesh electrode assembly

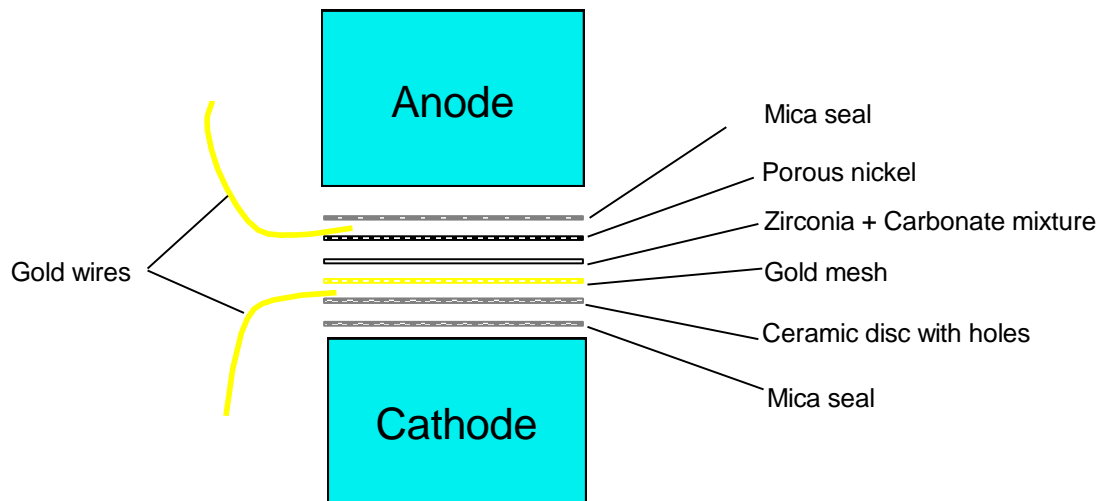


Figure 6.3: Porous nickel, zirconia, gold mesh electrode assembly with ceramic disc

The fourth and fifth arrangements are shown in Figures 6.4 and 6.5. The electrolyte consists of zirconia saturated in carbonated mixture and on either side are gold meshes.

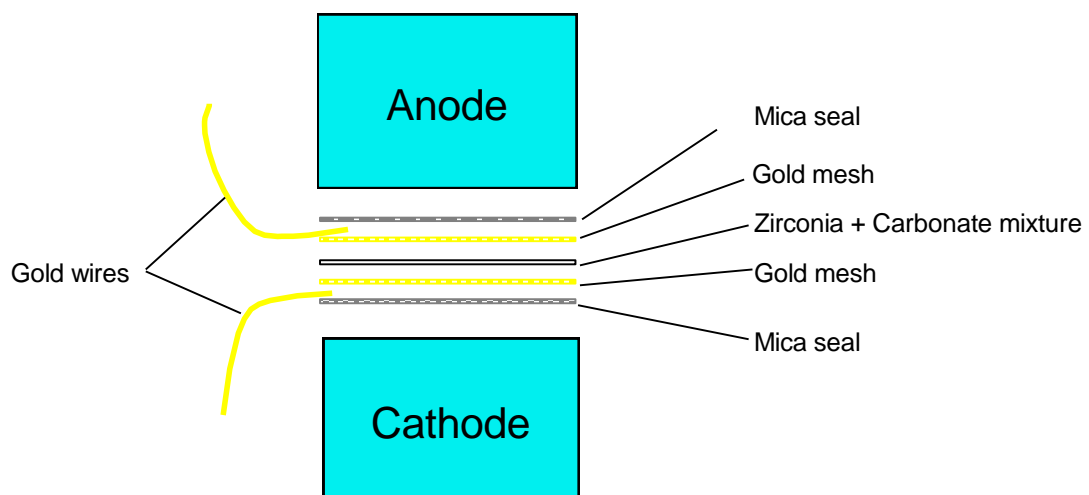


Figure 6.4: Gold mesh, zirconia, gold mesh electrode assembly

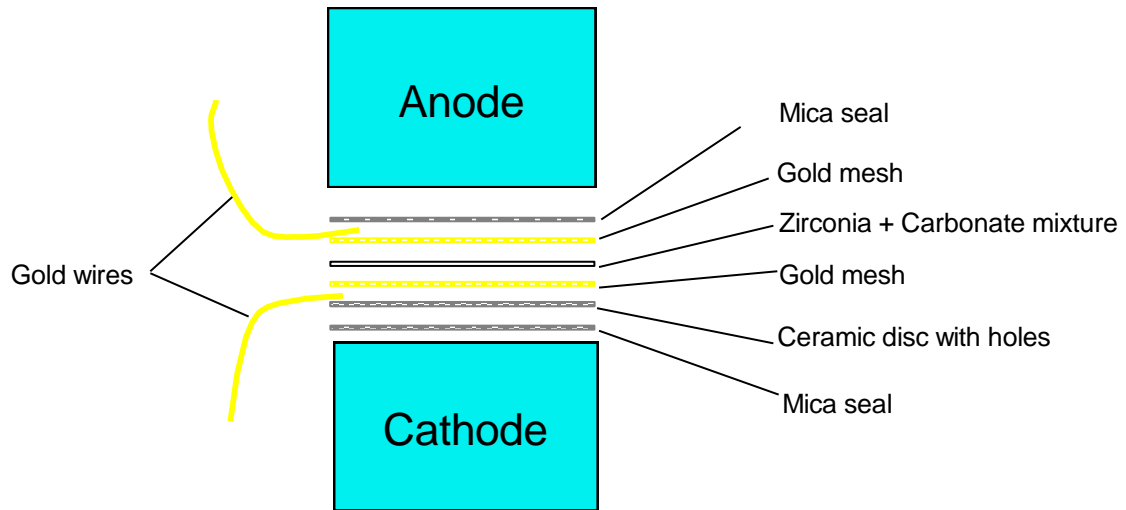


Figure 6.5: Gold mesh, zirconia, gold mesh electrode assembly with ceramic disc

This developed electrode assembly was further improved by introducing ceramic disc with holes, which acted as a support for the cathode side (Figure 6.5) as well as keeping the electrolyte flat and in proper contact with the electrode. This cell arrangement was discovered to be stable unlike the other two arrangements and was used for the MCDRFC operations. Figures 6.6 to 6.9 show some of the components of the MCDRFC.



Figure 6.6: Saturated zirconia electrolyte for MCDRFC.



Figure 6.7: Saturated zirconia and porous nickel electrode assembly

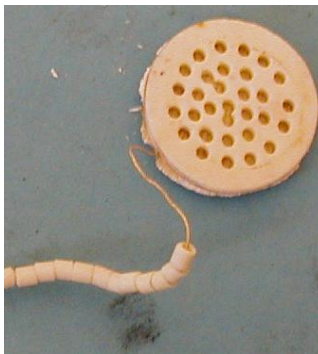


Figure 6.8: Ceramic disc, gold mesh, zirconia and gold wire electrode assembly

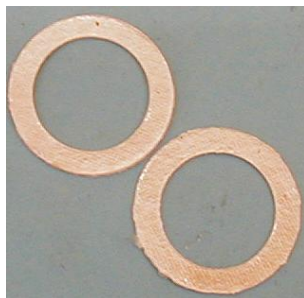


Figure 6.9: Mica seals used as protection for DCFC casing

6.3 Voltages from MDCFC Operations

6.3.1 Voltages from MDCFC using Carbon Black and Porous Nickel

The preliminary results obtained from the constructed MDCFC were based on the potential of the fuel cell to produce open circuit voltage (OCV) without generating current from the system. Figures 6.10 and 6.11 give the open circuit voltage of the tests carried out on the MDCFC using two different flow rates of CO₂. The OCV presented in Figure 6.10, has CO₂ flow rate at 140 cm³/min and air at 700 cm³/min. While for Figure 6.11, we have CO₂ flow rate at 250 cm³/min and air at 700 cm³/min. The difference between the two figures demonstrates the importance of CO₂ in the operation of the MDCFC as well as in other fuel cells.

At a lower flow rate of CO₂ (Figure 6.10), the voltage (0.18 V) generated was from 460°C and slightly increases until it got to a temperature of 480°C, there was a rapid increase in the voltage obtained between 480°C to 520°C. This rapid increase could be attributed to the point in which the electrolyte became molten and the carbonate ions became reactive in the MDCFC system. A maximum open circuit voltage of 0.710 V was observed between the temperatures of 530°C and 540°C, this gave the point in the MDCFC with maximum OCV performance. Between the temperature of 560°C and 570°C there was a sharp drop in voltage to 0.580 V, this illustrate a potential error at that point in the MDCFC operation, the reason attributed to this error is a sudden drop in the CO₂ pressure, a situation which is associated with the malfunctioning of the rotameter in maintaining the CO₂ pressure.

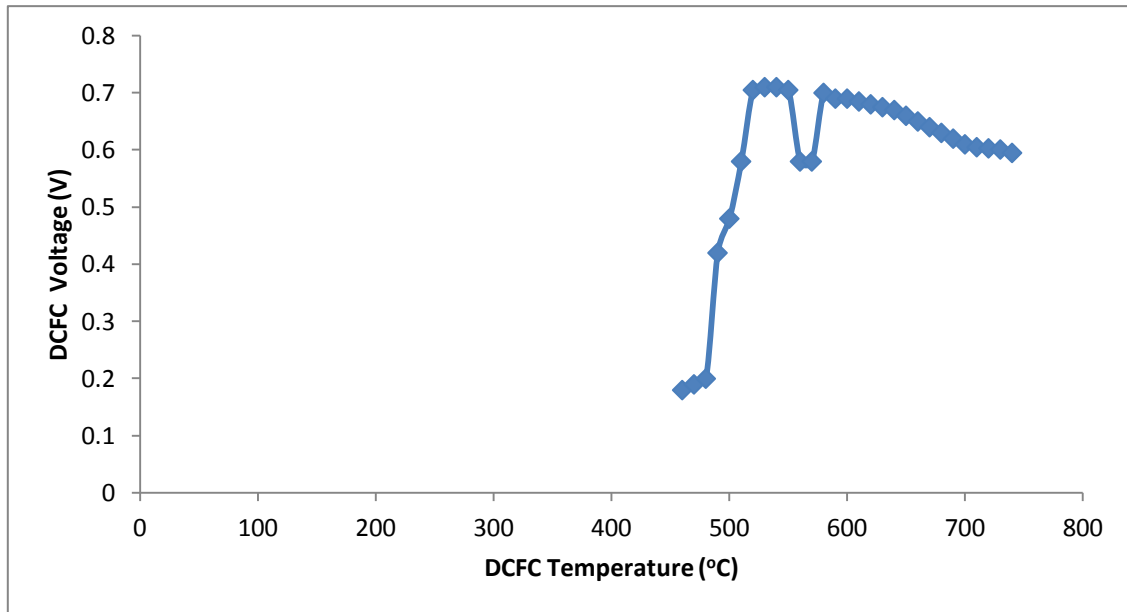


Figure 6.10: MDCFC open circuit voltage at varying temperature with CO₂ flow at 140 cm³/min

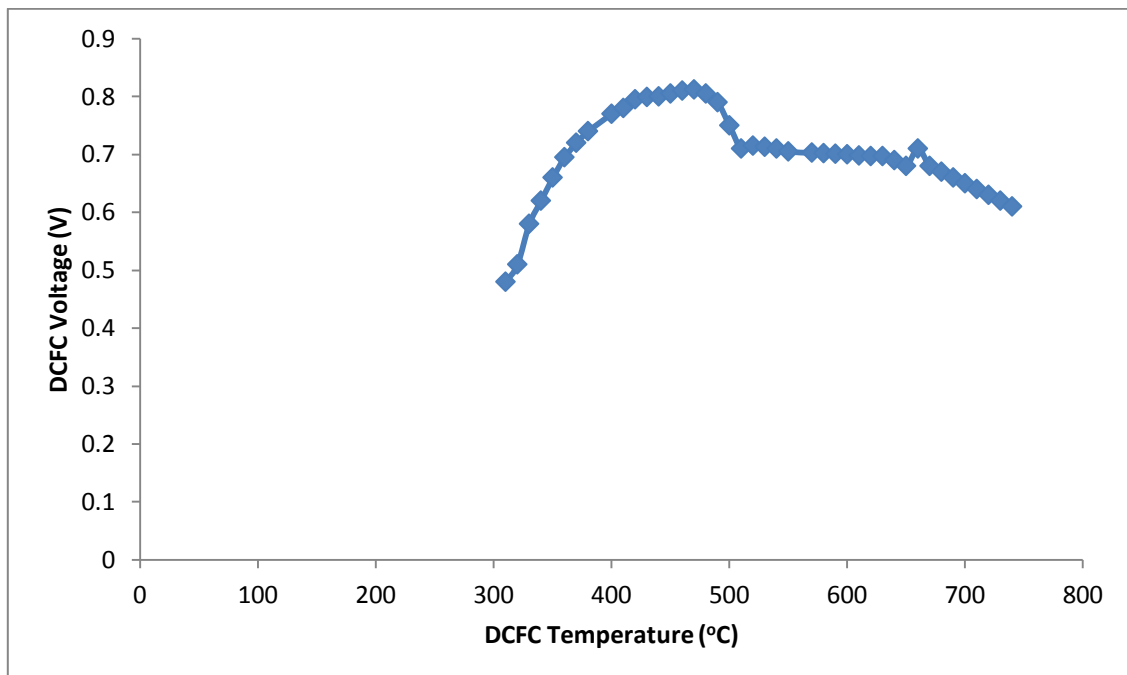


Figure 6.11: MDCFC open circuit voltage at varying temperature with CO₂ flow at 250 cm³/min

From a temperature of 590°C the voltage reading began to drop to 0.690 V and further continue to drop with increase in temperature, signifying a drop in the OCV performance of the MDCFC. The calculated maximum voltage efficiency for the MDCFC at this operating condition was 70%. Figure 6.11 shows an improved OCV performance from the cell as the CO₂ flow was increased to 250 cm³/min, it also gave higher voltage reading for the MDCFC above 0.8 V. The fuel cell OCV performances using industrial carbon black fuel from room temperature are presented in Figure 6.12.

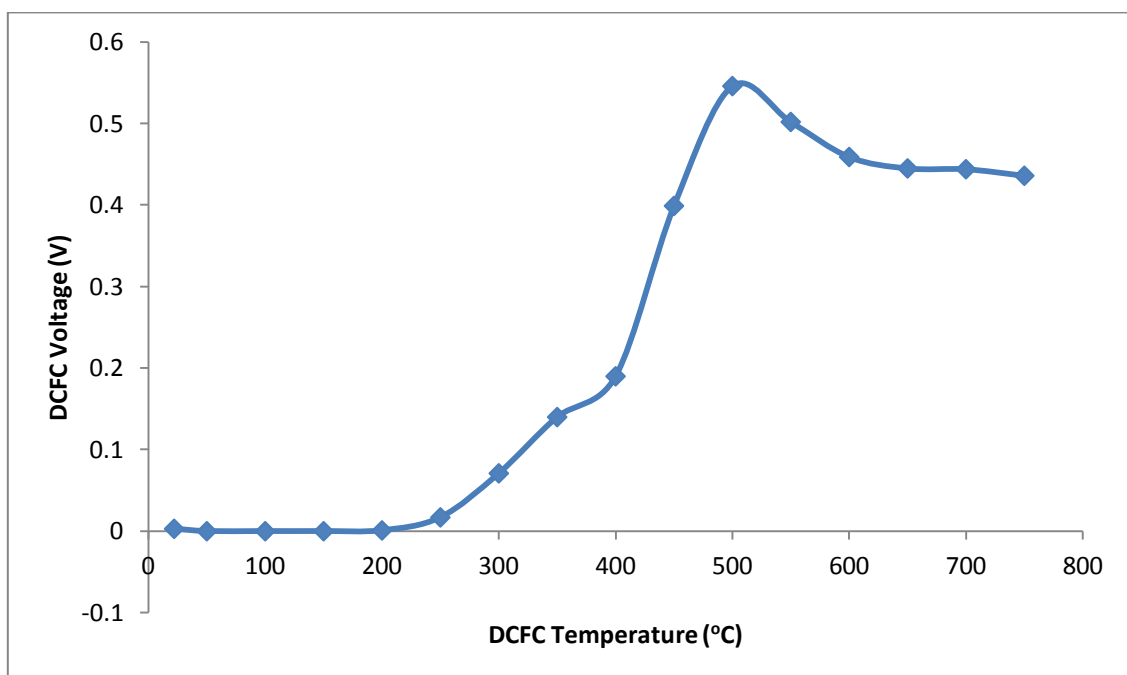


Figure 6.12: MDCFC OCV at varying temperature using carbon black

The MDCFC operation result given in Figure 6.11 is a better result than that of the Figure 6.10 with calculated voltage efficiency of 80%. In all these cases carbon black and carbonate mixture (lithium and potassium carbonates) were used as the fuel, gold wire connectors, gold mesh at the cathode, saturated zirconia electrolyte and porous nickel at the anode. In Figure 6.11 the OCV generated were recorded from 310°C and progressively increased till it reached a maximum open circuit voltage of 0.812 V at 470°C after which there was a gradual drop. Figure 6.12 shows the voltage profile generated from carbon black/carbonate fuel from room temperature to the final

operating temperature of 750°C having the highest voltage of 0.55 V. These preliminary tests on the MCDCCFC helped to achieve an optimum operating conditions of N₂ (200 cm³/min), CO₂ (600 cm³/min) and compressed air (1500 cm³/min). These were then applied for the rest of the MCDCCFC operations.

6.3.2 Voltages from MCDCCFC using Biomass and Gold Mesh-ZrO₂-Gold Mesh Electrode Assembly

Figure 6.13 shows the voltages (OCV) obtained using the six biomass fuels. Poplar fuel (Pop) gave the highest voltage of 1.1 V, and wheat fuel (Whe) the lowest at 0.8 V. Spruce fuel (Spr) gave the second highest voltage of 1.0 V, followed by miscanthus (Mis, 1.0 V), switchgrass (Swi, 0.9 V) and willow (Wil, 0.9 V) using gold mesh, saturated zirconia and gold mesh arrangement.

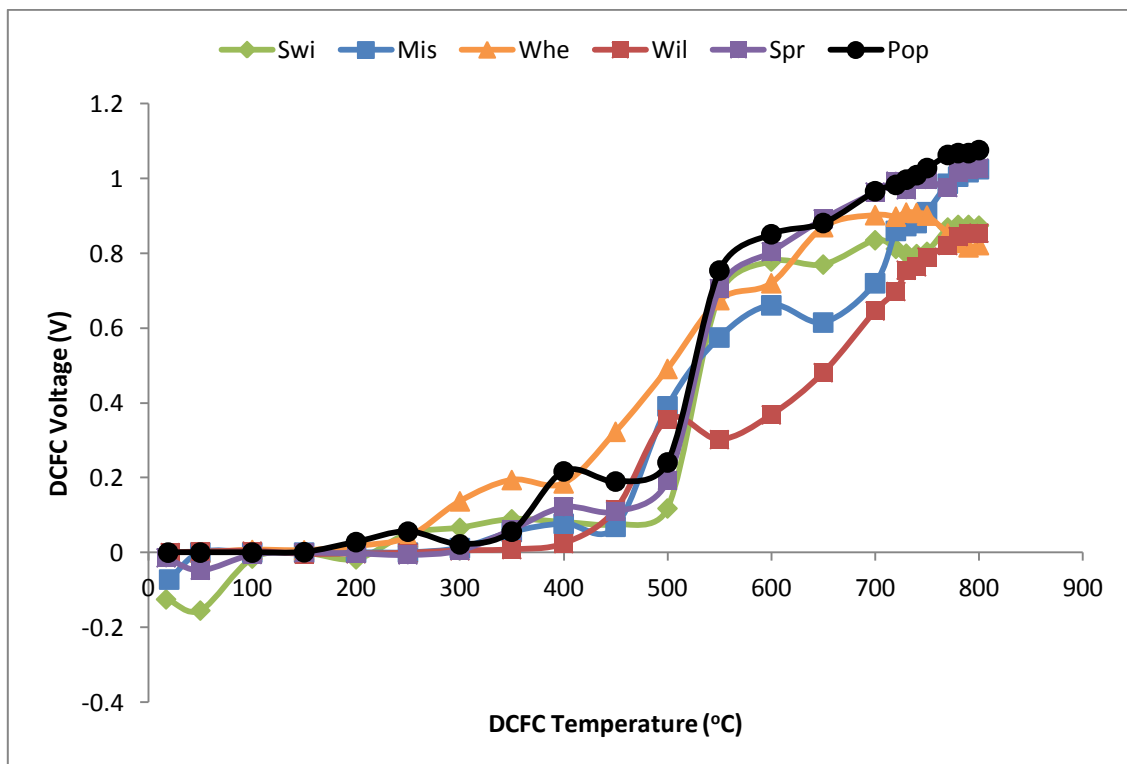


Figure 6.13: MCDCCFC OCV for the six biomass carbon fuels at different temperature

It was observed that the voltage increases with increase in temperature. Poplar and spruce display a similar pattern in the generation of voltage. The pattern generated by miscanthus, switchgrass, wheat and willow were different. There was a sharp rise in the OCV at 500°C (Figure 6.13), which is due to the ionic conduction in the phase of the molten carbonate and the melting of the carbonate salt mixture. The performances of the fuel cell was greatly enhanced as the temperature increases up to 800°C, this is attributed to the decrease in the viscosity of the molten carbonate phase and a corresponding enhancement of the ionic conduction rate of the electrolyte and the electrochemical reactions at the two electrodes (Jia *et al.*, 2010; Li *et al.*, 2009; Jain *et al.*, 2008; Hackett *et al.*, 2007; Cherepy *et al.*, 2005).

6.4 MCDRFC Performances with Porous Nickel- ZrO₂-Gold Mesh Electrode Assembly

The preliminary fuel cell arrangement are shown in Figures 6.2 and 6.3 which consists of the electrode assembly using porous nickel, zirconia saturated in carbonated mixture (lithium carbonate and potassium carbonate) and gold mesh. The direct carbon fuel cell performances are shown in Figures 6.14 to 6.22.

6.4.1 MCDRFC Performances using Carbon Black

Figures 6.14 to 6.16 show the results obtained from the MCDRFC using carbon black/carbonate fuel at four different temperature regions of 550°C, 600°C, 650°C and 700°C. Industrial carbon black was used (Acetylene, 100 % compressed, 99.9+% metal basis, Alfa Aesar, Johnson Matthey Co., USA). The current densities were calculated by dividing the cell voltages by the resistances and the active surface area of the cell (2.5 cm²). The power density was also calculated by squaring the voltages and dividing by the resistances and the active surface area of the cell.

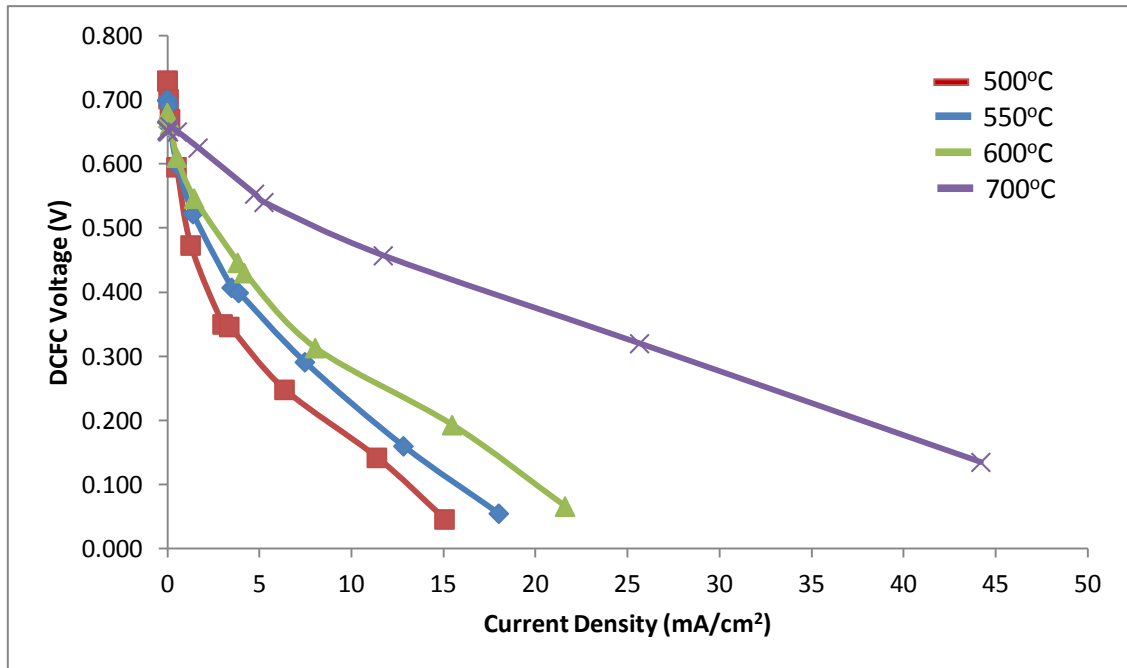


Figure 6.14: Voltage versus current density using carbon black at different temperature.

At the lowest temperature of 500°C the highest OCV (0.73 V) was obtained having the lowest current density of 15 mA/cm² (Figure 6.14). At 550°C we had a voltage of 0.70 V and a maximum current density of 18 mA/cm². For the 600°C point we had 0.68 V and a maximum current density of 22 mA/cm². The voltage was 0.65 V at 700°C and a maximum current density of 44 mA/cm². These corresponding drops in voltages at each temperature regions are as a result of the load (resistance) applied to the cell. Twelve resistances were applied (1.167 MΩ the highest and 1.2 Ω the lowest) across the cell for each temperature regime.

Figure 6.14 shows that the current density-voltage curves drop initially due to activation resistance. This activation resistance lead to activation losses or voltage drop in the fuel cell. This is caused by the slowness of the reactions taking place on the surfaces of the electrodes, a proportion of the voltage generated is lost in driving the chemical reaction that transfers the electrons to and from the electrode. The curves continue to decrease linearly due to the ohmic resistance of the fuel cell. The ohmic

resistance leads to ohmic losses or voltage drop, which is the resistance to the flow of electrons through the material of the electrodes and the different interconnections. Ohmic losses also include the resistance to the flow of ions through the electrolyte. The ohmic resistance is also known as the area specific resistance (ASR) of the fuel cell. Eventually the voltage decreases sharply at high current density due to mass transport or concentration losses. This is brought about from the change in the concentration of the reactants at the electrodes surface as the fuel is being consumed. The reduction in concentration leads to insufficient reactants transportation to the electrode surface and is otherwise known as mass transport loss (Li *et al.*, 2009; Jain *et al.*, 2008; Hackett *et al.*, 2007; O'Hayre *et al.*, 2006; Cherepy *et al.*, 2005; Larminie and Dicks, 2003; Hoogers, 2003). Figure 6.15 shows the corresponding power and current densities for the carbon black fuel using the same four temperature regimes.

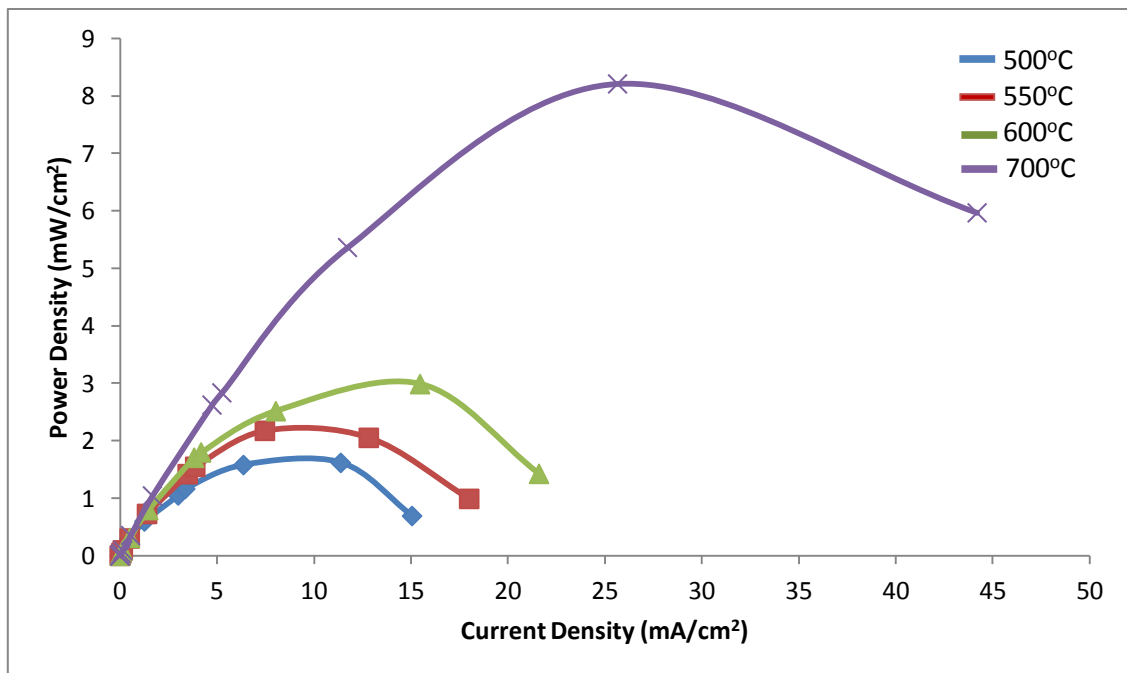


Figure 6.15: Power versus current density using carbon black at different temperature.

There were increases in the power and current densities with increasing temperatures. The highest power density was recorded at 700°C (8 mW/cm²) at the maximum current density of 44 mA/cm². The power greatly reduces to 3 mW/cm² at 600°C,

which further reduces at 550°C to 2 mW/cm². The value at 500°C was 1.5 mW/cm². Figure 6.16 combines the results from Figures 6.14 and 6.15 and gave the overall performances of the MDCFC. 500V and 500P represent the voltages and power densities at 500°C and this applies to the other temperatures.

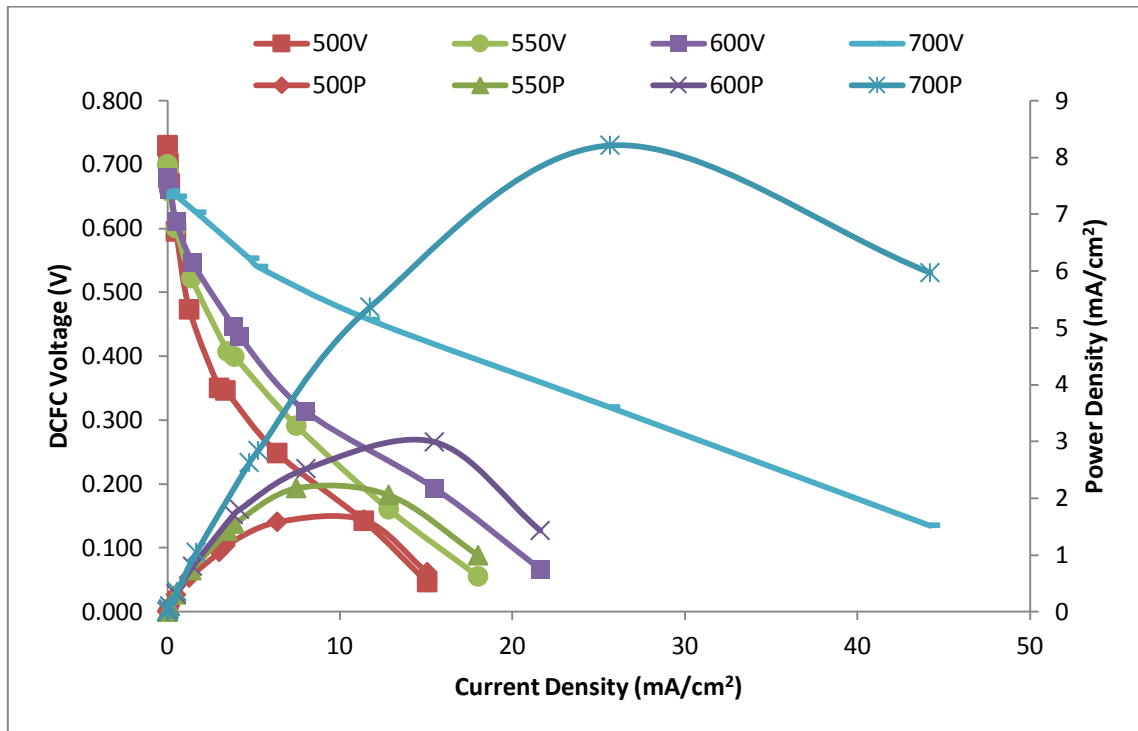


Figure 6.16: Voltage, power and current density using carbon black at different temperature.

Figure 6.16 gives an overall assessment of the MDCFC performances for the four temperature regimes. It shows that temperature has great effect on the performances of the MDCFC as reported by other researchers (Li *et al.*, 2009; Jain *et al.*, 2008; Cao *et al.*, 2007; Hackett *et al.*, 2007; Cherepy *et al.*, 2005; Zecevic *et al.*, 2003; Patton, 2003).

6.4.2 MCDRFC Performances using Miscanthus Carbon with Porous Nickel Electrode Assembly

The direct carbon fuel cell performances using porous nickel, saturated zirconia and gold mesh are shown in Figures 6.17 to 6.19. The performances recorded for the miscanthus and willow using the same type of cell arrangement as the carbon black was much better. In the case of miscanthus fuel we have an OCV of 1.0 V as against the 0.7 V for the carbon black and also higher current and power densities as presented in Figures 6.17 to 6.19.

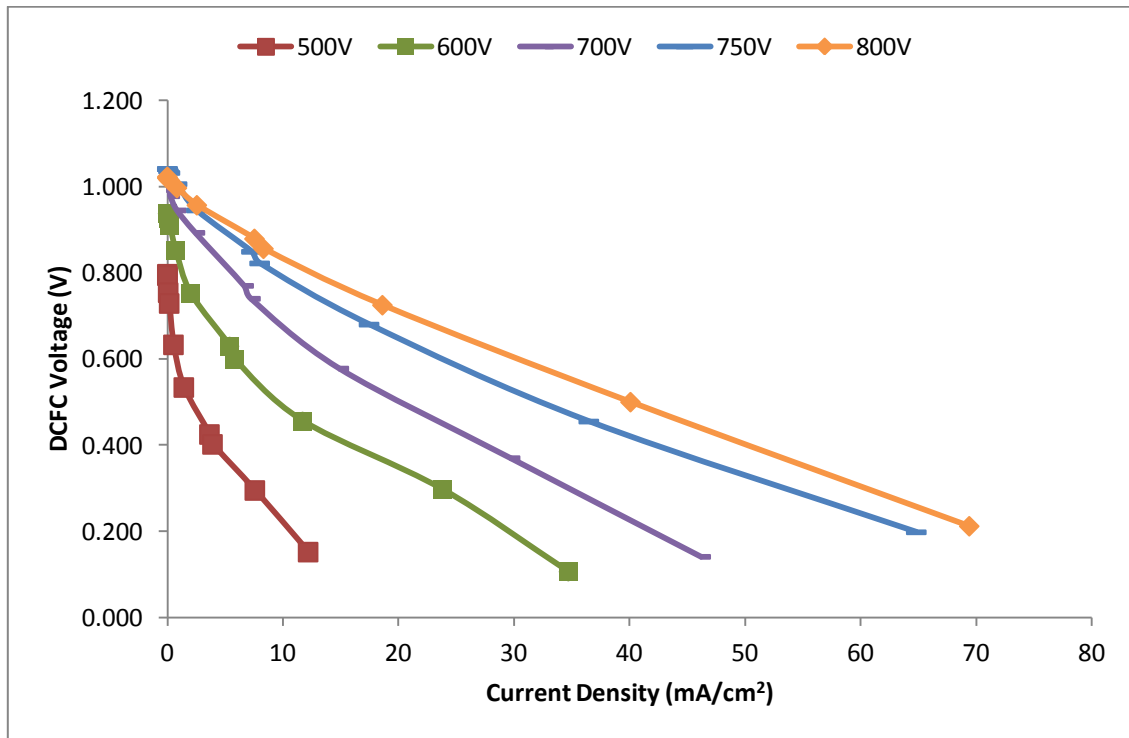


Figure 6.17: Voltage versus current density using miscanthus at different temperature

Figure 6.17 shows the voltages and current densities at five different temperature regimes for miscanthus fuel. Again the higher the temperature the higher the voltage recorded by the fuel cell. The highest temperature was at 800°C in which we have an OCV of 1.0 V and a maximum current density of 70 mA/cm². At 750°C the voltage is 1.0 V and 66 mA/cm² current density. At 700°C we have 0.95 V and 48 mA/cm² current density. At 600°C the voltage was 0.9 V and 35 mA/cm² current density. This further

reduces at 500°C to 0.8 V and 12 mA/cm² current density. Figure 6.18 shows the power and current density using miscanthus fuel at the same five different temperatures regimes. The highest power density was 20 mW/cm² for the temperature regime of 800°C. At 750°C we have 17 mW/cm². This reduces to 13 mW/cm² at 700°C. It was much smaller at 600°C with 7 mW/cm² and finally 2 mW/cm² at 500°C. Figure 6.19 show the combinations of Figures 6.17 and 6.18.

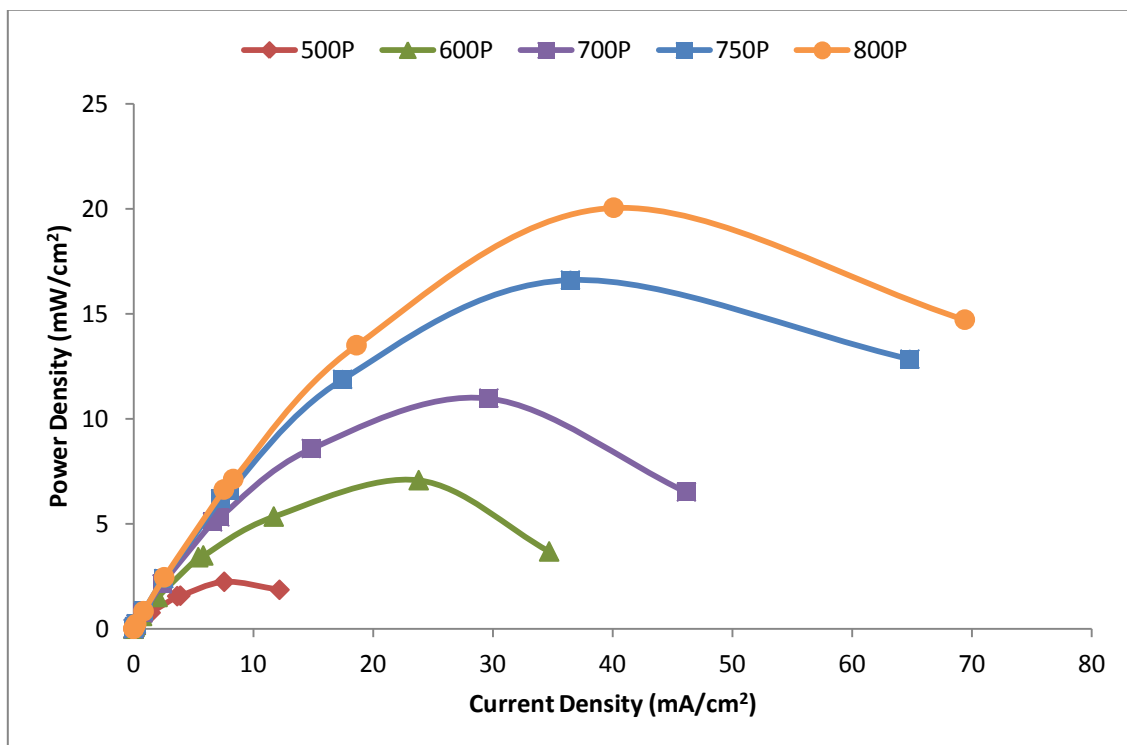


Figure 6.18: Power versus current densities using miscanthus at different temperature

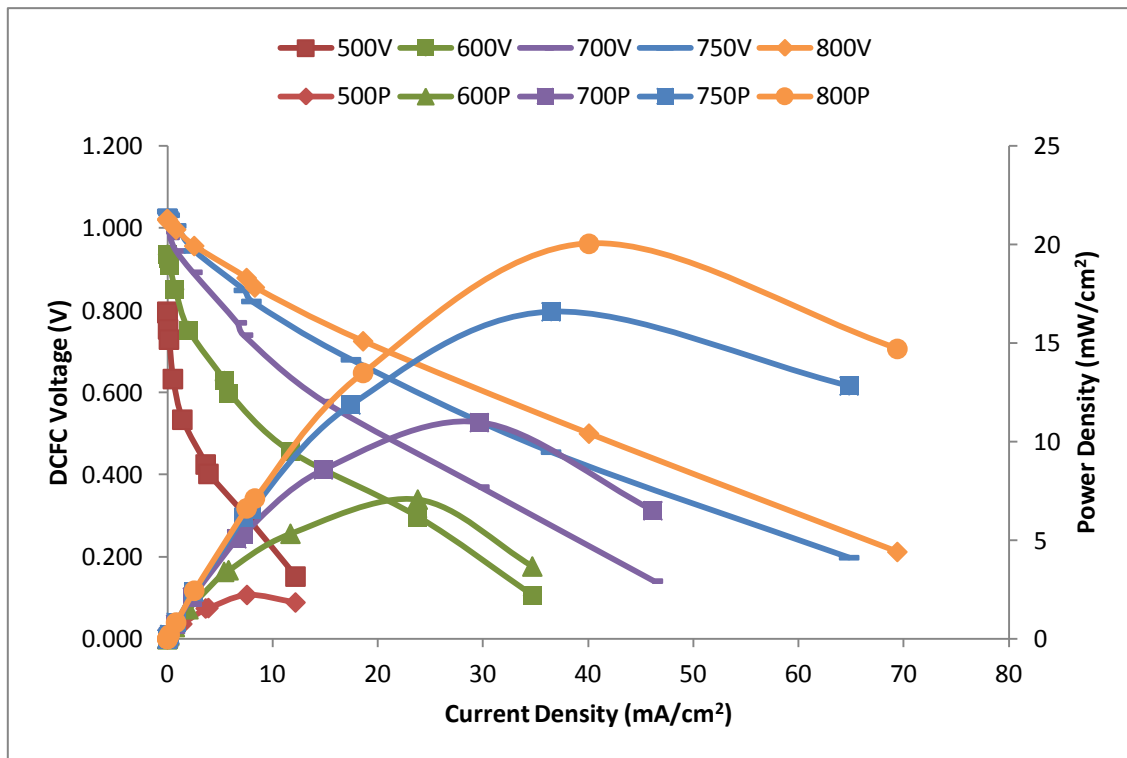


Figure 6.19: Voltage, power and current densities using miscanthus Fuel

6.4.3 MDCFC Performances using Willow Carbon

The performances recorded from the fuel cell operations using willow fuel in terms of the power and current densities were higher than those observed in the miscanthus fuel. Figures 6.20 to 6.22 show these performances. The same cell arrangement (porous nickel, saturated ZrO_2 and gold mesh) was still used for the willow fuel cell operations but a fresh electrolyte was used, the fuel cell was disassembled and thoroughly cleaned before reassembling. It was noticed that porous nickel apart from acting as the anode probably also acted as a catalyst thus giving good MDCFC performances.

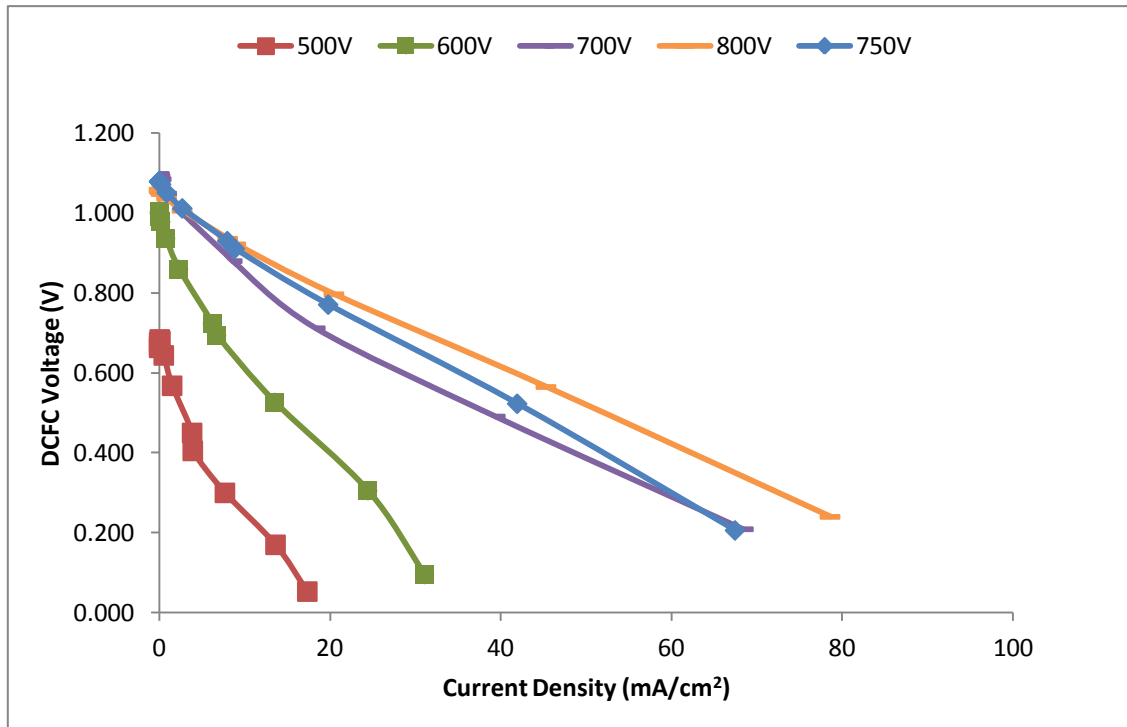


Figure 6.20: Voltage versus current density using willow at different temperature.

Figure 6.20 gives the voltages recorded using the willow fuel. The voltages recorded at 800°C was 1.1 V and a maximum current density of 80 mA/cm². The voltage at 750°C was 1.1 V and a current density of 70 mA/cm². This voltage was still 1.1 V at 700°C and 70 mA/cm². At 600°C we have 1.0 V and 32 mA/cm² but were much lower at 500°C with 0.7 V and 18 mA/cm².

Figure 6.21 shows the power and current density performances for the willow fuel, again here the performances were higher than that of miscanthus fuel. The highest power density was 25 mW/cm² at 800°C compared to 20 mW/cm² for miscanthus. At 750°C we have 22 mW/cm² with 17 mW/cm² for miscanthus. This reduces to 17 mW/cm² at 700°C as against 13 mW/cm² for miscanthus. It was much smaller at 600°C with 7 mW/cm² the same for miscanthus fuel. Finally 2 mW/cm² at 500°C also the same with miscanthus fuel. Figure 6.18 show the combinations of Figures 6.20 and 6.21.

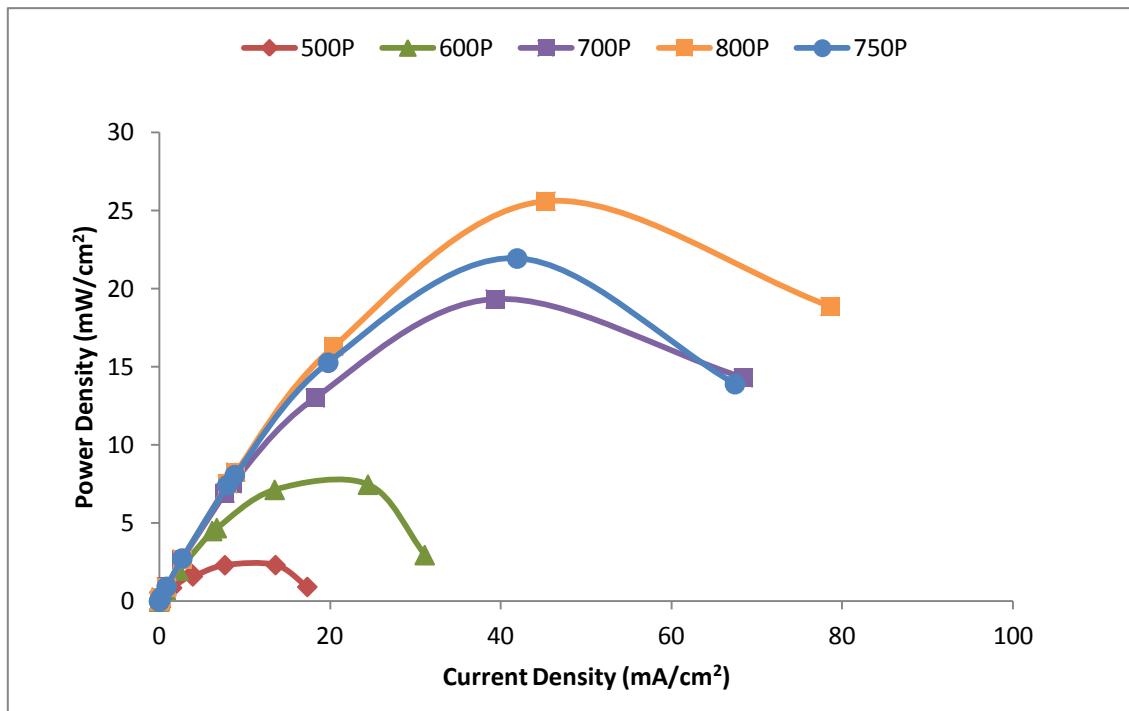


Figure 6.21: Power versus current density using willow at different temperature.

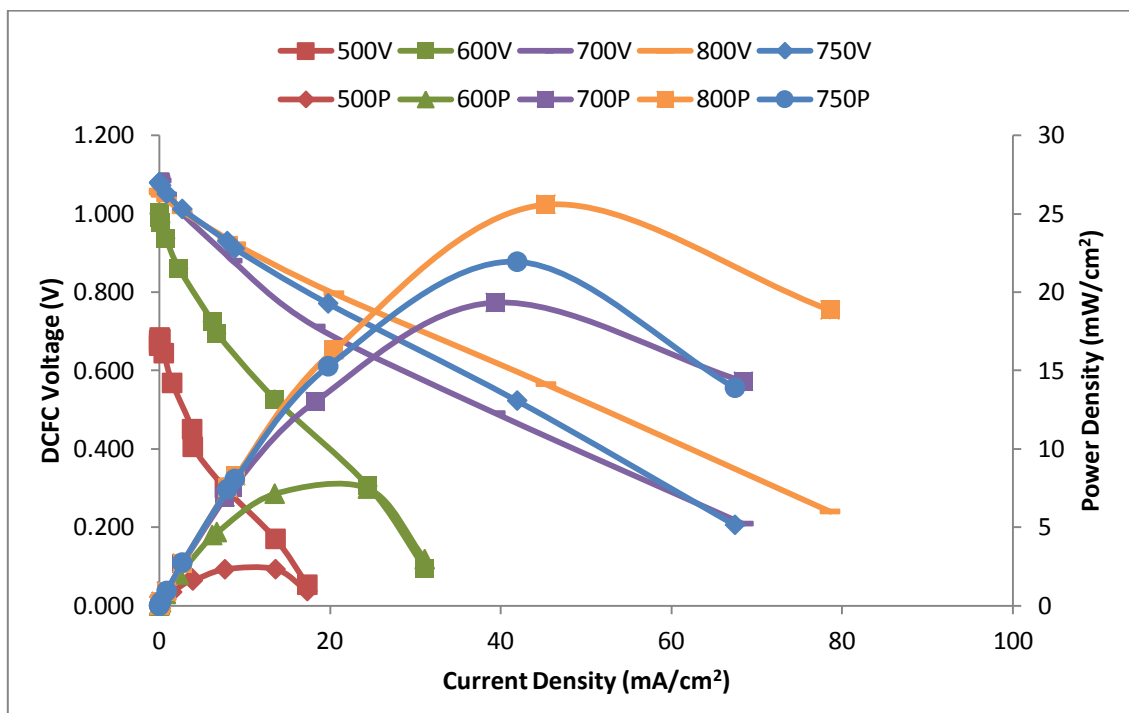


Figure 6.22: Voltage, power versus current density using willow at different temperature.

6.5 MCDRFC Performances with Gold Mesh- ZrO_2 -Gold Mesh Electrode Assembly

The MCDRFC performances recorded for the six biomass carbon fuels are presented in Figures 6.23 to 6.31. The molten carbonate direct carbon fuel cell electrode assembly were gold mesh, zirconia and gold mesh as shown in Figure 6.5. Figure 6.23 shows the voltage readings versus the current density supplied by the MCDRFC using hand milled (HM) biomass carbon fuels. The performances of the MCDRFC presented are for the first day while the second and third day operations are given in Appendix C.

6.5.1 First Day Performances of the MCDRFC using HM Biomass Carbon

Figures 6.23 to 6.25 show the voltage versus current densities results of the MCDRFC for the first day. Poplar fuel gave the highest results while willow fuel gave the lowest. The acronym MisV and MisP represent the voltages and power densities of miscanthus fuel and likewise for the other fuels of Swi (switchgrass), Spr (spruce), Pop (poplar), Whe (wheat) and Wil (willow) biomass carbon fuels.

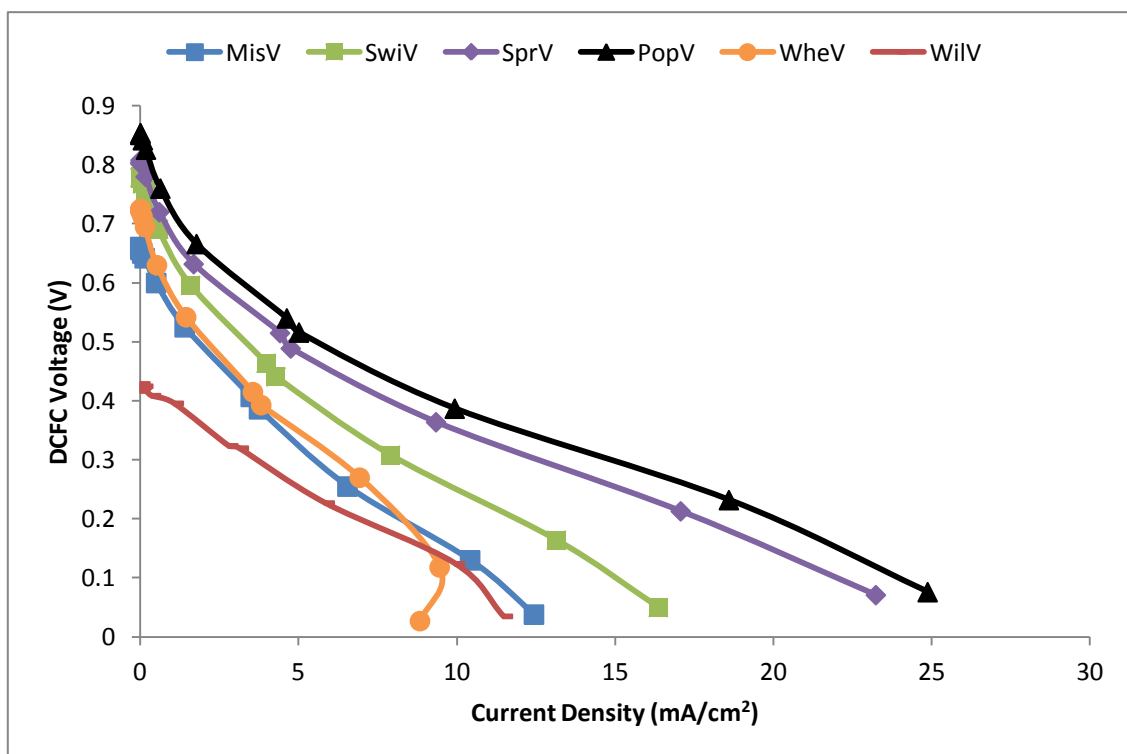


Figure 6.23: Voltage, current density for the 6 biomass fuels at 600°C (HM-Day 1).

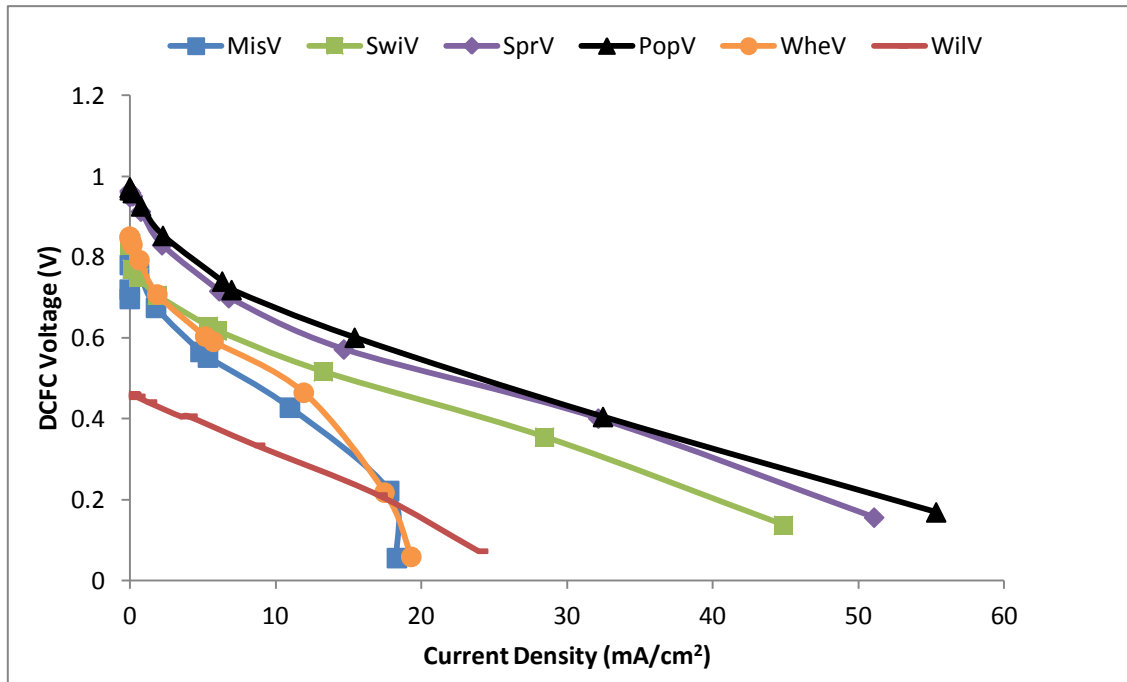


Figure 6.24: Voltage, current density for the 6 biomass fuels at 700°C (HM-Day 1).

At the operating temperature of 600°C, poplar fuel gave the highest open circuit voltage (OCV) (0.85 V) this is followed by spruce (0.83 V), switchgrass (0.79 V), wheat (0.72 V), miscanthus (0.66 V) and willow (0.42 V) fuels. The performances of poplar and spruce fuels could be attributed to the high calorific values they possess, in this work we reported 31 MJ/kg and 33 MJ/kg respectively which are in agreement with findings from other researchers (Nowakowski *et al.*, 2007; McKendry, 2002). These values are comparable to those presented in Tables 2.2 and 2.3 (Montross and Crofcheck, 2010; Klass, 1998) and our work (Tables 5.16 to 5.24). Generally the performances of all the fuels increase with increased temperature. At 700°C the performance of spruce fuel was close to that of poplar and slightly surpasses at 800°C within 30 to 60 mA/cm² of the current density axis (Figures 6.24 and 6.25).

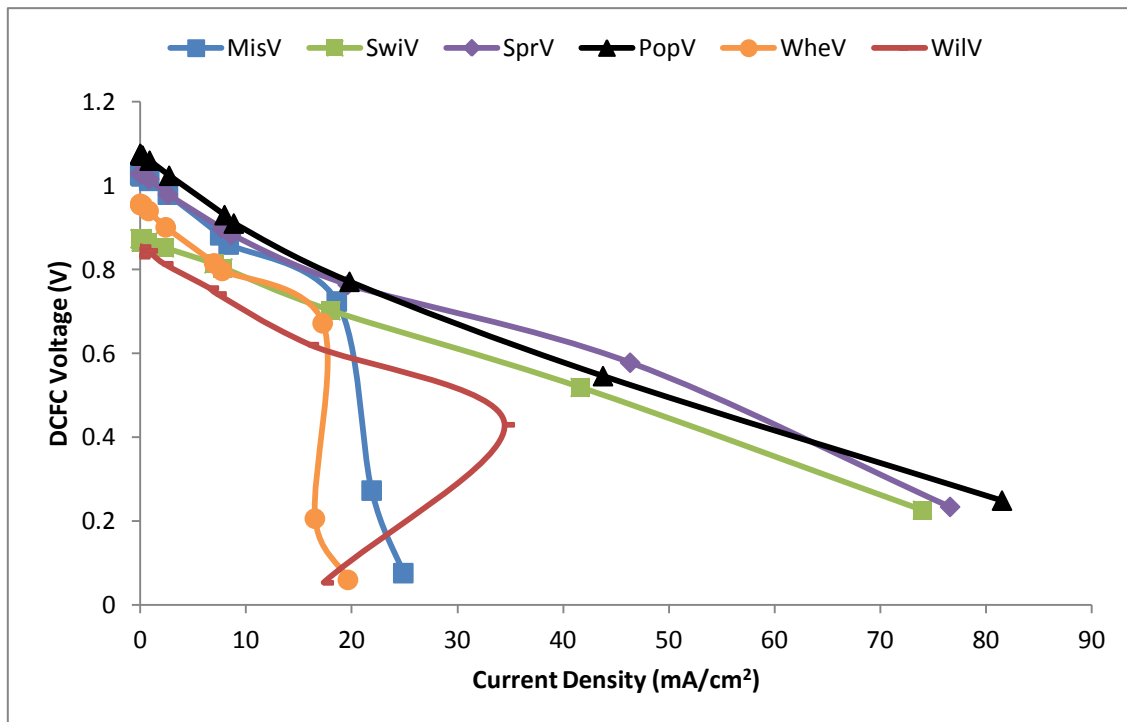


Figure 6.25: Voltage, current density for the 6 biomass fuels at 800°C (HM-Day 1).

Figures 6.23 to 6.25 show that the current density-voltage curves drop initially due to activation resistance. This activation resistance lead to voltage drop in the fuel cell. The curves continue to decrease linearly due to the ohmic resistance (ASR) of the MCDRFC. Table 6.1 gives the calculated ASR for the MCDRFC. Eventually the voltage decreases sharply at high current density due to mass transport or concentration losses (Li *et al.*, 2009; Jain *et al.*, 2008; Hackett *et al.*, 2007; O'Hayre *et al.*, 2006; Cherepy *et al.*, 2005; Larminie and Dicks, 2003).

At 700°C the OCV performances of wheat fuel was close to that of miscanthus but by 800°C the performance of miscanthus rose close to that of spruce but suddenly dropped after 20 mA/cm² (Figure 6.25), this could be due to the aging or degradation process of the cell during operations. Willow fuel performance picked up close to that of wheat fuel. There is a notable behaviour of the wheat, willow and miscanthus fuels patterns at higher current density which are more pronounced at higher temperatures giving rise to a curving back phenomenon (Figures 6.23 and 6.25). These curving back

phenomena of the fuels are attributed to the overconsumption of the carbon fuel at the anode compartment giving rise to gaps between the fuel contact and the electrolyte layers (Jia *et al.*, 2010). This was also reported by Jia and co-worker (2010) and their graphs are shown in Figure 6.26. The active surface area of the MDCFC was 2.5 cm^2 , this was used throughout the calculation of the current and power densities. The curve back phenomena lead to reduction in this active surface area but our calculations did not accommodate this change. This brings about lower values of the current and power densities and the patterns experience by some of the graphs presented.

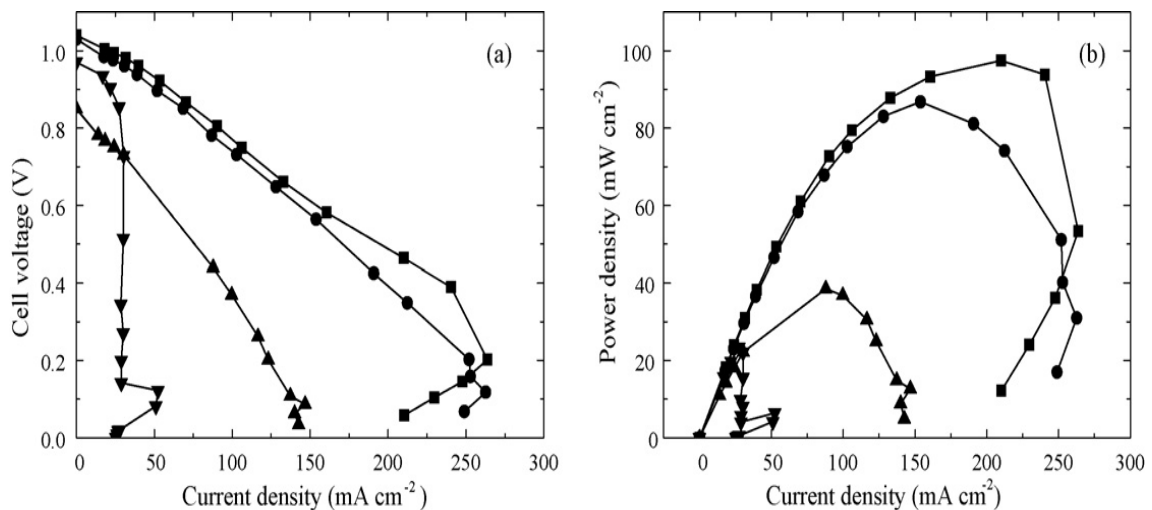


Figure 6.26: Voltage, Power and current density experiencing curving back phenomena at 700°C (Jia *et al.*, 2010).

Figures 6.27 to 6.29 show the power density versus the current density obtained from the MDCFC operations. Poplar still showed superior performance compared with the other fuels and willow showed the least performance in terms of the OCV, current and power densities.

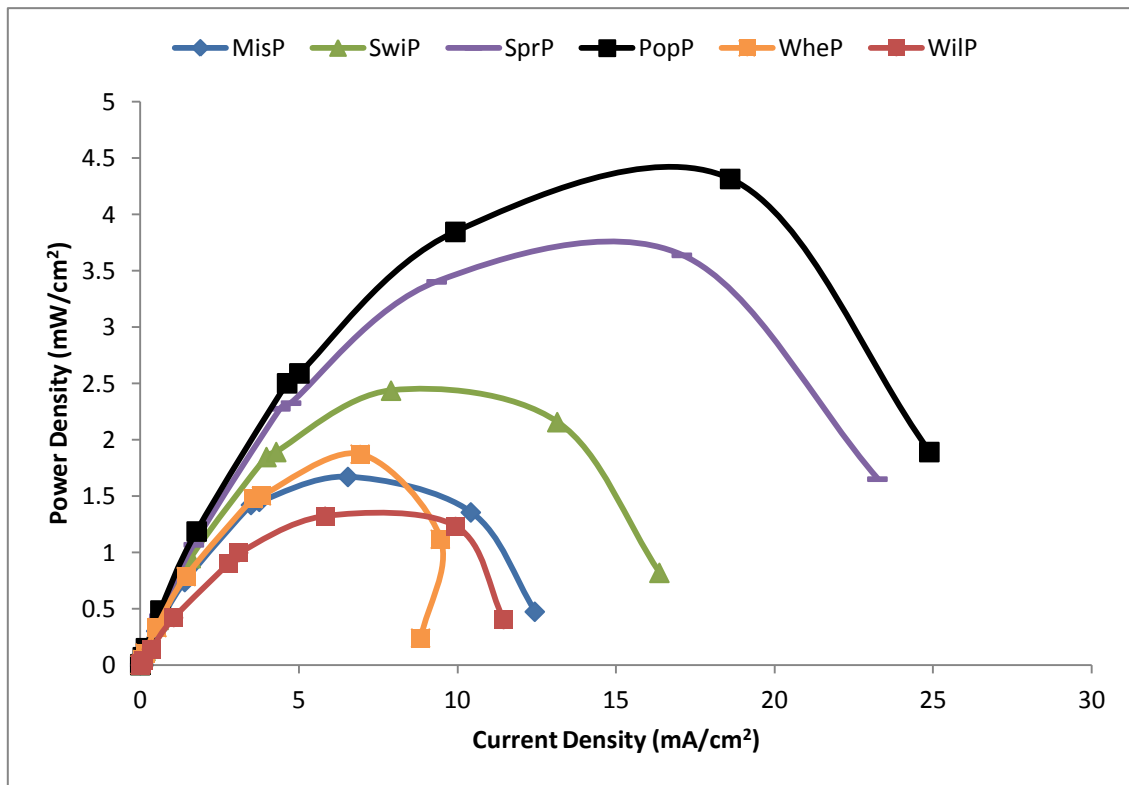


Figure 6.27: Power, current density for the 6 biomass fuels at 600°C (HM-Day 1).

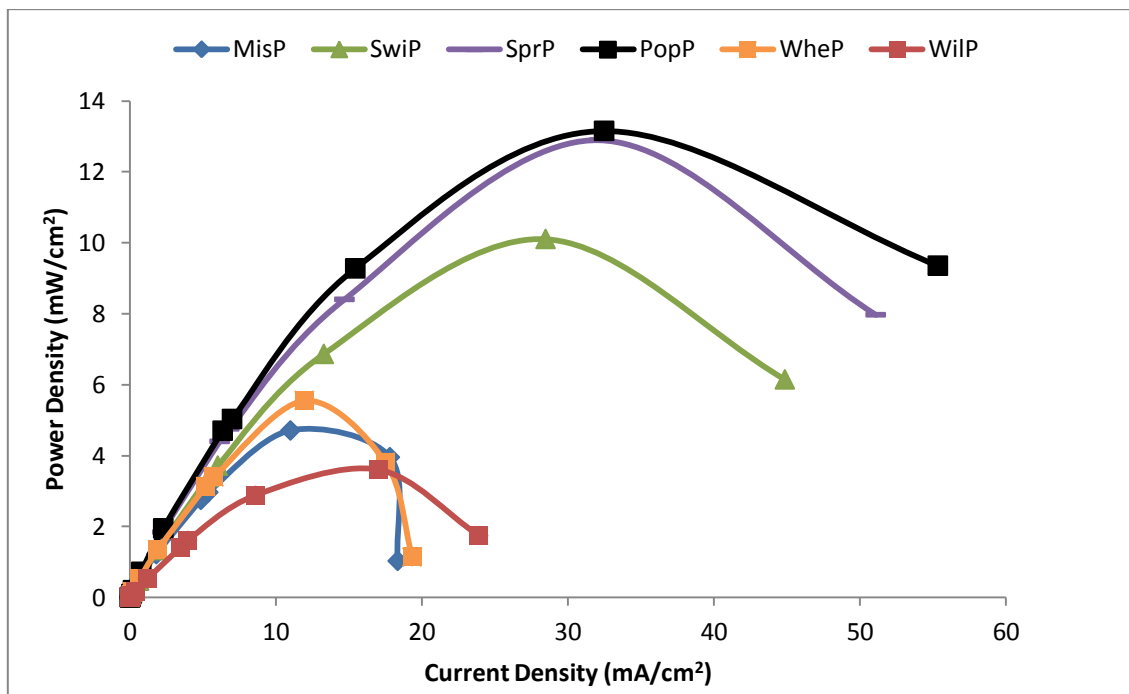


Figure 6.28: Power, current density for the 6 biomass fuels at 700°C (HM-Day 1).

From Table 2.3 (Chapter 2), spruce and poplar biomass have higher values of lignin compared to the other biomasses, this could be responsible for the high performance experienced from these biomass carbons (Montross and Crofcheck, 2010; Klass, 1998). Lignin is also known to be amorphous due its branched and partly random structure (Henriksson *et al.*, 2010). Lignin has relatively low oxygen content and large energy content and very stable solid material due to its chemical structure and highly cross-linked nature (Petrus and Noordermeer, 2006). At the temperature of 600°C poplar still gave the highest power density (4.32 mW/cm²), which was followed by spruce (3.64 mW/cm²), switchgrass (2.44 mW/cm²), wheat (1.7 mW/cm²), miscanthus (1.5 mW/cm²) and willow (1.4 mW/cm²) fuels (Figure 6.27). At 700°C there was sharp increase in the performance of the spruce and eventually surpassing poplar at 800°C for some regions. Figures 6.30 to 6.32 show the overall performances of the direct carbon fuel cell for the three different operating temperature regimes.

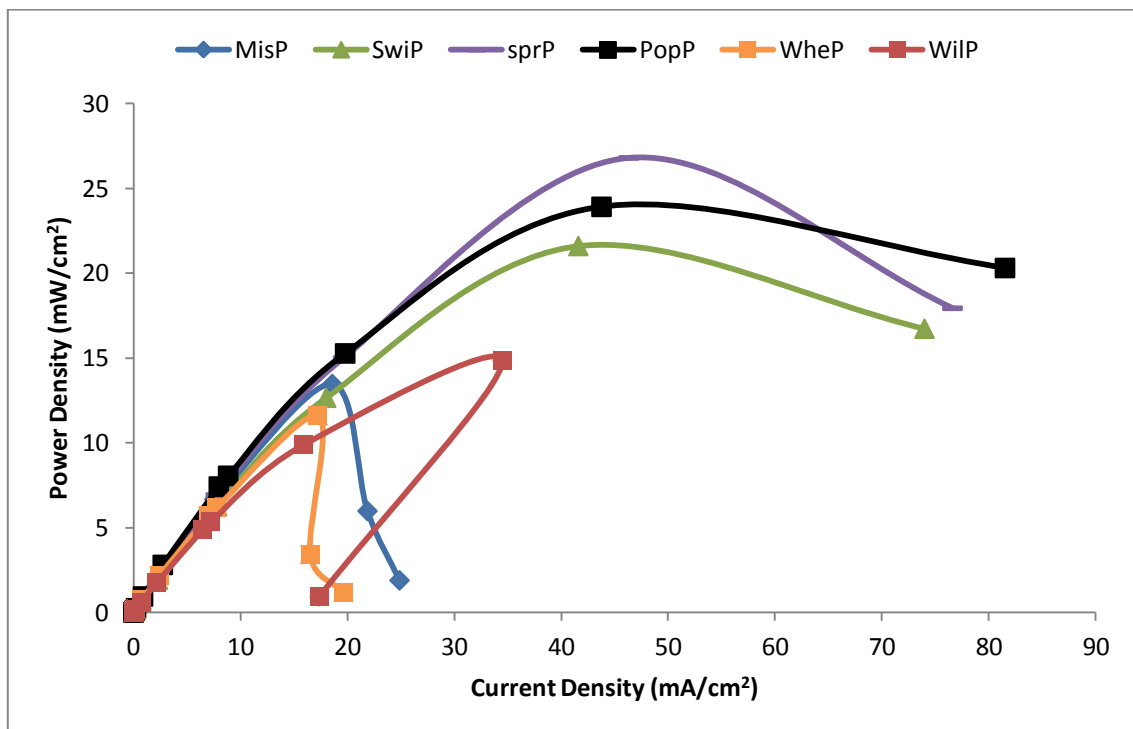


Figure 6.29: Power, current density for the 6 biomass fuels at 800°C (HM-Day 1)

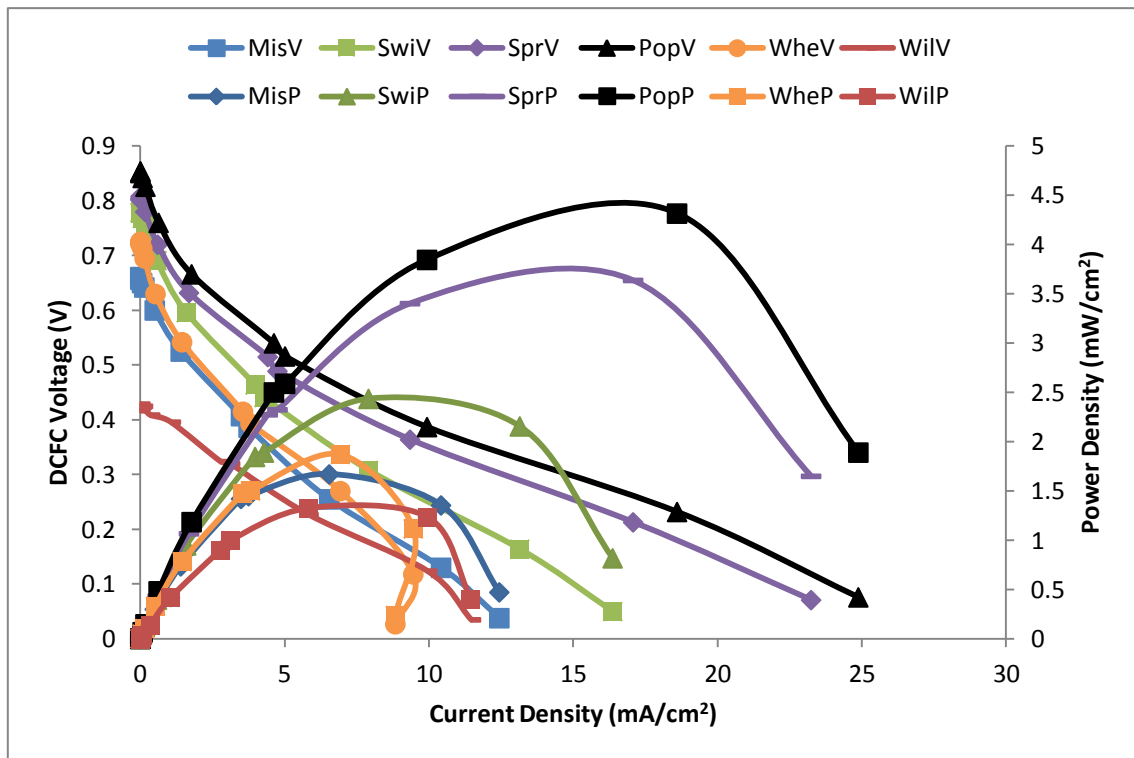


Figure 6.30: Overall performances for the 6 biomass fuels at 600°C (HM-Day 1)

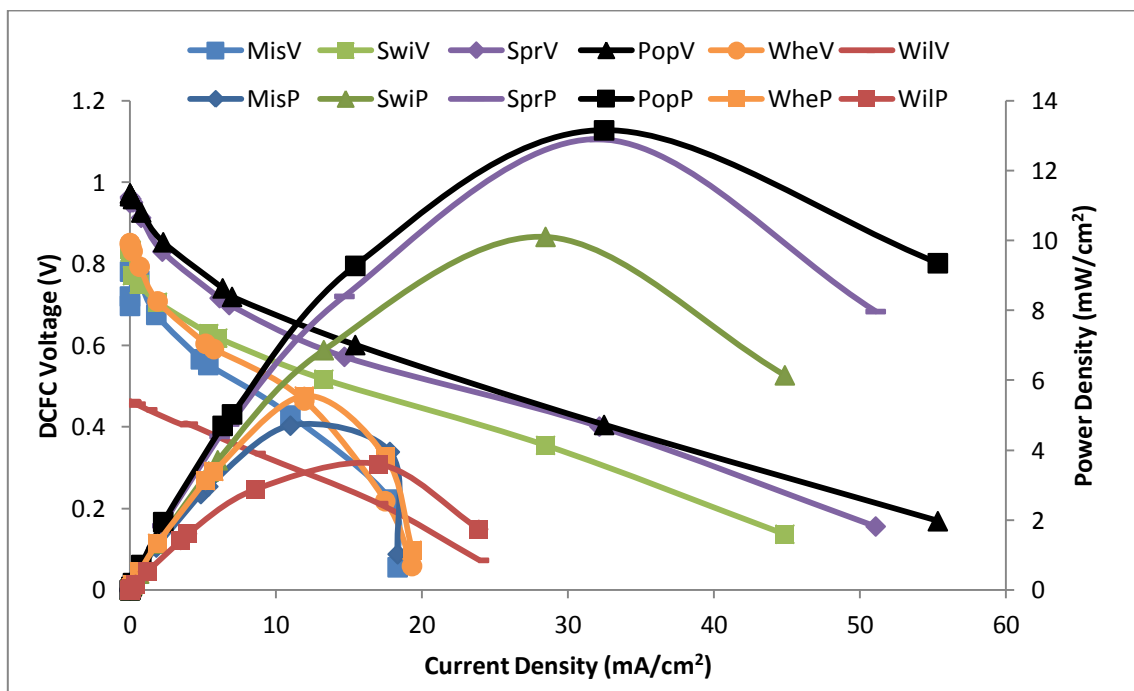


Figure 6.31: Overall performances for the 6 biomass fuels at 700°C (HM-Day 1)

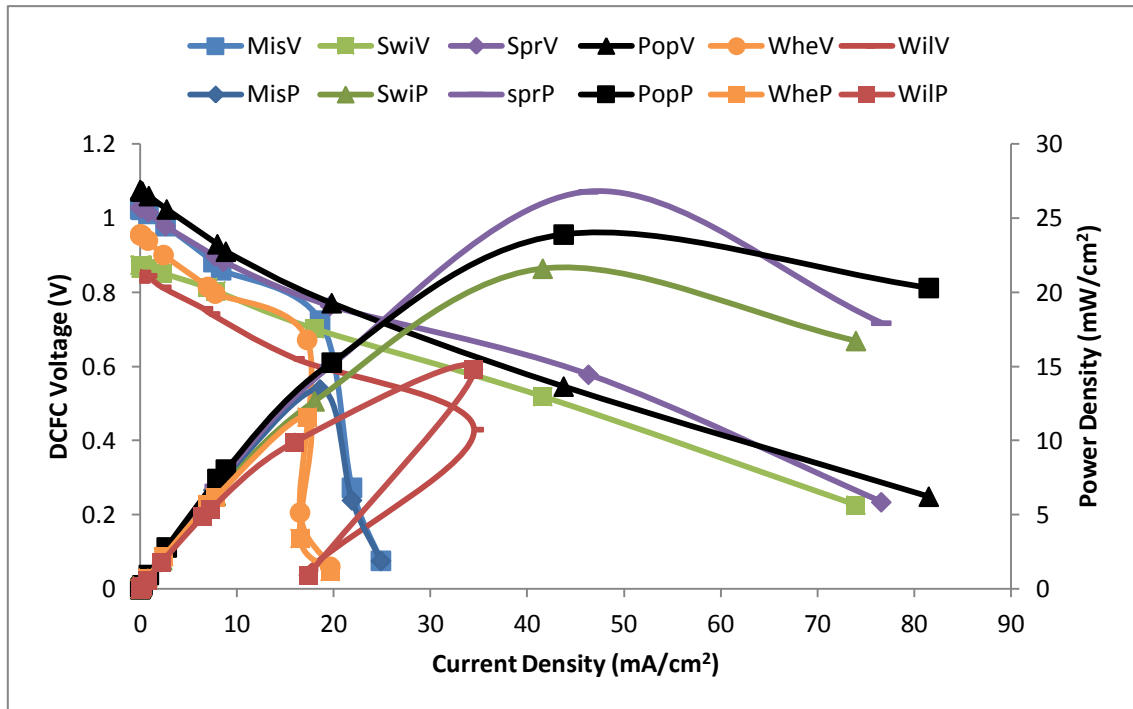


Figure 6.32: Overall performances for the 6 biomass fuels at 800°C (HM-Day 1)

Figures 6.29 and 6.32 show that miscanthus, wheat and willow fuel cell operations show some interesting phenomenon as reported earlier (Jia *et al.*, 2010, Figure 6.26). The DCFC power density increases with increasing current density, it reaches a maximum and finally falls at higher current densities (Li *et al.*, 2009; Hackett *et al.*, 2007). More results are presented in Appendix C.

6.5.2 Temperature Effects on MDCFC Performances with HM Carbon Fuel

The effects that temperature has on the performance of the MDCFC are shown in Figure 6.33 while the others are presented in Appendix C (Figures C5 and C6). The DCFC voltages presented on these figures are the open circuit voltage (OCV) of the cell. There is a sharp rise in the OCV above 400°C (Figure 6.33), which is due to the ionic conduction in the phase of the molten carbonate and the melting of the carbonate salt mixture which is in agreement with other reports (Jia *et al.*, 2010). The performance of the fuel cell was greatly enhanced as the temperature increases up to 800°C, also attributed to a decrease in the viscosity of the molten carbonate phase and a

corresponding enhancement of the ionic conduction rate of the electrolyte and the electrochemical reactions at the two electrodes (Jia *et al.*, 2010; Li *et al.*, 2009; Jain *et al.*, 2008; Hackett *et al.*, 2007; Cherepy *et al.*, 2005).

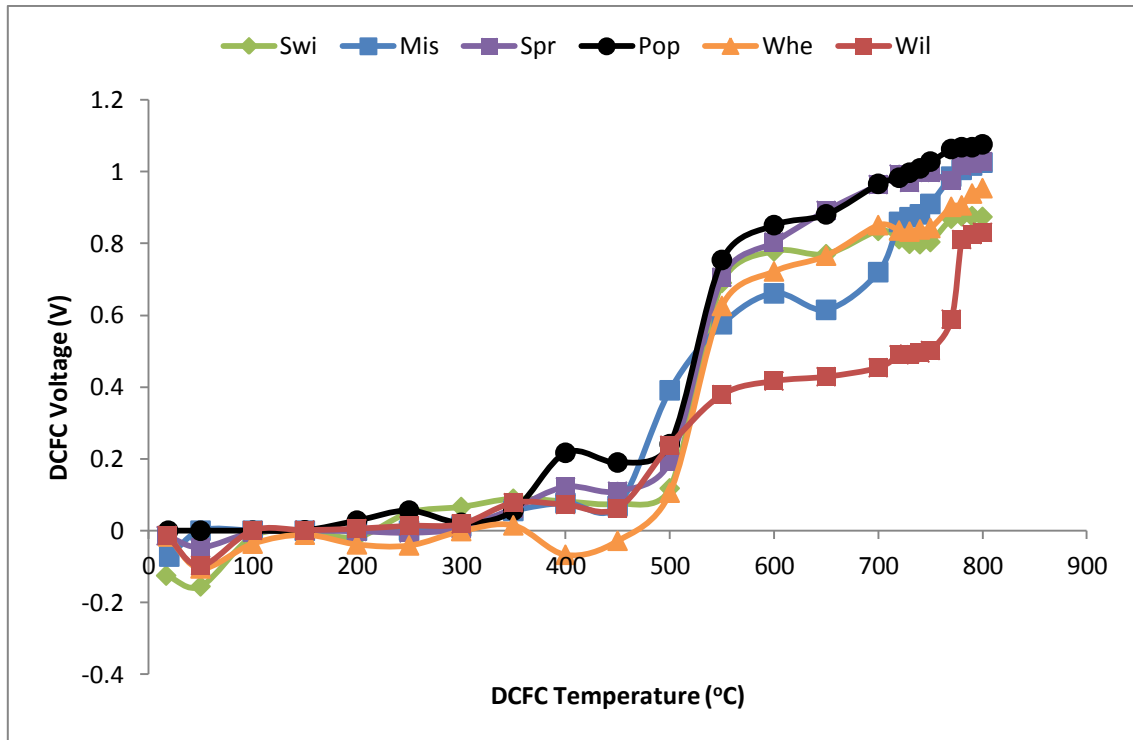


Figure 6.33: MDCFC voltages for the six biomass carbon fuels at different temperatures (HM-Day 1)

Figures C5 and C6 show that the sharp rise in the OCV starts at 400°C. At the start of the second and third day the existing DCFC set-up was used, additional fuel of 1.5 g was used for these days and the molten carbonate phase was reached much faster. It was observed that higher values of the OCV were obtained for the DCFC than the theoretical values, a situation which is attributed to low activities of CO or CO₂ at the anode compartment of the cell, which was help by the use of nitrogen gas purging the anode compartment (Jain *et al.*, 2008). At higher temperature there is a possibly of more CO₂ being produced which could decrease the voltage output of the cell if not properly removed (Hackett *et al.*, 2007).

6.5.3 MCDRFC Power Efficiency and ASR for HM Biomass Carbon Fuels

The power and voltage curves show characteristic behaviour for the single cell molten carbonate direct carbon fuel cell, and of particular interest are the effective open circuit voltage (OCV), peak power, current density and the area specific resistance (ASR) behaviours. A number of characteristic electrochemical parameters are presented in Table 6.1 and Tables D1 and D2 (Appendix D). Table 6.1 shows the electrochemical data for hand milled (HM) miscanthus and willow and it shows that the OCV, power and current densities increases with the temperature rise but the ASR decreases with rise in temperature. Wheat has the highest power efficiency of 71% at the highest operating condition and spruce has the lowest power efficiency of 26% at the lowest operating condition. The ASR is a measurement of the overall ohmic resistance from the biomass carbon fuels and electrolyte, the mechanical connections of the cell and the electrode materials. The ASR was calculated from the slope of the voltage versus the current density at the linear central region of the polarisation curves (Li *et al.*, 2009; Hackett *et al.*, 2007). The efficiency at peak power was calculated by dividing the voltage at peak power by the OCV and multiplying by 100%.

Table 6.1: MCDRFC Electrochemical data for miscanthus and willow (HM)

Cell Parameter	Miscanthus			Willow		
	Temperature °C			Temperature °C		
	600	700	800	600	700	800
Open circuit voltage (V)	0.66	0.72	1.03	0.42	0.45	0.83
Peak power density (mW/cm ²)	1.67	4.70	13.46	1.32	3.60	14.83
Maximum current density (mA/cm ²)	12.44	18.34	24.89	11.46	23.90	34.48
Current density at 0.8 V (mA/cm ²)	0	0.64	18.59	0	0	6.49
Voltage at peak power (V)	0.26	0.43	0.72	0.23	0.21	0.43
Area specific resistance (Ω cm ²)	46.88	22.05	13.30	34.22	15.50	13.86
Efficiency at peak power (%)	40.00	60.00	70.00	55.00	47.00	52.00

Table 6.1 gives the some area specific resistances (ASR) of the MCDRFC. It can occur from the mechanical connections, electrode materials and within the electrolyte itself. The values of ASR decrease with increase in temperature (Li *et al.*, 2009; Hackett *et al.*, 2007; Larminie and Dicks, 2003). For all the biomass carbon fuel the lower the ASR the better the performance recorded for the fuel cell. The six materials show increasing trend in performance with increasing temperature, with the peak power density at 800°C being slightly higher from one carbon to the other. Also shown are thermal efficiency values for conversion to electricity at peak power. The enthalpy of oxidation of pure carbon to carbon dioxide at the operating temperatures is 394 kJ/mol, whereas the available work from the cell is represented by the measures ΔG value based on $\Delta G = -n F E$. Efficiency values are also calculated for the cells operating at the maximum power condition, and it can be seen that these approach 70% for the miscanthus material at the highest temperature. These values emphasise the efficiency benefits achievable for electricity generation from biomass materials when compare with around 35% for generation from conventional combustion and steam cycle plant (Adeniyi and Ewan, 2011; Cao *et al.*, 2007). The current densities at 0.8 V corresponds to working at 80% voltage efficiency but at the expense of the current density as shown in Tables 6.1, D1 and D2.

6.6 MCDRFC Performances with BM Biomass Carbon Fuels

6.6.1 First Day Performances of the MCDRFC using BM Carbon Fuels

Figures 6.34 to 6.36 show the voltage versus current densities results of the MCDRFC for the first day of the ball milled (BM) biomass carbon particle fuels. The carbons were subjected to ball milling for forty minutes and the particle sizes reduce from 48 μm to 2 μm . Interestingly in terms of the OCV obtained willow gave the highest (0.75 V) but its maximum current density was low (5 mA/cm^2). Spruce fuel had the next highest OCV (0.7 V) and the highest maximum current density (18 mA/cm^2). Poplar fuel OCV was third (0.55 V) but had the second highest maximum current density (17 mA/cm^2). Switchgrass, wheat and miscanthus had low OCVs and low current densities.

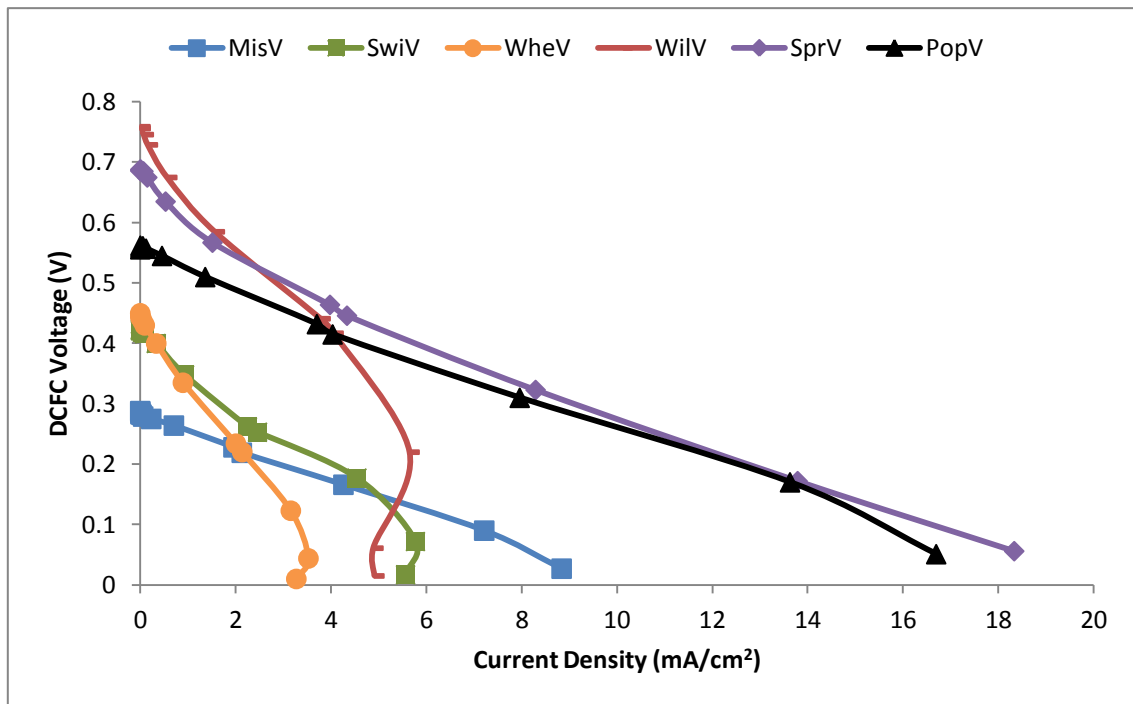


Figure 6.34: Voltage, current density for the 6 biomass fuels at 600°C (BM-Day 1).

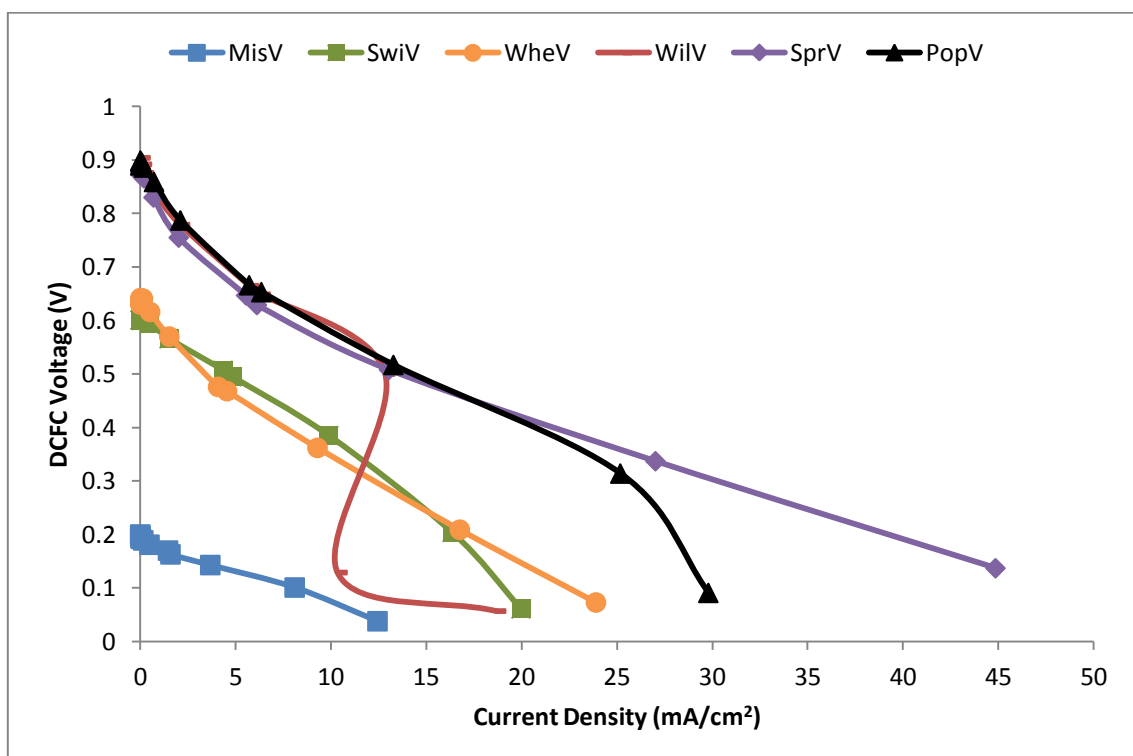


Figure 6.35: Voltage, current density for the 6 biomass fuels at 700°C (BM-Day 1).

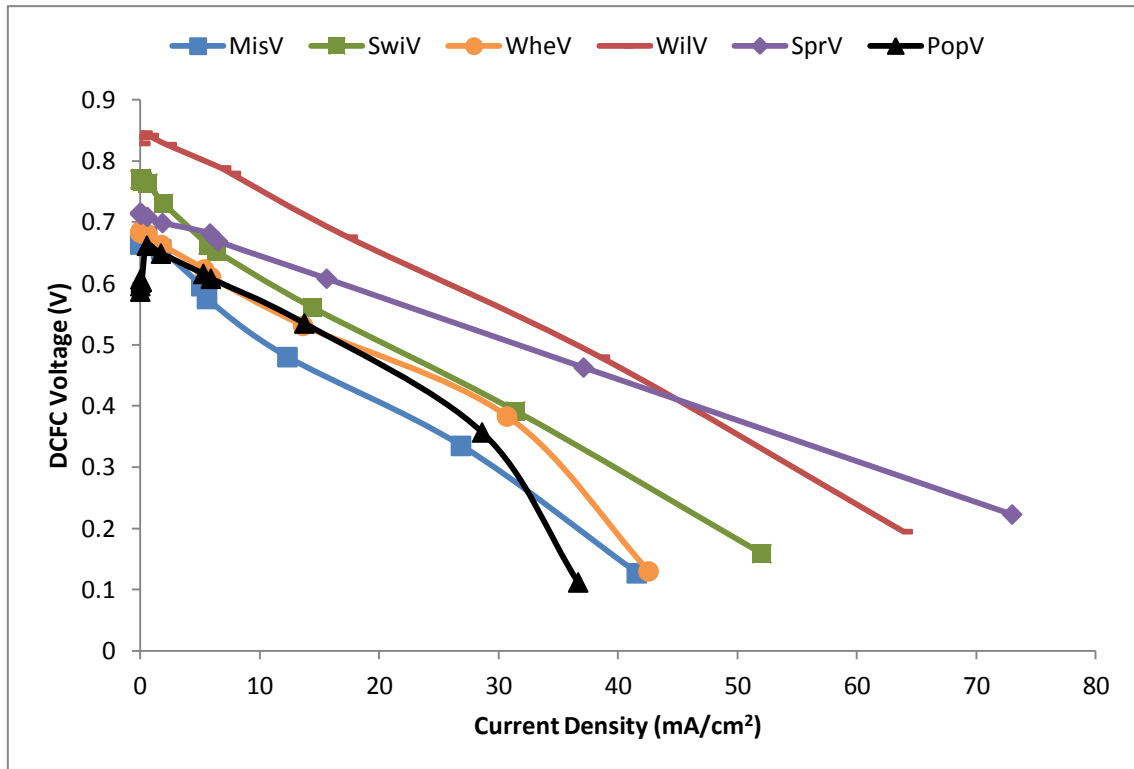


Figure 6.36: Voltage, current density for the 6 biomass fuels at 800°C (BM-Day 1).

Figures 6.35 and 6.38 show that at 700°C poplar fuel performance picked up while that of willow slides down. At 800°C willow performance increased greatly giving the best peak power density and the second best current density. Figures 6.34 to 6.42 show different degrees of the curve back phenomenon of the performances of these fuels a situation attributed to the overconsumption of the fuel at the anode compartment (Jia *et al.*, 2010). Figures 6.34 to 6.42 show that the current density-voltage curves drop due to activation resistance, ohmic resistance and mass transport limitation (Li *et al.*, 2009; Jain *et al.*, 2008; Hackett *et al.*, 2007; O'Hayre *et al.*, 2006; Cherepy *et al.*, 2005; Larminie and Dicks, 2003). Figures 6.37 to 6.39 give the power versus the current densities and Figures 6.40 to 6.42 show the overall performances of the biomass carbon fuels.

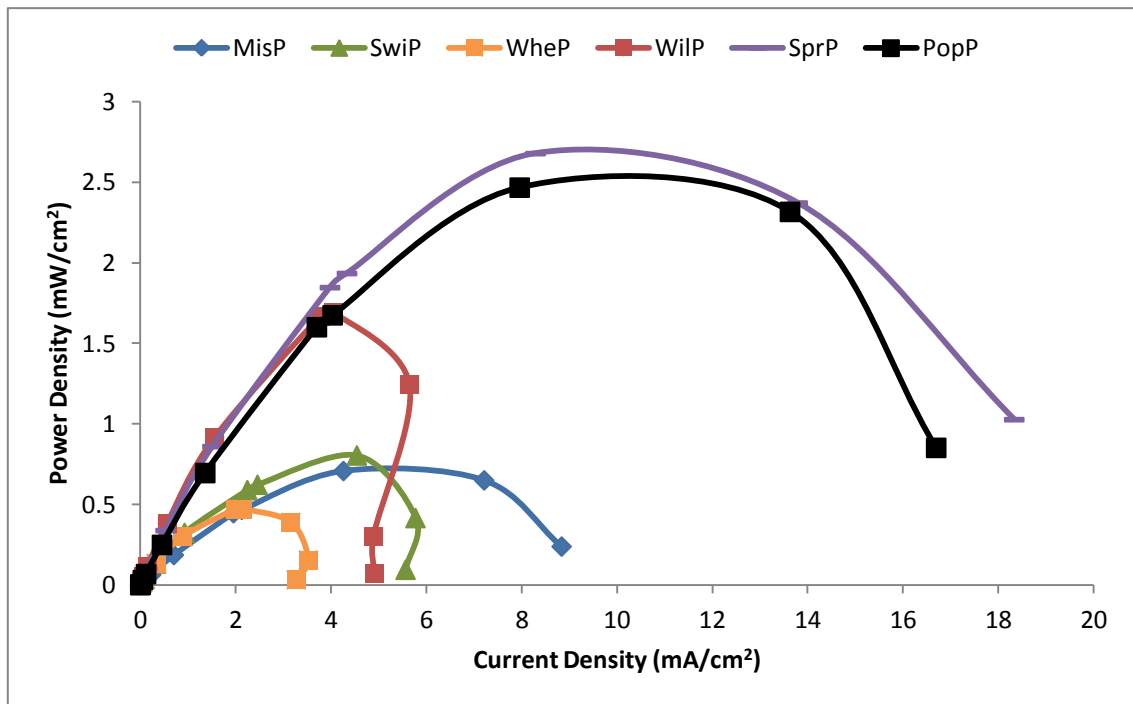


Figure 6.37: Power versus current density for the 6 biomass fuels at 600°C (BM-Day 1).

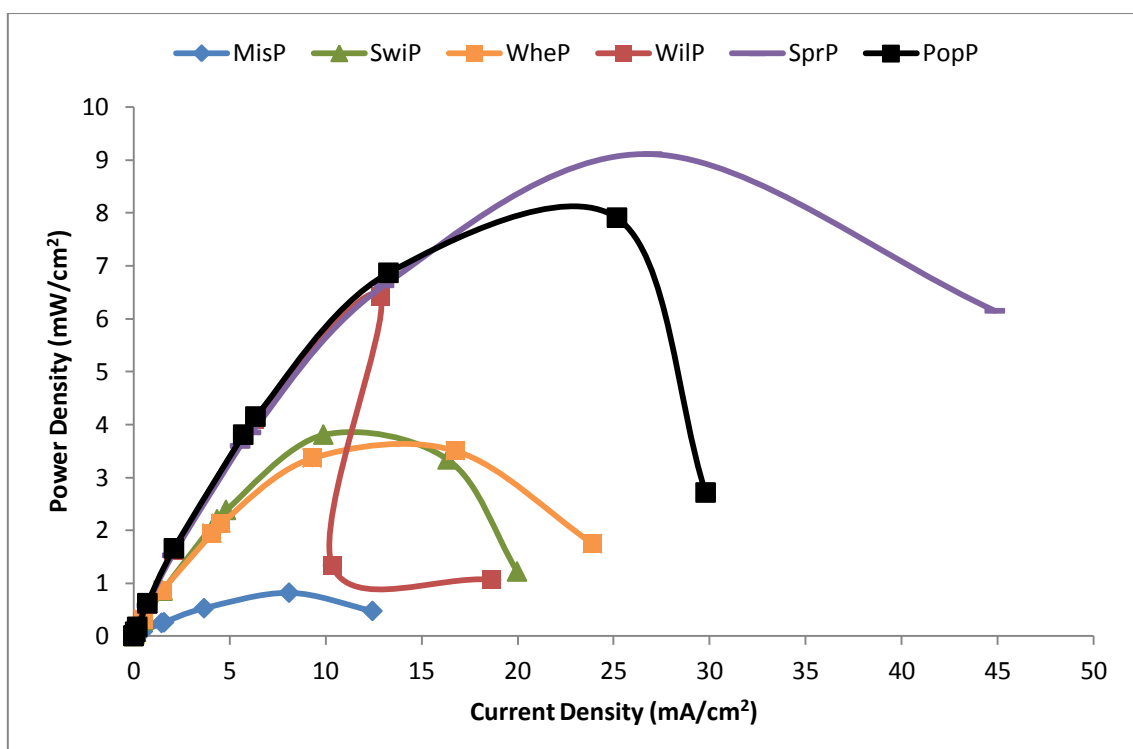


Figure 6.38: Power versus current density for the 6 biomass fuels at 700°C (BM-Day 1)

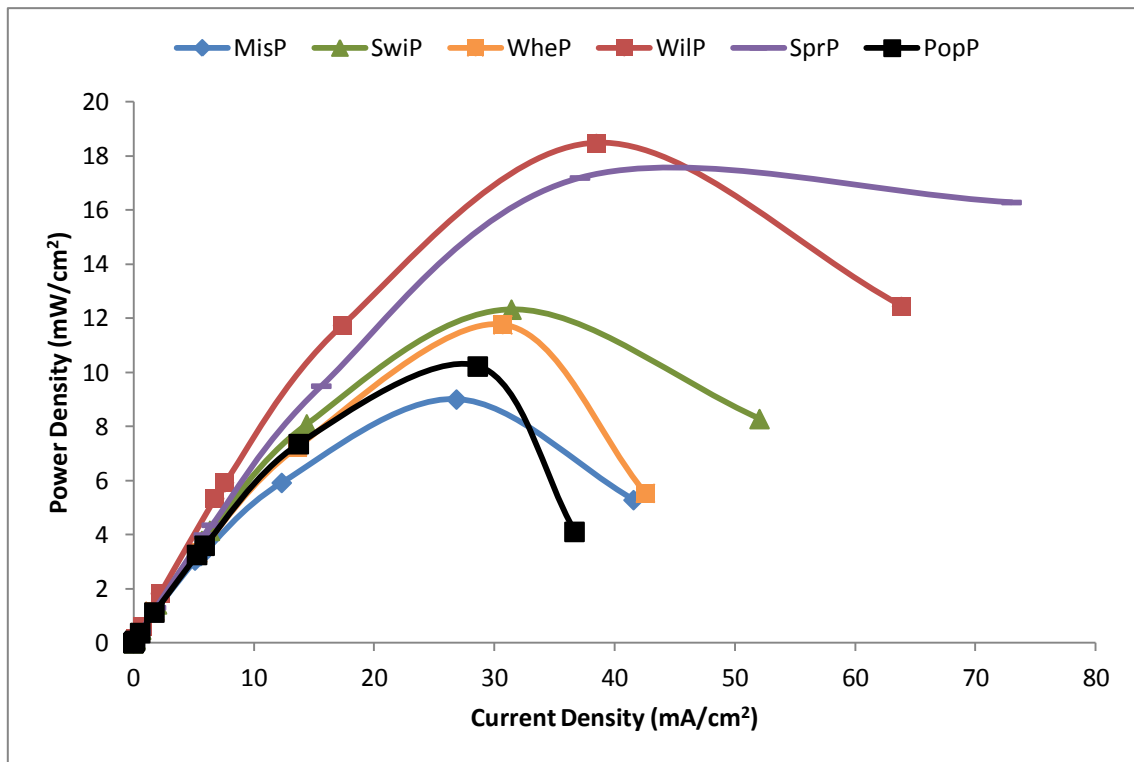


Figure 6.39: Power versus current density for the 6 biomass fuels at 800°C (BM-Day 1)

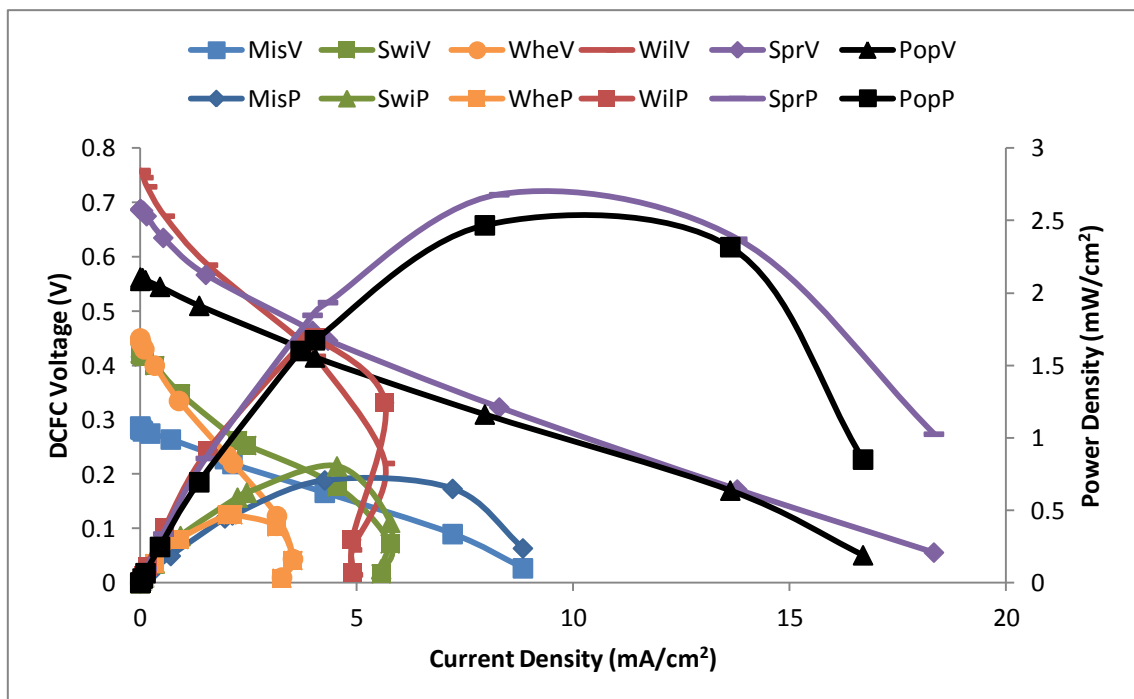


Figure 6.40: Overall performances for the 6 biomass fuels at 600°C (BM-Day 1)

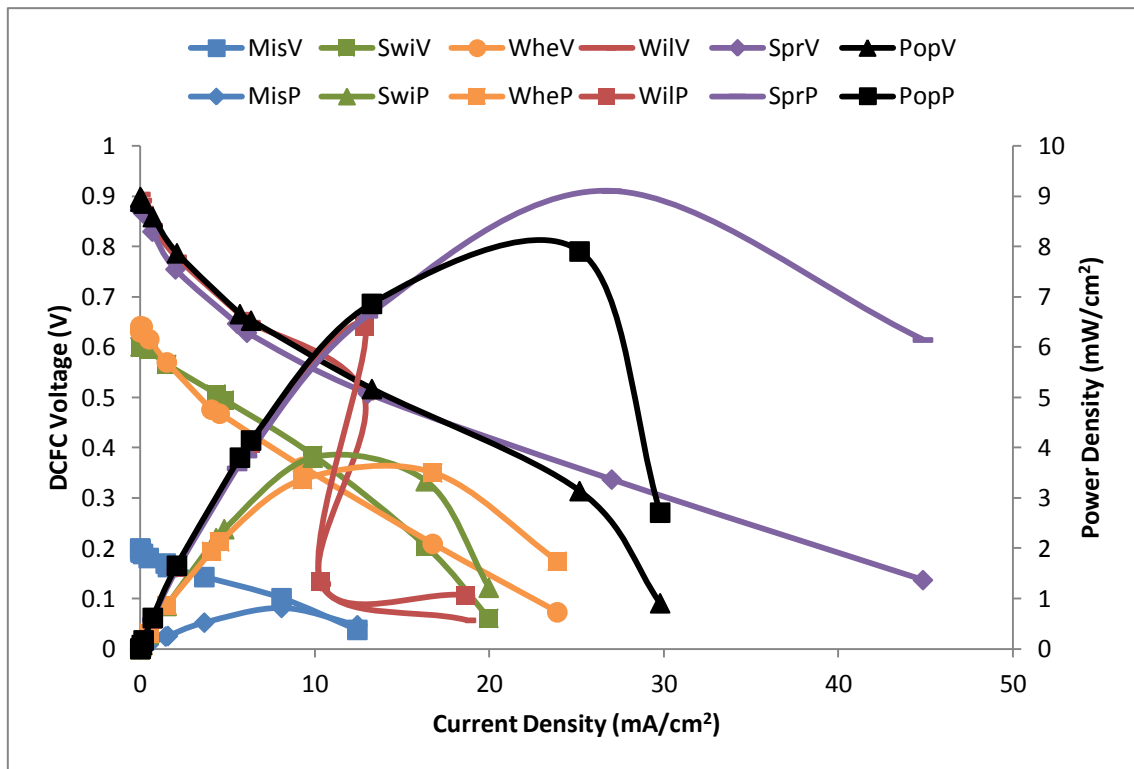


Figure 6.41: Overall performances for the 6 biomass fuels at 700°C (BM-Day 1)

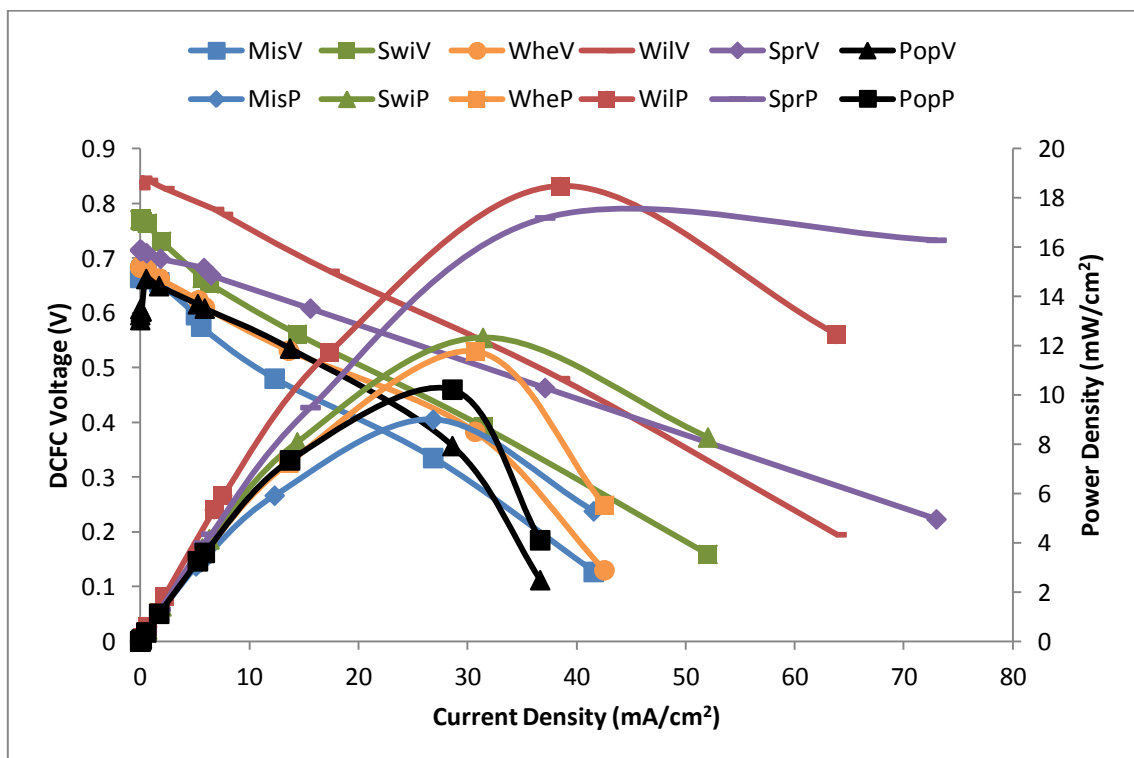


Figure 6.42: Overall performances for the 6 biomass fuels at 800°C (BM-Day 1)

The ball milling of willow carbon fuel from 44 μm to 3 μm show some influence on its performance in the MDCFC, as shown by Figures 6.34 to 6.42 others results are shown in Appendix C (Figures C7 to C10). The chemical reactivity of carbons to oxidations are said to be strongly dependent on structure particularly the extent of graphitization and surface area (Cherepy *et al.*, 2005). The specific surface area of willow fuel increased from 0.42 m^2/g to 2.23 m^2/g for HM and BM respectively.

6.6.2 Temperature Effects on MDCFC Performances with BM Carbon Fuels

For the ball milled biomass carbon fuels, the effects that temperature has on the performances of the MDCFC are shown in Figure 6.43 and in Appendix C (Figures C11 and C12). The performances of the fuel cell was greatly enhanced as the temperature increases from 400°C to 800°C, this is attributed to enhancement of the ionic conduction rate of the electrolyte and the electrochemical reactions at the electrodes (Jia *et al.*, 2010; Li *et al.*, 2009; Jain *et al.*, 2008; Hackett *et al.*, 2007; Cherepy *et al.*, 2005). The patterns generated here are similar to those of the hand milled biomass carbon fuels.

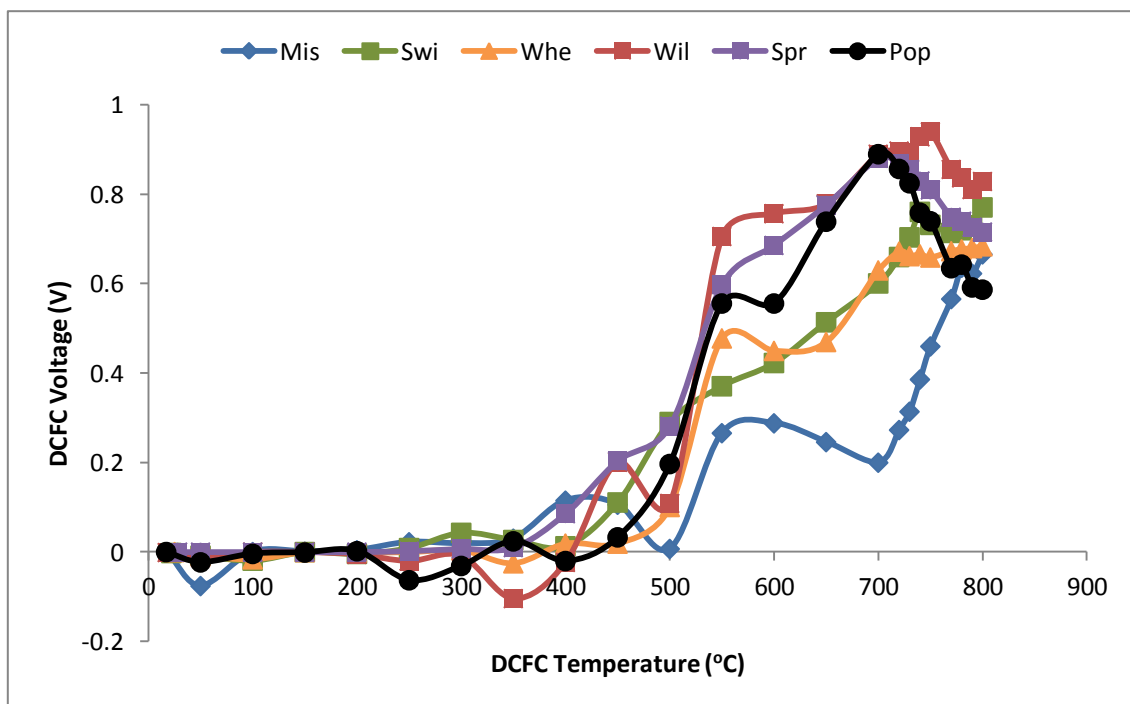


Figure 6.43: MDCFC OCV for the six biomass carbon fuels at different temperature (BM-Day 1)

Figures 6.43, C11 and C12 show that the sharp rises in the OCV start below 400°C which is due to faster ionic conduction in the molten carbonate phase. At the start of the second and third day the existing DCFC set-up was used, additional fuel of 1.5 g was used for each day.

6.6.3 MCDRFC Performance Efficiency using BM Biomass Carbon Fuels

Figures 6.34 to 6.43 show the characteristics of power and voltage curves behaviour for a single cell molten carbonate electrolyte direct carbon fuel cell (MCDRFC). A number of characteristic electrochemical parameters are presented in Table 6.2 and Tables D3 and D4 (Appendix D). Switchgrass has the highest power efficiency of 65% at 700°C and wheat the lowest power efficiency of 33% at the 700°C operating condition. Interestingly the low efficiency recorded for willow for the hand milled fuel has risen to 58% at the highest temperature for the ball milled (BM) fuel.

Table 6.2: MCDRFC Electrochemical data for miscanthus and willow (BM)

Cell Parameter	Miscanthus			Willow		
	Temperature °C			Temperature °C		
	600	700	800	600	700	800
Open circuit voltage (V)	0.28	0.20	0.67	0.76	0.89	0.83
Peak power density (mW/cm ²)	0.71	0.82	9.00	1.69	6.42	18.48
Maximum current density (mA/cm ²)	8.84	12.44	41.58	4.91	18.66	63.85
Current density at 0.8 V (mA/cm ²)	0	0	0	0	2.08	6.77
Voltage at peak power (V)	0.17	0.10	0.34	0.42	0.50	0.48
Area specific resistance (Ω cm ²)	24.85	9.58	14.11	123.6	22.82	10.64
Efficiency at peak power (%)	61.00	50.00	51.00	55.00	56.00	58.00

Comparison between Tables 6.2, D3 and D4 and Tables 6.1, D1 and D2 shows that the OCV for the BM fuels were lower than those of the HM fuels with the exception of willow BM fuel. The peak power densities were relatively lower in the BM than the HM fuels, again with willow being an exception. The maximum current densities were lower in the BM than the HM with some few exceptions at 800°C. The current densities were lower in the BM than the HM with willow being an exception. The voltages at peak power were lower in the BM than the HM with willow being an exception. The ASR was higher for the BM fuels with miscanthus and poplar as exceptions.

6.7 Comparison of MCDRFC Performances for HM and BM Carbon Fuels

6.7.1 Miscanthus (*Miscanthus x giganteus*) Carbon Fuel

The differences between the hand and ball milled biomass carbon fuels in the MCDRFC performances using miscanthus fuel at 600°C, 700°C and 800°C are shown in Figures 6.44 to 6.46. The figures show that the hand milled miscanthus carbon fuel had better performance than the ball milled ones. Hand milled carbon fuel had an average particle size of 29 µm while the ball milled was 8 µm (Tables 5.25 and 5.26). It seems that at this particle sizes the effect of milling was not significant to produce better electrochemical reactions using the miscanthus fuel. The specific surface area also increased from 0.57 m²/g for the hand milled to 0.95 m²/g for the ball milled, again this effect was not enough to enhance the electrochemical discharge rate using this carbon fuel (Cherepy *et al.*, 2005). The graphs of comparison shown here are for miscanthus and switchgrass the other four biomasses are presented in Appendix C (Figures C13 to C20).

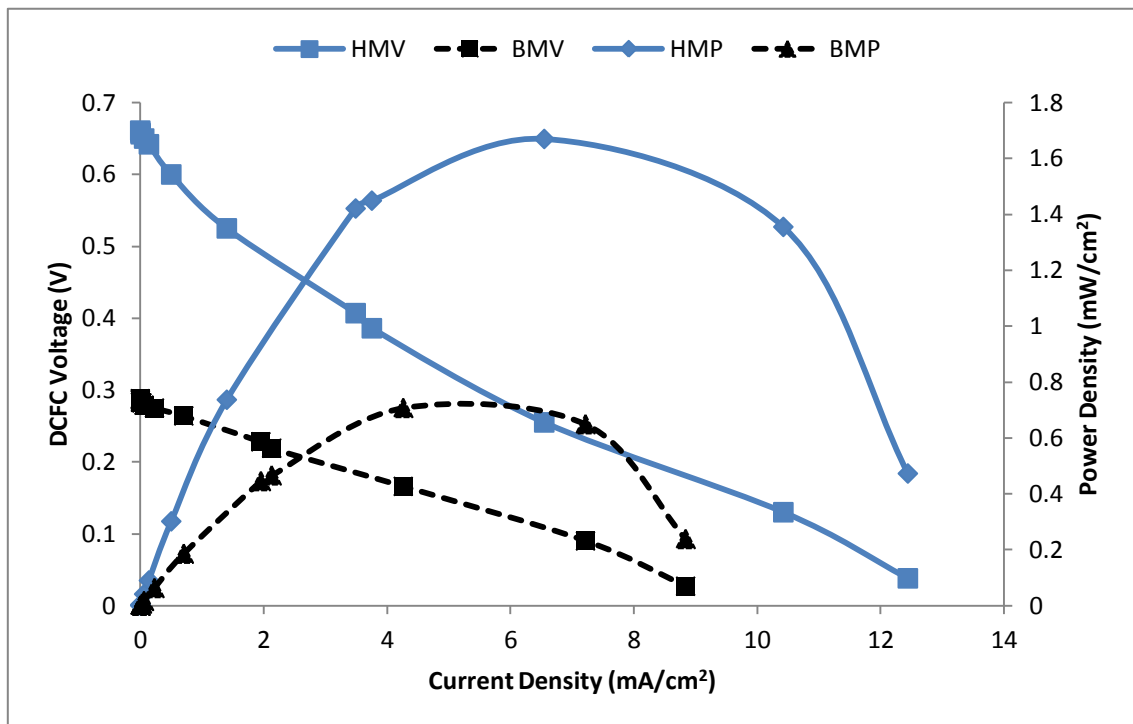


Figure 6.44: Miscanthus performances for hand and ball milled fuels at 600°C.

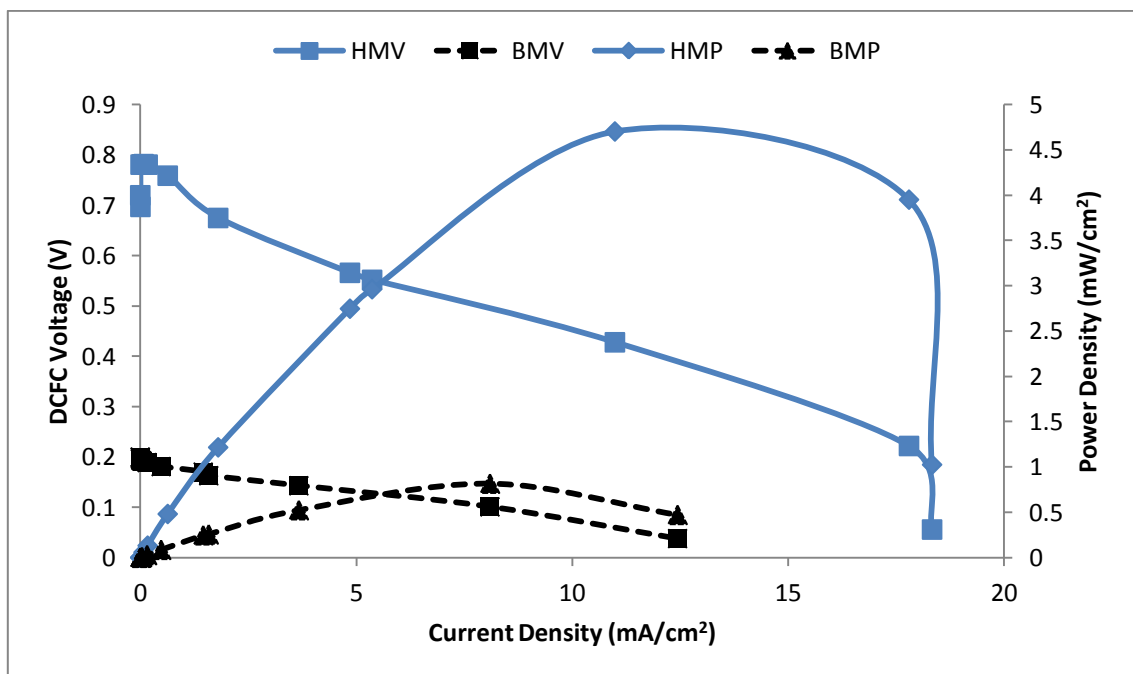


Figure 6.45: Miscanthus performances for hand and ball milled fuels at 700°C.

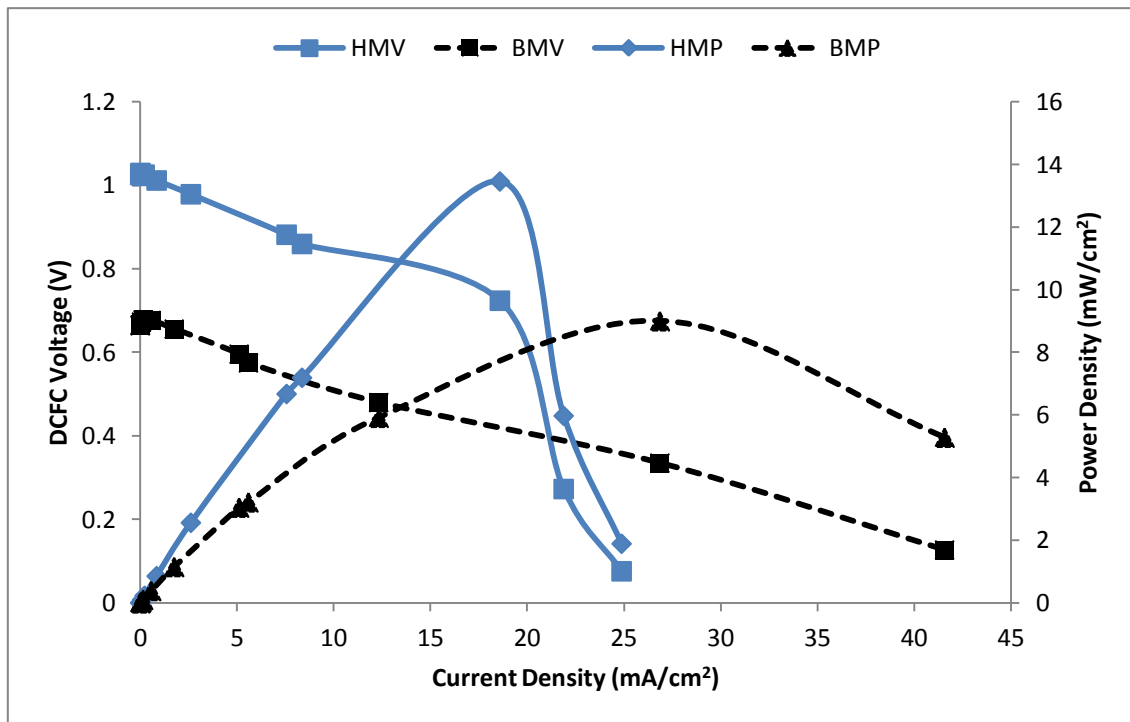


Figure 6.46: Miscanthus performances for hand and ball milled fuels at 800°C.

Figure 6.46 present the miscanthus fuel performance at an operating temperature of 800°C, it was observed that the hand milled fuel has high power density but low current density. The hand milled fuel was affected by the overconsumption of the carbon fuel at the anode which leads to gap between the fuel and the electrolyte surfaces and thus causing low current generation, but for this occurrence the current output could have been better (Jia *et al.*, 2010). Figures 6.47 and 6.48 show the SEM micrographs of the miscanthus carbon fuels. These micrographs show that there are different particle sizes and shapes, the connectivity of the particles in aggregates for the hand and ball milled carbon fuels look similar.

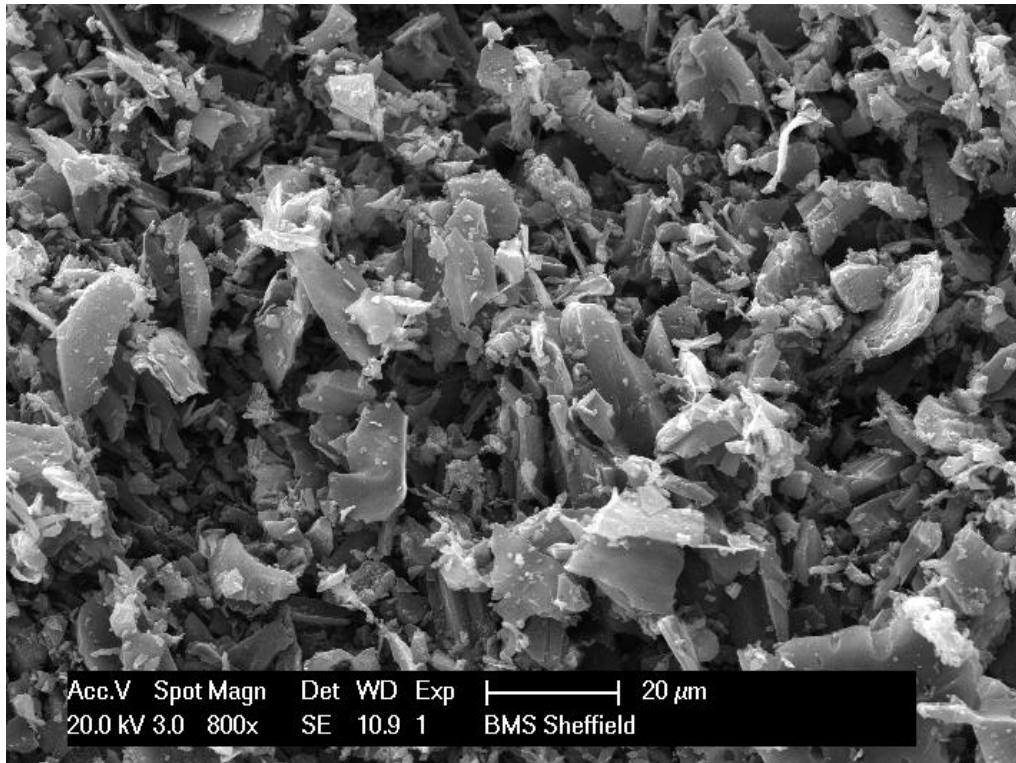


Figure 6.47: SEM micrograph of hand milled miscanthus carbon particles (800x)

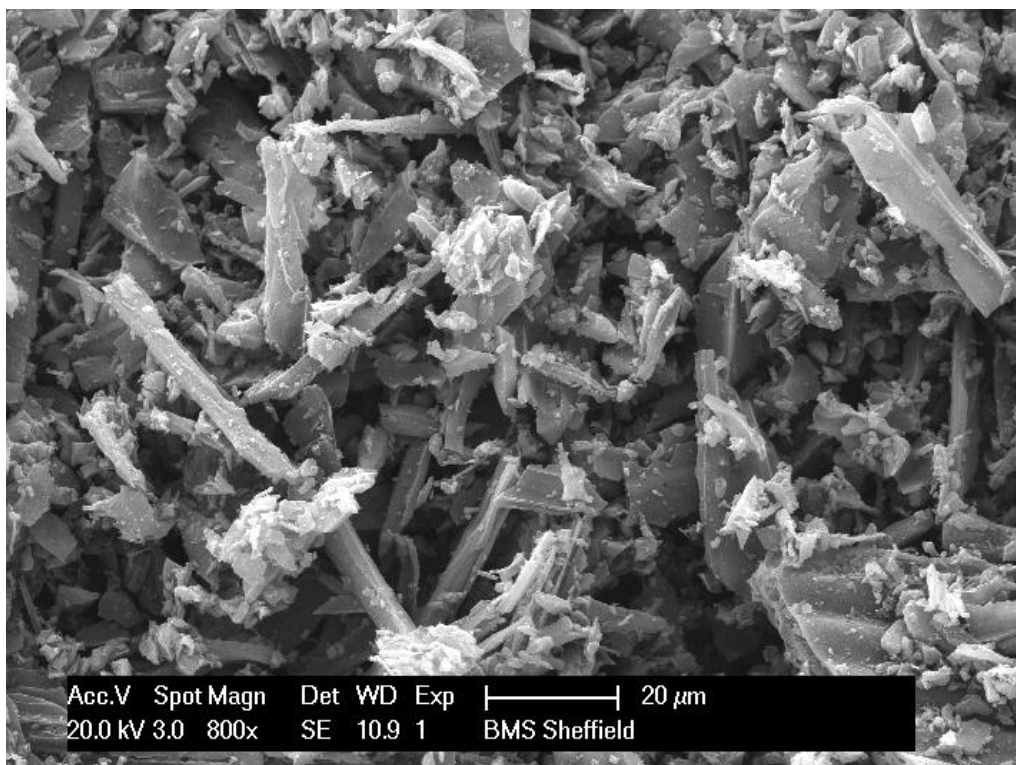


Figure 6.48: SEM micrograph of ball milled miscanthus carbon particles (800x)

6.7.2 Switchgrass (*Panicum virgatum*) Carbon Fuel

The difference between the MCDRFC performances using switchgrass HM and BM fuels at 600°C, 700°C and 800°C are shown in Figures 6.49 to 6.51. The figures show that the hand milled switchgrass carbon fuels gave better performances than the ball milled. Hand milled carbon fuel have an average particle size of 30 μm while the ball milled was 2 μm (Tables 5.25 and 5.26). Again it seems that at this particle sizes the effect of milling was negative in the electrochemical performances. The specific surface area also increased from 0.63 m^2/g for the hand milled to 2.55 m^2/g for the ball milled as given in Tables 5.25 and 5.26 (Cherepy *et al.*, 2005).

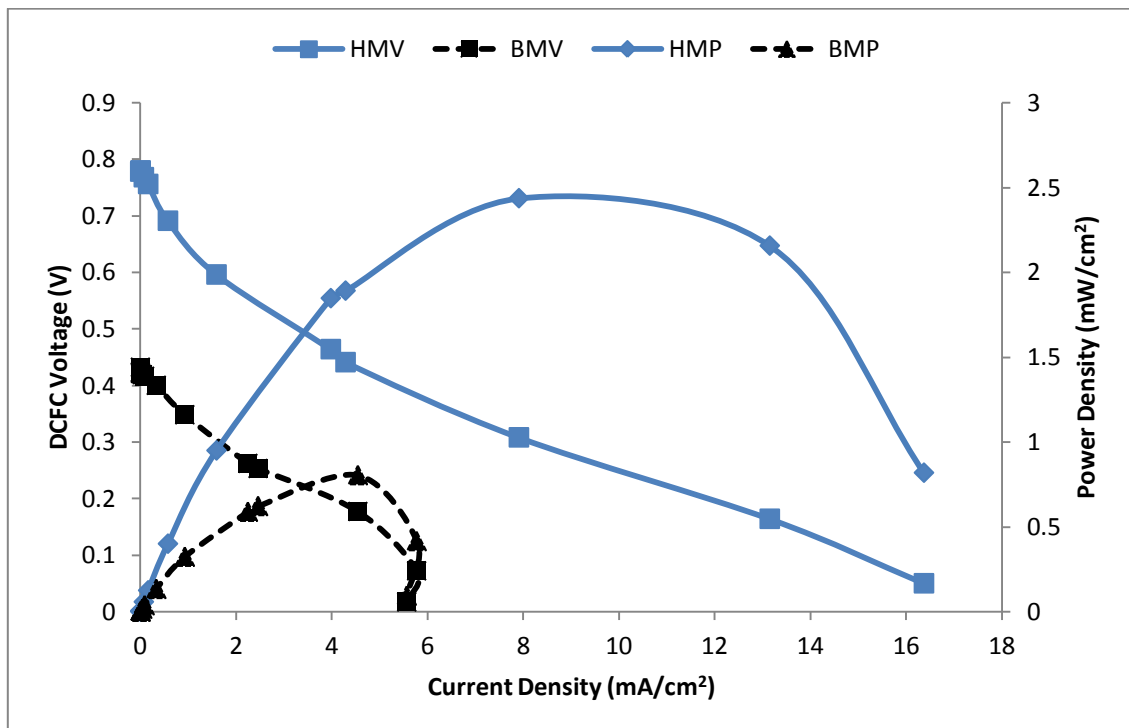


Figure 6.49: Switchgrass performances for hand and ball milled fuels at 600°C.

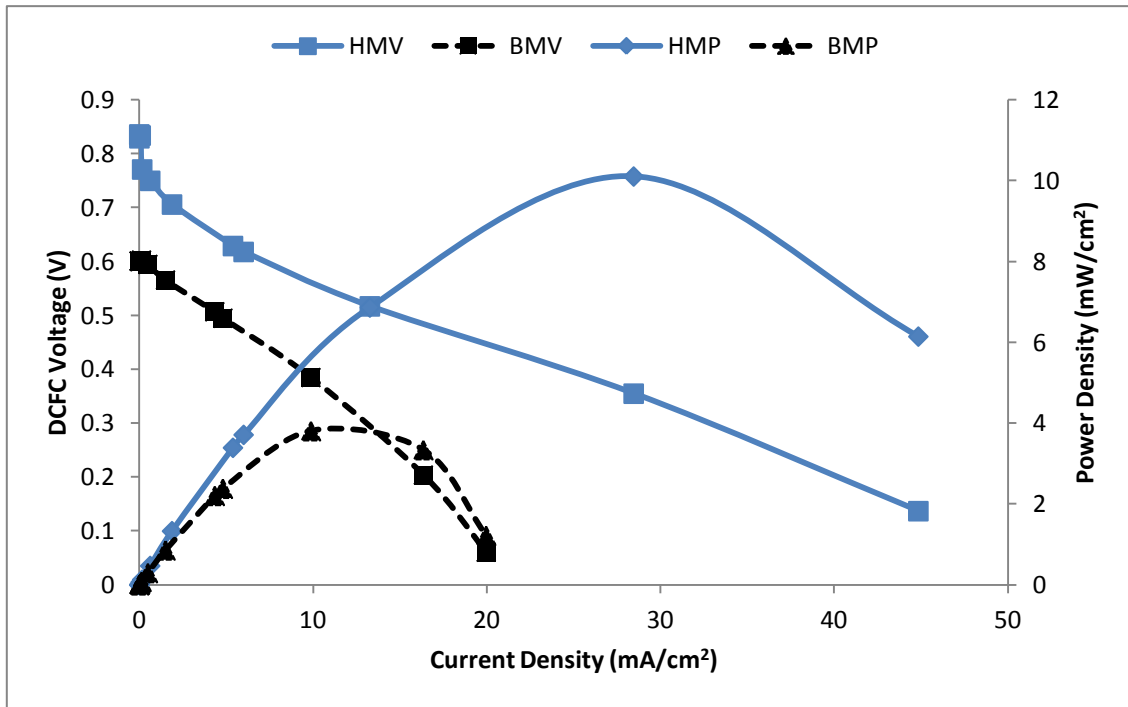


Figure 6.50: Switchgrass performances for hand and ball milled fuels at 700°C.

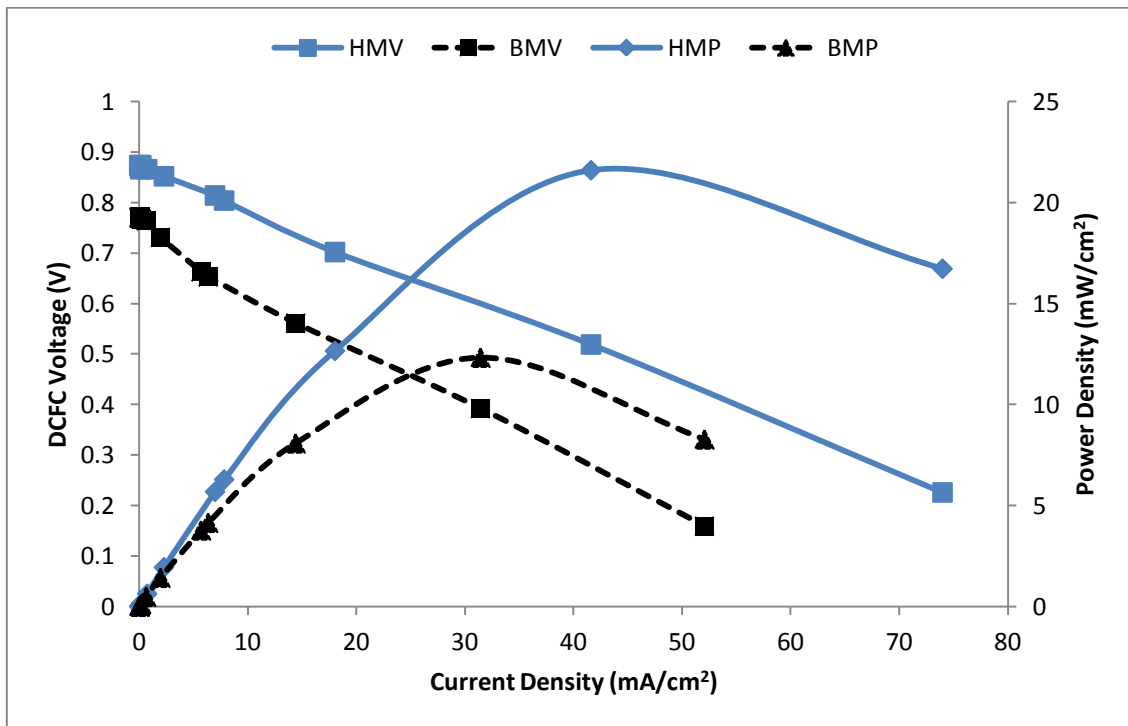


Figure 6.51: Switchgrass performances for hand and ball milled fuels at 800°C.

Figures 6.49 to 6.51 show that the performances of switchgrass in this case was better than the miscanthus fuel with HM peak power density of 22 mW/cm^2 for switchgrass as against 14 mW/cm^2 for miscanthus at 800°C . Figures 6.52 and 6.53 shows the SEM micrographs of the switchgrass carbon fuels. The HM SEM show larger particles than those of the BM as expected but contrary to expectations the hand milled fuel performed better than the ball milled carbon fuels.

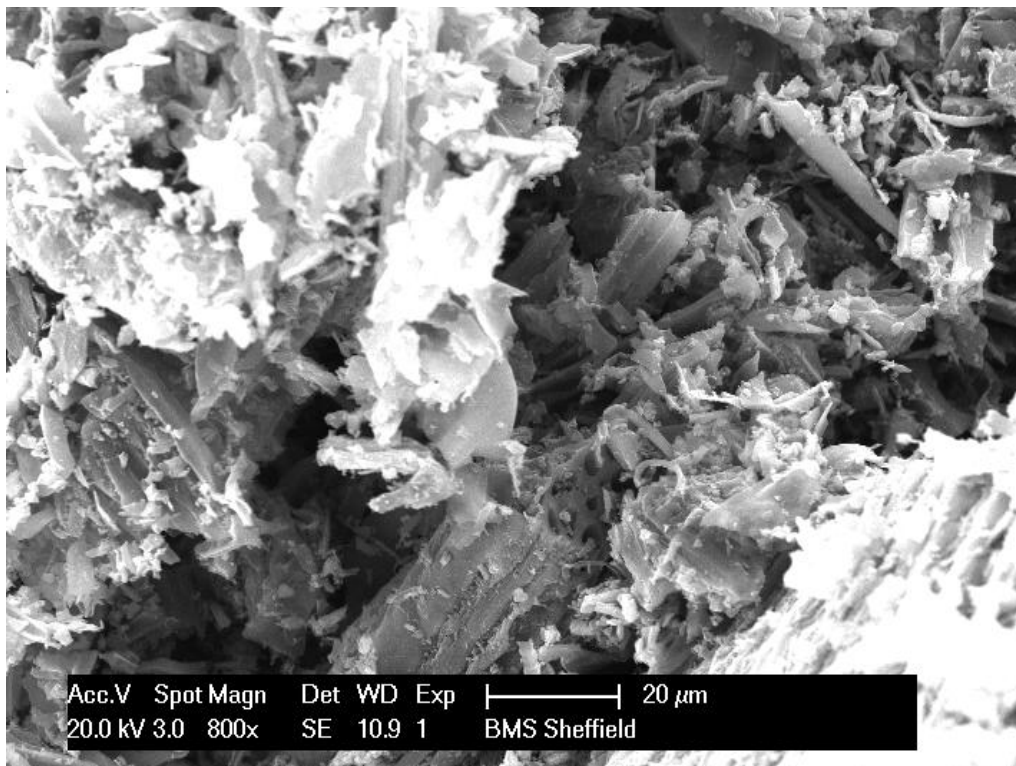


Figure 6.52: SEM micrograph of hand milled switchgrass carbon particles (800x)

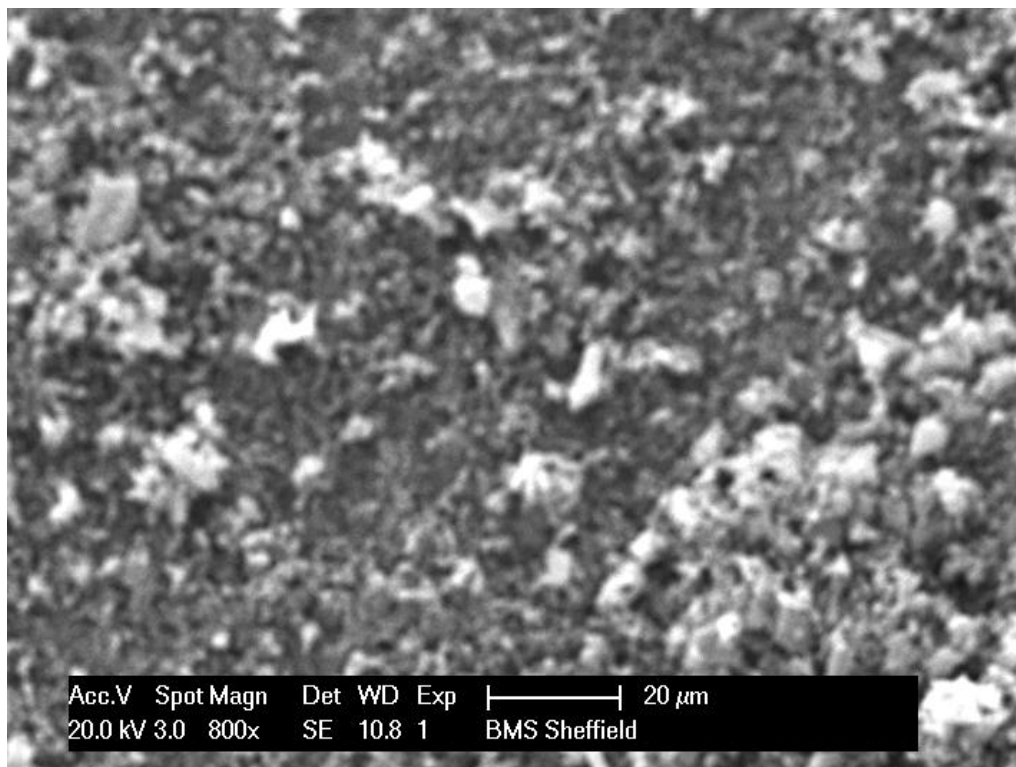


Figure 6.53: SEM micrograph of ball milled switchgrass carbon particles (800x)

6.8 Summary

Table 6.3 summarises the outcome of the MCDRFC electrochemical performances for both the hand (HM) and ball milled (BM) biomass carbon fuels at 800°C. The performances of the hand milled biomass fuels were higher than those experienced with the ball milled with the exception of willow fuel. In terms of the open circuit voltage, poplar fuel (1.08 V) had the best for the HM and willow fuel (0.83 V) for the BM. The best peak power density was recorded for spruce fuel (26.79 mW/cm²) for the HM and willow fuel (18.48 mW/cm²) for the BM. Poplar fuel (81.53 mA/cm²) gave the maximum current density for the HM while spruce fuel (73.02 mA/cm²) for the BM. For the current density at 80% voltage efficiency poplar fuel (19.80 mA/cm²) was superior for the HM and willow fuel (6.67 mA/cm²) for the BM. Miscanthus fuel (0.72 V) show the highest voltage at peak power for the HM and willow fuel (0.48 V) for the BM. The peak power efficiency evaluated show that wheat fuel (71%) gave the highest value for the hand milled and spruce carbon fuel (64%) for the ball milled.

Table 6.3: MDCFC Electrochemical performance at 800°C (HM and BM)

MDCFC Parameter		Miscanthus	Switchgrass	Wheat	Willow	spruce	Poplar
Open circuit voltage (V)	HM	1.03	0.87	0.95	0.83	1.03	1.08
	BM	0.67	0.77	0.68	0.83	0.72	0.59
Peak power density (mW/cm ²)	HM	13.46	21.60	11.60	14.83	26.79	23.91
	BM	9.00	12.32	11.76	18.48	17.19	10.22
Maximum current density (mA/cm ²)	HM	24.89	74.00	19.65	34.48	76.62	81.53
	BM	41.58	52.06	42.57	63.85	73.02	36.67
Current density at 0.8 V (mA/cm ²)	HM	18.59	7.82	7.75	6.49	19.62	19.80
	BM	0	0	0	6.77	0	0
Voltage at peak power (V)	HM	0.72	0.52	0.67	0.43	0.58	0.55
	BM	0.34	0.39	0.38	0.48	0.46	0.36
Efficiency at peak power (%)	HM	70.00	60.00	71.00	52.00	56.00	51.00
	BM	51.00	51.00	56.00	58.00	64.00	61.00

Chapter Seven

SODCFC Single Cell Performances

7.1 Introduction

A single cell solid oxide electrolyte direct carbon fuel cell (SODCFC) with the six biomass carbon fuels performances are presented in this chapter. The results obtained from the SODCFC are reproducible, the variation observed in the results are also due to a number of factors such as ohmic resistance, activation losses, mass transport limitation and the aging process of the electrochemical cell system. This chapter presents the SODCFC electrochemical cell design and components. The performances recorded for the SODCFC with the biomass carbon fuels with the hand and ball milled biomass carbon fuels are presented. The temperature effects on the performances of the SODCFC and the tables of the summary of the electrochemical results for the six biomass fuels are also given. A comparison between the ball and hand milled biomass carbon fuels on the performances of the SODCFC are presented along with the comparison between the MCDCFC and the SODCFC.

7.2 SODCFC Electrochemical Cell Design and Development

The major design that was explored for the electrochemical cell system of the solid oxide electrolyte direct carbon fuel cell (SODCFC) is presented in Figure 7.1. Button cells from Fuel Cell Materials Ltd., USA were used. The composition of the cell are lanthanum oxide, manganese oxide, strontium oxide, cerium (IV) oxide, gadolinium oxide, nickel (II) oxide, zirconium oxide, yttrium oxide, and scandium oxide. The cells consisted of Ni/Yttrium-stabilized zirconium (YSZ) anode support layer, Ni/scandium-stabilized zirconium (ScSZ) anode active interlayer, ScSZ electrolyte layer and lanthanum strontium manganese (LSM)/ScSZ cathode layer. The anode and the cathode layers are 1.2 cm in diameter and the cells are 2.5 cm in diameter with an active surface area of 1.1 cm². Because of their relatively simple experimental setup and good reproducibility, these button cells were employed in the SODCFC experiments (Li *et al.*, 2011a,b; Wu *et al.*, 2009; Ihara *et al.*, 2004; Nakagawa *et al.*, 1988).

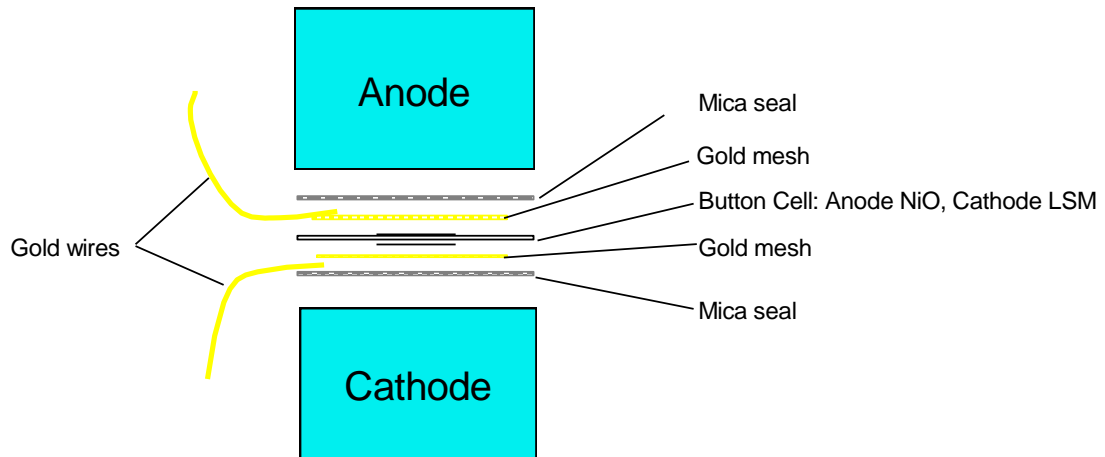


Figure 7.1: SODCFC Button cell, Gold mesh, Ni/YSZ, LSM/ScSZ, gold mesh electrode assembly.

Figure 7.2 shows the button cells before high temperature operation at 900°C to reduce the nickel oxide to nickel cermets. Figure 7.3 shows what the button cell looks like after reduction and gold mesh bonded on each side to serve as the current collector. Figures 7.4 to 7.6 show some of the components of SODCFC for high temperature operations. The preparation procedures were explained in Section 4.7.5 (Chapter 4).



Figure 7.2: Button cell for the SODCFC, cathode (black-LSM), anode (green- NiO_2)

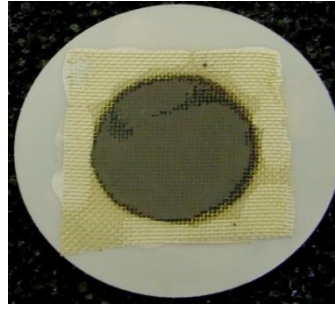


Figure 7.3: Button cell bond with gold mesh on each side as the electrolyte



Figure 7.4: Assembled SODCFC ready for high temperature operation



Figure 7.5: SODCFC during high temperature operation

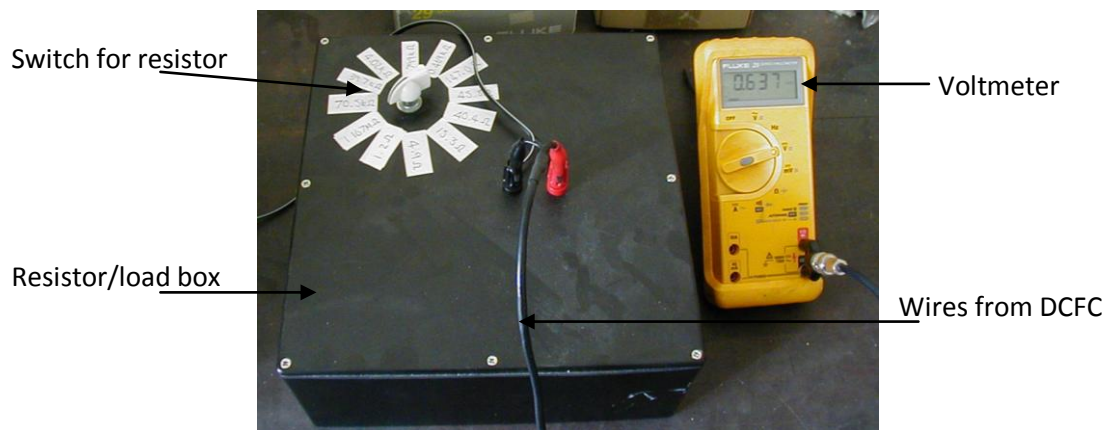


Figure 7.6: Resistor box and voltmeter connected to SODCFC

7.3 SODCFC Performance with Ball Milled (BM) Biomass Carbon Fuels

7.3.1 First Day Performance of the SODCFC

Figures 7.7 to 7.9 show the voltage versus current densities of the SODCFC for the first day of the ball milled carbon particle fuels for the operating temperatures of 600°C to 800°C. As in the case of the MDCFC the carbons were subjected to ball milling for forty minutes to obtain particle sizes of 2 μm . From Figure 7.7 in terms of the OCV, switchgrass gave the highest (0.87 V) with a maximum current density of 56 mA/cm^2 . Wheat fuel had the next highest OCV (0.87 V) but a lower current density 18 mA/cm^2 . Poplar fuel OCV was 0.82 V but had the third highest current density (33 mA/cm^2). Spruce and willow fuels had low OCV and low current densities.

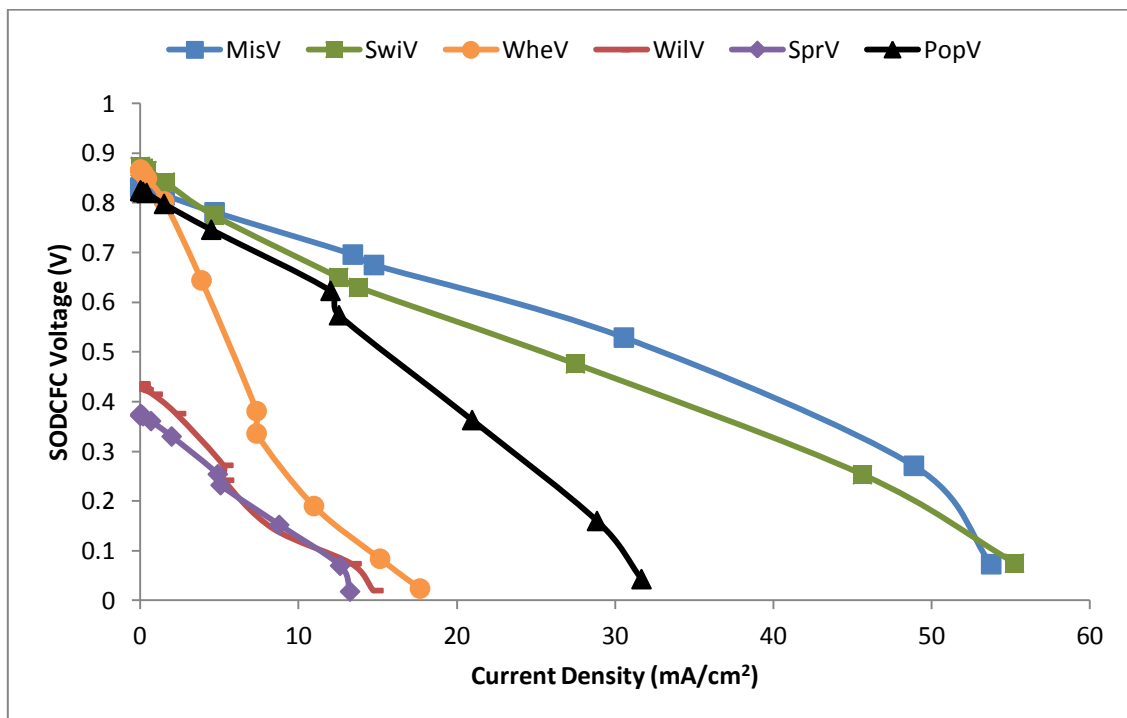


Figure 7.7: SODCFC voltage, current density for the 6 biomass fuels at 600°C (BM).

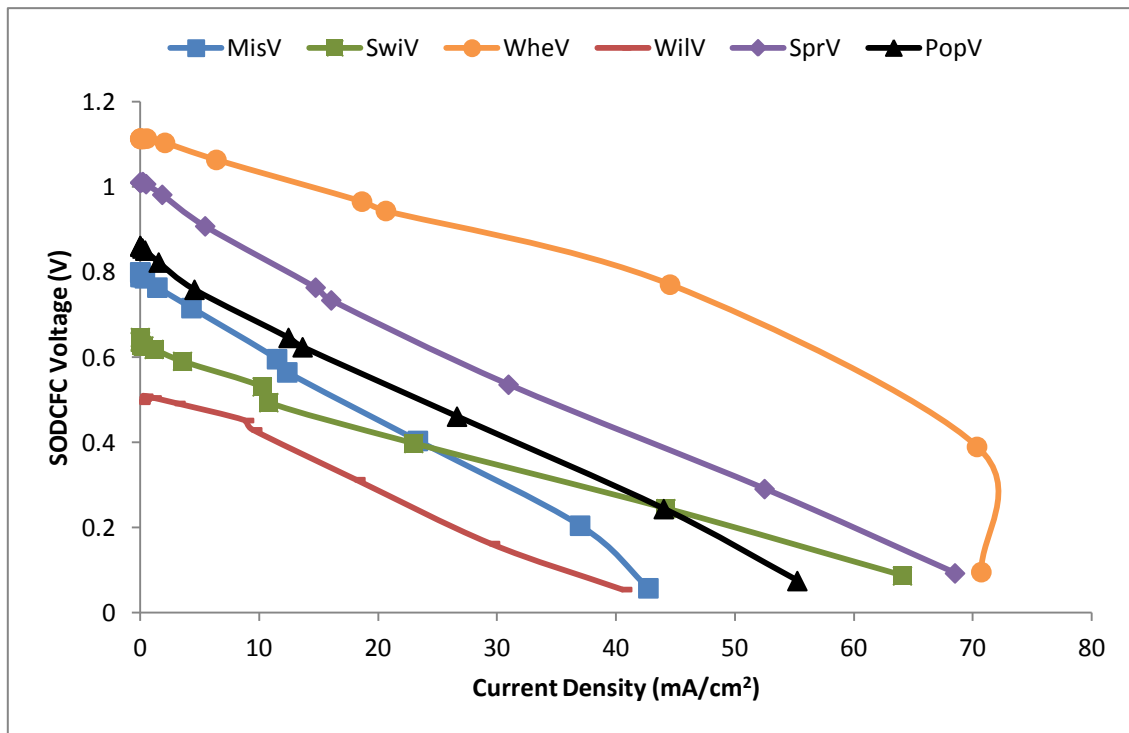


Figure 7.8: SODCFC voltage, current density for the 6 biomass fuels at 700°C (BM).

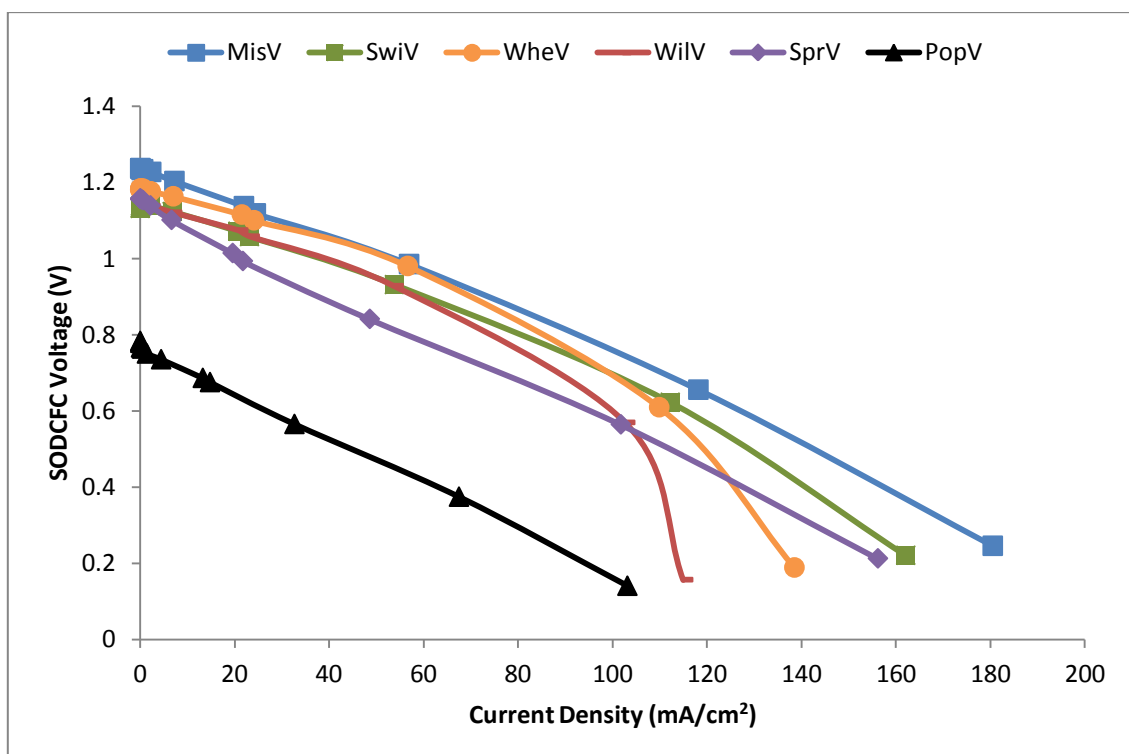


Figure 7.9: SODCFC voltage, current density for the 6 biomass fuels at 800°C (BM).

Figure 7.8 shows that at 700°C wheat, spruce and poplar fuels performances picked up while that of willow was still down. At 800°C miscanthus performance increased greatly giving the best voltage and the best current density. Figures 7.7 to 7.9 show mild degrees of the curve back phenomenon on the performance of these fuels a situation attributed to the overconsumption of the fuel at the anode compartment giving rise to gaps between the fuel and the electrolyte surface leading to reduction of the current density measured (Li *et al.*, 2009; Jain *et al.*, 2008; Hackett *et al.*, 2007; O'Hayre *et al.*, 2006; Cherepy *et al.*, 2005; Larminie and Dicks, 2003). Figures 7.10 to 7.12 give the power versus the current densities and Figures 7.13 to 7.15 show the overall performances of the biomass carbon fuels.

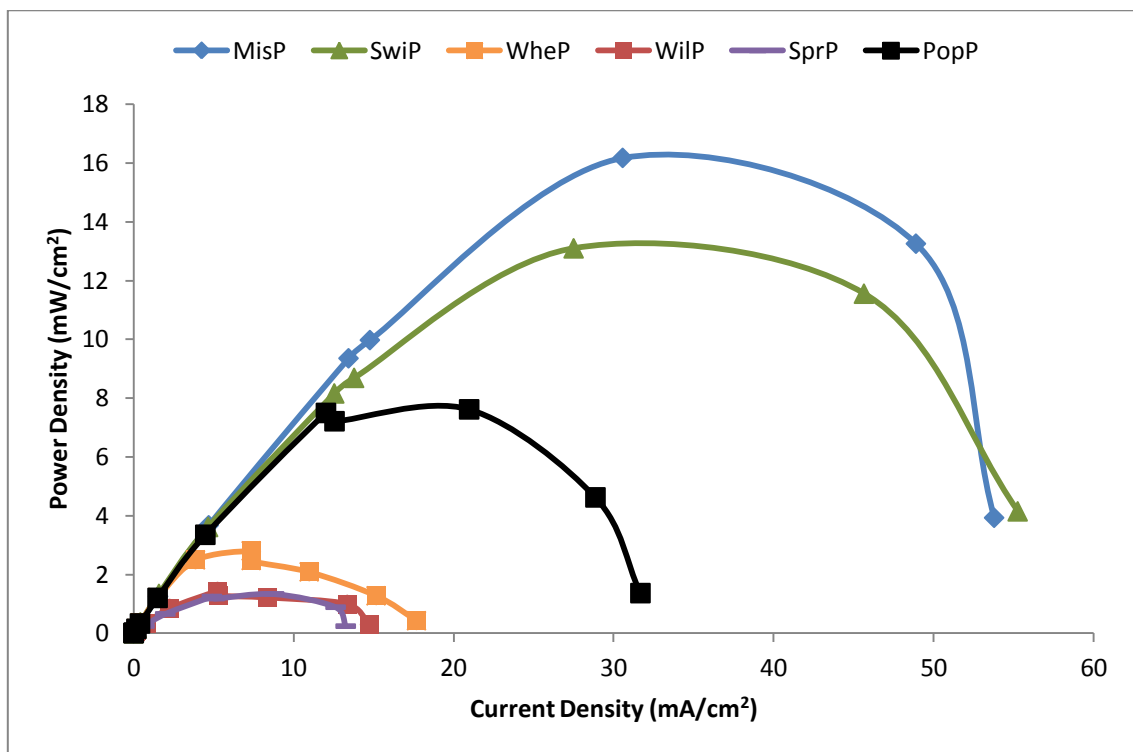


Figure 7.10: SODCFC power, current density for the 6 biomass fuels at 600°C (BM).

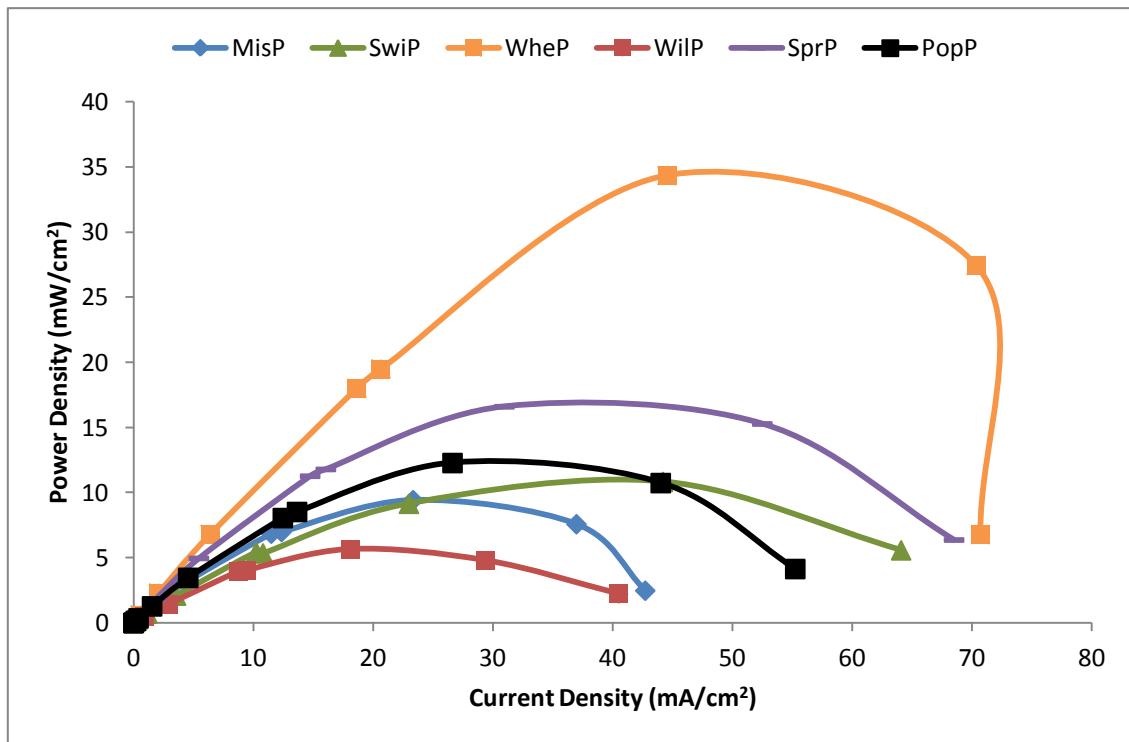


Figure 7.11: SODCFC power, current density for the 6 biomass fuels at 700°C (BM).

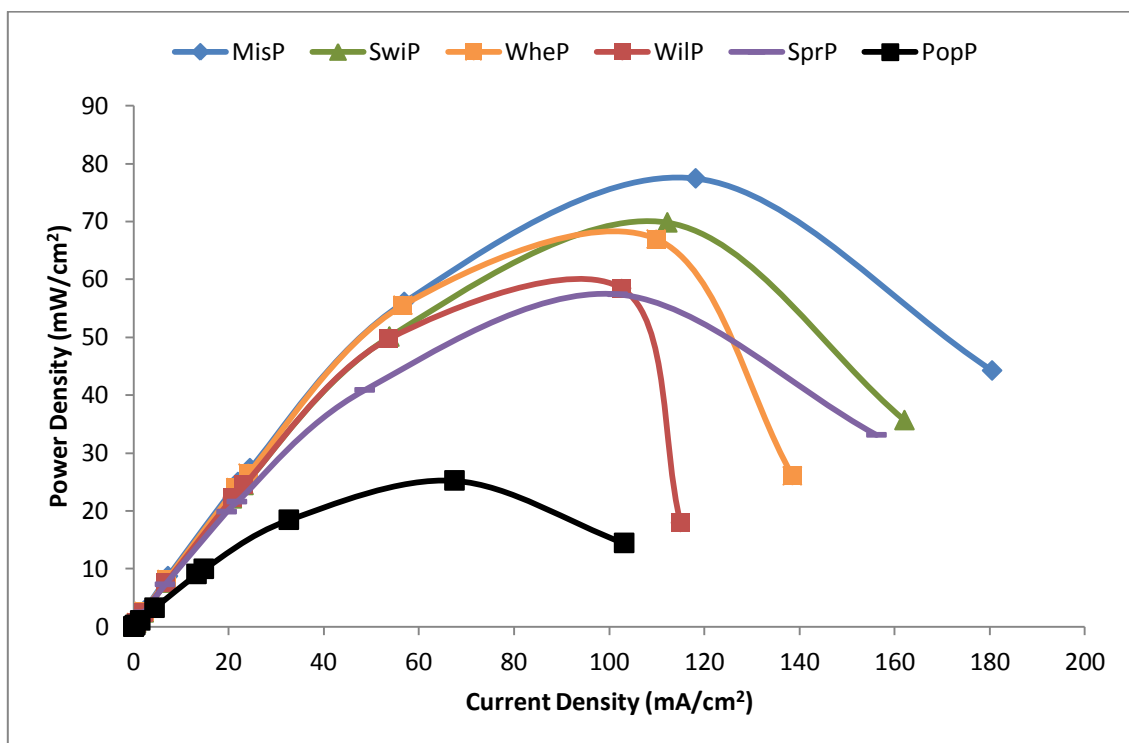


Figure 7.12: SODCFC power, current density for the 6 biomass fuels at 800°C (BM).

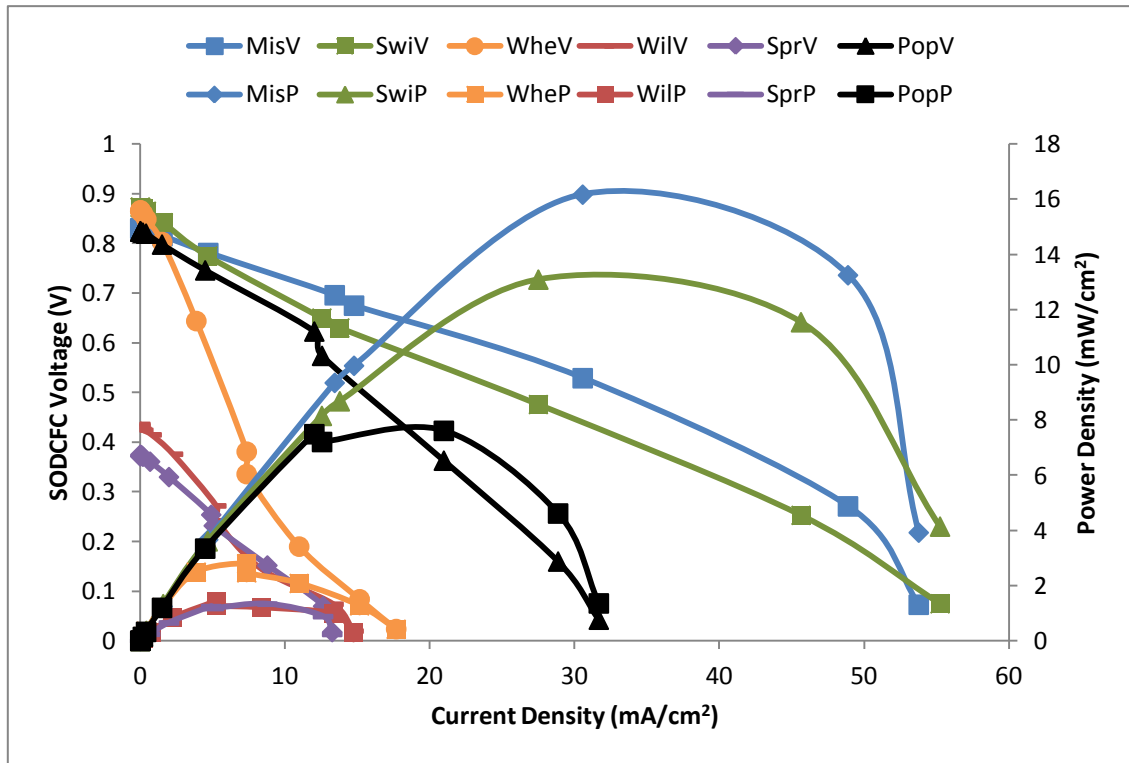


Figure 7.13: SODCFC overall performances for the 6 biomass fuels at 600°C (BM).

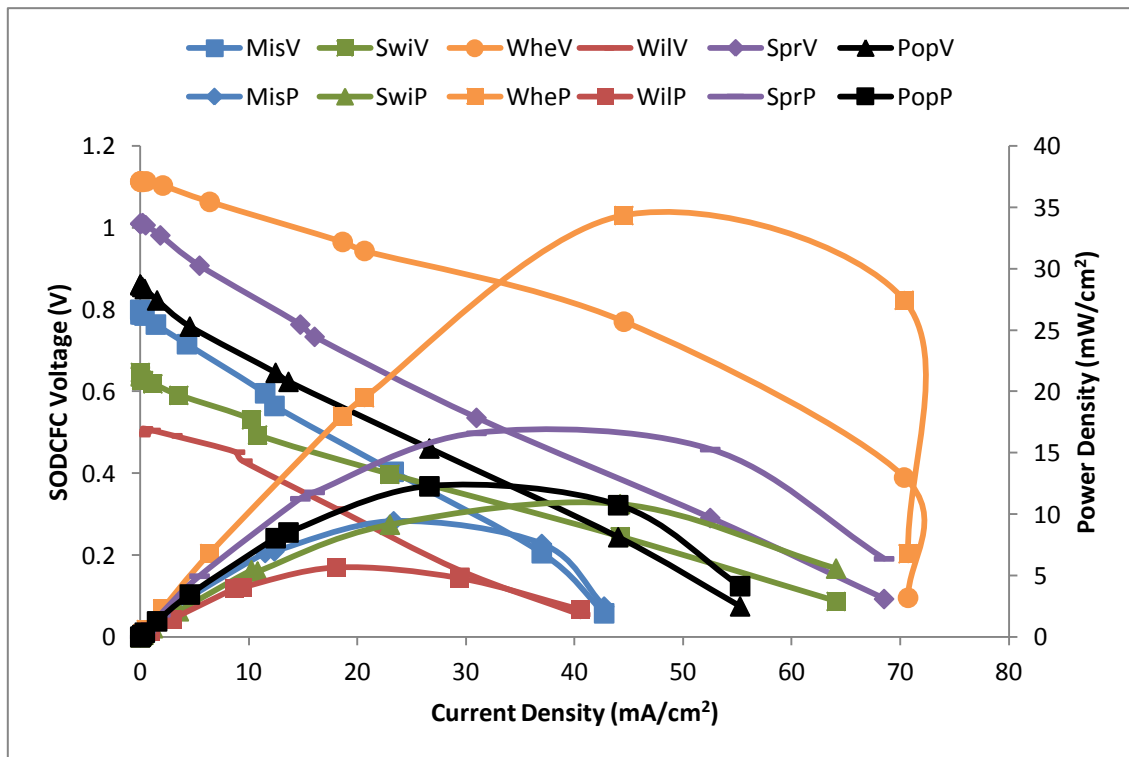


Figure 7.14: SODCFC overall performances for the 6 biomass fuels at 700°C (BM).

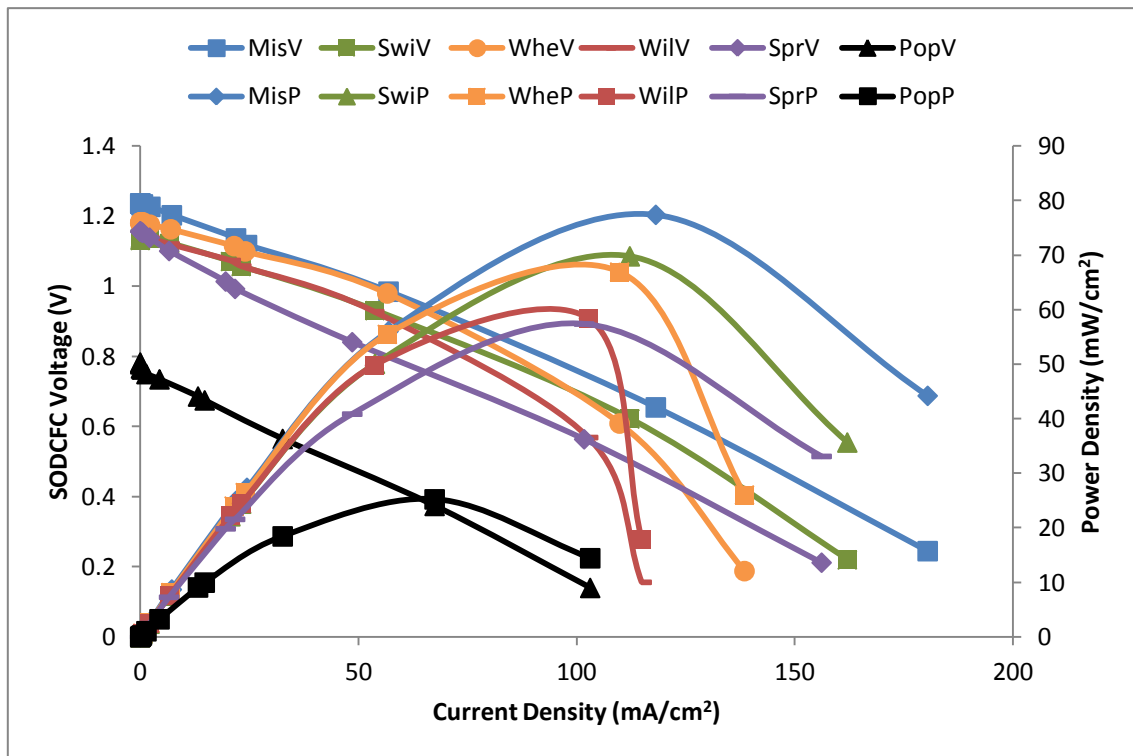


Figure 7.15: SODCFC overall performances for the 6 biomass fuels at 800°C (BM).

Figure 7.14 show that wheat fuel cell operation gave some interesting improvement. The SODCFC power density and current density increases with increase in temperature, reaches a maximum and finally falls at higher current densities (Li *et al.*, 2009; Hackett *et al.*, 2007). At 800°C miscanthus shows some improvement in the performance possessing the highest OCV, current and power densities. Perhaps the nickel components on the buttons cells acted as catalyst during the electrochemical reactions.

7.3.2 Temperature Effects on SODCFC Performances with BM Carbon Fuel

The effects of temperature on the performance of the SODCFC using the ball milled (BM) biomass carbon fuels are shown in Figure 7.16. There is a sharp rise in the OCV above 200°C, indicating ionic conduction in the SODCFC. This is quite different for the case of MDCFC which was around 400°C and shows that the electrochemical reactions of the carbon fuels in the SODCFC were faster than the MDCFC. The

performance of the fuel cell was greatly enhanced as the temperature increases up to 800°C, this is attributed to the decrease in the viscosity of the molten carbonate phase and a corresponding enhancement of the ionic conduction rate of the electrolyte and the electrochemical reactions at the two electrodes (Jia *et al.*, 2010; Li *et al.*, 2009; Jain *et al.*, 2008; Hackett *et al.*, 2007; Cherepy *et al.*, 2005;).

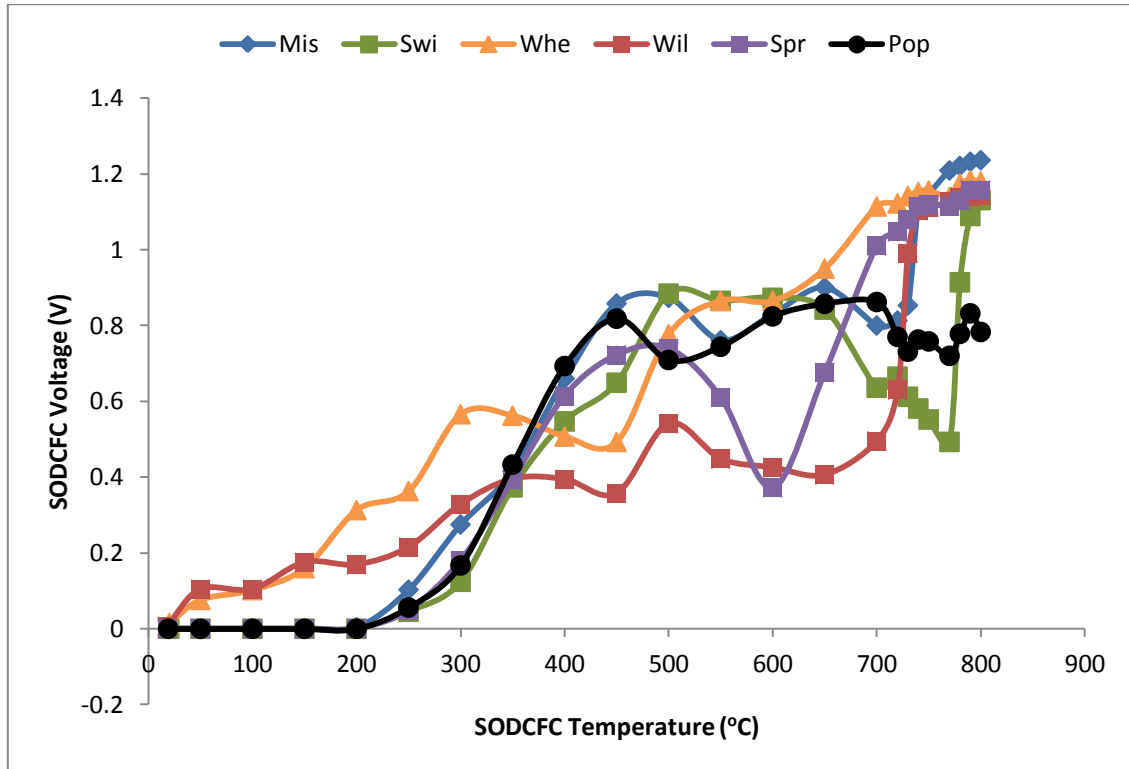


Figure 7.16: SODCFC open circuit voltage for the six biomass carbon fuels at different temperature (Ball milled)

The performances of the SODCFC at higher temperatures differ from the MDCFC. Miscanthus and wheat appears to have higher OCVs with poplar fuel recording lower OCV. Generally at 800°C the OCV for most of the biomass carbon fuels were higher than 1.0 V but poplar fuel gave 0.8 V (Figures 7.15 and 7.16).

7.3.3 SODCFC Performance Efficiency using BM Biomass Carbon Fuel

The current, power and voltage curves show characteristic behaviour of the single cell solid oxide electrolyte direct carbon fuel cell (SODCFC), and of particular interest are the effective open circuit voltage (OCV), peak power, current density and the area specific resistance (ASR) behaviours. The characteristic electrochemical performances are presented in Table 7.1, Tables D5 and D6 (Appendix D). Tables 7.1, D5 and D6 show the electrochemical properties of the six biomass carbon fuels, it reveals that the OCV, power and current densities increases with increase in temperatures while the area specific resistance (ASR) decreases with rise in temperature. Wheat has the highest power efficiency of 69% at 700°C operating condition and switchgrass in contrast has the lowest power efficiency of 39% also at 700°C. Interestingly the low efficiency recorded for MDCFC willow fuel has been greatly enhanced to 63% for the ball mill (BM) fuel at 600°C.

Table 7.1: SODCFC Electrochemical performances for miscanthus and willow (BM)

SODCFC Parameter	Miscanthus			Willow		
	Temperature °C			Temperature °C		
	600	700	800	600	700	800
Open circuit voltage (V)	0.83	0.80	1.24	0.43	0.50	1.14
Peak power density (mW/cm ²)	16.17	9.43	77.41	1.43	5.66	58.42
Maximum current density (mA/cm ²)	53.79	42.74	180.52	14.74	40.52	114.94
Current density at 0.8 V (mA/cm ²)	4.70	0.01	100.00	0	0	80.00
Voltage at peak power (V)	1.54	0.40	0.66	0.27	0.31	0.57
Area specific resistance (Ω cm ²)	9.24	14.66	4.10	31.46	13.48	4.27
Efficiency at peak power (%)	64.00	50.00	53.00	63.00	62.00	50.00

Tables 7.1, D5 and D6 summarise the results of the SODCFC electrochemical performances for the ball milled (BM) biomass carbon fuels at 600°C, 700°C and 800°C. The SODCFC performances of the BM biomass fuels were higher than those experienced with the MDCFC ball milled fuels. For the SODCFC in terms of the open circuit voltage, miscanthus fuel (1.24 V at 800°C) had the best for the BM and spruce fuel (0.37 V at 600°C) the least for the BM. The best peak power density was recorded for miscanthus fuel (77.41 mW/cm² at 800°C) and spruce fuel (1.34 mW/cm² at 600°C) the least. Again miscanthus fuel (180.52 mA/cm² at 800°C) gave the maximum current density while spruce fuel (13.26 mA/cm² at 600°C) gave the minimum. For the current density at 80% voltage efficiency miscanthus fuel (100 mA/cm² at 800°C) and wheat fuel (90 mA/cm² at 800°C) were superior. Miscanthus fuel (1.54 V) shows the highest voltage at peak power and spruce fuel (0.15 V) the lowest. The ASR evaluation show that wheat fuel gave the highest (40.26 Ω cm² at 600°C) and lowest values (3.69 Ω cm² at 800°C), the reduction in the ohmic resistance could have been responsible for the higher peak power efficiency observed at 700°C for wheat fuel.

7.4 SODCFC Performance with Hand Milled (HM) Biomass Carbon Fuels

7.4.1 First Day Performances of the SODCFC

Figures 7.17 to 7.19 show the voltage versus current densities results of the SODCFC for the first day of the hand milled carbon particle fuels operating at 600°C, 700°C and 800°C. From Figure 7.17 in terms of the OCV, miscanthus fuel had the highest OCV (0.83 V) and the highest current density 36 mA/cm². Spruce fuel OCV was 0.82 V but had the third highest current density (25 mA/cm²). Willow, poplar and wheat did not perform very well in this case.

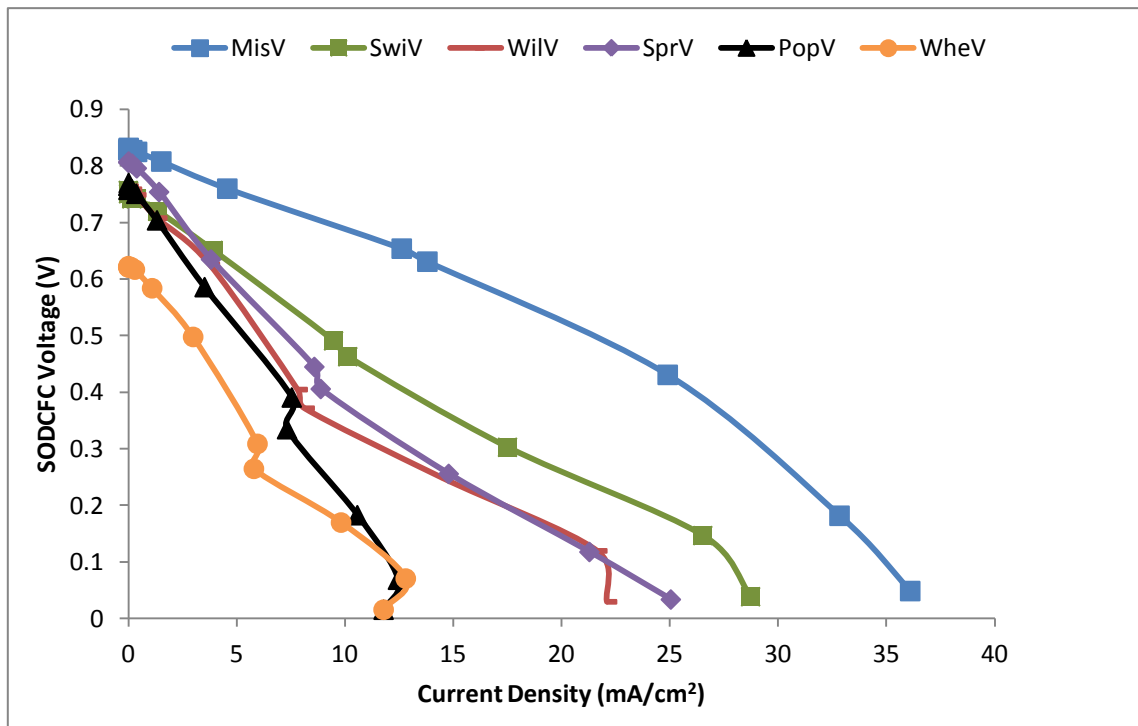


Figure 7.17: SODFCF voltage, current density for the 6 biomass fuels at 600°C (HM).

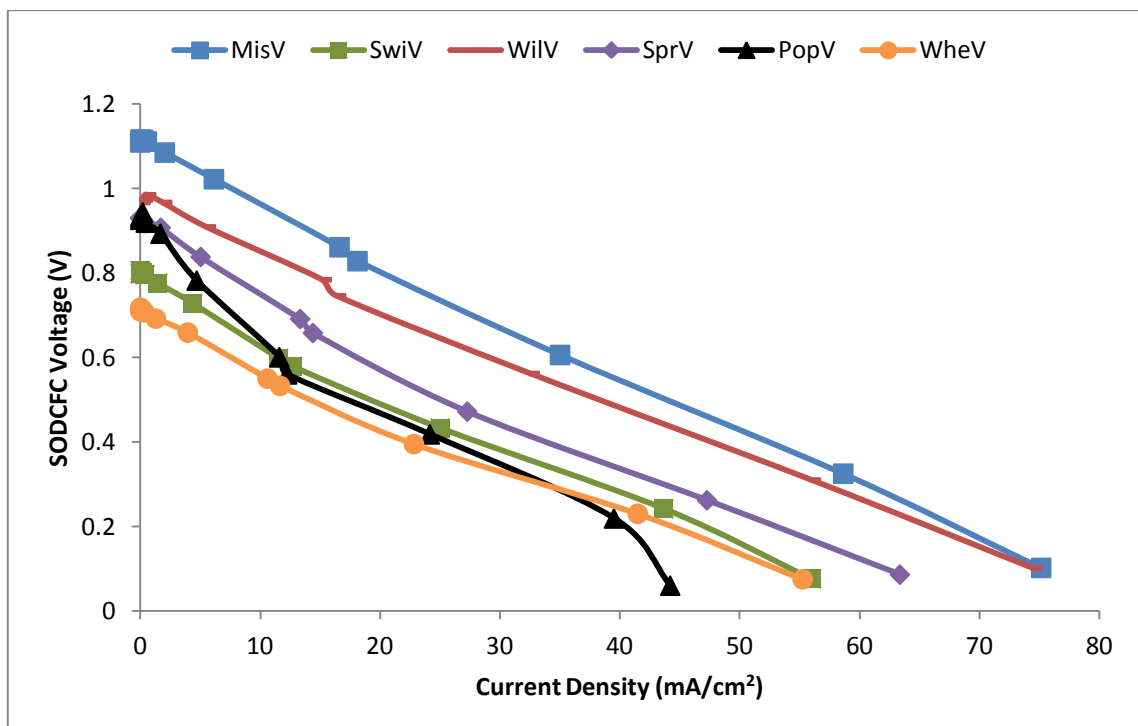


Figure 7.18: SODFCF voltage, current density for the 6 biomass fuels at 700°C (HM).

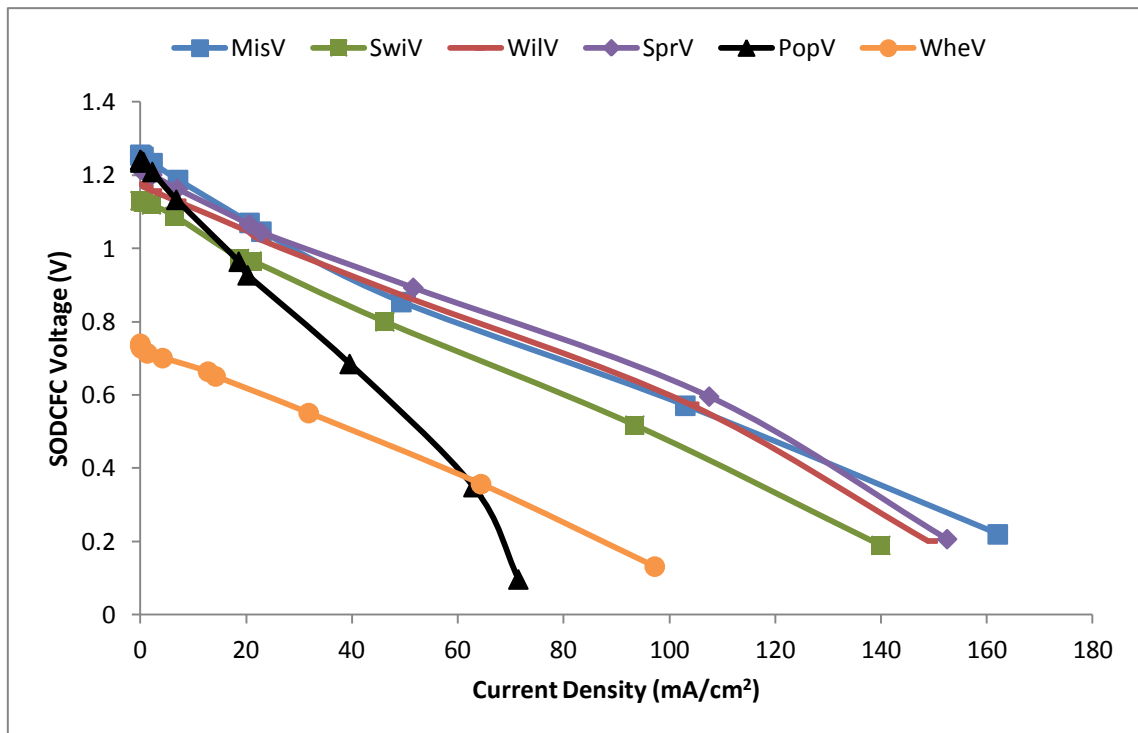


Figure 7.19: SODFC voltage, current density for the 6 biomass fuels at 800°C (HM).

Figure 7.18 shows that at 700°C miscanthus, willow and spruce fuels performances picked up while that of wheat was still down. At 800°C spruce and willow performances increased greatly. Figures 7.17 to 7.19 show some slight degrees of the curve back phenomena of the performance of the biomass fuels again attributed to the overconsumption of the fuel at the anode compartment (Li *et al.*, 2009; Jain *et al.*, 2008; Hackett *et al.*, 2007; O'Hayre *et al.*, 2006; Cherepy *et al.*, 2005; Larminie and Dicks, 2003). Figures 7.20 to 7.22 show the power versus the current densities and Figures 7.23 to 7.25 shows the overall performances of the biomass carbon fuels.

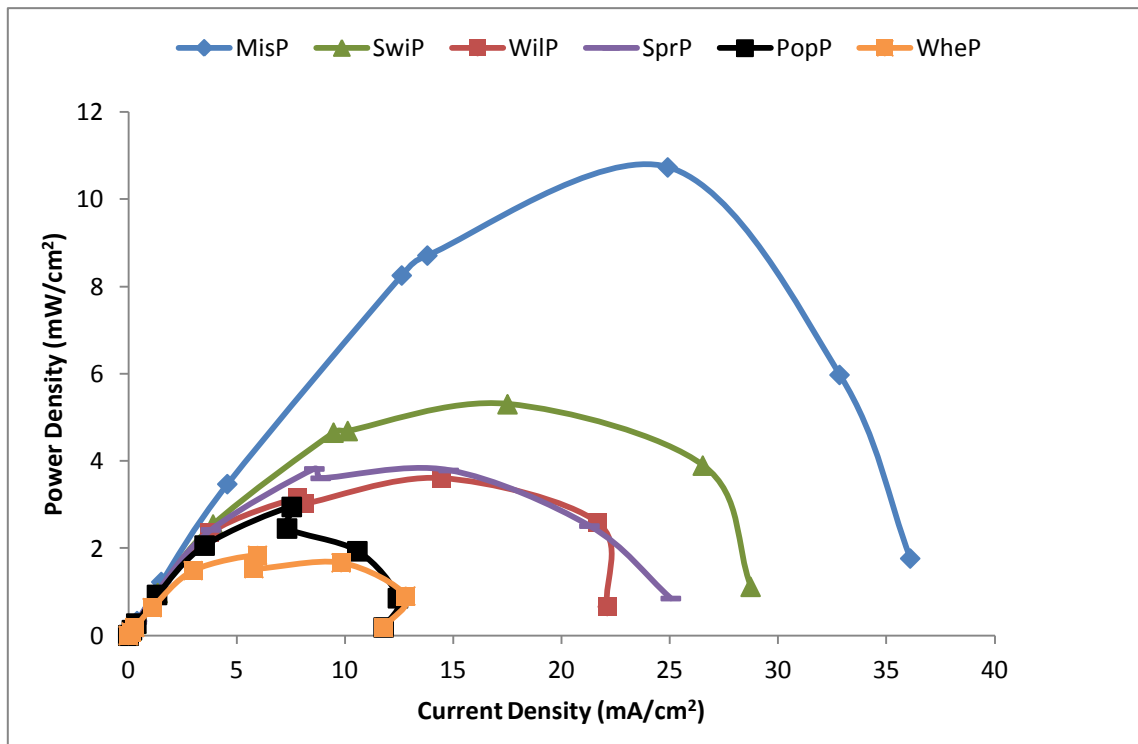


Figure 7.20: SODFC power versus current density for the 6 biomass fuels at 600°C (HM).

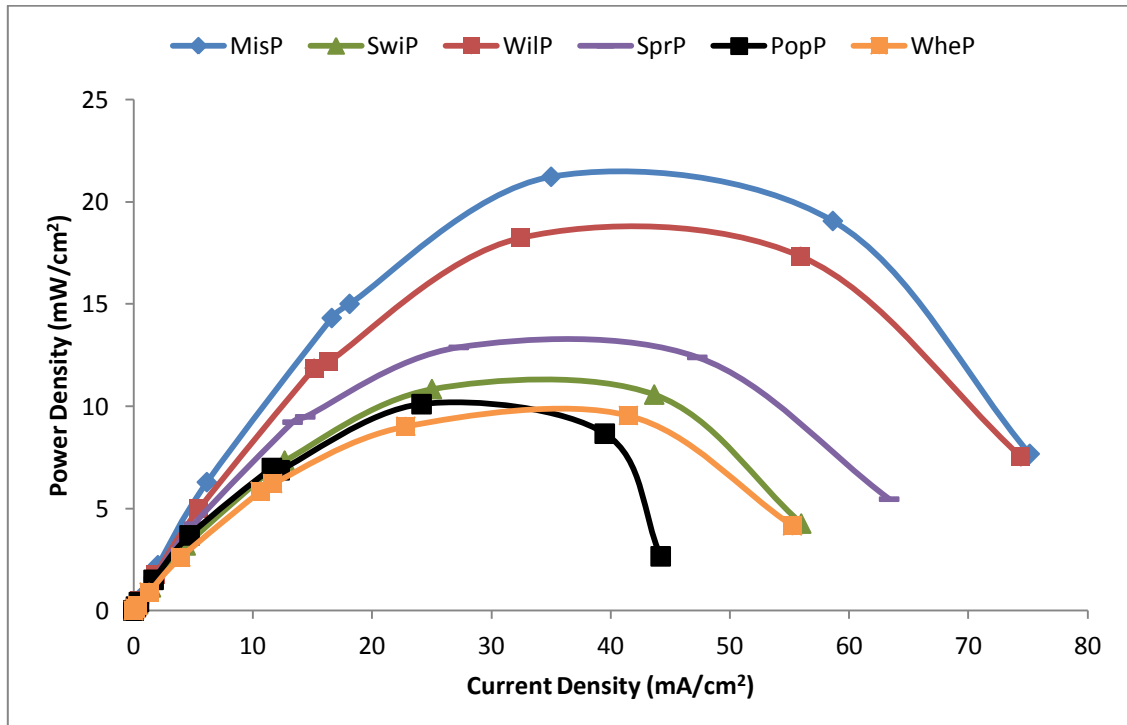


Figure 7.21: SODFC power versus current density for the 6 biomass fuels at 700°C (HM).

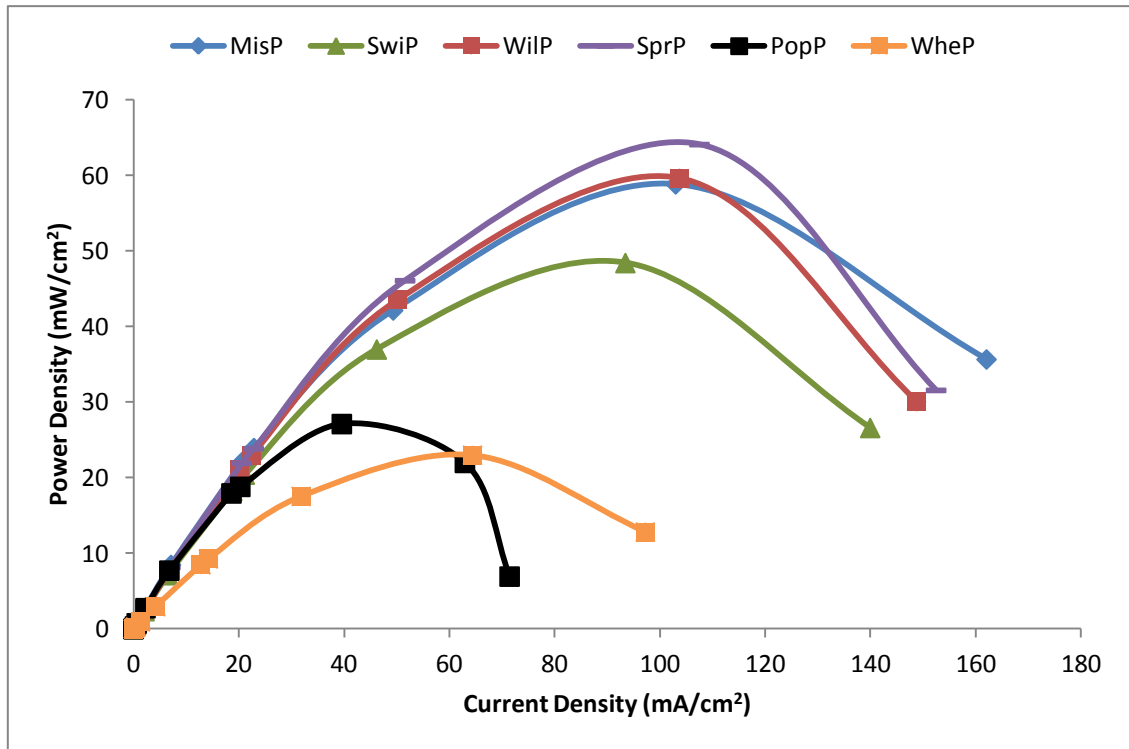


Figure 7.22: SODCFC power versus current density for the 6 biomass fuels at 800°C (HM).

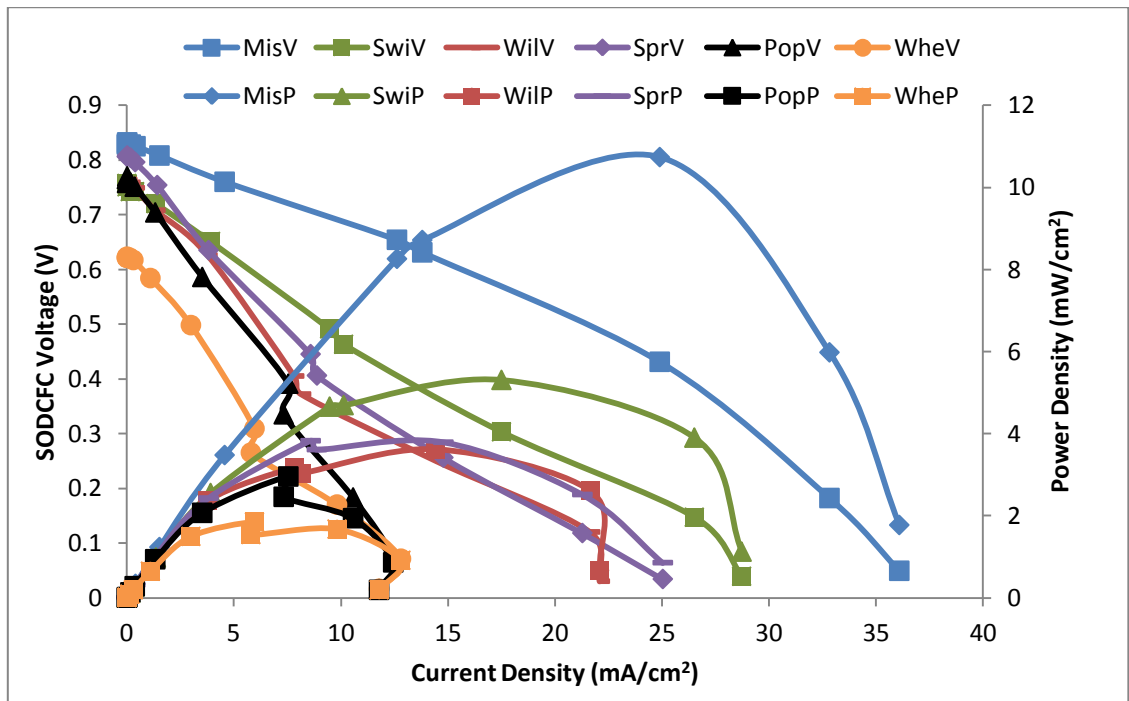


Figure 7.23: SODCFC overall performances for the 6 biomass fuels at 600°C (HM).

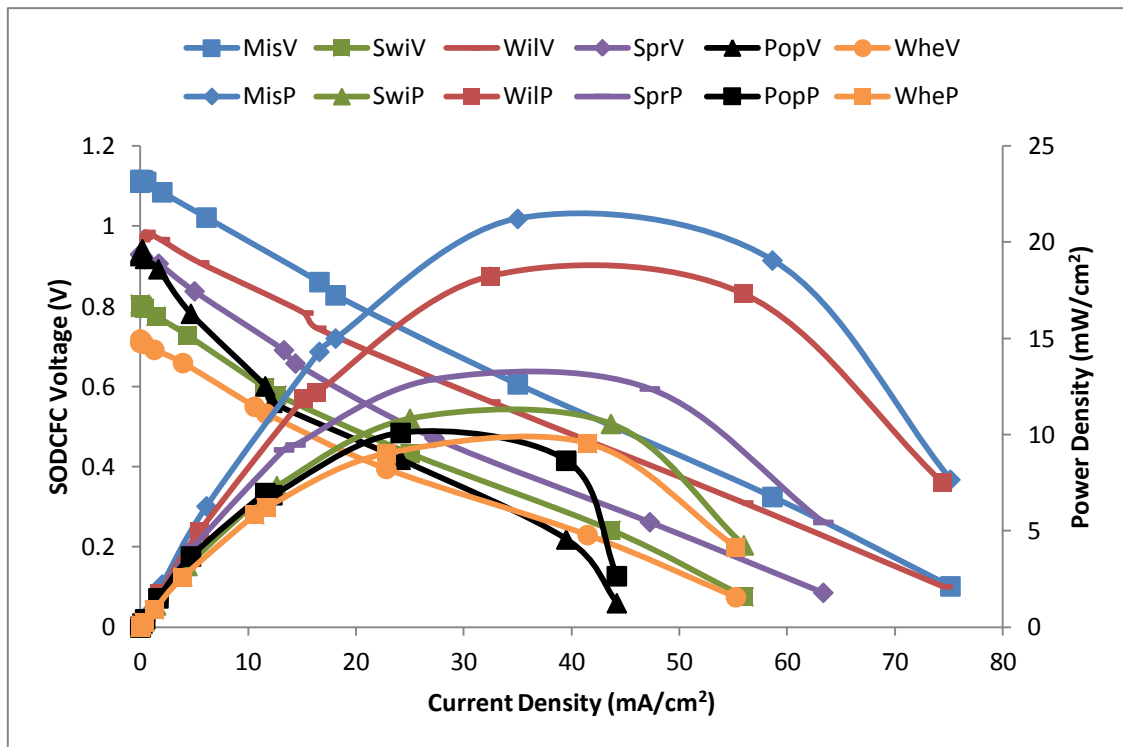


Figure 7.24: SODCFC overall performances for the 6 biomass fuels at 700°C (HM).

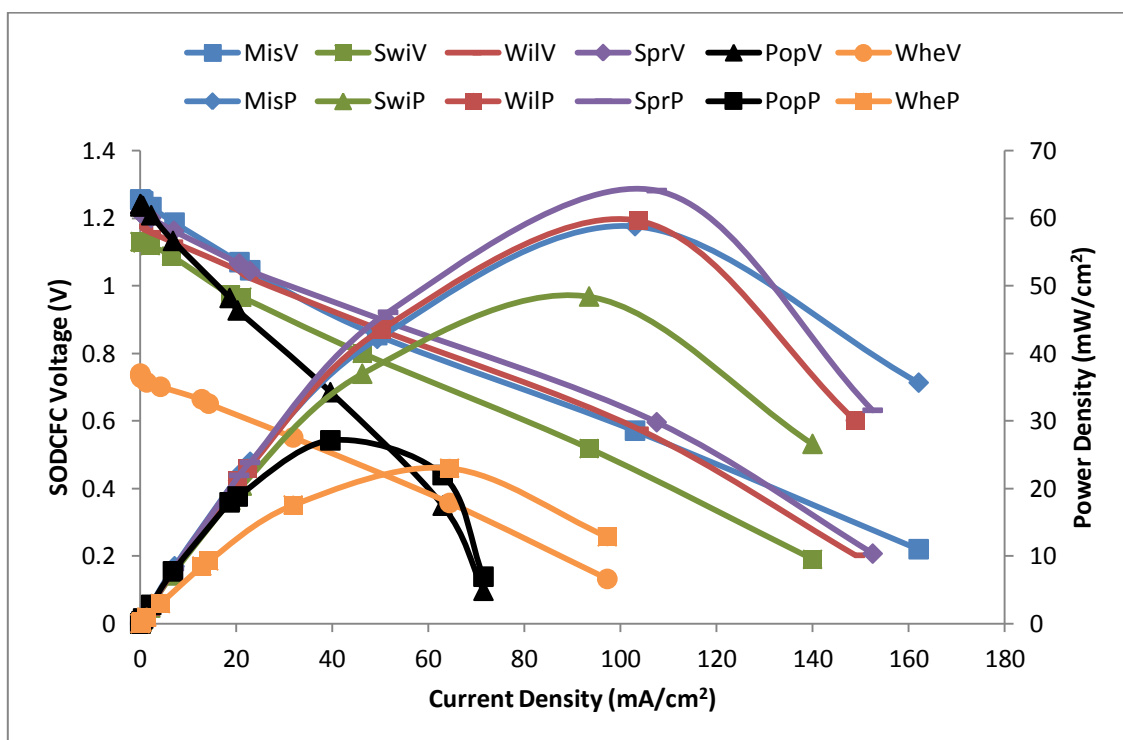


Figure 7.25: SODCFC overall performances for the 6 biomass fuels at 800°C (HM).

Figures 7.23 and 7.25 show that overall picture of the performances of these biomass fuels. Miscanthus and willow fuel cell operations show some interesting improvement. Spruce fuel finally proved its superiority in performance at higher temperatures. Surprisingly poplar started with high OCV but ended up with weak performances.

7.4.2 Temperature Effects on SODCFC Performances with HM Carbon Fuel

The effects of temperature on the performance of the SODCFC using the hand milled (HM) biomass carbon fuels are shown in Figure 7.26. There is a sharp rise in the OCV above 300°C, this is slightly different from the BM fuels starting at 200°C. This is different from the case of MDCFC which was at 500°C and shows that the electrochemical reactions of the carbon fuels in the SODCFC were faster than the MDCFC, this could be as a result of the nickel anode component of the SODCFC which not only acted as an anode but could have catalysed the reactions. The reaction of the SODCFC with the hand milled (300°C) fuels lag behind that of the ball milled (200°C) because the reactions with smaller particles (having higher surface area) lead to a reduction in activation loss and gave higher OCV (Kim *et al.*, 2010). The performance of the fuel cell was greatly enhanced as the temperature increases up to 800°C, this is attributed to an enhancement of the ionic conduction rate of the electrolyte and the electrochemical reactions at the two electrodes (Jia *et al.*, 2010; Li *et al.*, 2009; Jain *et al.*, 2008; Hackett *et al.*, 2007; Cherepy *et al.*, 2005).

The performances of the SODCFC with the hand milled fuels at higher temperature were also higher than the MDCFC hand milled fuels. Miscanthus seems to give the highest OCV recorded for the HM fuels and wheat gave the least (Figure 7.26).

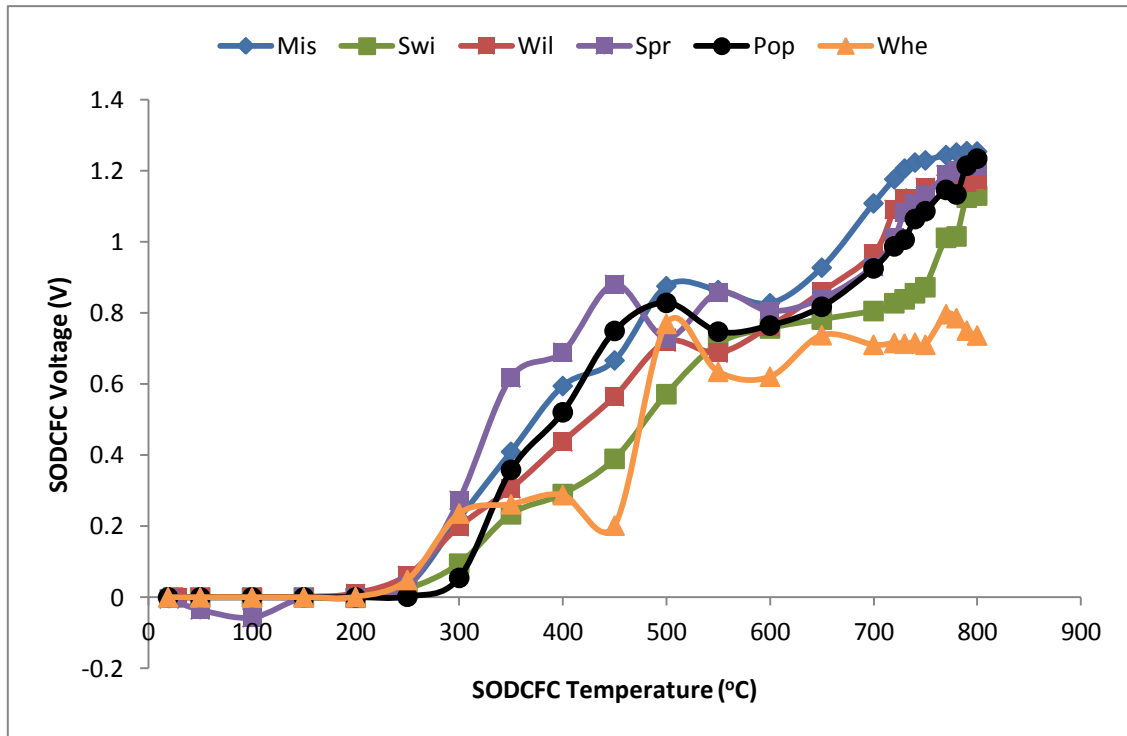


Figure 7.26: SODCFC open circuit voltage for the six biomass carbon fuels at different temperature (HM)

7.4.3 SODCFC Performance Efficiency using HM Biomass Carbon Fuel

Tables 7.2, D7 and D8 (Appendix D) give the current, power and voltage characteristic behaviour of the SODCFC, showing the effective open circuit voltage (OCV), peak power, current density, voltage at peak power, area specific resistance (ASR) and the efficiency at peak power. Tables 7.2, D7, D8 show the electrochemical performances for the six biomass carbon fuels, it reveals that the OCV, power and current densities increases with increase in temperature while the ASR decreases with increase in temperature. Switchgrass has the highest power efficiency of 61% at 600°C operating condition and wheat in contrast has the lowest power efficiency of 32% also at the 700°C operating condition.

Table 7.2: SODCFC Electrochemical performances for miscanthus and willow (HM)

SODCFC Parameter	Miscanthus			Willow		
	Temperature °C			Temperature °C		
	600	700	800	600	700	800
Open circuit voltage (V)	0.83	1.11	1.26	0.76	0.97	1.18
Peak power density (mW/cm ²)	10.73	21.22	58.83	3.61	18.25	59.66
Maximum current density (mA/cm ²)	36.10	75.15	162.10	22.10	74.42	148.84
Current density at 0.8 V (mA/cm ²)	1.52	24.00	70.00	0	15.14	78.00
Voltage at peak power (V)	0.43	0.61	0.57	0.25	0.56	0.58
Area specific resistance (Ω cm ²)	18.02	13.14	7.26	19.35	11.39	5.66
Efficiency at peak power (%)	52.00	55.00	45.00	33.00	58.00	49.00

Tables 7.2, D7, D8 summarise the results of the SODCFC electrochemical performances for the hand milled (HM) biomass carbon fuels at 600°C, 700°C and 800°C. Again the SODCFC performances of the HM biomass fuels were higher than those of the MDCFC hand milled fuels. The BM fuels have better performances than the HM fuels in the SODCFC, detailed comparison are given in section 7.5. For the hand milled fuels SODCFC in terms of the open circuit voltage, miscanthus fuel (1.26 V at 800°C) had the best and wheat fuel (0.62 V at 600°C) the least. The best peak power density was recorded for spruce fuel (64.10 mW/cm² at 800°C) and wheat fuel (1.84 mW/cm² at 600°C) the least. Miscanthus fuel (162.10 mA/cm² at 800°C) gave the maximum current density while poplar fuel (11.79 mA/cm² at 600°C) gave the minimum. For the current density at 80% voltage efficiency spruce fuel (90 mA/cm² at 800°C) and willow fuel (78 mA/cm² at 800°C) were superior. Poplar fuel (0.69 V) shows the highest voltage at peak power and wheat fuel (0.23 V) the lowest. The ASR evaluations show that poplar fuel gave the highest (46.85 Ω cm² at 600°C) and spruce fuel the lowest values (5.25 Ω cm² at 800°C). The ASR recorded for the SODCFC were much higher than those recorded in literatures and this could contribute to the lowering of the performances of the fuel cell (Li *et al.*, 2009; Hackett *et al.*, 2007; Larminie and Dicks, 2003).

7.5 Comparison of SODCFC Performances for HM and BM Carbon Fuels

7.5.1 Miscanthus Carbon Fuel

The differences between the SODCFC performances using hand and ball milled miscanthus fuel at 600°C, 700°C and 800°C are shown in Figures 7.27 to 7.29. The figures show that the BM miscanthus carbon fuels have better performance at 600°C and 800°C while the HM has at 700°C. Hand mill carbon fuel had an average particle size of 29 μm while the ball mill was 8 μm (Tables 5.25 and 5.26). The specific surface area was 0.57 m^2/g for the HM and 0.95 m^2/g for the BM (Tables 5.25 and 5.26). H MV and HMP represent the hand milled carbon fuel voltage and power density and likewise for the ball milled carbon fuels (BMV and BMP).

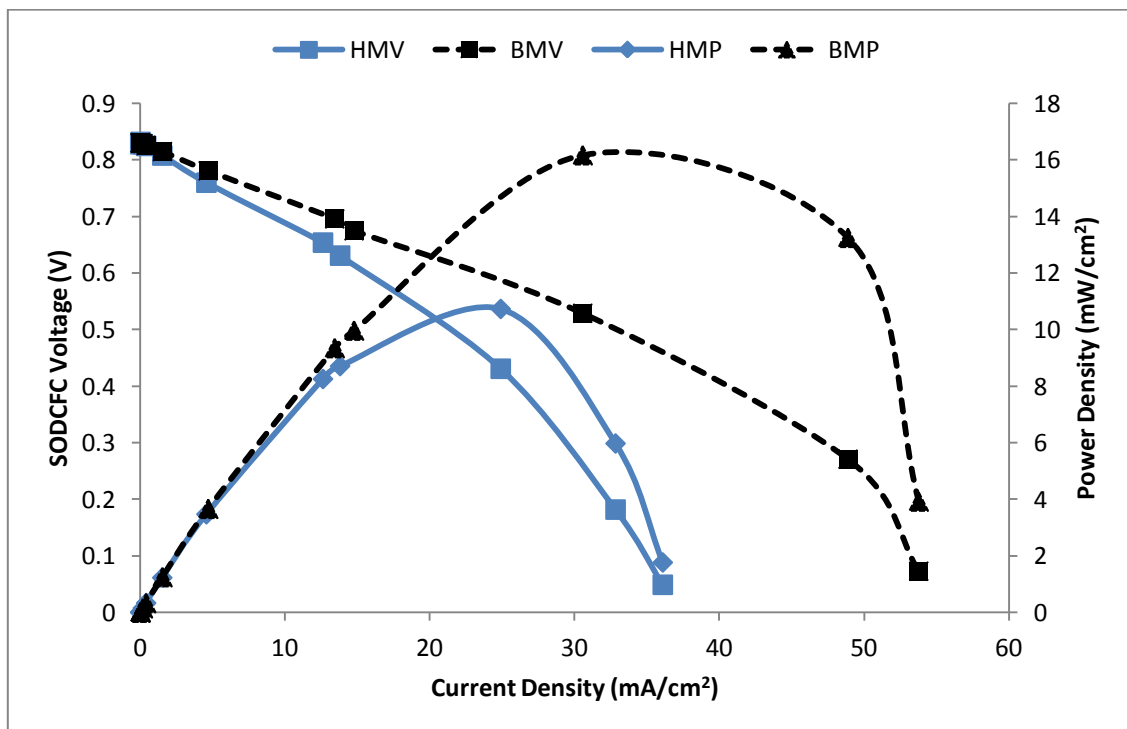


Figure 7.27: SODCFC miscanthus performances for HM and BM fuels at 600°C.

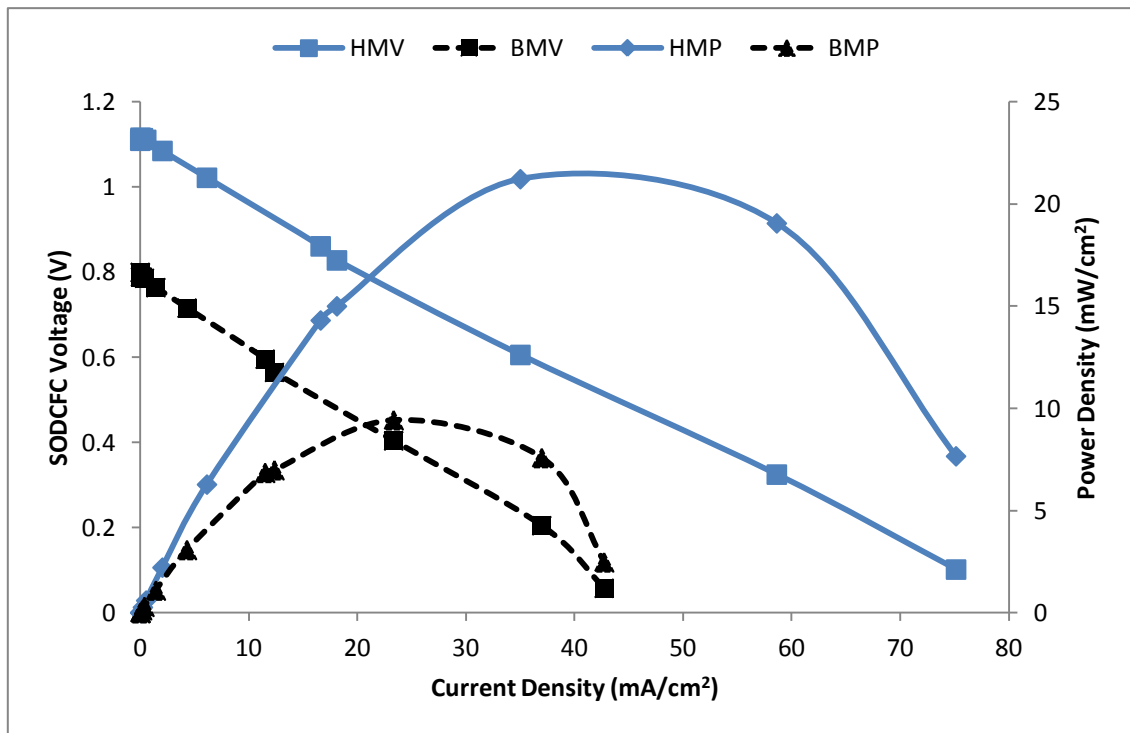


Figure 7.28: SODFCF miscanthus performances for HM and BM fuels at 700°C.

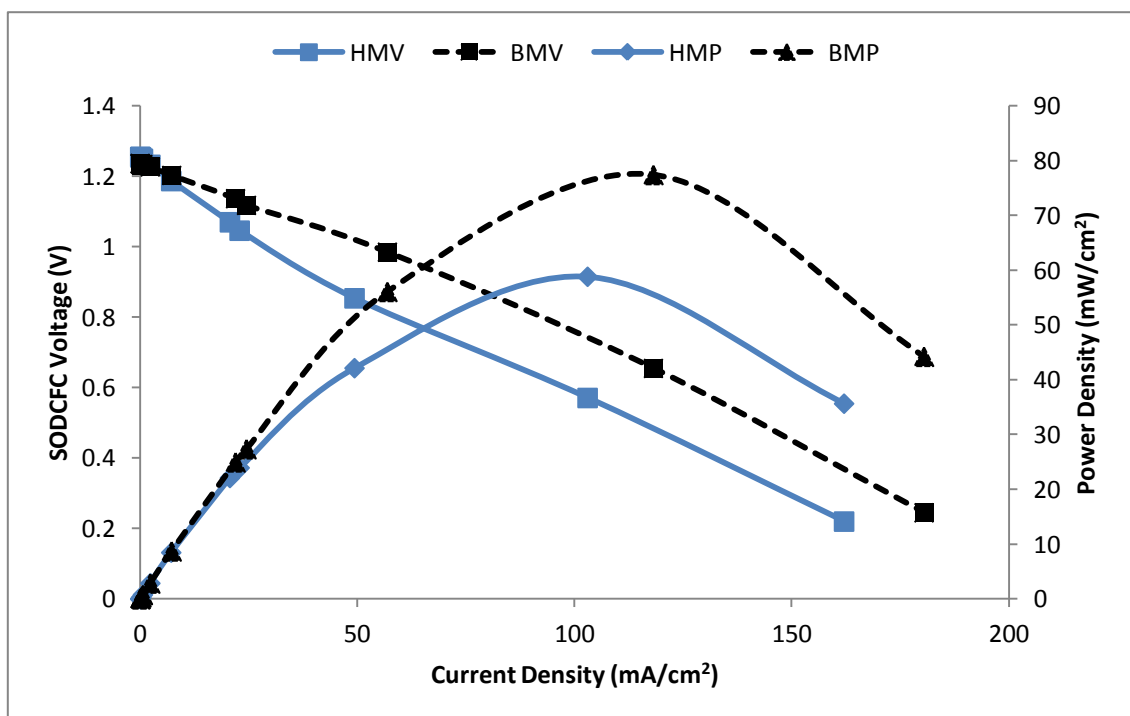


Figure 7.29: SODFCF miscanthus performances for HM and BM fuels at 800°C.

The performances presented in Figures 7.27 to 7.29 support the observations that reactions with smaller particles could enhance positively or negatively the active reactions sites on the biomass carbon fuel (Kim *et al.*, 2010; Hackett *et al.*, 2008; Cherepy *et al.*, 2005).

7.5.2 Switchgrass Carbon Fuel

The difference between the SODCFC performances using switchgrass fuel at 600°C, 700°C and 800°C are shown in Figures 7.30 to 7.32. The figures show that the BM switchgrass carbon fuel have better performance than the HM. Hand milled carbon fuel had an average particle size of 30 μm while the ball milled had 2 μm . The specific surface area was 0.63 m^2/g for the hand milled and 2.55 m^2/g for the ball milled (Tables 5.25 and 5.26). These show some positive and negative effects on the electrochemical discharge with the BM carbon fuel (Cherepy *et al.*, 2005).

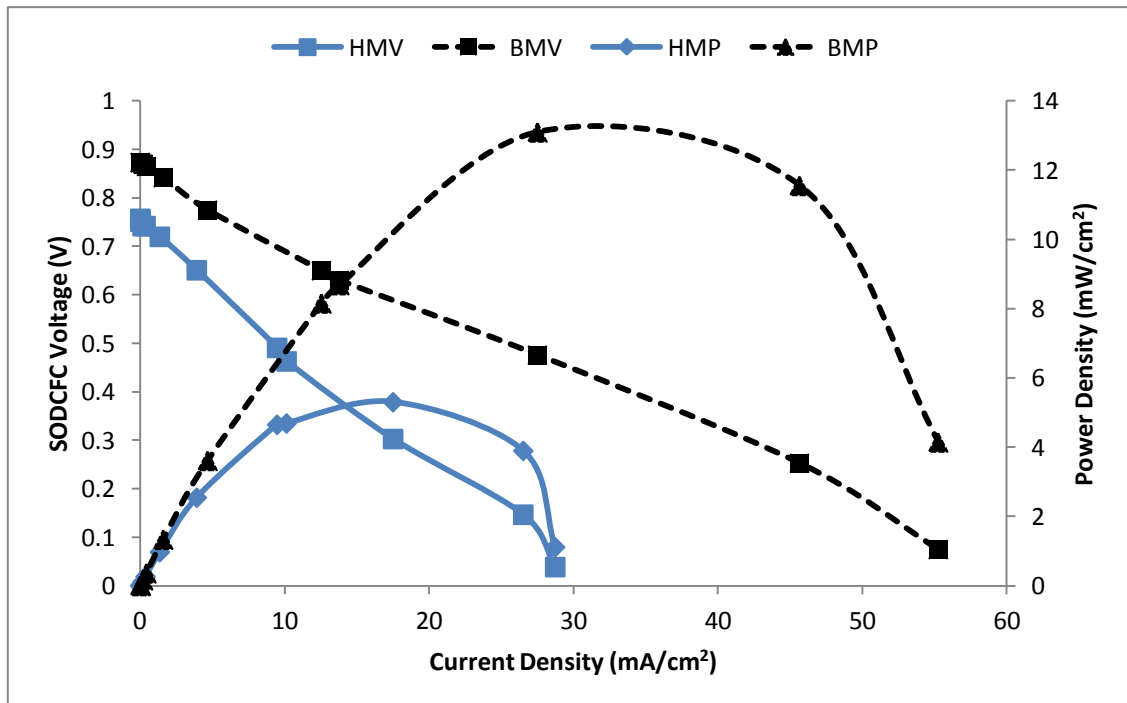


Figure 7.30: SODCFC switchgrass performances for HM and BM fuels at 600°C.

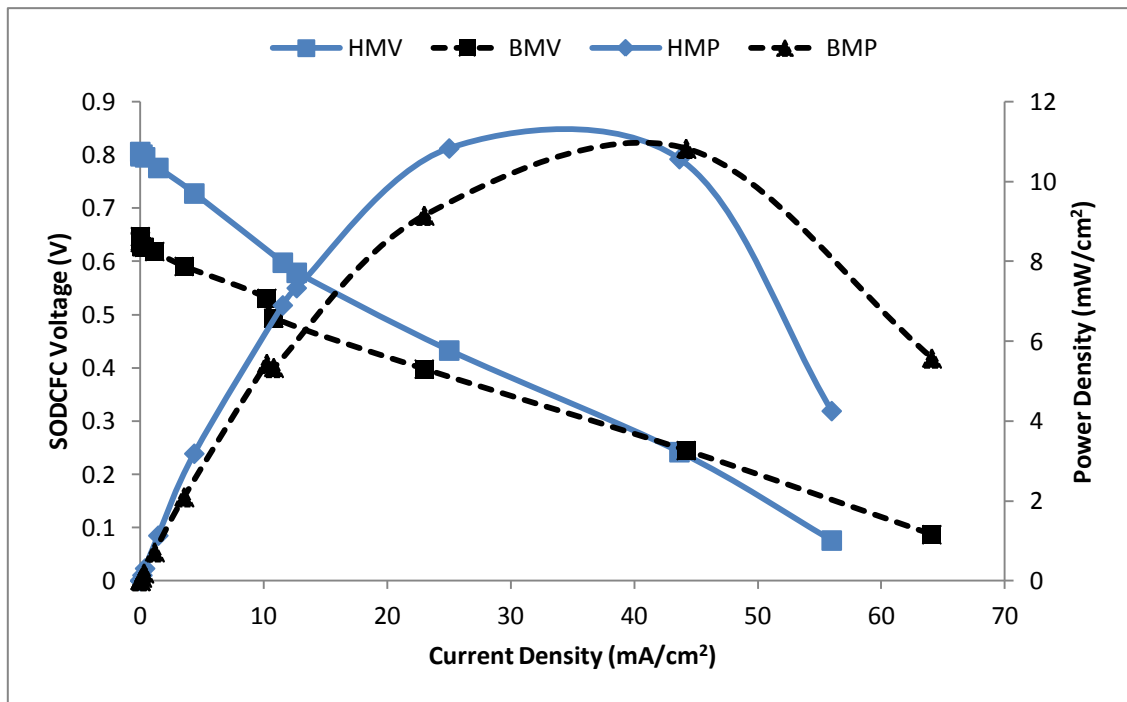


Figure 7.31: SODCFE switchgrass performances for HM and BM fuels at 700°C.

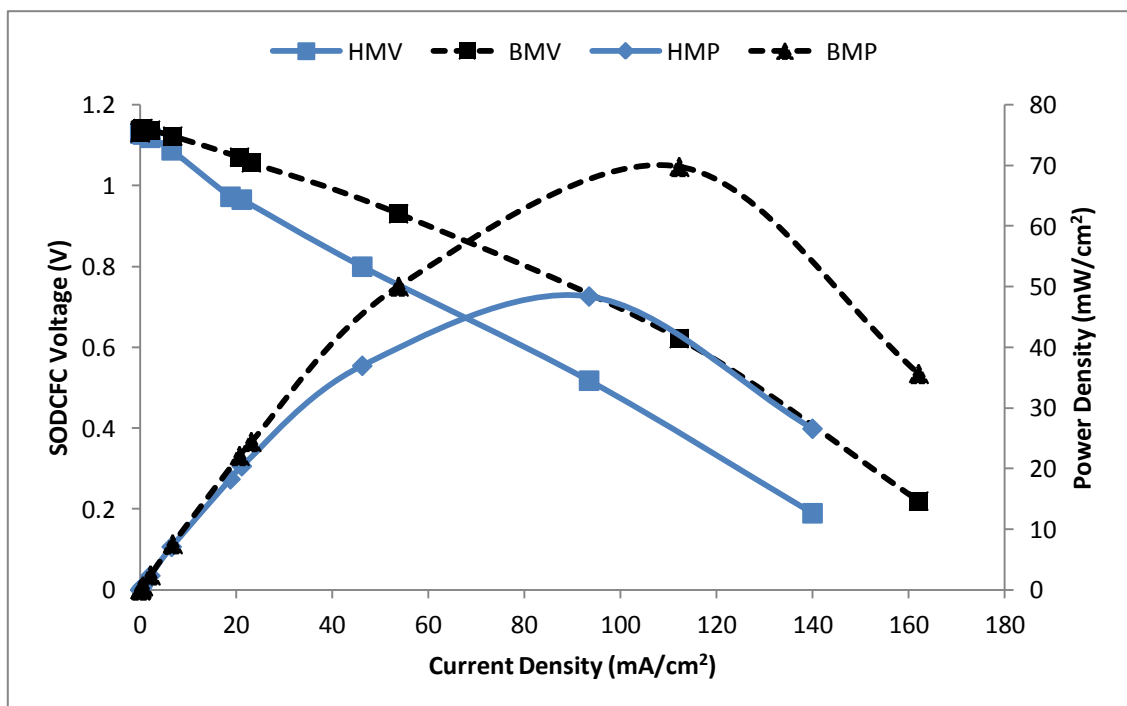


Figure 7.32: SODCFE switchgrass performances for HM and BM fuels at 800°C.

Figures 7.30 to 7.32 show that reactions with smaller particles (BM) led to positive and negative effects on the active reactions sites on the switchgrass BM fuel. The ASR

recorded for the HM ($6.62 \Omega \text{ cm}^2$ at 800°C) was higher than those of the BM ($4.11 \Omega \text{ cm}^2$ at 800°C) as given in Tables D5 and D7 (Appendix D). The higher the ASR value, the higher the ohmic resistance on the SODCFC operations and invariably the lower the electrochemical discharge rate from the cell (Kim *et al.*, 2010; Hackett *et al.*, 2008; Cherepy *et al.*, 2005).

7.6 Comparison of SODCFC and MDCFC Performance for BM Carbon Fuels

7.6.1 Miscanthus Carbon Fuel

The performances of the SODCFC were better than the MDCFC. The difference between these performances using miscanthus fuel at 600°C , 700°C and 800°C are shown in Figures 7.33 to 7.35. The open circuit voltage, power and current densities outputs from the SODCFC were superior to those of the MDCFC.

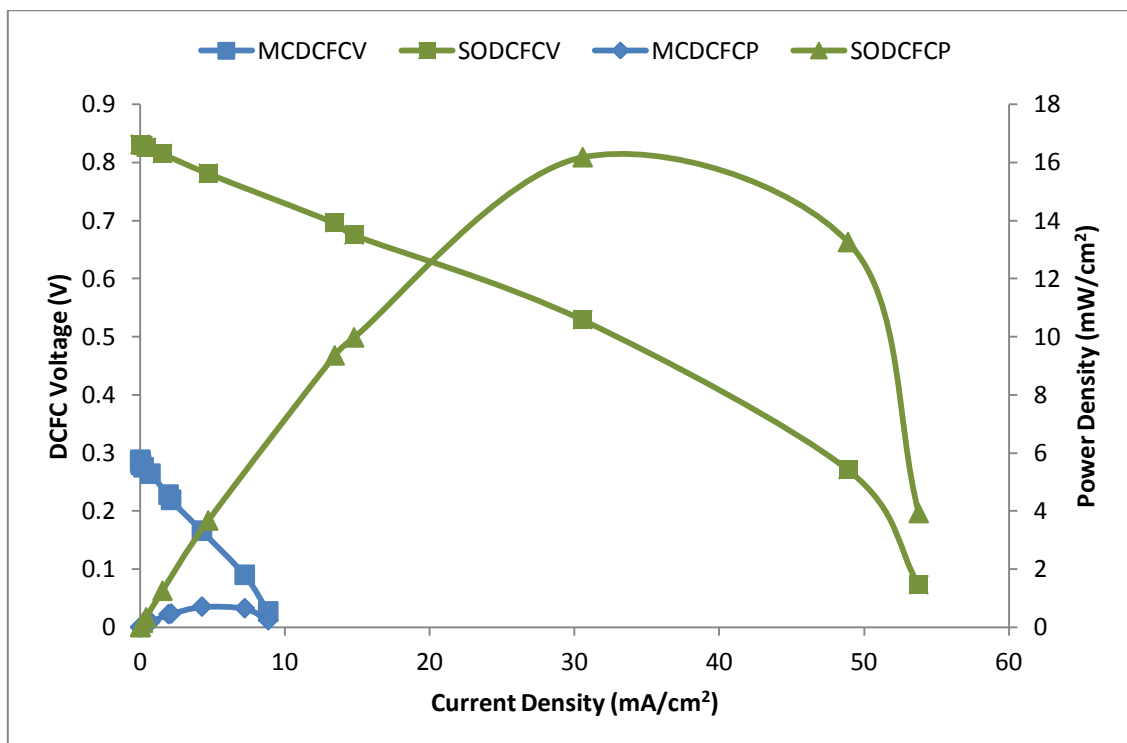


Figure 7.33: BM Miscanthus performances for SODCFC and MDCFC at 600°C .

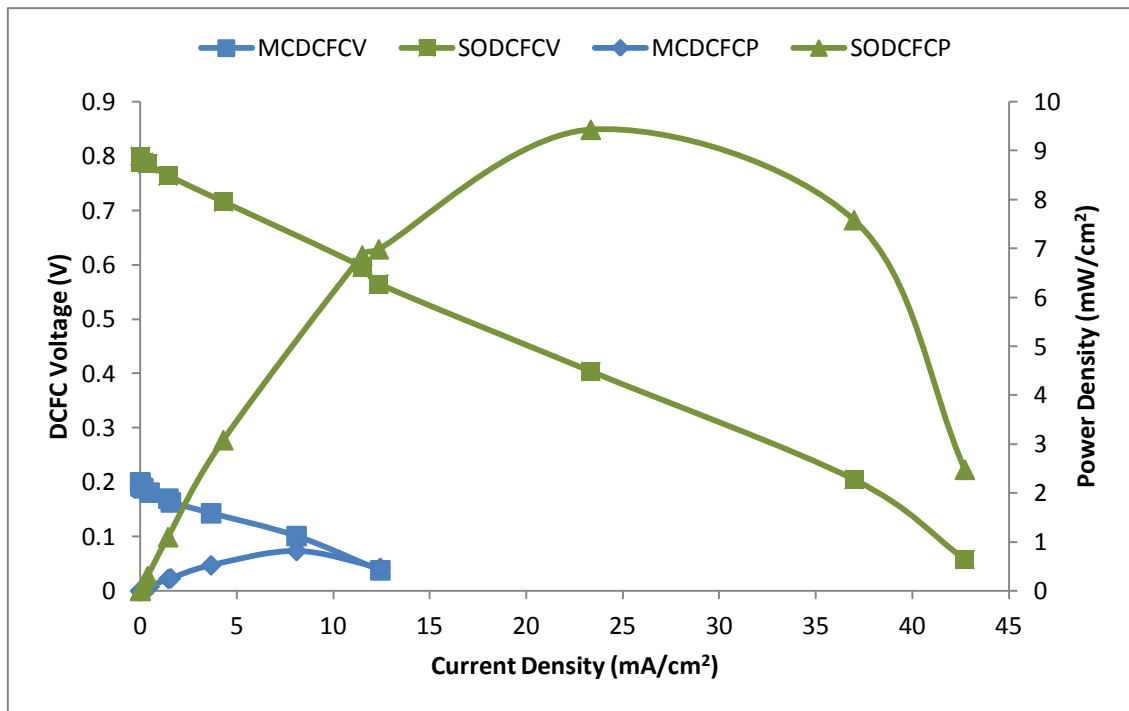


Figure 7.34: BM Miscanthus performances for SODCFC and MDCFC at 700°C.

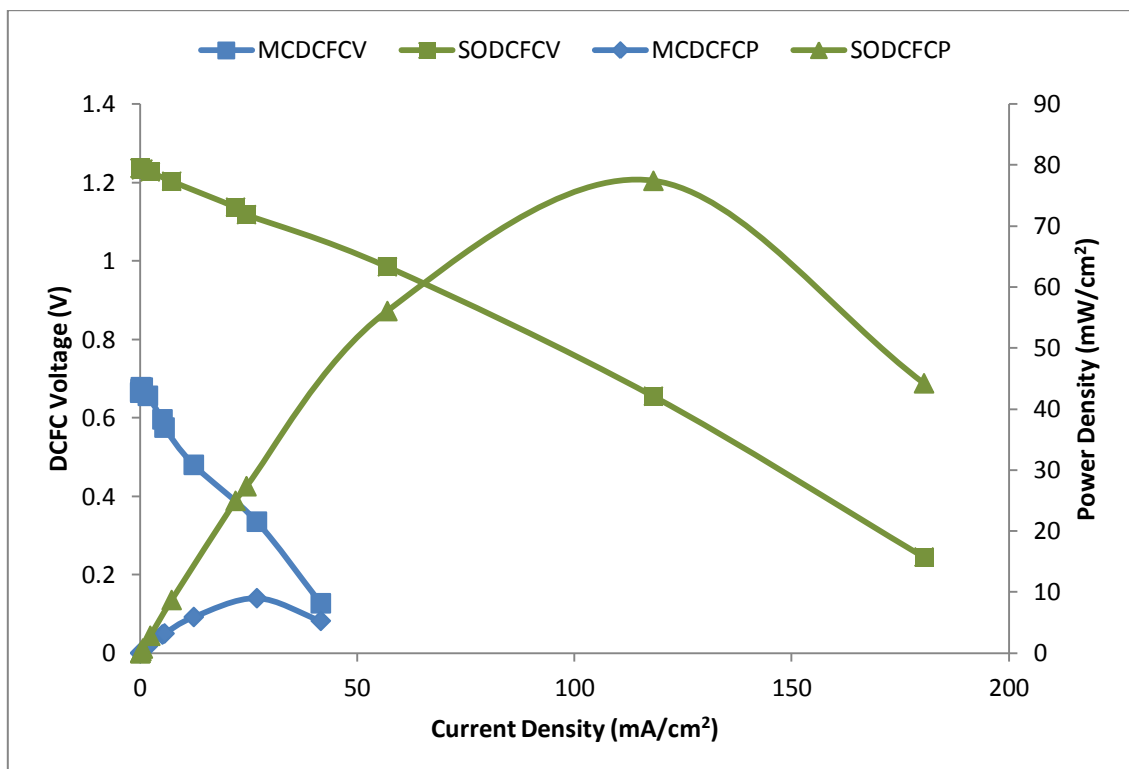


Figure 7.35: BM Miscanthus performances for SODCFC and MDCFC at 800°C.

Figures 7.33 to 7.35 shows enhanced performances with increase in temperature of the fuel cell. The OCV increased from 0.82 V to 1.2 V for the SODCFC as compared with 0.3 V to 0.7 V for the MCDCFC (600°C to 800°C). The peak power at 800°C was 80 mW/cm² (SODCFC) and 5 mW/cm² (MCDCFC) with a corresponding current of 180 mA/cm² and 46 mA/cm². Button cells of SOFC have been reported to have higher conductivity because of the composite electrolyte they are made-up of, they have faster kinetics, better electrodes activity and higher efficiency. This could explain the higher performances we have recorded for the SODCFC (Li *et al.*, 2011a,b; Jia *et al.*, 2010; Liu *et al.*, 2010; Zhu, 2003).

7.6.2 Switchgrass Carbon Fuel

The comparison between the SODCFC and MCDCFC performances using switchgrass fuel at 600°C, 700°C and 800°C are shown in Figures 7.36 to 7.38. The figures show that again the SODCFC switchgrass carbon fuel had better performance than the MCDCFC one.

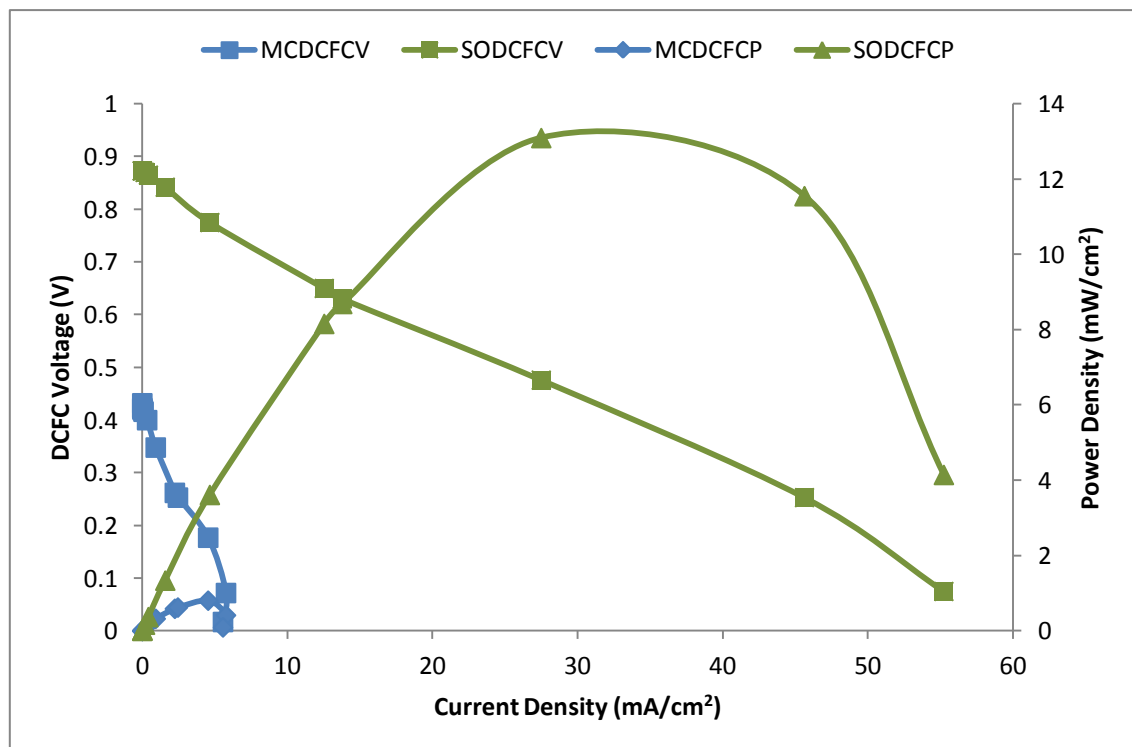


Figure 7.36: BM Switchgrass performances for SODCFC and MCDCFC at 600°C.

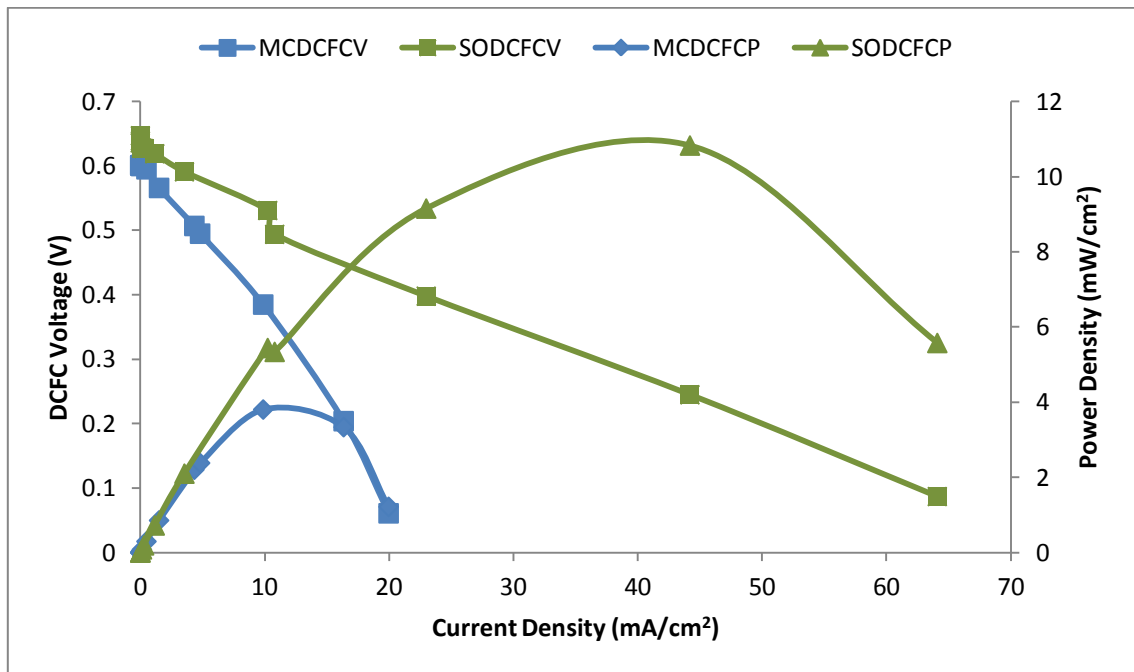


Figure 7.37: BM Switchgrass performances for SODCFC and MDCFC at 700°C.

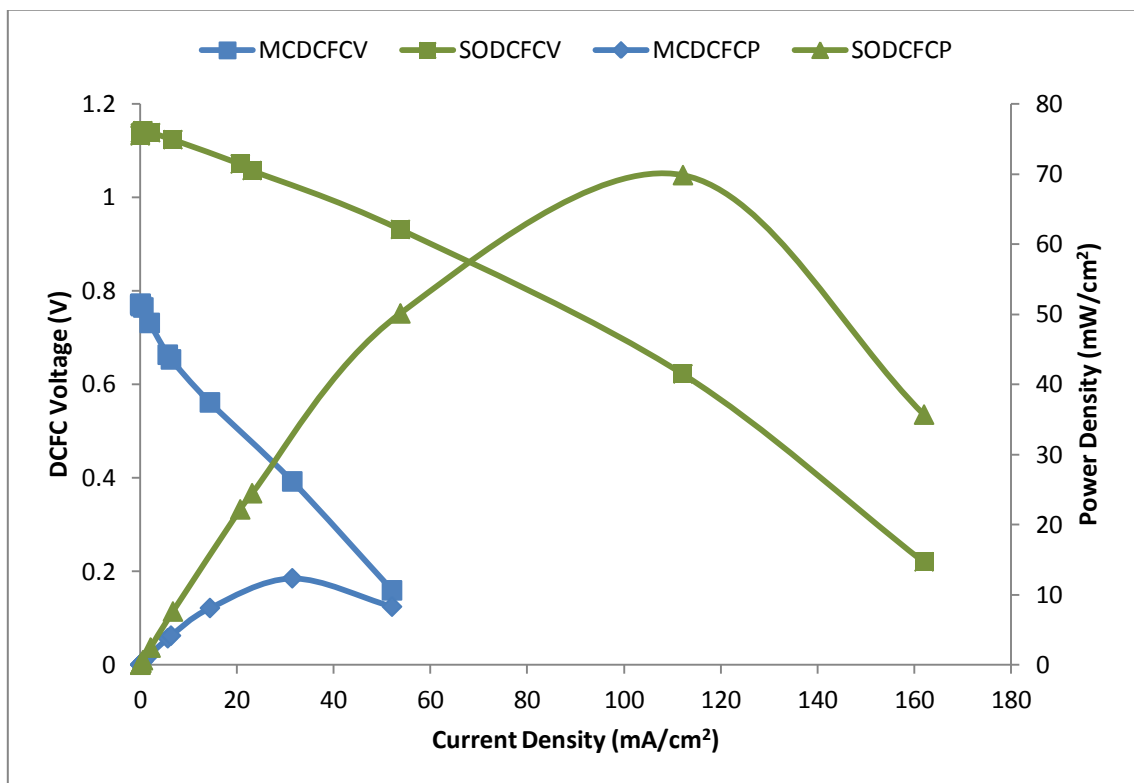


Figure 7.38: BM Switchgrass performances for SODCFC and MDCFC at 800°C.

From Figures 7.36 to 7.38, the OCV at 600°C were 0.88 V and 0.45 V which changed at 700°C to 0.65 and 0.60 V and finally at 800°C changed to 1.1 V and 0.8 V for SODCFC and MCDCFC respectively. Also the peak power generated at 600°C was 12 and 1 mW/cm², and increased at 800°C to 70 mW/cm² and 10 mW/cm² for SODCFC and MCDCFC respectively. The current density increased from 55 mA/cm² to 160 mA/cm² for the SODCFC while for the MCDCFC there was an increment from 5 mA/cm² to 50 mA/cm². The comparison graphs for the other four biomasses are shown in Figures C21 to C30 (Appendix C).

7.7 Energy Strategy of Electricity Generation from Biomass

Considering two major routes of electricity generation from biomass. Route 1 is the burning of biomass in a power plant to generate electricity from steam cycle with a conversion efficiency of 35%. Route 2 is the DCFC integrated route in which pyrolysis gas and liquid are used to power gas turbine cycle (having 50% conversion efficiency) to generate electricity and the biomass char is used in the direct carbon fuel cell to further generate electricity with a known conversion efficiency of 80% (Desclaux *et al.*, 2010; Cao *et al.*, 2007). Figure 7.39 illustrates the two possible routes and the evaluations are given in Tables 7.3 and 7.4.

Assuming that 1.0 kg of miscanthus biomass carbon has a heating value of 18.5 MJ (Ioannidou *et al.*, 2011; Kim *et al.*, 2011; Neves *et al.*, 2011; Kwapinski *et al.*, 2010; He *et al.*, 2009; Garcia-Perez *et al.*, 2007; McKendry 2002; Klass, 1998; Raveendran *et al.*, 1996, 1995). The first route gives the option of burning in power plant with a conversion of 35% giving 6.5 MJ of electricity produced from the system. For the second route, it is estimated that 23 wt.% of char is generated and subjected to electrochemical conversion of 80% giving 5.4 MJ of electricity (Adeniyi and Ewan, 2011; Desclaux *et al.*, 2010; Cao *et al.*, 2007; Cherepy *et al.*, 2005; Cooper, 2004; Zecevic *et al.*, 2004). The pyrolysis gas and liquid could be use to power gas turbines with 50% conversion yielding a further 7.4 MJ of electricity. The total electricity

production from the second route is 12.8 MJ which is far higher than the first route. Tables 7.3 and 7.4 give the breakdown of the energy evaluation.

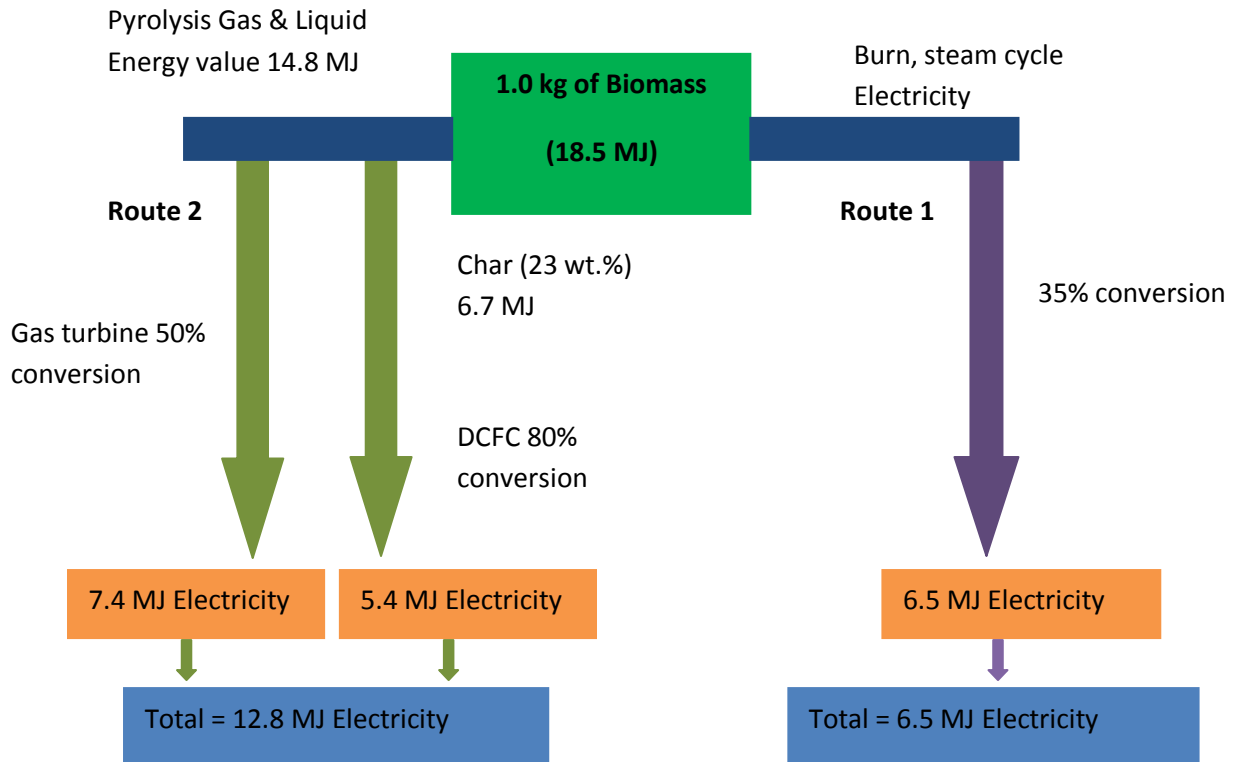


Figure 7.39: Routes of electricity generation from biomass

Table 7.3: Mass and percentage of biomass fractions

Biomass	Carbon (kg)	Liquid (kg)	Gas (kg)	Carbon (wt.%)	Liquid (wt.%)	Gas (wt.%)
Miscanthus	0.226	0.228	0.546	22.59	22.84	54.58
Switchgrass	0.262	0.157	0.581	26.20	15.65	58.15
Wheat	0.287	0.128	0.585	28.71	12.78	58.51
Willow	0.247	0.234	0.519	24.69	23.77	51.54
Spruce	0.223	0.276	0.501	22.27	27.64	50.09
Poplar	0.201	0.216	0.583	20.12	21.59	58.29

Table 7.4: Heating values of biomass fractions

Biomass	Carbon (MJ)	Liquid (MJ)	Gas (MJ)	HV1 (MJ)	HV2 (MJ)	HV3 (MJ)
Miscanthus	5.453	5.686	9.069	14.755	7.378	12.778
Switchgrass	6.322	3.916	9.650	13.566	6.783	12.183
Wheat	6.925	3.192	9.717	12.909	6.455	11.855
Willow	5.960	5.836	8.621	14.457	7.229	12.629
Spruce	5.381	6.883	8.322	15.205	7.603	13.003
Poplar	4.850	5.387	9.684	15.071	7.536	12.936

HV1- Gas plus liquid heating value, HV2- Gas and liquid heating value at 50% conversion, HV3- Total energy for Route 2.

7.8 Summary

Table 7.5 summarises the SODCFC (called SO) and MDCFC (called MC) electrochemical performances for the ball milled (BM) biomass carbon fuels at 800°C. The performances of the SODCFC biomass fuels were higher than those experienced with the MDCFC. In most of the ball milled fuels electrochemical cases, miscanthus fuels performs best in the SODCFC while willow in the MDCFC. In terms of the open circuit voltage, miscanthus fuel (1.24 V) had the best value for SODCFC while willow fuel (0.83 V) for MDCFC. The best peak power density was recorded for miscanthus fuel (77.41 mW/cm²) in the SODCFC and willow fuel (18.48 mW/cm²) in the MDCFC. Miscanthus fuel (180.52 mA/cm²) gave the maximum current density for the SODCFC while spruce fuel (73.02 mA/cm²) for the MDCFC. For the current density at 80% voltage efficiency miscanthus fuel (100 mA/cm²) was superior for the SODCFC and willow fuel (6.67 mA/cm²) for MDCFC. Miscanthus fuel (0.66 V) shows the highest voltage at peak power for the SODCFC and willow fuel (0.48 V) for the MDCFC. The peak power efficiency evaluated show that switchgrass fuel (55%) gave the highest value for the SODCFC and spruce carbon fuel (64%) for the MDCFC.

Table 7.5: SODCFC and MDCFC electrochemical performance at 800°C (BM)

DCFC Parameter	DCFC	Miscanthus	Switchgrass	Wheat	Willow	spruce	Poplar
Open circuit voltage (V)	SO	1.24	1.13	1.18	1.14	1.16	0.78
	MC	0.67	0.77	0.68	0.83	0.72	0.59
Peak power density (mW/cm ²)	SO	77.41	69.81	66.92	58.42	57.40	25.24
	MC	9.00	12.32	11.76	18.48	17.19	10.22
Maximum current density (mA/cm ²)	SO	180.52	162.10	138.52	114.94	156.20	103.15
	MC	41.58	52.06	42.57	63.85	73.02	36.67
Current density at 0.8 V (mA/cm ²)	SO	100.00	85.00	90.00	80.00	60.00	0
	MC	0	0	0	6.77	0	0
Voltage at peak power (V)	SO	0.66	0.62	0.61	0.57	0.56	0.37
	MC	0.34	0.39	0.38	0.48	0.46	0.36
Efficiency at peak power (%)	SO	53.00	55.00	52.00	50.00	48.00	47.00
	MC	51.00	51.00	56.00	58.00	64.00	61.00

SO-SODCFC, MC-MDCFC

Chapter Eight

Conclusions and Recommendations

10.1 Conclusions

The aim of this research is to investigate the use of biomass carbon fuels in a direct carbon fuel cell (DCFC) while taking advantage of the higher efficiencies available for electricity production. This Ph.D research was conducted through thorough review of literatures, theory and experimental techniques. Based on these major experimental areas were identified in the thermochemical treatment of biomass and the application of the biomass carbon fuels in a single cell direct carbon fuel cell using molten carbonate and solid oxide electrolyte systems. The significant outcomes from this research are:

- ❖ Material characterisation of the six biomasses investigated showed that they consist of different compositions. Proximate analysis reveals that there were moisture, ash, volatiles and fixed carbon. The ultimate analysis reveals that there were carbon and hydrogen. The results obtained were within recorded values from literatures (Montross and Crofcheck, 2010; Nowakowski *et al.*, 2007; Mckendry, 2002; Klass, 1998; Raveendran *et al.*, 1995, 1996).
- ❖ Major pyrolysis parameters and method of analysing the biomass carbon quality were identified through experimental runs and literature reviews. Notable are the temperature and the heating rate. Optimum operating parameters used were: temperature of 800°C, heating rate of 7°C/min, while using nitrogen gas flow rate of 4000 cm³/min for purging.
- ❖ Pyrolysis reaction greatly enhanced the properties of the biomass carbon produced. Results obtained reveals that there were increases in the carbon (80 wt.%) and calorific values (30 MJ/kg) and reductions in the moisture contents (4 wt.%) and the hydrogen (1.2 wt.%) compositions.
- ❖ The CV results from these biomasses were compared to those in literatures and found to be commensurate for these biomasses and comparable with coal. Among the woody materials spruce carbon gave the highest CV of 32.53 MJ/kg, while among the grass materials miscanthus has the highest of 29.11 MJ/kg. The least value was obtained from wheat (23.36 MJ/kg).
- ❖ The results obtained from the XRD analyses reveals that the carbon produced from these biomasses were amorphous in nature. The SEM on the other hand

reveals that the shape and sizes of the biomass carbon fuels produced were of different sizes and shapes. Results from the hand milled carbon fuels reveal that we have particle size range of 29.23 μm to 48.07 μm while for the ball milled we have 2.22 μm to 8.13 μm . The specific surface areas obtained from the hand mill carbon fuels were smaller than those of the ball milled carbon fuels.

- ❖ The Performances of the hand milled biomass carbon fuels were tested in a single cell MCDCFC using different electrochemical cell arrangement and industrial carbon black fuel. In each of these cases the performances of the biomass fuels were superior to those obtained from the industrial carbon black. Using porous nickel-zirconia-gold mesh electrode assembly and carbon black fuel we obtained an OCV of 0.73 V, maximum current density of 44 mA/cm^2 , peak power density of 8 mW/cm^2 at 700°C. While using willow carbon fuel with the same cell arrangements and temperature we obtained a maximum OCV of 1.10 V, maximum current density of 70 mA/cm^2 , peak power density 17 mW/cm^2 . This corresponds to 112.5% increment in terms of power density.
- ❖ Because of the possibilities of the porous nickel oxidising during the electrochemical reactions at the high operating temperatures of the MCDCFC a more stable electrochemical cell arrangement of gold mesh-zirconia-gold mesh was explored. At 800°C the performances of the hand milled biomass fuels were higher than those experienced with the ball milled with the exception of willow fuel. In terms of the open circuit voltage, poplar fuel (1.08 V) had the best for the HM and willow fuel (0.83 V) for the BM. The best peak power density was recorded for spruce fuel (26.79 mW/cm^2) for the HM and willow fuel (18.48 mW/cm^2) for the BM. Poplar fuel (81.53 mA/cm^2) gave the maximum current density for the HM while spruce fuel (73.02 mA/cm^2) for the BM. For the current density at 80% voltage efficiency, poplar fuel (19.80 mA/cm^2) was superior for the HM and willow fuel (6.67 mA/cm^2) for the BM. Miscanthus fuel (0.72 V) show the highest voltage at peak power for the HM and willow fuel (0.48 V) for the BM. The peak power efficiency evaluated show that wheat fuel (71%) gave the highest value for the hand milled and spruce carbon fuel (64%) for the ball milled.

- ❖ The Performances of the BM and HM biomass carbon fuels were also investigated in a single cell SODCFC using gold mesh-Ni anode-ScSZ-LSM cathode-gold mesh electrochemical cell arrangement. The electrochemical reactions of the SODCFC were better than the MCDCFC with ion conduction starting above 200°C when compared to 500°C of MCDCFC. Using ball milled willow carbon fuel in MCDCFC at 800°C we obtained an OCV of 0.83 V, maximum current density of 64 mA/cm², and peak power density 18 mW/cm². While using ball milled willow carbon fuel in SODCFC at 800°C we obtained an OCV of 1.14 V, maximum current density of 115 mA/cm², and peak power density 58 mW/cm². This corresponds to 222.2% increment in terms of power density.
- ❖ In the SODCFC at 800°C the performances of the ball milled biomass fuels were higher than those experienced with the hand milled with the exception of willow fuel. In terms of the open circuit voltage, miscanthus fuel (1.26 V) had the best for the HM and miscanthus fuel (1.24 V) for the BM. The best peak power density was recorded for spruce fuel (64.10 mW/cm²) for the HM and miscanthus fuel (77.41 mW/cm²) for the BM. Miscanthus fuel (162.10 mA/cm²) gave the maximum current density for the HM while miscanthus fuel (180.52 mA/cm²) for the BM. For the current density at 80% voltage efficiency spruce fuel (90 mA/cm²) was superior for the HM and miscanthus fuel (100 mA/cm²) for the BM. Poplar fuel (0.69 V) show the highest voltage at peak power for the HM and miscanthus fuel (0.66 V) for the BM. The peak power efficiency evaluated show that poplar fuel (56%) gave the highest value for the hand milled and switchgrass carbon fuel (55%) for the ball milled.
- ❖ The performances of the SODCFC biomass fuels were generally higher than those experienced with the MCDCFC. In most of the ball milled fuels electrochemical cases, miscanthus fuels performs best in the SODCFC while willow in the MCDCFC. In terms of the open circuit voltage, miscanthus fuel (1.24 V) had the best value for SODCFC while willow fuel (0.83 V) for MCDCFC. The best peak power density was recorded for miscanthus fuel (77.41 mW/cm²) in the SODCFC and willow fuel (18.48 mW/cm²) in the MCDCFC. Miscanthus fuel (180.52 mA/cm²) gave the maximum current density for the

SODCFC while spruce fuel (73.02 mA/cm^2) for the MCDCFC. For the current density at 80% voltage efficiency, miscanthus fuel (100 mA/cm^2) was superior for the SODCFC and willow fuel (6.67 mA/cm^2) for MCDCFC. Miscanthus fuel (0.66 V) shows the highest voltage at peak power for the SODCFC and willow fuel (0.48 V) for the MCDCFC. The peak power efficiency evaluated show that switchgrass fuel (55%) gave the highest value for the SODCFC and spruce carbon fuel (58%) for the MCDCFC.

- ❖ There were dramatic improvements in the performances of the SODCFC biomass fuels than the MCDCFC biomass fuels. These were observed from the large differences in the peak power density and the fuel cell current density at 80% voltage efficiency. For ball milled miscanthus carbon fuel operation at 800°C the peak power densities were 77.41 mW/cm^2 (SODCFC) and 9.00 mW/cm^2 (MCDCFC). The current densities at 80% voltage efficiency were 100 mA/cm^2 (SODCFC) and 0 mA/cm^2 (MCDCFC) for miscanthus fuel. Also for BM spruce carbon fuel operated at 800°C the peak power densities were 57.40 mW/cm^2 (SODCFC) and 17.19 mW/cm^2 (MCDCFC). The current densities for spruce BM at 80% voltage efficiency were 60 mA/cm^2 (SODCFC) and 0 mA/cm^2 (MCDCFC).
- ❖ The overall energy strategy considering two major routes of electricity generation from biomass were investigated. The first route is the burning of biomass in a power plant to generate 6.5 MJ of electricity and the second is the DCFC integrated route using biomass to generate 12.8 MJ of electricity. The DCFC integrated route show superior output of energy generation with an overall conversion efficiency of 70% as compared with the 35% of the first route.

10.2 Recommendations for Future Work

Based on the limitations of this research, the discussion of results and our conclusions, the following recommendations for future work within this field are given:

- ❖ The performance studies on a wider range of biomass materials would be advantageous using both the MDCFC and SDCFC. Another area worth investigation is the use of bio-briquette, that is, the mixture of biomass carbon with coal in the MDCFC and SDCFC which could be highly beneficial at industrial level helping to reduce carbon emission from power plants. The performances of various carbonaceous fuels such as the refused derived fuel (RDF) and municipal solid waste (MSW) in the MDCFC and SDCFC would be of great industrial benefits.
- ❖ The recording of the results from the various test on the DCFC were carried out manually, which is subject to some human errors. Automation of data recording through LabView or other methods is recommended as this could greatly reduced error associated with manual collections of data.
- ❖ The degradation studies of the electrochemical cell system of the DCFC would be advantageous as this could give better insight into what is causing the fluctuations of the data obtained from the different operations and the best way to solve them, so that maximum efficiency could be maintained throughout the DCFC operations. Investigation into the build-up of ash and other impurities on the electrolyte would give good information on the performance of the DCFC with different biomass fuel.
- ❖ The biomass carbon particle sizes investigated in this research were within micro-particle range it would be interesting to investigate how the biomass carbon fuels within the nano-particle range performs in the DCFC. The electrochemical reactions of carbon in DCFC are known to be enhanced by the degree of disorderliness of the carbon structures subjected to mechanical treatments, investigation within the nano-particle range might reveal some interesting phenomena in the DCFC.
- ❖ The performance studies of the DCFC operations were recorded for a few hours (10 hours) it would be interesting to investigate the DCFC performances at

different temperature for longer period of operation while studying the performances and degradation rates.

- ❖ Using porous nickel as the anode side of the MDCFC anode compartment show some promising results. More investigation with porous nickel at the anode compartment with different biomass and other fuels would be beneficiary.
- ❖ Large-scale electrochemical reaction of the direct carbon fuel cell would be advantageous. Scaling up of the DCFC would allow large varieties of carbonaceous materials (biomass, coal, bio-briquette, RDF, MSW, etc.) to be electrochemically converted using the higher efficiencies available through the DCFC and contributing to electricity generated to the national grid and heating for domestic and industries. The information gained from such tests would benefits the industrial usage of these materials as fuel sources.
- ❖ This research shows that biomass and other carbonaceous fuels could be used for combine heat and power (CHP) generation from the DCFC at higher efficiency. Detailed economic studies of the process, equipment, tax incentives and logistics are recommended for industrial purposes.

References

Adeniyi O.D. (2008) "Molten carbonate fuel cell (MCFC) and the use of biomass", Research Training Programme assignment for CPE 6002, Department of Chemical and Process Engineering, The University of Sheffield, Sheffield, Autumn Semester.

Adeniyi O.D. and Ewan B.C.R. (2011) "Performance study on the use of biomass carbon in a direct carbon fuel cell", *Proceedings of the Bioten Conference, SUPERGEN Bioenergy (Birmingham, U.K.)*, CPL Press, pp. 407-419, 21-23th September 2010.

Alder Wright C. R. and Thompson C. (1889) "Note on the Development of Voltaic Electricity by Atmospheric Oxidation of Combustible Gases and Other Substances", *Proceedings of the Royal Society of London*, **46**, 372-376.

Andujar J.M. and Segura F. (2009) "Fuel cells: History and updating. A walk along two centuries", *Renewable and Sustainable Energy Review*, **13**, 2309-2322.

Antal Jr. M.J. and Nihous G.C. (2008) "Thermodynamics of an aqueous-alkaline/carbonate carbon fuel cell", *Industrial and Engineering Chemistry Research*, **47**, 2442-2448.

Babu B.V. (2007) "Chemical kinetics and dynamics of plasma assisted pyrolysis of assorted, non nuclear waste", *Proceedings of one-day discussion meeting on 'New Research directions in the use of power beams for environmental application (RPDM-PBEA-2007)'*, Laser & Plasma Technology Division, Bhabha Atomic Research Centre (BARC), Mumbai, September 18.

Babu B.V. (2008) "Biomass pyrolysis: A State-of-the-art Review", Society of Chemical Industry and John Wiley & Sons, Ltd., *Biofuels, Bioproducts & Biorefining*, **2**:393-414.

Bacon F.T. (1954) "Research into the properties of hydrogen-oxygen fuel Cell", *BEAMA Journal*, **61**, 6-12.

Bacon F.T. (1969) "Fuel Cells: past, present and future", *Electrochimica Acta*, **14**, 569-585.

Bacon F.T. (1979) "The Fuel Cell: Some thoughts and recollections", *Journal of Electrochemical Society*, **126**,7C-17C.

Balachov I.I., Dubois L.H., Hornbostel M.D. and Lipilin A.S. (2005) "Direct coal fuel cells: Clean electricity from coal and carbon based fuels", Presented in Fuel Cell Seminar, Direct Carbon Fuel Cell Workshop, Palm Springs, CA, USA, 14th November, 2005, Proceedings online, Retrieved on 8th January 2009, http://www.fuelcellseminar.com/pdf/Direct_Carbon_Fuel_Cell_Workshop/Balachov_louri.pdf

Baur E. and Brunner R. (1937) "Über die Eisenoxyd-Kathode in der Kohle-Luft-Kette", *Zeitschrift für Elektrochemie und Angewandte Physikalische Chemie*, **43**, 94-96.

Baur E. and Ehrenberg H. (1912) "Über neue Brennstoffketten", *Zeitschrift für Elektrochemie*, **18**, 1002-1011.

Baur E. and Preis H. (1937) "Über Brennstoffketten mit Festleitern", *Zeitschrift für Elektrochemie*, **43**, 727-732.

Berkovich A.J. (2003) "Low severity extraction of coal for production of carbon fuel for direct carbon fuel cells", Direct Carbon Fuel Cell Workshop, NETL, Pittsburgh, PA, 30th July.

Boehm H.P. (1996) in: D.Eley, H. Pines, P. Weisz, (ed.), *Advances in Catalysis and Related Subjects*, Vol. 16, p. 179.

Boyle G.C. (2004) "*Renewable energy: Power for a sustainable future*", 2nd ed., Oxford University Press, Oxford.

Boyle G.C., Evereth R. and Ramage J. (eds) (2003) "*Energy systems and sustainability: power for a sustainable future*", Oxford University Press in association with Open University, Oxford.

Broers G.H.J and Ketelaar J.A.A. (1960a) "High-temperature fuel cells", in *Fuel Cells*, Young, G.J., (ed.), Reinhold publishing Corporation, New York, pp. 78-93.

Broers G.H.J and Ketelaar J.A.A. (1960b), "High temperature fuel cells", *Industrial and Engineering Chemistry*, **52**, 303-306.

Bujalski W., Dikwal C.M. and Kendall K. (2007) "Cycling of three solid oxide fuel cell types", *Journal of Power Sources*, **171**, 96-100.

Cao D., Sun Y., Wang G. (2007) "Direct carbon fuel cell: Fundamentals and recent developments", *Journal of Power Sources*, **167**(2), 250-257.

Chan S.H., Low C.F. and Ding O.L. (2002) "Energy and exergy analysis of simple solid-oxide fuel-cell power systems", *Journal of Power Sources*, **103**, 188-200.

Chen G., Yu Q. and Sjöström K. (1997) "Reactivity of char from pyrolysis of birch wood", *Journal of Analytical and Applied Pyrolysis*, **40-41**, 491-499.

Cherepy N.J., Krueger R., Fiet K.J., Jankowski A.F. and Cooper J.F. (2005) "Direct conversion of carbon fuels in a molten carbonate fuel cell", *Journal of the Electrochemical Society*, **152**(1) A80-A87.

Chuang S.S.C. (2005) "Catalysis of coal-based fuel cells", Presented in Fuel Cell Seminar, Direct Carbon Fuel Cell Workshop, Palm Springs, CA, USA, 14th November, 2005, Proceedings online, Retrieved on 8th January 2009, http://www.fuelcellseminar.com/pdf/Direct_Carbon_Fuel_Cell_Workshop/Chuang_Steve.pdf

- Coggins C. (2009) "Towards and energy from waste hierarchy: Including waste as an energy resource", Seminar Presentation, Department of Chemical and Process Engineering, Sir Robert Hadfield Building, The University of Sheffield, Mappin Street, Sheffield, United Kingdom, 13th March.
- Cohen J.M. (1956) "*The Life of Ludwig Mond*", Methuen, London, pp. 280-282.
- Cohen R. (1966) "Gemini Fuel Cell System", *Proceedings of the 20th Annual Power Sources Conference*, New Jersey, 24-26 May, pp. 21-24.
- Cooper J.F. (2003a) "Design, efficiency and materials for carbon/air fuel cell", Presented at the Direct Carbon fuel Cell Workshop, NETL, Pittsburgh, PA, July 30th. (US DOE Ref. UCRL-PRES-154748).
- Cooper J.F. (2003b) "Reaction of the carbon anode in the molten carbonate electrolyte", Presented at the Direct Carbon fuel Cell Workshop, NETL, Pittsburgh, PA, July 30th. (US DOE Ref. UCRL-PRES-154747).
- Cooper J.F. (2004) "Direct conversion of coal in fuel cells, keynote address", Second International Conference on Fuel Cell Science, Engineering and Technology, ASME, Rochester, NY, pp. 14-16.
- Cooper J.F. and Berner K. (2005) "The carbon/air fuel cell, conversion of coal-derived carbons", The Carbon fuel Cell Seminar, Palm Spring, CA, November 14th, UCRL-PRES-216953, pp. 1-16.
- Cooper J.F. and Cherepy N. (2008) "Carbon fuel particles used in direct carbon conversion fuel cells", US Patent Pub. No. US 2008/0274382 A1.
- Cooper J.F., Krueger R., and Cherepy N. (2004) "Fuel cell apparatus and method thereof", US Patent No. US 6815105 B2.
- Cullity B.D. and Stock S.R. (2001) "Elements of X-ray diffraction", 3rd Edition, Prentice Hall Inc., New Jersey, pp.4-19.
- Dasgupta K. and Sathiyamoorthy D. (2003) "Disordered carbon- its preparation, structure and characterisation", *Materials Science and Technology*, **19**, 995-1002.
- Demirbas A. (2001) "Bioresources facilities and biomass conversion processing for fuels and chemicals", *Energy Conversion and Management*, **42**, 1357-1378.
- Desclaux P., Nürnberger S., and Stimming U. (2010) "Direct carbon fuel cells", in R. Steinberger-Wilckens, W. Lehnert (eds.) *Innovations in Fuel Cell Technologies*, RSC Energy and Environment Series No. 2, Royal Society of Chemistry, Cambridge, pp. 190-210.

- Di Blasi C., Signorelli G., Di Russo C. and Rea G. (1999) "Product distribution from pyrolysis of wood and agricultural residues", *Industrial and Engineering Chemistry Research*, **38**, 2216-2224.
- Dicks A.L (1996) "Hydrogen generation from natural gas for the fuel cell systems of tomorrow", *Journal of Power Sources*, **61**, 113-124.
- Dicks A.L. (2006) "The role of carbon in fuel cells", *Journal of Power Sources*, **156**, 128-141
- Dikwal C.M., Bujalski W., and Kendall K. (2008) "Characterization of the electrochemical performance of micro-tubular SOFC in partial reduction and oxidation conditions", *Journal of Power Sources*, **181**, 267-273.
- DIN 53582, German standard method for the iodine adsorption number.
- Drummond A.F. and Drummond I.W. (1996) "Pyrolysis of sugarcane bagasse in a wire-mesh reactor", *Industrial and Engineering Chemistry Research*, **35**, 1263-1268.
- Dunn S. (2001) "Routes to a Hydrogen Economy", *Renewable Energy World*, **4**, 18.
- Duskin A. and Gur T.M. (2005) "Direct coal fuel cell", Presented in Fuel Cell Seminar, Direct Carbon Fuel Cell Workshop, Palm Springs, CA, USA, 14th November, 2005, Proceedings online, Retrieved on 8th January 2009, http://www.fuelcellseminar.com/pdf/Direct_Carbon_Fuel_Cell_Workshop/duskin_alvin.pdf
- EG&G Services (2000) "Fuel cell Handbook", 5th ed., Parsons inc., Science application International Corporation, U.S. Department of Energy, office of Fossil Energy, National Energy Technology Laboratory, Morgantown, WV.
- Elliot S.R (1990) "Physics of amorphous materials", 2nd ed., Longman scientific & technical, England.
- Encinar J.M., Beltran F.J., Ramiro A., and Gonzalez J.F. (1998) "Pyrolysis/gasification of agricultural residues by carbon dioxide in presence of different additives: Influence of variables", *Fuel Processing Technology*, **55**, 219-233.
- Epstein E., Kostrin H., and Alpert J. (1978) In Energy from biomass and waste, D.L. Klass and W.W. Waterman (eds.), p.769, Institute of Gas Technology, Chicago.
- Frank W.B. and Haupin W.E. (1985) Ullmann's Encyclopaedia of Industrial Chemistry, Vol. A1, fifth ed., VCH, Deerfield Beach, FL, USA.
- Franklin R.E. and Watt J. D. (1957) "Changes in the structure of carbon during oxidation", *Nature*, **180**, 1190-1191

- Franklin R.E. (1950) "On the structure of carbon", *Journal De Chimie Physique Et De Physico-Chimie Biologique*, **47**(5-6), 573-575
- Franklin R.E. (1951) *Acta Cryst.*, **4**, 423.
- Franklin R.E. (1957) *Proceedings of the Royal Society.*, London, A, **209**, 196
- Freni S. and Maggio G. (1997) "Energy balance of different internal reforming MCFC configurations", *International Journal of Energy Research*, **21**, 253-264.
- Fukunaga T., Nagano K., Mizuntani U., Wakayama H. and Fukushima Y. (1998) "Structural change of graphite subjected to mechanical milling", *Journal of Non-Crystalline Solids*, **232-234**, 416-420.
- Garcia-Perez M., Adams T.T., Goodrum J.W., Geller D.P. and Das K.C. (2007) "Production and fuel properties of pine chip bio-oil/biodiesel blends", *Energy and Fuels*, 2363-2372.
- Goret J. and Tremillon B. (1966) *Bull. Soc. Chim. France*, **67**, 2827.
- Goret J. and Tremillon B. (1967) *Electrochim. Acta*, **12**, 1065.
- Goyal H.B., Diptendu S. and Saxena R.C. (2008) "Bio-fuels from thermochemical conversion of renewable resources: A review", *Renewable & Sustainable Energy Reviews*, **12**, 504-517.
- Grove W.R. (1839) "On voltaic Series and the Combination of Gases by Platinum", *Philosophical magazine and Journal of Science*, Series 3, **14**, 127-130.
- Grove W.R. (1842) "On a Gaseous Voltaic Battery", *London and Edinburgh philosophical Magazine and Journal of Science*, Series 3, **21**, 417-420.
- Grove W.R. (1843) "Experiments of the Voltaic Battery, with a view of ascertaining the rational of its action and on its applications to eudiometry", *Proceedings of the Royal Society of London*, **4**, 463-465.
- Grove W.R. (1845) "On a Gas Voltaic Battery: Voltaic action of Phosphorus, sulphur and hydrocarbons", *Proceedings of the Royal Society of London*, **5**, 557-558.
- Grubb W.T. and Niedrach L.W. (1960) "Batteries with solid ion-exchange membrane electrolyte II: Low temperature hydrogen oxygen fuel cells", *Journal of the Electrochemical Society*, **107**, 131-135.
- Guddeti R.R., Knight R. and Grossmann E.D. (2000) "Depolymerization of Polyethylene using induction-coupled plasma technology", *Plasma Chem Plasma P*, **20**, 37-64.

- Haber F. and Bruner (1904) "Das Kollenelement, eine Knallgaskette", *Zeitschrift für Elektrochemie*, **10**, 697-713.
- Hackett G.A., Zondlo J.W. and Svensson R. (2007) "Evaluation of carbon materials for use in a direct carbon fuel cell", *Journal of Power Sources*, **168**, 111-118.
- Hardwick F. (2009) "Waste, energy and the future", Seminar presentation, Department of Chemical and Processing Engineering, Sir Robert Hadfield Building, The University of Sheffield, Mappin Street, Sheffield, United Kingdom, 27th February.
- Haupin W.E. and Frank W.B. (1981) "Comprehensive Treatise of Electrochemistry", *Electrochemical Processings*, in: J.O.M. Bockris, B.E. Conway, E. Yeager, R.E. White (Eds.), Vol. 2, Plenum Press, NY, USA, pp. 301–305.
- Hauser V.E. (1964) "A study of carbon anode polarization in fused carbonate fuel cells", Ph.D. Dissertation, Oregon State University, Corvallis, OR, USA.
- He R., Ye X. P., English B. C. and Satrio J. A. (2009) "Influence of pyrolysis condition on switchgrass bio-oil yield and physicochemical properties", *Bioresource Technology*, **100**, 5305-5311.
- Hemmes K. (2003) "Using the full exergetic quality of solid fuels", Direct Carbon Fuel Cell Workshop, NETL, Pittsburgh, PA, 1st August.
- Hemmes K., Houwing M. and Woudstra N. (2005) *Proceedings of the 3rd International Conference on Fuel Cell Science, Engineering, and Technology*, Ypsilanti, MI, USA, May 23–25, 2005, p. 499.
- Henriksson G., Li J., Zhang L. and Lindström M.E. (2010) "Lignin utilization", in M. Crocker (ed.) *Thermochemical Conversion of Biomass to Liquid Fuels and Chemicals*, RSC Energy and Environment Series No. 1, Royal Society of Chemistry, Cambridge, pp.222-259.
- Heuvel E.J.M.T. van den (1994) "The potential of miscanthus", *Energy for sustainable Development Letters*, **1**(2), 41-44.
- Holliday A.K., Hughes G. and Walker S.M. (1973) "The Chemistry of carbon: organometallic Chemistry", Pergamon Press Ltd., Vol. 6, Oxford, England, pp.1173-1203
- Hoogers G. (2003) "Fuel Cell Technology Handbook", CRC Press LLC, Florida.
- Hoogers G. and Potter L.C. (1999) "Fuel cells: Their potential as the Ultimate source of clean power", *Renewable Energy World*, **2**, 50.
- Huang H. and Tang L. (2007) "Treatment of organic waste using thermal plasma pyrolysis technology", *Energy Conversion and Management*, **48**, 1331-1337.

- Huang H., Tang L. and Wu C.Z. (2003) "Characterization of gaseous and solid product from thermal plasma pyrolysis of waste rubber", *Environmental Science and Technology*, **37**, 4463-4467.
- Hyatt N. (2008) "Principle and practice of powder diffraction", Lecture note on MAT 6051, Department of Engineering Materials, The University of Sheffield, Sheffield, autumn.
- Ihara M., Matsuda K., Sato H., and Yokoyama C. (2004) "Solid state fuel storage and utilization through reversible carbon deposition on a SOFC anode", *Solid State Ionics*, **175**:51-54.
- Ioannidou O., Jung C.G. and Zabaniotou A. (2011) "A thermogravimetric model to predict yield product distribution in pyrolysis of agricultural biomass", *Catalysis Today*, **167**, 129-134.
- Jacques W.W. (1896) "Electricity Direct from Coal", *Harper's New Monthly Magazine*, **94**,144-150.
- Jain S.L., Nabae Y., Lakeman B.J., Pointon K.D. and Irvine J.T.S. (2008) "Solid state electrochemistry of direct carbon/air fuel cell", *Fuel Cells Bulletin*, pp. 10-13.
- Jenkins B.M., Baxter L.L., Miles Jr. T.R. and Miles T.R. (1998) "Combustion properties of biomass", *Fuel Processing Technology*, **54**, 17-46.
- Jenkins R. and Synder R.L. (1996) "*Introduction to X-ray Powder diffractometry*", John Wiley and Son Inc., New York , NY, pp.2-5
- Jia L., Tian Y., Liu Q., Chun X., Yu J., Wang Z., Zhao Y. and Li Y. (2010) "A direct carbon fuel cell with (molten carbonate)/(doped ceria) composite electrolyte", *Journal of Power Sources*, **195**, 5581-5586.
- Kern M. and Sprick W. (2001)"Abschaetzung des potenzials an regenerativen Energietraegern im Restmuell", in *Bio-und Restabfallbehandlung V, Biologisch-Mechanisch-Thermisch*, Wiemer, K. and Kern, M., eds., Witzenhausen, p. 149.
- Kim J., Lee S-M., Srinivasan S., and Chamberlin C.E. (1995) "Modelling of proton exchange membrane fuel cell performance with an empirical equation", *Journal of the Electrochemical Society*, **142**(8), 2670–2674.
- Kim J-P., Lim H., Jeon C-H., Chang Y-J., Koh K-N., Choi S-M. and Song J-H. (2010) "Performance evaluation of tubular fuel cells fuelled by pulverized graphite", *Journal of Power Sources*, **195**, 7568-7573.
- Klass D.L. (1998) "*Biomass for renewable energy, fuels, and chemicals*", San Diego, CA, Academic Press.

- Klass D.L. and Ghosh S. (1977) In *Clean fuels from biomass and wastes*, W.W. Waterman ed., p.323, Institute of Gas Technology, Chicago.
- Koßmehl S.-O. and Heinrich H. (1998) "Assessment of the use of Biofuels in passenger vehicles", in *Sustainable Agricultural for Food, Energy and Industry*, James & James, London, pp. 867-875.
- Köttner M. (2001) "Biogas in agricultural and Industry: potentials, present use and perspectives", *Renewable Energy World*, **4**,132.
- Kunz H.R. (1987) "Transport of Electrolyte in Molten Carbonate Fuel Cells", *Journal of the Electrochemical Society*, **134**, 105
- Kwant K. W. (2001) "Status of biomass gasification", *Renewable Energy World*, **4**,122.
- Kwapinski W., Byrne C.M.P., Kryachko E., Wolfram P., Adley C., Leahy J.J., Novotny E.H. and Hayes M.H.B. (2010) "Biochar from biomass and waste", *Waste Biomass Valor*, **1**, 177-189.
- Lanzetta M. and Di Blasi C. (1998) "Pyrolysis kinetics of wheat and corn straw", *Journal of Analytical and Applied Pyrolysis*, **44**, 181-192
- Larminie J. and Dicks A. (2003) "*Fuel cell systems explained*", 2nd edition, John Wiley & Sons Ltd., England.
- Laurencelle F., Chahine R., Hamelin J., Fournier M., Bose T.K., and Laperriere A. (2001) "Characterization of a Ballard MK5-E proton exchange membrane stack", *Fuel Cells*, **1**(1), 66–71.
- Lauzon J.-C., Preng R., Sutton B., and Pavlovic B. (2007) "Survey of Energy Resources", World Energy Council, London, U.K.
- Lehmann A. -K., Russel A.E. and Hoogers G. (2001) "Renewable fuel cell power from biogas", *Renewable Energy World*, **4**,76.
- Li C., Shi Y, and Cai N. (2011a) "Mechanism for carbon direct electrochemical reactions in a solid oxide electrolyte direct carbon fuel cell", *Journal of Power Sources*, **196**, 754-763.
- Li C., Shi, Y and Cai N. (2011b) "Effect of contact type between anode and carbonaceous fuels on direct carbon fuel cell reaction characteristics", *Journal of Power Sources*, **196**, 4588-4593.
- Li S., Lee A.C., Mitchell R.E., Gur T.M. (2008) "Direct carbon conversion in a helium fluidized bed fuel cell", *Solid State Ionics*, **179**, 1549-1552.

Li X., Zhu Z, Chen J., De Marco R., Dicks A., Bradley J. and Lu G. (2009) "Surface modification of carbon fuels for direct carbon fuel cells", *Journal of Power Sources*, **186**, 1-9.

Liu R., Zhao C., Li J., Zeng F., Wang S., Wen T. and Wen Z. (2010) "A novel direct carbon fuel cell by approach of tubular solid oxide fuel cells", *Journal of Power Sources*, **195**, 480-482.

McKendry P. (2002) "Energy production from biomass (part 1): overview of biomass", *Bioresource Technology*, **83**, 37-46

McPhee W. and Tao T. (2008) "Direct conversion of coal and bio-mass using a liquid tin anode fuel cell", Fuel Cell Seminar, 29th October.

Minkova V., Marinov S.P., Zanzi R., Björnbom E., Budinova T., Stefanova M. and Lakov L. (2000) "Thermochemical treatment of biomass in a flow of steam or in a mixture of steam and carbon dioxide", *Fuel Processing Technology*, **62**,45-52.

Mond L. and Langer C.A. (1889) "A new form of Gas Battery", *Proceedings of the Royal Society of London*, **46**, 296-304.

Montross M. and Crofcheck C. (2010) "Energy crops for the production of biofuels", in M. Crocker (ed.) *Thermochemical Conversion of Biomass to Liquid Fuels and Chemicals*, RSC Energy and Environment Series No. 1, Royal Society of Chemistry, Cambridge, pp.26-42.

Moore J. (2009) "Hydrogen-a central player in tomorrow's energy mix", *Energy World*, Energy Institute, London, February, No. 368, pp. 14-15

Murray J.N. and Grimes P.G. (1963) "Methanol Fuel cell", in *Fuel Cells*, CEP Technical Manual, American Institute of Chemical Engineers (Progress Technical Manual) pp. 57-65.

Nabae Y., Pointon K.D. and Irvine J.T.S. (2008) "Electrochemical oxidation of solid carbon in hybrid DCFC with solid oxide and molten carbonate binary electrolyte", *Energy and Environmental Science*, **1**,148-155.

Nakagawa N., and Ishida M. (1988) "Performance of an internal direct-oxidation fuel cell and its evaluation by graphic exergy analysis", *Industrial and Engineering Chemistry Research*, **27**, 1181-1185.

Nema S. and Ganesh P.K.S. (2002) "Plasma pyrolysis of medical waste", *Current Science*, India, **83**, 271-278.

Neves D., Thunman H., Matos A., Tarelho L. and Gomez-Barea A. (2011) "Characterization and prediction of biomass pyrolysis products", *Progress in Energy and Combustion Science*, **37**, 611-630.

- Nowakowski D.J., Jones J.M., Brydson R.M.D. and Ross A.B. (2007) "Potassium catalysis in the pyrolysis behaviour of short rotation willow coppice", *Fuel*, **86**, 2389-2402.
- Nürnberg S., Bußar R., Desclaux P., Franke B., Rzepka M. and Stimming U. (2010) "Direct carbon conversion in a SOFC-system with a non-porous anode", *Energy and Environmental Science*, **3**, 150-153.
- O'Hayre R.P., Cha S.-W., Colella W. and Prinz F.B. (2006) "*Fuel Cell fundamentals*", John Wiley & Sons Ltd., New York.
- Oberlin A., Bonnany S. And Lafde K. (1998) in *Carbon fibres*, ed. J.B. Donnet et al., 3rd edn., 85-150, New York, NY, Dekker.
- Okada O., Tabata T., Takami S., Hirao K., Masuda M., Futjita H., Iwasa N., and Okhama T. (1992) "Development of an advanced reforming system for fuel cells", International Gas Conference, Orland Florida, USA, Nov. 15-19.
- Onay O, and Kockar O.M. (2004) "Fixed bed pyrolysis of rapeseed (*Brassica napus L.*)", *Biomass Bioenergy*, **26**, 289-299.
- Onay O, Beis S.H. and Kockar O.M. (2001) "Fast pyrolysis of rapeseed in well-swept fixed bed reactor", *Journal of Analytical and Applied Pyrolysis*, **58-59**, 995-1007.
- Ozbay N., Putun A.E., Uzun B.V. and Putun E. (2001) "Biocrude from biomass: pyrolysis of cotton seed cake", *Renewable Energy*, **24**, 615-625.
- Patton E.M. (2003) "SARA's direct carbon fuel cell: history, status and joint industry program", Presented in Direct Carbon Fuel Cell Workshop, NETL, Pittsburg, PA, USA, 30th July, 2003, Proceedings online, Retrieved on 8th January 2009, <http://www.netl.doe.gov/publications/proceedings/03/dcfw/Patton.pdf>
- Petrus L. and Noordermeer M.A. (2006) "Biomass to biofuel, a chemical perspective", *Green Chemistry*, **8**, 861-867.
- Popov V.N and Lambin P. (2006) "Carbon nanotubes: From basic research to nanotechnology", NATO Science Series, Series II, Dordrecht Springer Science & Business Media.
- Putun A.E., Ozcan A., Gercel H.F. and Putun E. (2001) "Production of biocrude from biomass in a fixed bed tubular reactor", *Fuel*, **80**, 1371-1378.
- Raveendran K., Ganesh A. and khilar K.C. (1995) "Influence of mineral matter on biomass pyrolysis characteristics", *Fuel*, **74**(12), 1812-1822.
- Raveendran K., Ganesh A. and khilar K.C. (1996) "Heating value of biomass and biomass pyrolysis products", *Fuel*, **75**(15), 1712-1720.

- Rayleigh L. (1882) "On a new form of Gas Battery", *Proceedings of the Cambridge Philosophical Society*, **4**, 198.
- Razuan R., Chen Q., Zhang X., Sharifi V. and Swithenbank J. (2010) "Pyrolysis and combustion of oil palm stone and palm kernel cake in fixed-bed reactors", *Bioresource Technology*, **101**, 4622-4629.
- Reeves N. (2005) "Basic Instructions for WinX^{POW} ", Manual on STOE Win XPOW 1.10, X-ray Laboratory, Department of Engineering Materials, The University of Sheffield, Sheffield.
- Reich S., Thomsen C., Maultzsch J. (2004) "Carbon nanotubes: Basic concepts and physical properties", Wiley-Vch
- Robertson J. (1986) *Advances in Physics*, **35**, 317
- Ruyter H.P. (1982) *Fuel*, **61**, 1182
- Ryu C., Yang Y.B., Khor A., Yates N.E., Sharifi V.N. and Swithenbank J. (2006) "Effect of fuel properties on biomass combustion: Part I. Experiments-fuel type, equivalence ratio and particle size", *Fuel*, **85**, 1039-1046.
- Saddawi A. (2005) "Carbon Fuels for the Direct Carbon Fuel Cell", Master Thesis, West Virginia University, Morgantown, WV, USA.
- Salver-Disma F., Tarascon J.-M., Clinard C. and Rouzaud J.-N. (1999) "Transmission electron microscopy studies on carbon materials prepared by mechanical milling", *Carbon*, **37**, 1941-1959.
- Schneider J.M. (2005) "AEP's coal fired generation technologies", Presented in Fuel Cell Seminar, Direct Carbon Fuel Cell Workshop, Palm Springs, CA, USA, 11th November, 2005, Proceedings online: http://www.fuelcellseminar.com/pdf/Direct_Carbon_Fuel_Cell_Workshop/Schneider_John.pdf, Retrieved on 8th January 2009.
- Selman R.J. (2003) "Anodic oxidation in molten carbonate, Why molecular mechanism may be less relevant than wetting behaviour", DOE Direct Carbon Fuel Cell Workshop, NETL, Pittsburgh, PA, July 30th.
- Sensöz S. (2003) "Slow pyrolysis of wood barks from *Pinus brutia* Ten. and product composition", *Bioresource Technology*, **89**, 307-311.
- Sensöz S., Angin D., and Yorgun S. (2000) "Influence of particle size on the pyrolysis of rapeseed (*Brassica napus* L.): fuel properties of bio-oil", *Biomass and Bioenergy*, **19**, 271-279.

- Sharifi V.N. (2009) "Thermal waste and biomass treatment technologies (CPE 6060)", Lecture series, Department of Chemical and Process Engineering, Sir Robert Hadfield Building, The University of Sheffield, Mappin Street, Sheffield, spring 2008/2009.
- Sørensen B. (2000) "*Renewable Energy*" (2nd ed.), Academic Press, p.3
- Sørensen B. (2005) "*Hydrogen and fuel cell: emerging technologies and applications*", Elsevier Academic Press, USA.
- Strahan, D. (2009) "Will hydrogen always be the fuel for the future?" *Energy World*, Energy Institute, London, April, no.370, p.17.
- Tamaru S., and Kamada M. (1935) *Z. Elektrochem.*, **41**,93.
- Tao T. (2003) "Direct carbon conversion", Presented in Direct Carbon Fuel Cell Workshop, NETL, Pittsburg, PA, USA, 30th July, 2003, Proceedings online, Retrieved on 8th January 2009, <http://www.netl.doe.gov/publications/proceedings/03/dcfcw/Tao.pdf>
- Tao T. (2005) "Liquid anode fuel cell for direct carbon conversion", Presented in Fuel Cell Seminar, Direct Carbon Fuel Cell Workshop, Palm Springs, CA, USA, 14th November, 2005, Proceedings online, Retrieved on 8th January 2009, <http://www.fuelcellseminar.com/pdf/Direct Carbon Fuel Cell Workshop/Tao Tom.pdf>
- Tarmy B.L. and Ciprios G. (1965) "The Methanol Fuel Cell Battery", *Engineering Development in Energy Conversion*, ASME, pp. 272-283.
- Tewksbury C. (1991) In "*Energy from biomass and waste*", D.L. Klass ed., p.95, Institute of Gas technology, Chicago.
- Tuinstra E. and Koenig K.L. (1970) *Journal of Chemical Physics*, **53**, 1126.
- Twidell J. (1998) "Biomass energy", *Renewable Energy World*, **3**, 38-39.
- Twidell J. and Weir A. (1986) *Renewable Energy Resources*, London, E & FN Spon.
- Vutetakis D.G., Skidmore D.R., and Byker H.J. (1987) "Measured coulombic efficiencies of slurries of carbon particles in molten salt", *Journal of the Electrochemical Society*, **134**, 3027–3035.
- Vutetakis D.J. (1985) "Electrochemical oxidation of carbonaceous materials dispersed in molten salt", Ph.D. Dissertation, Ohio State University, Columbus, OH, USA.
- Warren B.E. (1941) *Physical Review*, **59**,(9), 693
- Warren B.E. and Bodenstein P. (1966) *Acta Crystallographica*, **20**, 602.

Weaver R.D., Leach S.C., and Nanis L. (1981) *Proceedings of the 16th Intersociety Energy Conversion Engineering Conference*, ASME, NY, USA, p. 717.

Weaver R.D., Leach S.C., Bayce A.E. and Nanis L. (1979) "Direct Electrochemical Generation of Electricity from Coal", SRI, Menlo Park, CA, USA (Report SAN-0115/105-1, National Technical Information Service, NTIS).

Weaver R.D., Tietz L., and Cubicciotti D. (1975) "Direct use of Coal in a Fuel Cell: Feasibility Investigation", Report for USAEPA, Office of R&D, EPA-650/2-75-040.

Weston J.A. (1963) "A direct carbon fuel cell", Master Thesis, Department of Fuel Technology and Chemical Engineering, University of Sheffield, March.

William K.R., Andrew M.R., and Jones F. (1965) "Some Aspect of the Design and Operation of Dissolved Methanol Fuel cells", in *Hydrogen Fuel cell Technology*, Baker, B.S., Ed., Academic Press, New York, pp. 143-149.

Wolk R.H., Scott L., Gelber S. and Holcomb F.H. (2007) "Direct carbon fuel cells: Converting waste to electricity", ERDC/CERL fuel cell program, U.S. Army Corps of Engineers, Washington D.C., Final report, Sept.

Wornat, M.J., Hurt, R.H., Yang, N.Y.C. and Headley, T.J. (1995) "Structural and compositional transformations of biomass chars during combustion", *Combustion and Flame*, **100**, 131-143.

Wu Y., Su C., Zhang C., Ran R. and Shao Z. (2009) "A new carbon fuel cell with high power output by integrating with in situ catalytic reverse Boudouard reaction", *Electrochemistry Communications*, **11**, 1265-1268.

Xia J., Noda K., Kagawa S., and Wakao N., (1999) "Production of activated carbon from bagasse (waste) of sugarcane grown in Brazil", *Journal of Chemical Engineering of Japan*, **31**, 987

Yaman S. (2004) "Pyrolysis of biomass to produce fuels and chemical feedstocks", *Energy Conversion and Management*, **45**, 651-671.

Zanzi R, Bai X., Capdevila P. and Björnbom E. (2001) "Pyrolysis of biomass in presence of steam for preparation of activated carbon, liquid and gaseous products", 6th World Congress of Chemical Engineering, Melbourne, Australia, 23-27 September.

Zaror C.A. and Pyle D.L. (1982) *Proceedings Indian Academics of Science (Engineering Science)*, **5(4)**269

Zecevic S., Patton E.M. and Parhami P. (2003) "Electrochemistry of direct carbon fuel cell based on metal hydroxide electrolyte", Presented in Direct Carbon Fuel Cell Workshop, NETL, Pittsburg, PA, USA, 30th July, 2003, Proceedings online, Retrieved on

8th January 2009,
<http://www.netl.doe.gov/publications/proceedings/03/dcfw/Zecevic.pdf>.

Zecevic S., Patton E.M. and Parhami P. (2004a) *Proceedings of the 2nd International Conference on Fuel Cell Science, Engineering and Technology*, Rochester, NY, USA, June 14–16, pp. 387–394.

Zecevic S., Patton E.M. and Parhami P. (2004b) “Carbon-air fuel cell without a reforming process”, *Carbon*, **42**, 1983-1993.

Zecevic S., Patton E.M. and Parhami P. (2005a) “Direct electrochemical power generation from carbon in fuel cells with molten hydroxide electrolyte”, *Chemical Engineering Communications*, **192**, 1655–1670.

Zecevic S., Patton E.M. and Parhami P. (2005b) *Proceedings of the 3rd International Conference on Fuel Cell Science, Engineering, and Technology*, Ypsilanti, MI, USA, May 23–25, pp. 507–514.

Zhou W.L, Ikuhara Y., Zhao W. and Tang J. (1995) “A transmission electron microscopy study of amorphization of graphite by mechanical milling”, *Letters to the editor*, 1177-1180.

Zhu B. (2003) “Functional ceria-salt-composite materials for advanced ITSOFC applications”, *Journal of Power Sources*, **114**, 1-9.

Appendix A

Malvern Biomass Carbon Particle Analysis

Table A1: Miscanthus biomass carbon particle analysis (Hand milled)

ID: 040211misFi		Run No: 16		Measured: 4/2/2011 13:05			
File: KP120810		Rec. No: 109		Analysed: 4/2/2011 13:05			
Path: C:\SIZERS\DATA\VIKRANT\				Source: Analysed			
Range: 300 mm		Beam: 10.00 mm		Sampler: MS64		Obs': 17.0 %	
Presentation: 3TJD		Analysis: Polydisperse		Residual: 0.912 %			
Modifications: None							
Conc. = 0.0044 %Vol		Density = 1.390 g/cm ³		S.S.A.= 0.5356 m ² /g			
Distribution: Volume		D[4, 3] = 32.88 um		D[3, 2] = 8.06 um			
D(v, 0.1) = 3.46 um		D(v, 0.5) = 18.52 um		D(v, 0.9) = 78.04 um			
Span = 4.028E+00		Uniformity = 1.332E+00					
Size (um)	Volume In %	Size (um)	Volume In %	Size (um)	Volume In %	Size (um)	Volume In %
0.494	0.06	3.21	0.97	20.84	2.25	135.3	0.54
0.532	0.06	3.46	1.05	22.46	2.26	145.8	0.48
0.574	0.09	3.73	1.14	24.20	2.27	157.2	0.44
0.618	0.13	4.02	1.22	26.08	2.28	169.4	0.40
0.667	0.15	4.33	1.31	28.11	2.28	182.5	0.36
0.718	0.17	4.66	1.40	30.29	2.28	196.7	0.33
0.774	0.18	5.03	1.49	32.65	2.28	212.0	0.28
0.834	0.20	5.42	1.57	35.18	2.29	228.5	0.24
0.899	0.22	5.84	1.65	37.92	2.27	246.2	0.19
0.969	0.24	6.29	1.72	40.86	2.23	265.4	0.14
1.04	0.26	6.78	1.79	44.04	2.16	286.0	0.05
1.13	0.28	7.31	1.85	47.46	2.08	308.2	0.00
1.21	0.30	7.88	1.91	51.15	1.98	332.1	0.00
1.31	0.32	8.49	1.96	55.12	1.87	358.0	0.00
1.41	0.35	9.15	2.00	59.41	1.75	385.8	0.00
1.52	0.38	9.86	2.04	64.02	1.61	415.7	0.00
1.64	0.42	10.62	2.07	69.00	1.47	448.1	0.00
1.76	0.46	11.45	2.10	74.36	1.33	482.9	0.00
1.90	0.50	12.34	2.12	80.14	1.20	520.4	0.00
2.05	0.55	13.30	2.15	86.36	1.07	560.8	0.00
2.21	0.61	14.33	2.17	93.07	0.95	604.4	0.00
2.38	0.67	15.45	2.19	100.3	0.85	651.4	0.00
2.56	0.74	16.65	2.20	108.1	0.75	702.0	0.00
2.76	0.81	17.94	2.22	116.5	0.67	756.5	0.00
2.98	0.88	19.33	2.23	125.6	0.60	815.3	0.00
3.21		20.84		135.3		878.7	

Table A2: Switchgrass biomass carbon particle analysis (Hand milled)

ID: 040211swiDi		Run No: 10		Measured: 4/2/2011 12:43			
File: KP120810		Rec. No: 103		Analysed: 4/2/2011 12:43			
Path: C:\SIZERS\DATA\VIKRANT\				Source: Analysed			
Range: 300 mm		Beam: 10.00 mm		Sampler: MS64		Obs': 17.5 %	
Presentation: 3TJD		Analysis: Polydisperse		Residual: 0.991 %			
Modifications: None							
Conc. = 0.0082 %Vol		Density = 1.390 g/cm ³		S.S.A.= 0.2977 m ² /g			
Distribution: Volume		D[4, 3] = 101.45 um		D[3, 2] = 14.50 um			
D(v, 0.1) = 5.99 um		D(v, 0.5) = 59.02 um		D(v, 0.9) = 267.16 um			
Span = 4.425E+00		Uniformity = 1.343E+00					
Size (um)	Volume In %	Size (um)	Volume In %	Size (um)	Volume In %	Size (um)	Volume In %
0.494	0.03	3.21	0.48	20.84	1.32	135.3	2.02
0.532	0.03	3.46	0.52	22.46	1.36	145.8	2.02
0.574	0.05	3.73	0.56	24.20	1.41	157.2	2.01
0.618	0.07	4.02	0.60	26.08	1.46	169.4	2.01
0.667	0.08	4.33	0.64	28.11	1.51	182.5	2.00
0.718	0.09	4.66	0.68	30.29	1.56	196.7	1.98
0.774	0.10	5.03	0.72	32.65	1.61	212.0	1.94
0.834	0.11	5.42	0.76	35.18	1.67	228.5	1.90
0.899	0.12	5.84	0.79	37.92	1.72	246.2	1.83
0.969	0.13	6.29	0.83	40.86	1.77	265.4	1.74
1.04	0.14	6.78	0.86	44.04	1.81	286.0	1.62
1.13	0.15	7.31	0.90	47.46	1.85	308.2	1.47
1.21	0.17	7.88	0.93	51.15	1.89	332.1	1.31
1.31	0.18	8.49	0.96	55.12	1.92	358.0	1.12
1.41	0.19	9.15	0.98	59.41	1.94	385.8	0.93
1.52	0.21	9.86	1.01	64.02	1.96	415.7	0.75
1.64	0.23	10.62	1.04	69.00	1.98	448.1	0.60
1.76	0.24	11.45	1.06	74.36	1.99	482.9	0.44
1.90	0.27	12.34	1.09	80.14	2.00	520.4	0.17
2.05	0.29	13.30	1.11	86.36	2.01	560.8	0.00
2.21	0.32	14.33	1.14	93.07	2.01	604.4	0.00
2.38	0.35	15.45	1.17	100.3	2.02	651.4	0.00
2.56	0.38	16.65	1.20	108.1	2.02	702.0	0.00
2.76	0.41	17.94	1.24	116.5	2.02	756.5	0.00
2.98	0.44	19.33	1.28	125.6	2.02	815.3	0.00
3.21		20.84		135.3		878.7	

Table A3: Wheat biomass carbon particle analysis (Hand milled)

ID: 040211wheEi		Run No: 13		Measured: 4/2/2011 12:55			
File: KP120810		Rec. No: 106		Analysed: 4/2/2011 12:55			
Path: C:\SIZERS\DATA\VIKRANT\				Source: Analysed			
Range: 300 mm		Beam: 10.00 mm		Sampler: MS64		Obs': 17.8 %	
Presentation: 3TJD		Analysis: Polydisperse		Residual: 1.253 %			
Modifications: None							
Conc. = 0.0126 %Vol		Density = 1.390 g/cm ³		S.S.A.= 0.2012 m ² /g			
Distribution: Volume		D[4, 3] = 127.12 um		D[3, 2] = 21.45 um			
D(v, 0.1) = 8.88 um		D(v, 0.5) = 89.96 um		D(v, 0.9) = 304.72 um			
Span = 3.289E+00		Uniformity = 1.029E+00					
Size (um)	Volume In %	Size (um)	Volume In %	Size (um)	Volume In %	Size (um)	Volume In %
0.494	0.01	3.21	0.32	20.84	1.05	135.3	2.53
0.532	0.01	3.46	0.35	22.46	1.08	145.8	2.58
0.574	0.02	3.73	0.39	24.20	1.12	157.2	2.62
0.618	0.03	4.02	0.42	26.08	1.16	169.4	2.66
0.667	0.03	4.33	0.46	28.11	1.20	182.5	2.65
0.718	0.04	4.66	0.49	30.29	1.24	196.7	2.62
0.774	0.04	5.03	0.53	32.65	1.29	212.0	2.58
0.834	0.05	5.42	0.57	35.18	1.35	228.5	2.51
0.899	0.05	5.84	0.60	37.92	1.40	246.2	2.41
0.969	0.06	6.29	0.64	40.86	1.46	265.4	2.28
1.04	0.07	6.78	0.67	44.04	1.53	286.0	2.12
1.13	0.07	7.31	0.70	47.46	1.59	308.2	1.94
1.21	0.08	7.88	0.73	51.15	1.66	332.1	1.73
1.31	0.09	8.49	0.76	55.12	1.73	358.0	1.51
1.41	0.10	9.15	0.79	59.41	1.80	385.8	1.29
1.52	0.11	9.86	0.82	64.02	1.87	415.7	1.07
1.64	0.12	10.62	0.84	69.00	1.94	448.1	0.86
1.76	0.14	11.45	0.86	74.36	2.01	482.9	0.65
1.90	0.15	12.34	0.89	80.14	2.09	520.4	0.41
2.05	0.17	13.30	0.91	86.36	2.16	560.8	0.18
2.21	0.19	14.33	0.93	93.07	2.23	604.4	0.04
2.38	0.21	15.45	0.95	100.3	2.29	651.4	0.00
2.56	0.24	16.65	0.97	108.1	2.36	702.0	0.00
2.76	0.26	17.94	1.00	116.5	2.42	756.5	0.00
2.98	0.29	19.33	1.02	125.6	2.47	815.3	0.00
3.21		20.84		135.3		878.7	

Table A4: Willow biomass carbon particle analysis (Hand milled)

ID: 040211wilCi		Run No: 7		Measured: 4/2/2011 12:28			
File: KP120810		Rec. No: 100		Analysed: 4/2/2011 12:28			
Path: C:\SIZERS\DATA\VIKRANT\		Source: Analysed					
Range: 300 mm		Beam: 10.00 mm		Sampler: MS64		Obs': 18.2 %	
Presentation: 3TJD		Analysis: Polydisperse				Residual: 0.896 %	
Modifications: None							
Conc. = 0.0060 %Vol		Density = 1.390 g/cm ³		S.S.A.= 0.4188 m ² /g			
Distribution: Volume		D[4, 3] = 64.87 um		D[3, 2] = 10.31 um			
D(v, 0.1) = 3.99 um		D(v, 0.5) = 38.58 um		D(v, 0.9) = 169.57 um			
Span = 4.292E+00		Uniformity = 1.315E+00					
Size (um)	Volume In %	Size (um)	Volume In %	Size (um)	Volume In %	Size (um)	Volume In %
0.494	0.05	3.21	0.75	20.84	1.47	135.3	1.79
0.532	0.05	3.46	0.80	22.46	1.51	145.8	1.71
0.574	0.08	3.73	0.85	24.20	1.57	157.2	1.63
0.618	0.10	4.02	0.90	26.08	1.62	169.4	1.54
0.667	0.12	4.33	0.95	28.11	1.68	182.5	1.44
0.718	0.14	4.66	0.99	30.29	1.74	196.7	1.34
0.774	0.15	5.03	1.03	32.65	1.80	212.0	1.23
0.834	0.17	5.42	1.07	35.18	1.87	228.5	1.11
0.899	0.19	5.84	1.10	37.92	1.92	246.2	0.96
0.969	0.21	6.29	1.13	40.86	1.98	265.4	0.81
1.04	0.23	6.78	1.15	44.04	2.03	286.0	0.67
1.13	0.25	7.31	1.18	47.46	2.07	308.2	0.51
1.21	0.27	7.88	1.19	51.15	2.11	332.1	0.25
1.31	0.29	8.49	1.21	55.12	2.14	358.0	0.11
1.41	0.31	9.15	1.22	59.41	2.16	385.8	0.05
1.52	0.34	9.86	1.24	64.02	2.17	415.7	0.00
1.64	0.37	10.62	1.25	69.00	2.18	448.1	0.00
1.76	0.40	11.45	1.26	74.36	2.19	482.9	0.00
1.90	0.44	12.34	1.27	80.14	2.19	520.4	0.00
2.05	0.48	13.30	1.29	86.36	2.15	560.8	0.00
2.21	0.52	14.33	1.31	93.07	2.11	604.4	0.00
2.38	0.56	15.45	1.33	100.3	2.06	651.4	0.00
2.56	0.61	16.65	1.36	108.1	2.00	702.0	0.00
2.76	0.65	17.94	1.39	116.5	1.94	756.5	0.00
2.98	0.70	19.33	1.43	125.6	1.87	815.3	0.00
3.21		20.84		135.3		878.7	

Table A5: Spruce biomass carbon particle analysis (Hand milled)

ID: 040211sprAi		Run No: 1		Measured: 4/2/2011 12:03			
File: KP120810		Rec. No: 94		Analysed: 4/2/2011 12:03			
Path: C:\SIZERS\DATA\VIKRANT\				Source: Analysed			
Range: 300 mm		Beam: 10.00 mm		Sampler: MS64		Obs': 18.7 %	
Presentation: 3TJD		Analysis: Polydisperse		Residual: 0.519 %			
Modifications: None							
Conc. = 0.0151 %Vol		Density = 1.390 g/cm ³		S.S.A.= 0.1754 m ² /g			
Distribution: Volume		D[4, 3] = 143.77 um		D[3, 2] = 24.61 um			
D(v, 0.1) = 11.46 um		D(v, 0.5) = 110.10 um		D(v, 0.9) = 328.46 um			
Span = 2.879E+00		Uniformity = 8.969E-01					
Size (um)	Volume In %	Size (um)	Volume In %	Size (um)	Volume In %	Size (um)	Volume In %
0.494	0.02	3.21	0.25	20.84	0.88	135.3	2.75
0.532	0.02	3.46	0.27	22.46	0.91	145.8	2.83
0.574	0.03	3.73	0.29	24.20	0.95	157.2	2.91
0.618	0.03	4.02	0.32	26.08	0.99	169.4	2.97
0.667	0.04	4.33	0.34	28.11	1.03	182.5	2.98
0.718	0.05	4.66	0.37	30.29	1.08	196.7	2.96
0.774	0.05	5.03	0.40	32.65	1.13	212.0	2.91
0.834	0.05	5.42	0.42	35.18	1.19	228.5	2.84
0.899	0.06	5.84	0.45	37.92	1.25	246.2	2.73
0.969	0.06	6.29	0.48	40.86	1.32	265.4	2.60
1.04	0.07	6.78	0.50	44.04	1.39	286.0	2.43
1.13	0.07	7.31	0.53	47.46	1.47	308.2	2.23
1.21	0.08	7.88	0.55	51.15	1.55	332.1	2.01
1.31	0.09	8.49	0.58	55.12	1.64	358.0	1.77
1.41	0.09	9.15	0.60	59.41	1.73	385.8	1.54
1.52	0.10	9.86	0.63	64.02	1.82	415.7	1.31
1.64	0.11	10.62	0.65	69.00	1.92	448.1	1.07
1.76	0.12	11.45	0.67	74.36	2.02	482.9	0.84
1.90	0.13	12.34	0.70	80.14	2.12	520.4	0.62
2.05	0.14	13.30	0.72	86.36	2.22	560.8	0.39
2.21	0.16	14.33	0.74	93.07	2.32	604.4	0.14
2.38	0.17	15.45	0.77	100.3	2.42	651.4	0.00
2.56	0.19	16.65	0.79	108.1	2.51	702.0	0.00
2.76	0.21	17.94	0.82	116.5	2.60	756.5	0.00
2.98	0.23	19.33	0.85	125.6	2.68	815.3	0.00
3.21		20.84		135.3		878.7	0.00

Table A6: Poplar biomass carbon particle analysis (Hand milled)

ID: 040211popBi		Run No: 4		Measured: 4/2/2011 12:16			
File: KP120810		Rec. No: 97		Analysed: 4/2/2011 12:16			
Path: C:\SIZERS\DATA\VIKRANT\				Source: Analysed			
Range: 300 mm		Beam: 10.00 mm		Sampler: MS64		Obs': 18.3 %	
Presentation: 3TJD		Analysis: Polydisperse		Residual: 1.127 %			
Modifications: None							
Conc. = 0.0102 %Vol		Density = 1.390 g/cm ³		S.S.A.= 0.2513 m ² /g			
Distribution: Volume		D[4, 3] = 125.39 um		D[3, 2] = 17.17 um			
D(v, 0.1) = 7.07 um		D(v, 0.5) = 83.48 um		D(v, 0.9) = 310.03 um			
Span = 3.629E+00		Uniformity = 1.140E+00					
Size (um)	Volume In %	Size (um)	Volume In %	Size (um)	Volume In %	Size (um)	Volume In %
0.494	0.02	3.21	0.41	20.84	1.07	135.3	2.30
0.532	0.03	3.46	0.44	22.46	1.10	145.8	2.35
0.574	0.04	3.73	0.48	24.20	1.13	157.2	2.41
0.618	0.06	4.02	0.51	26.08	1.17	169.4	2.47
0.667	0.06	4.33	0.55	28.11	1.21	182.5	2.50
0.718	0.08	4.66	0.59	30.29	1.26	196.7	2.51
0.774	0.08	5.03	0.62	32.65	1.30	212.0	2.50
0.834	0.09	5.42	0.66	35.18	1.35	228.5	2.47
0.899	0.10	5.84	0.69	37.92	1.40	246.2	2.40
0.969	0.11	6.29	0.72	40.86	1.45	265.4	2.30
1.04	0.11	6.78	0.75	44.04	1.50	286.0	2.16
1.13	0.12	7.31	0.78	47.46	1.56	308.2	1.99
1.21	0.13	7.88	0.81	51.15	1.61	332.1	1.79
1.31	0.14	8.49	0.83	55.12	1.66	358.0	1.56
1.41	0.15	9.15	0.85	59.41	1.71	385.8	1.34
1.52	0.17	9.86	0.87	64.02	1.75	415.7	1.12
1.64	0.18	10.62	0.89	69.00	1.80	448.1	0.91
1.76	0.20	11.45	0.90	74.36	1.86	482.9	0.69
1.90	0.22	12.34	0.92	80.14	1.91	520.4	0.46
2.05	0.24	13.30	0.94	86.36	1.96	560.8	0.24
2.21	0.26	14.33	0.95	93.07	2.02	604.4	0.07
2.38	0.29	15.45	0.97	100.3	2.07	651.4	0.00
2.56	0.31	16.65	0.99	108.1	2.13	702.0	0.00
2.76	0.34	17.94	1.01	116.5	2.19	756.5	0.00
2.98	0.37	19.33	1.04	125.6	2.24	815.3	0.00
3.21		20.84		135.3		878.7	

Appendix B

Information Dissemination

B1 Departmental Seminar

- ❖ Adeniyi O.D. (2011) “The Use of Biomass carbon in a Direct Carbon Fuel Cell”, 30 month seminar, Department of Chemical and Biological Engineering, The University of Sheffield, Sheffield, U.K., 11th May 2011.
- ❖ Adeniyi O.D. and Ewan B.C.R. (2010) “Performance study on the Use of Biomass carbon in a Direct Carbon Fuel Cell”, Poster Presentation, Department of Chemical and Biological Engineering, The University of Sheffield, Sheffield, U.K., 10th November 2010.
- ❖ Adeniyi O.D. (2009) “The Use of Biomass in the Direct Carbon Fuel Cell”, MPhil to Ph.D Transfer Seminar, Department of Chemical and Process Engineering, The University of Sheffield, Sheffield, U.K., 20th October 2009, 186 pp.

B2 Conference Presentation

- ❖ Adeniyi O.D. and Ewan B.C.R. (2010) “Performance study on the use of biomass carbon in a direct carbon fuel cell”, Poster Presented at the Bioten Conference, SUPERGEN Bioenergy, Birmingham, U.K., 21-23th September 2010.

B3 Conference Proceeding

- ❖ Adeniyi O.D. and Ewan B.C.R. (2011) “Performance study on the use of biomass carbon in a direct carbon fuel cell”, *Conference Proceedings of the Bioten Conference on biomass, bioenergy and biofuels 2010, SUPERGEN Bioenergy*, Birmingham, CPL Press, U.K., pp. 407-419 (21-23th September 2010).

B4 Journal Publication

- ❖ Adeniyi O.D. and Ewan B.C.R. (2011) “Comparison of the performance of biomass carbons in direct carbon fuel cells”, *Green Chemistry*, (submitted for publication).

Appendix C

Graphs of DCFC Performances

C1 Graph of Performances of the MDCFC using HM Carbon Fuels

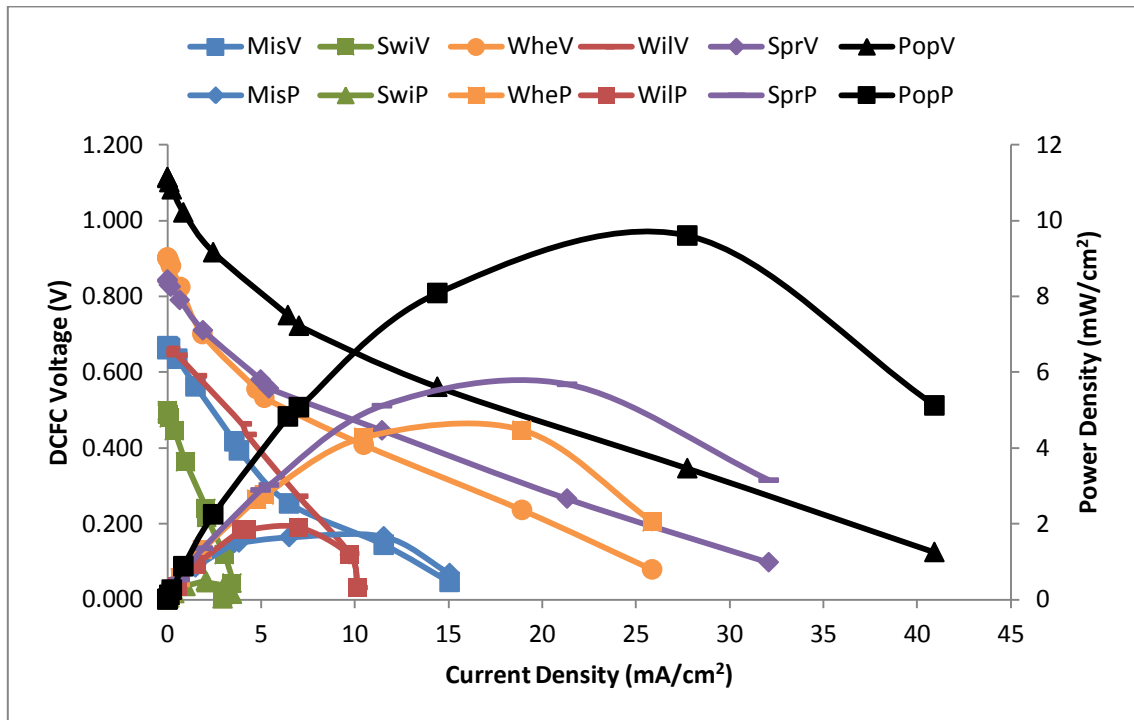


Figure C1: Overall performances for the 6 biomass fuels at 700°C (HM-Day 2)

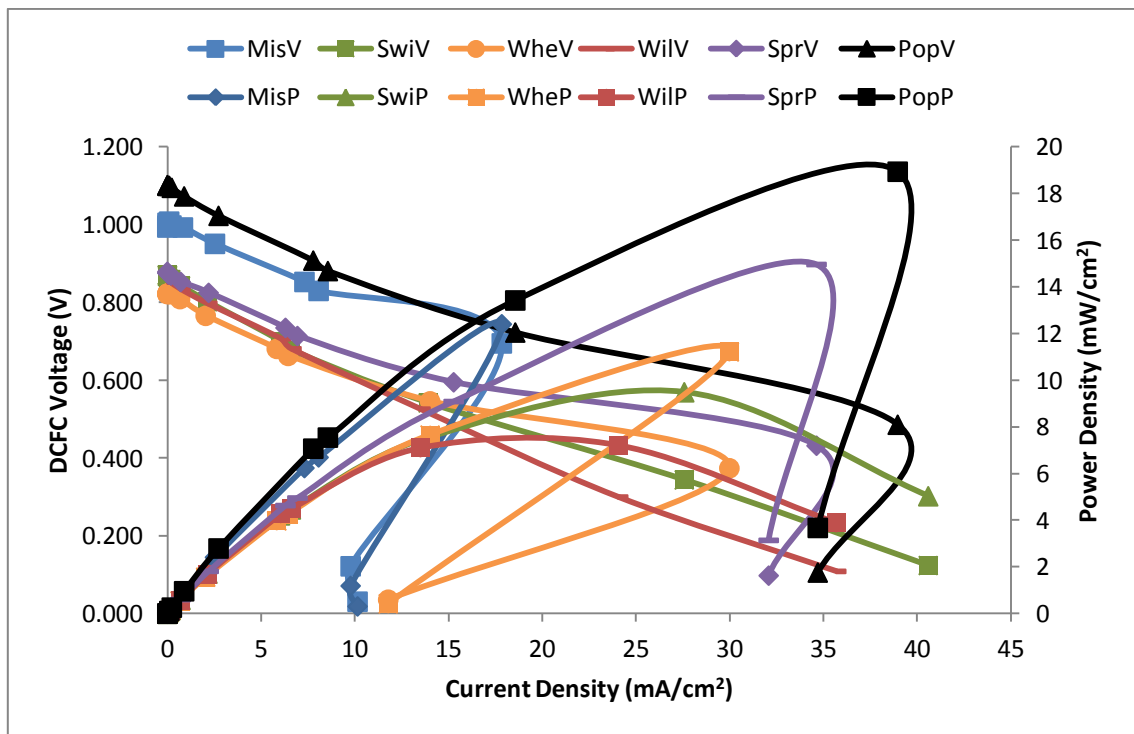


Figure C2: Overall performances for the 6 biomass fuels at 800°C (HM-Day 2)

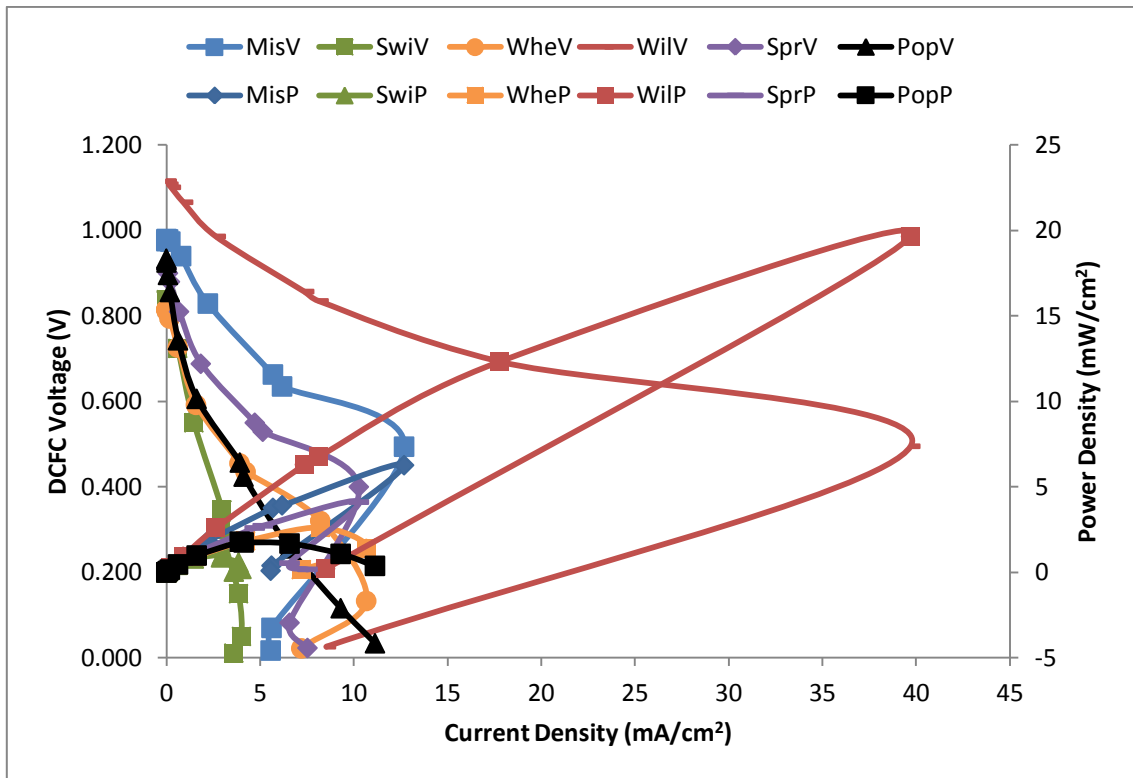


Figure C3: Overall performances for the 6 biomass fuels at 700°C (HM-Day 3)

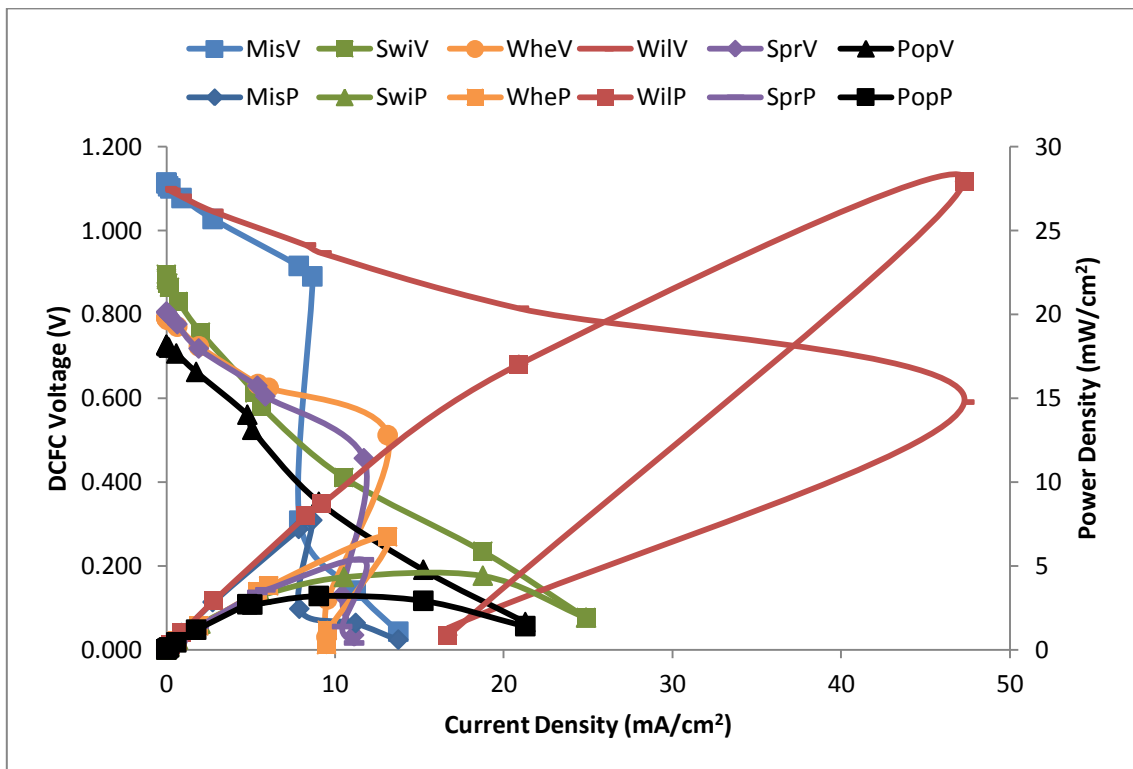


Figure C4: Overall performances for the 6 biomass fuels at 800°C (HM-Day 3)

C2 Temperature Effects on MDCFC Performances with HM Carbon Fuel

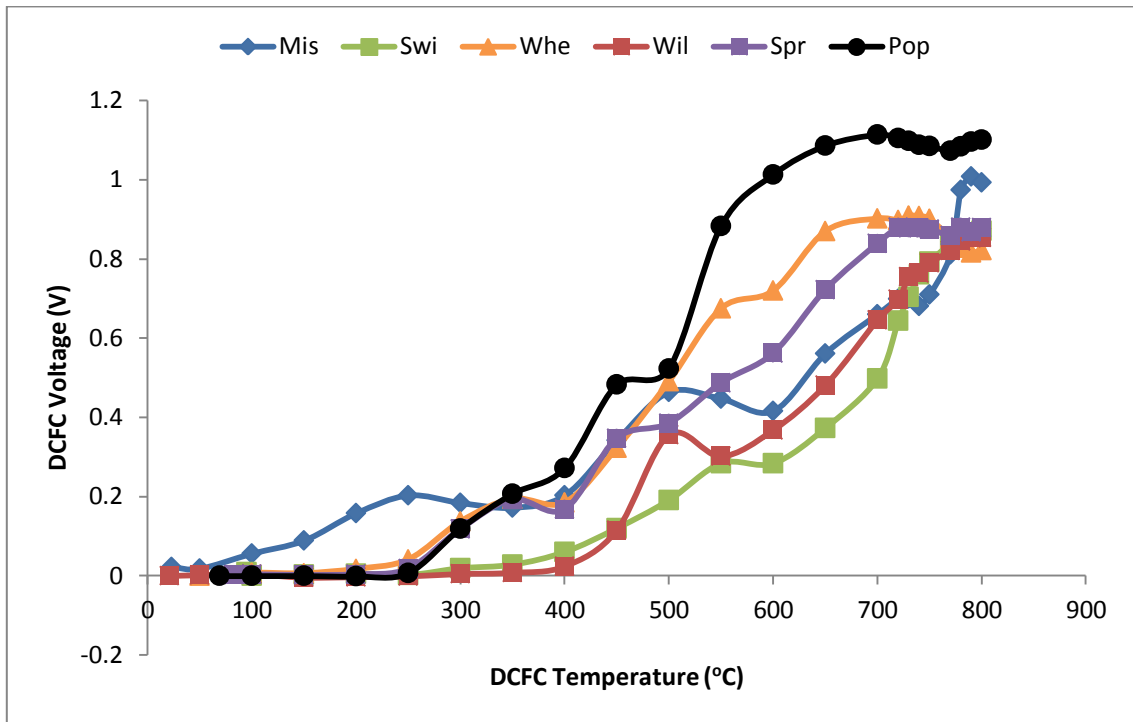


Figure C5: MDCFC voltages for the six biomass carbon fuels at different temperatures (HM-Day 2)

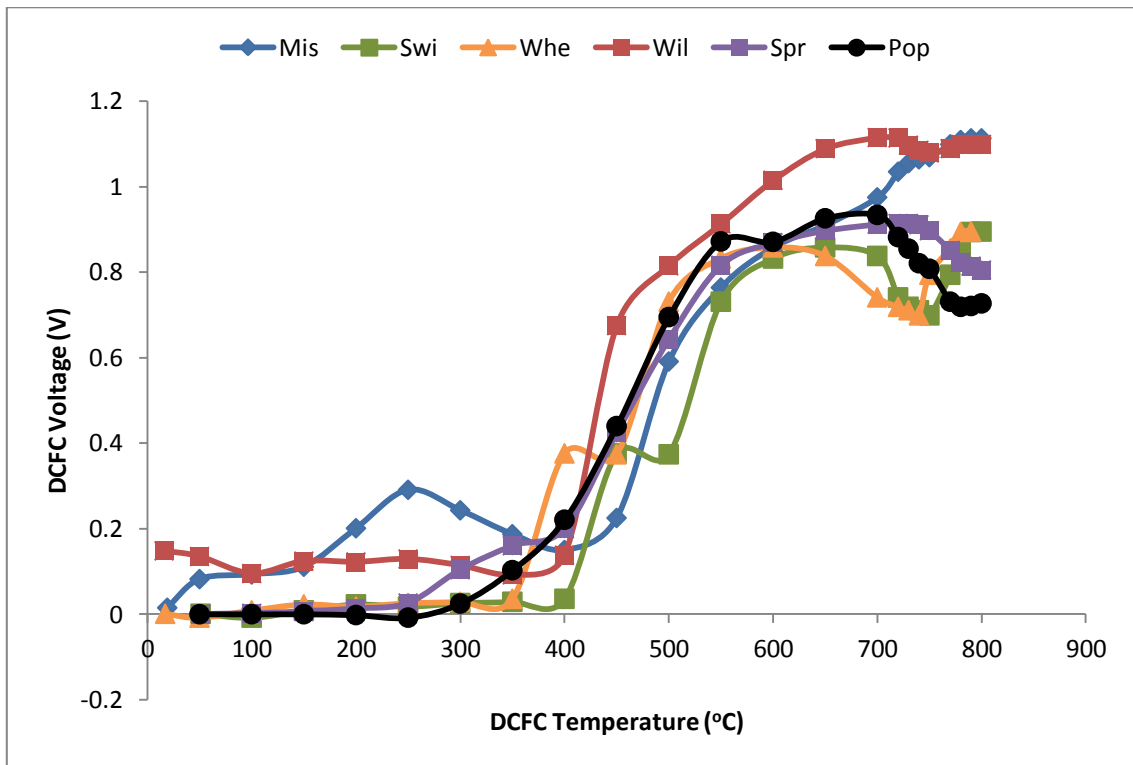


Figure C6: MDCFC voltages for the six biomass carbon fuels at different temperatures (HM-Day 3)

C3 Graphs of 2nd Day Performances of the MDCFC using BM Carbon Fuels

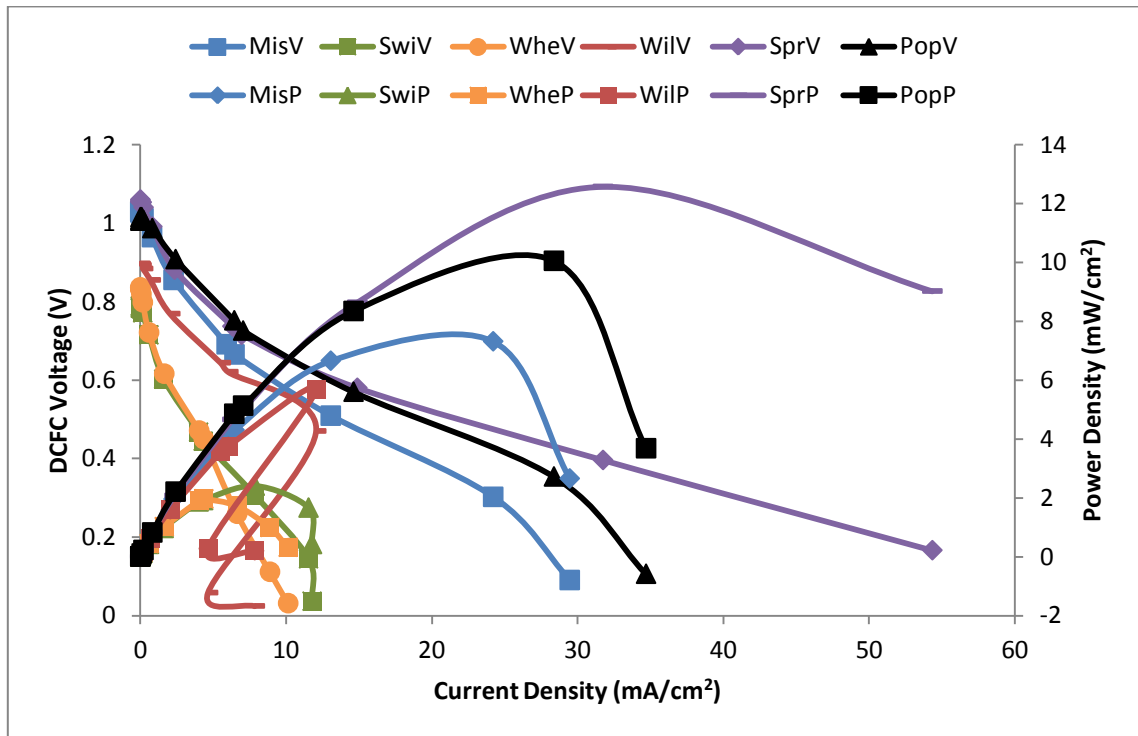


Figure C7: Overall performances for the 6 biomass fuels at 700°C (BM-Day 2)

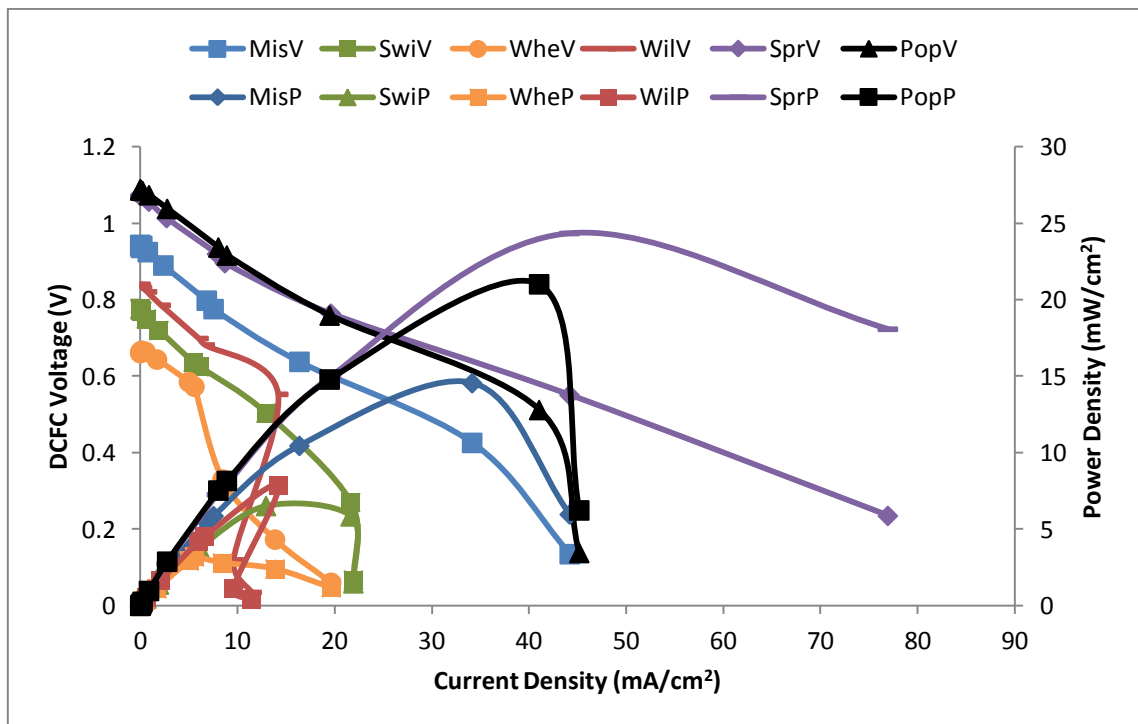


Figure C8: Overall performances for the 6 biomass fuels at 800°C (BM-Day 2)

C4 Graph of 3rd Day Performances of the MDCFC using BM Carbon Fuels

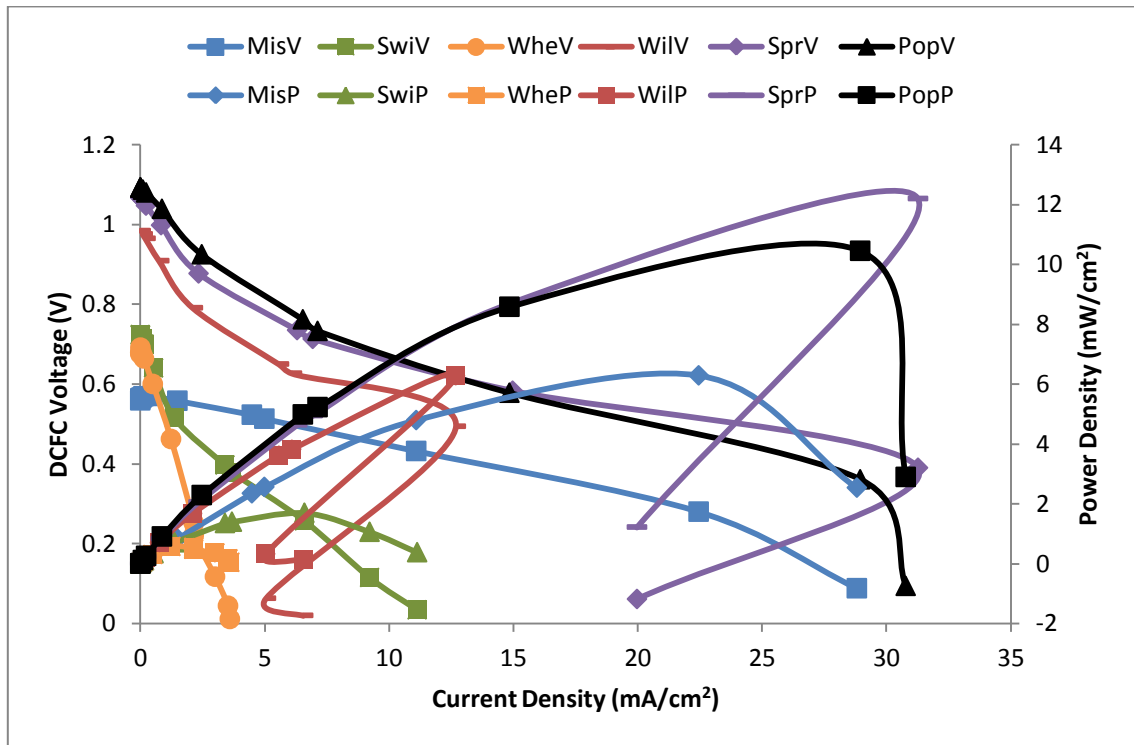


Figure C9: Overall performances for the 6 biomass fuels at 700°C (BM-Day 3)

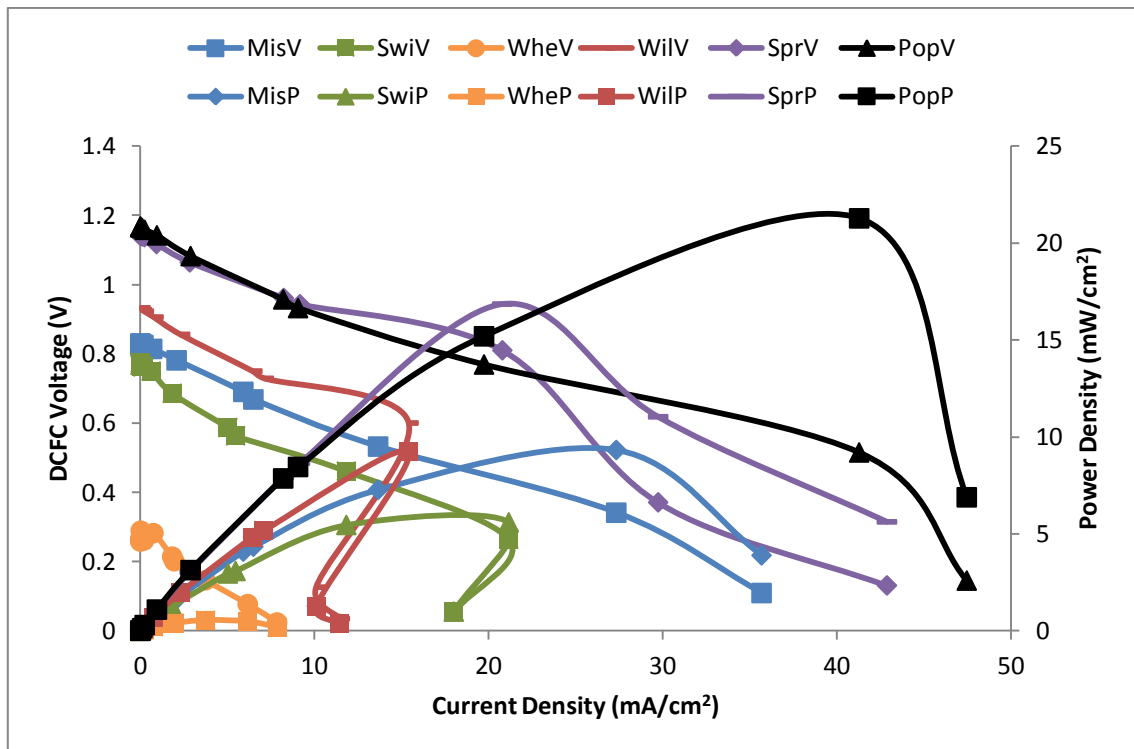


Figure C10: Overall performances for the 6 biomass fuels at 800°C (BM-Day 3)

C5 Graph of Temperature Effects on MDCFC Performances with BM Fuel

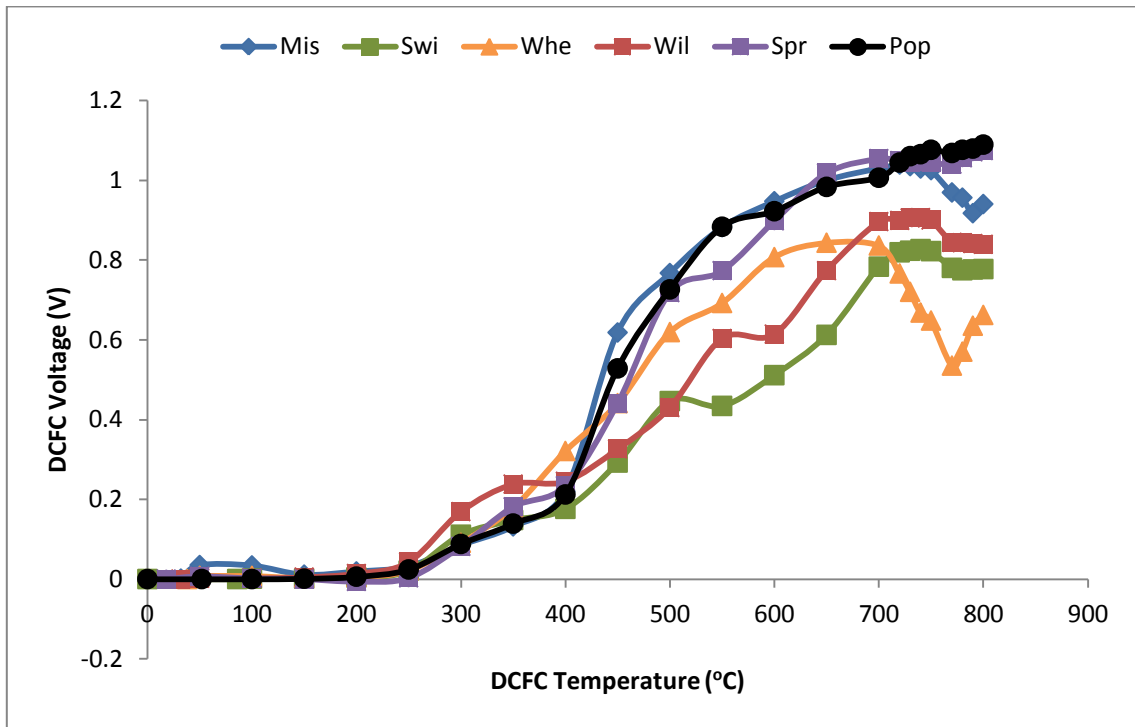


Figure C11: MDCFC OCV for the six biomass carbon fuels at different temperature (BM-Day 2)

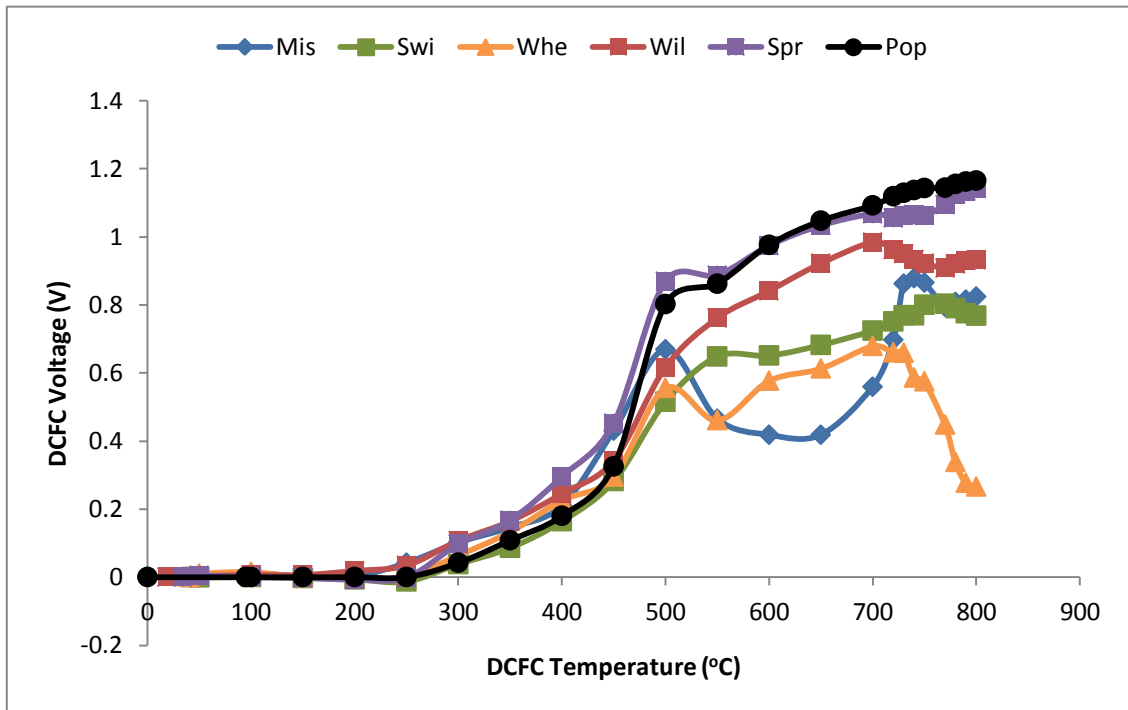


Figure C12: MDCFC OCV for the six biomass carbon fuels at different temperature (BM-Day 3)

C6 Graph of Comparison of MCDFC Performances for HM and BM Carbon Fuels

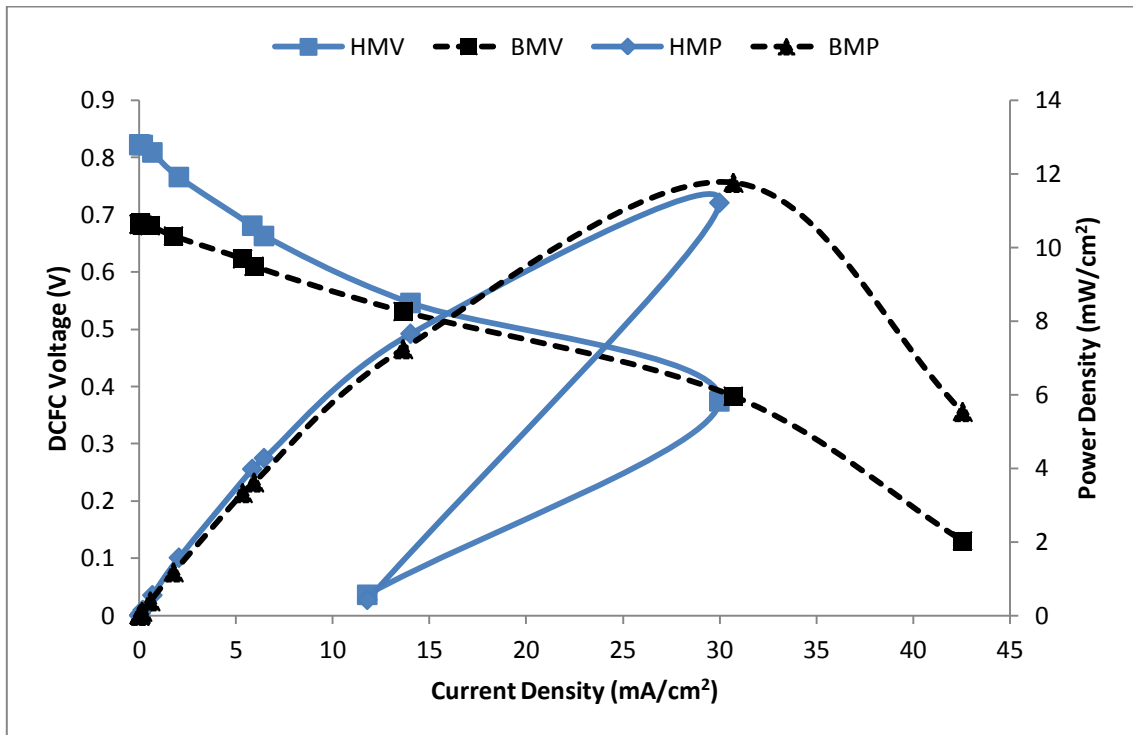


Figure C13: Wheat performances for hand and ball milled fuels at 800°C.

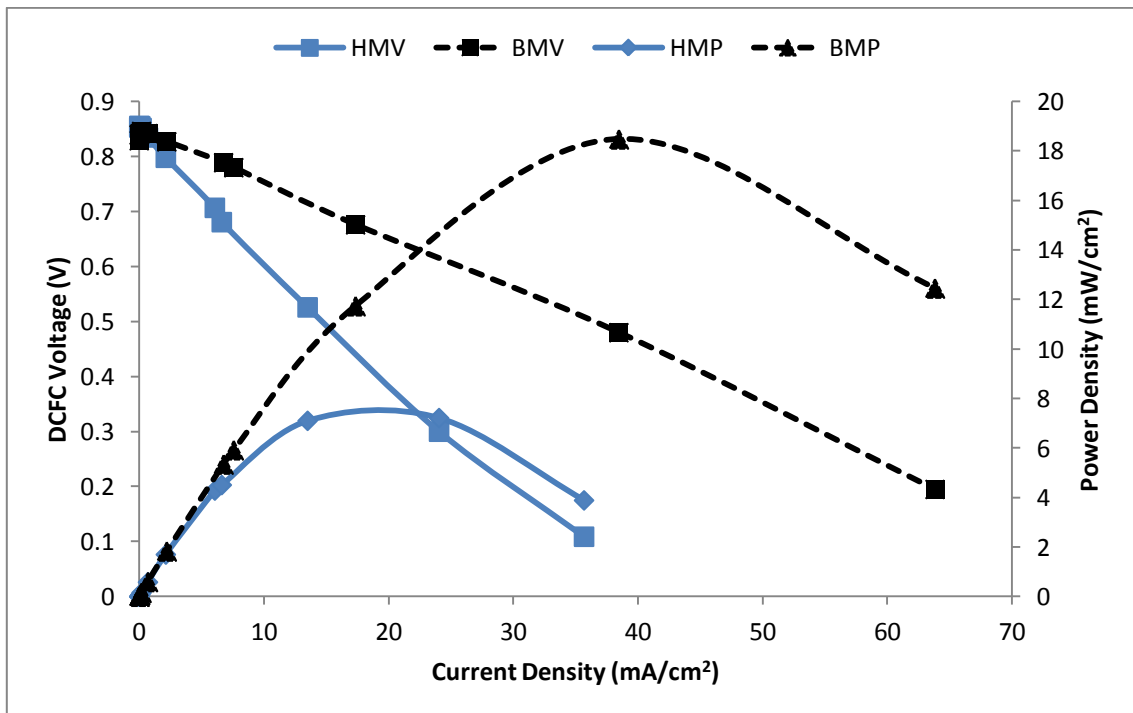


Figure C14: Willow performances for hand and ball milled fuels at 800°C.

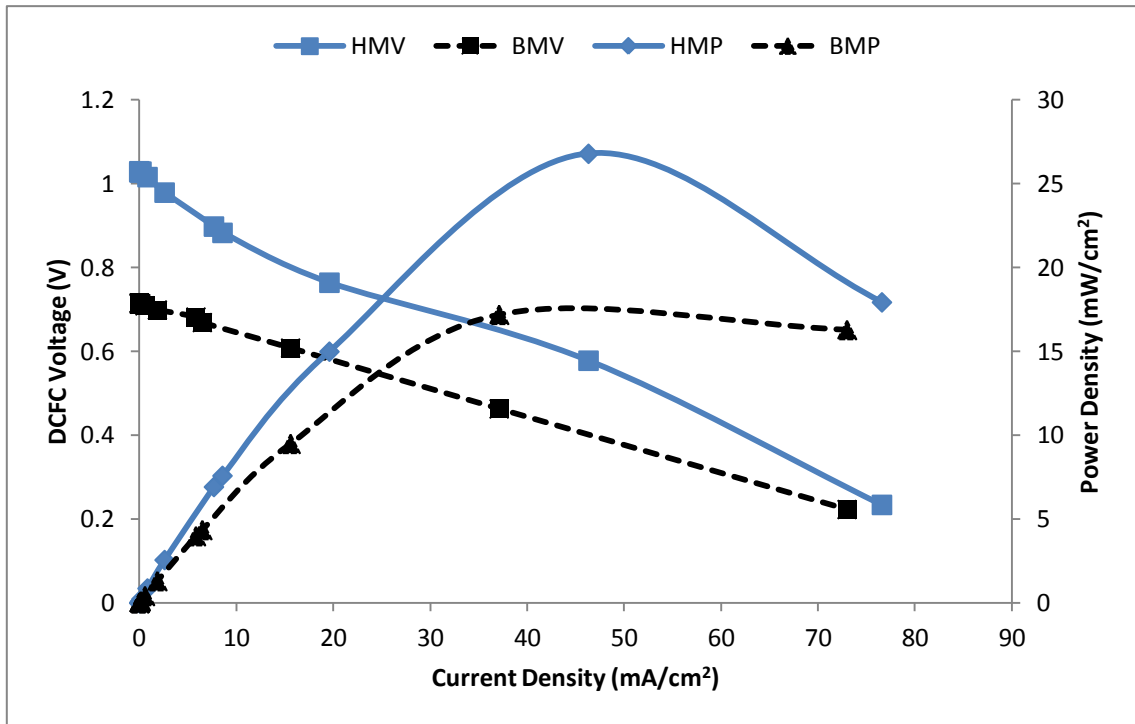


Figure C15: Spruce performances for hand and ball milled fuels at 800°C.

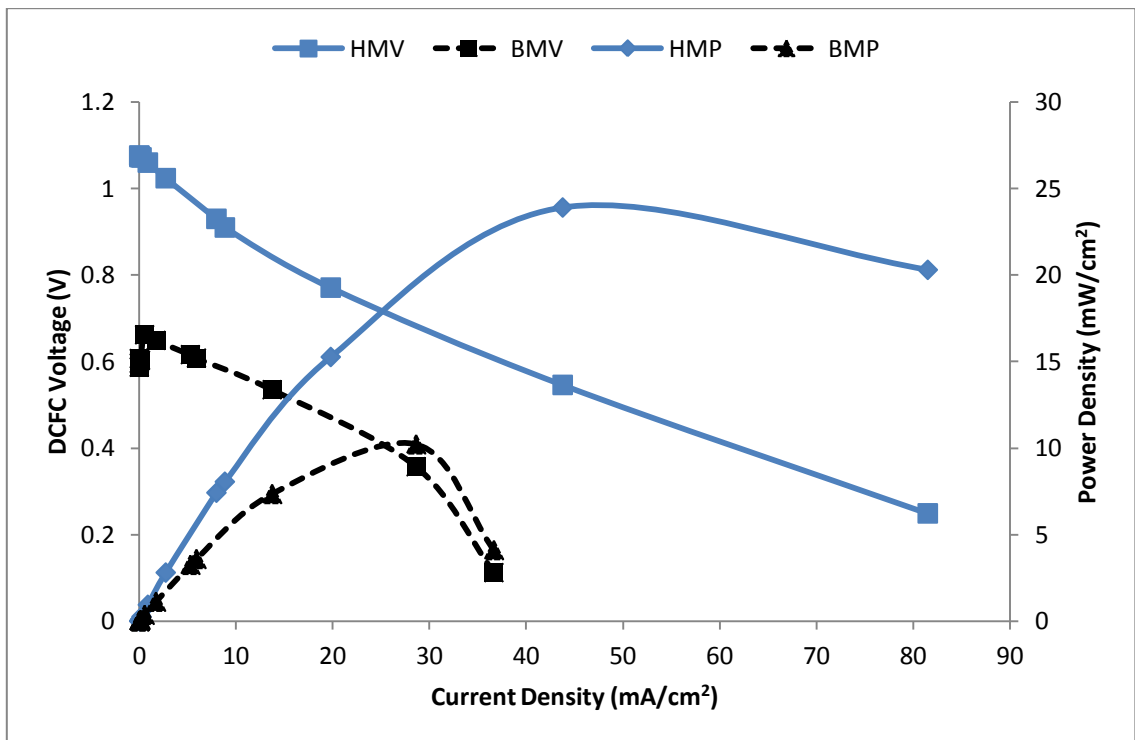


Figure C16: Poplar performances for hand and ball milled fuels at 800°C.

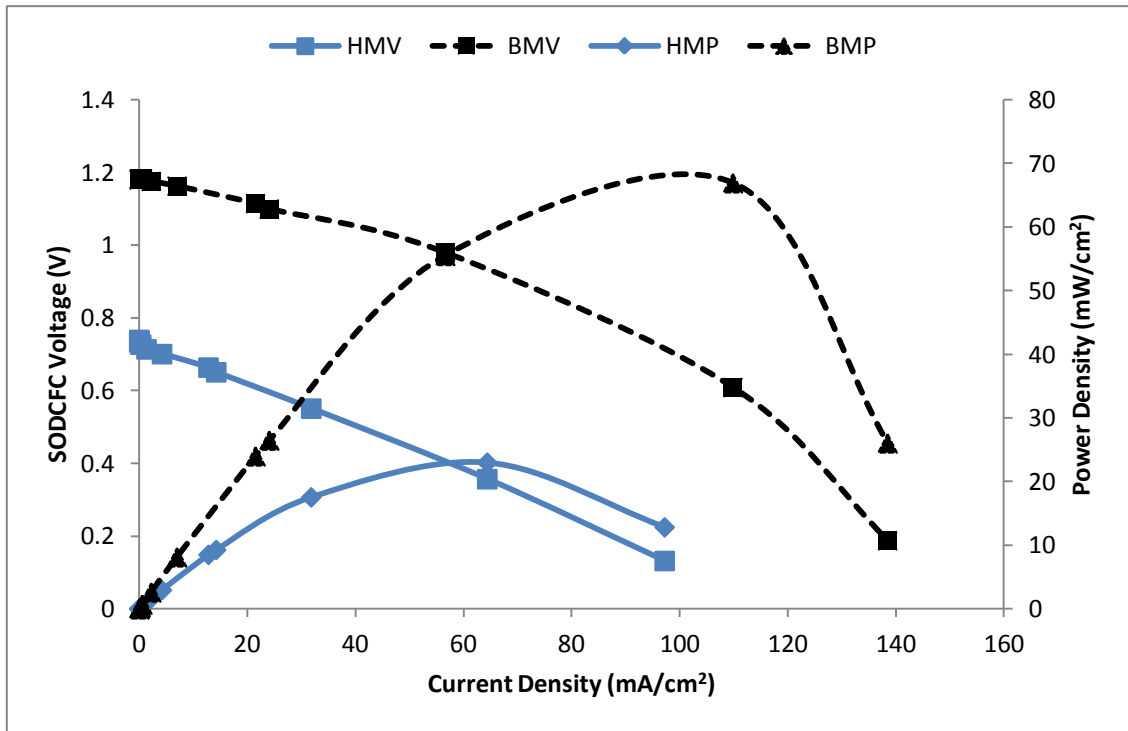


Figure C17: SODCFC wheat performances for HM and BM fuels at 800°C.

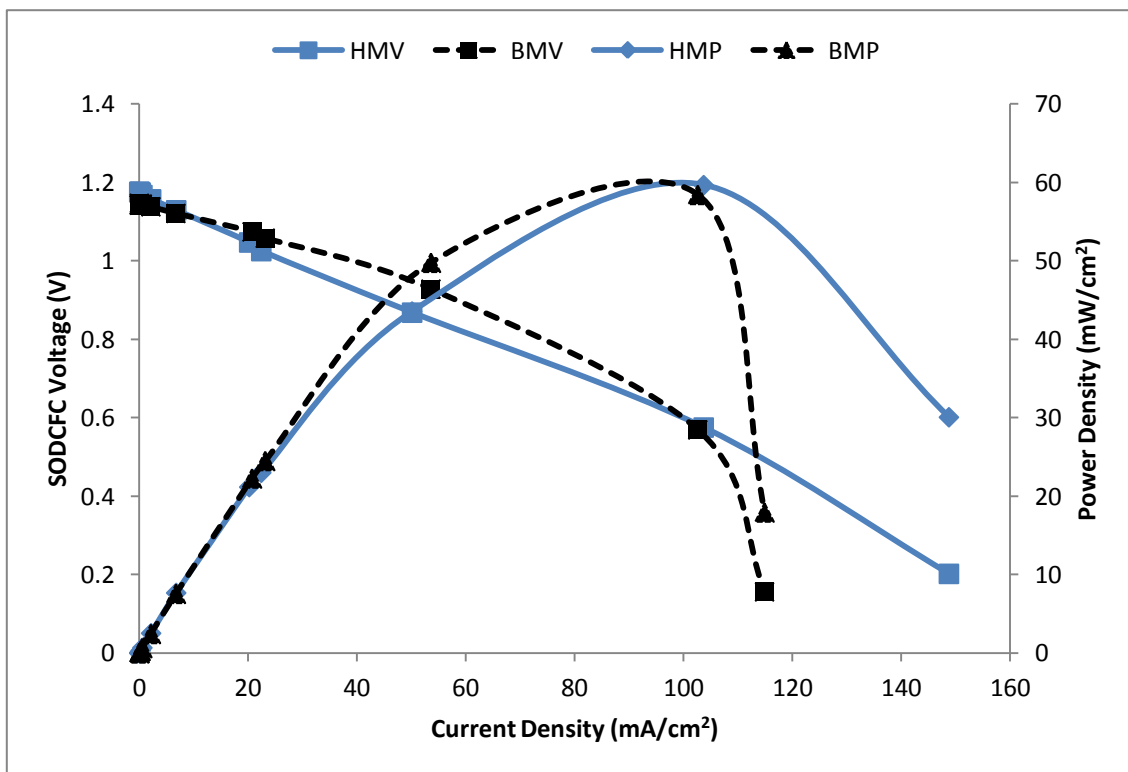


Figure C18: SODCFC willow performances for HM and BM fuels at 800°C.

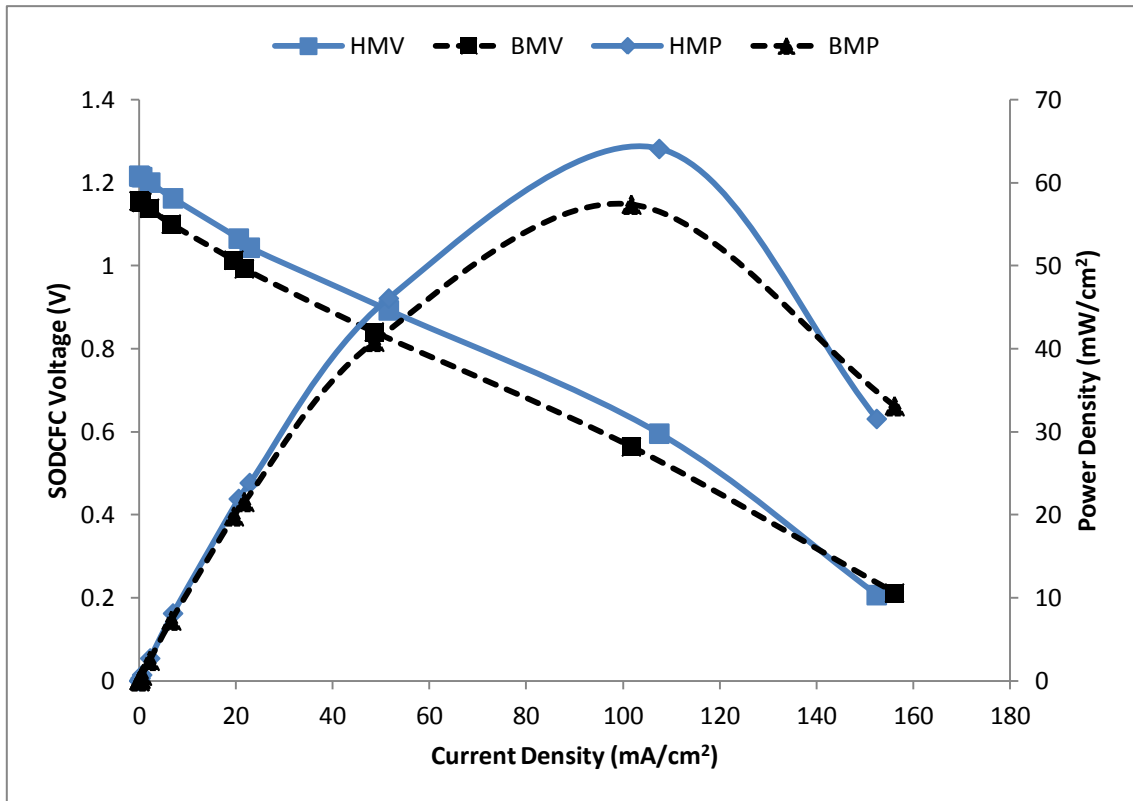


Figure C19: SODCFC spruce performances for HM and BM fuels at 800°C.

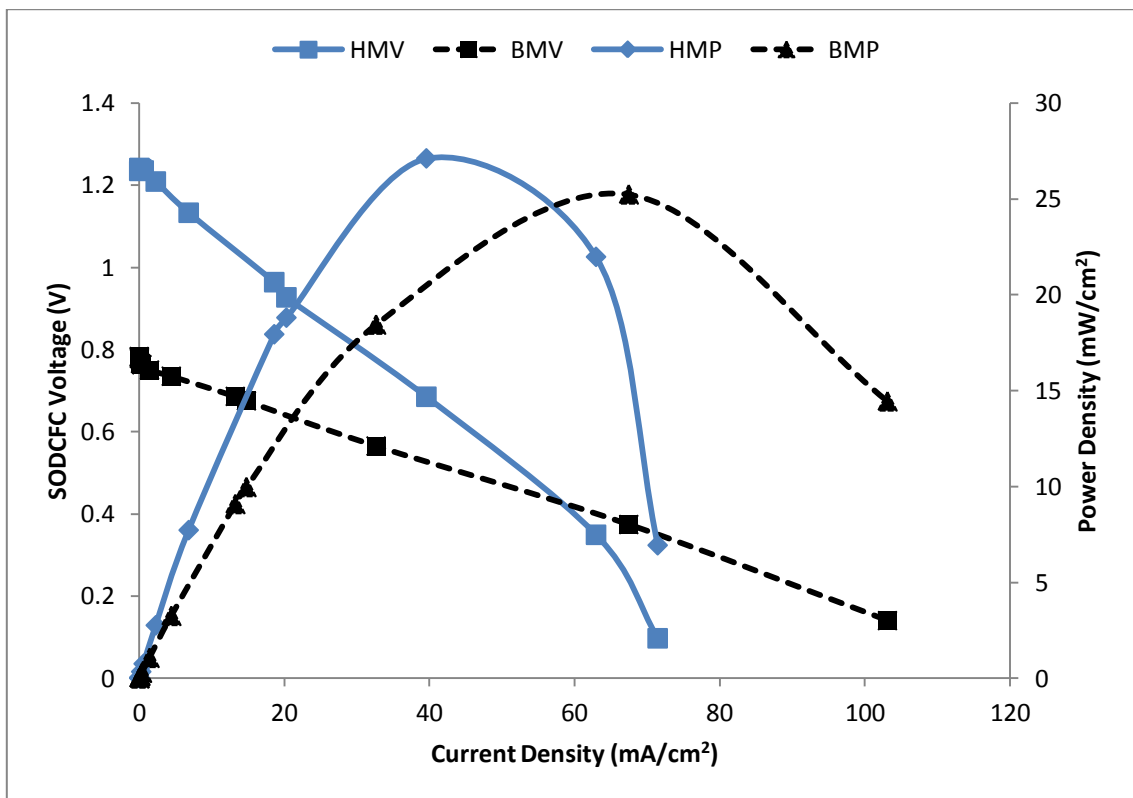


Figure C20: SODCFC poplar performances for HM and BM fuels at 800°C.

C7 Graph of Comparison of SODCFC and MDCFC Performance for BM Fuels

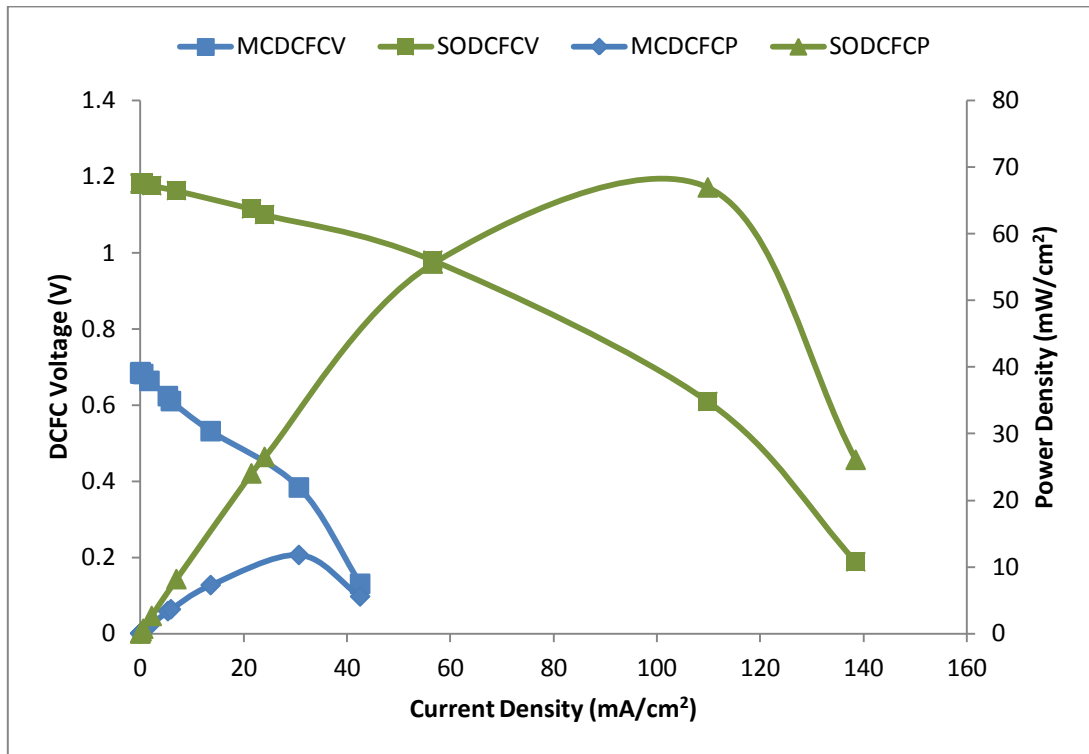


Figure C21: BM Wheat performances for SODCFC and MDCFC at 800°C.

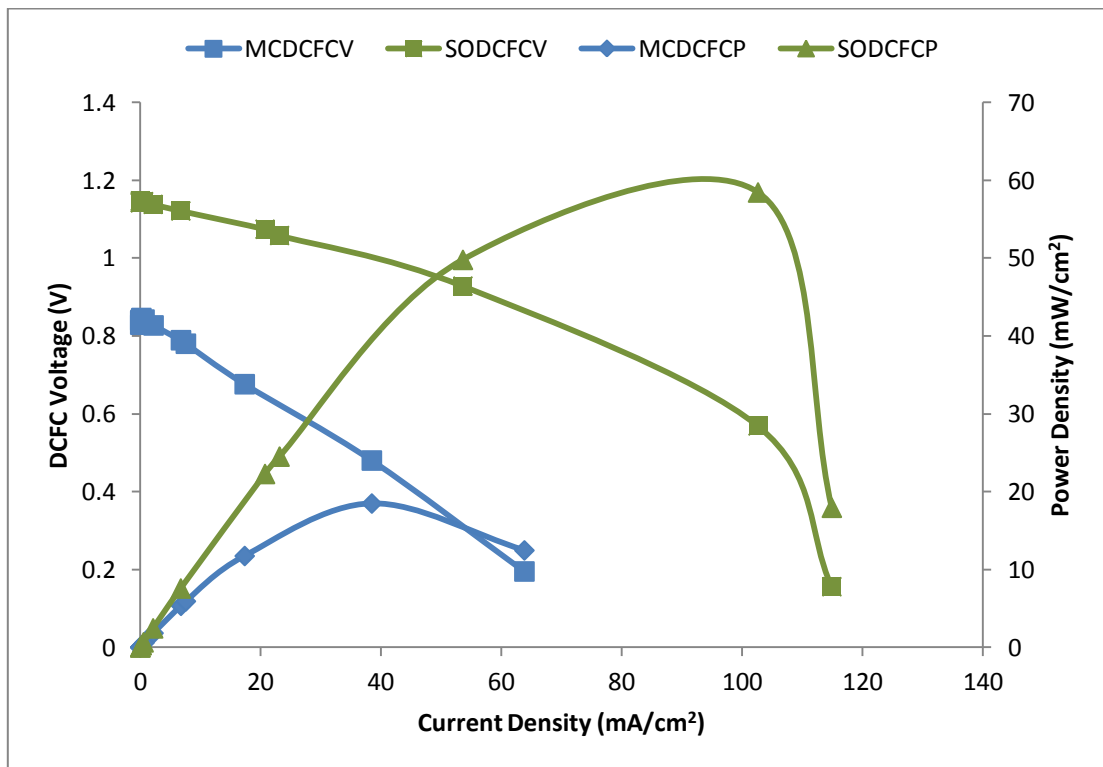


Figure C22: BM Willow performances for SODCFC and MDCFC at 800°C.

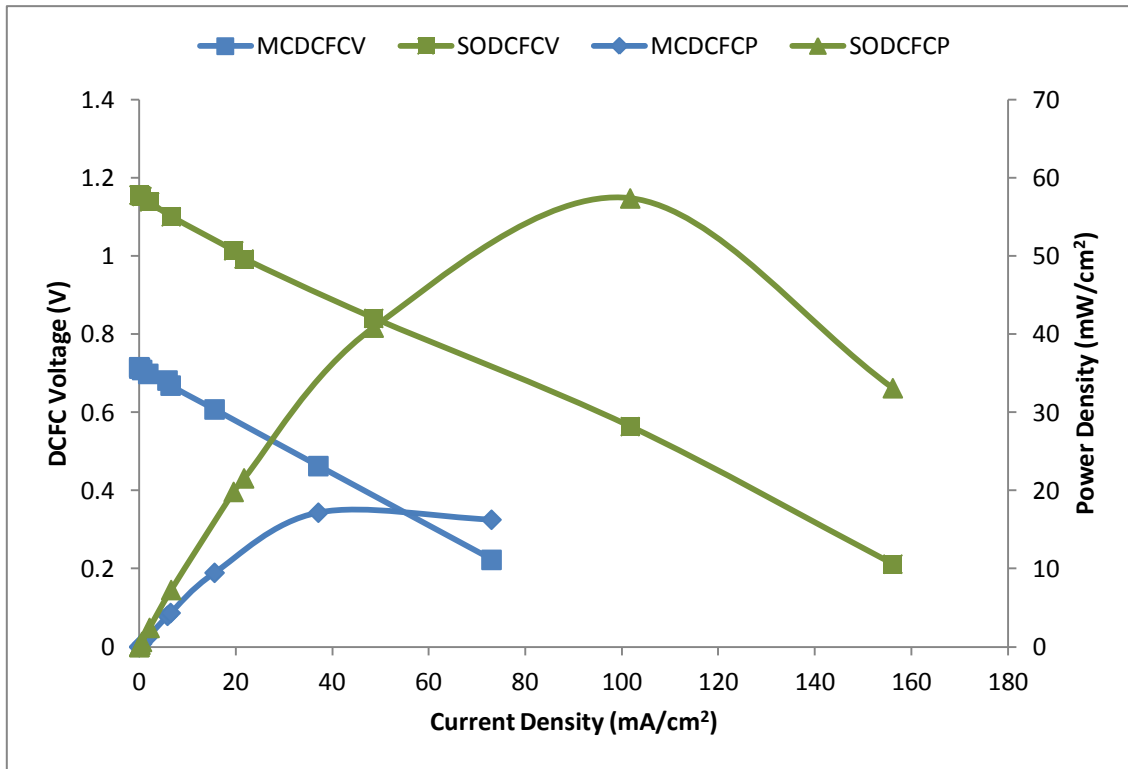


Figure C23: BM Spruce performances for SODFCV and MDCFCV at 800°C.

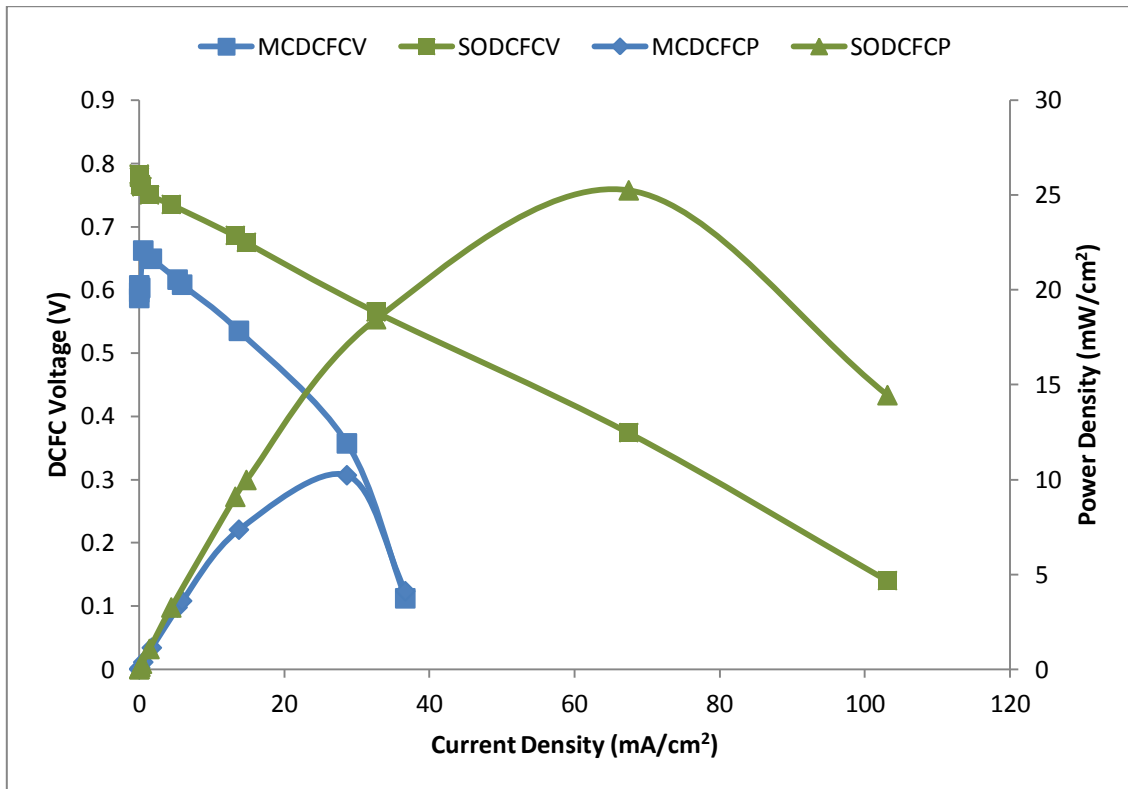


Figure C24: BM Poplar performances for SODFCV and MDCFCV at 800°C.

C8 Graph of Comparison of SODCFC and MDCFC performance for HM fuels

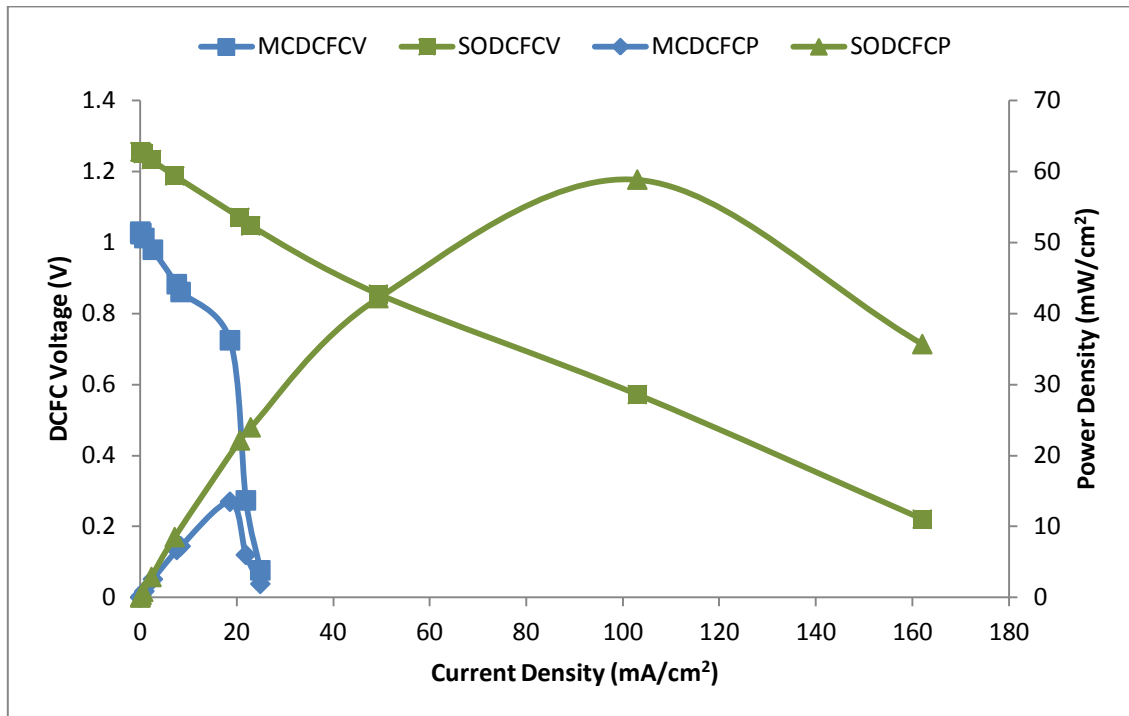


Figure C25: HM Miscanthus performances for SODCFC and MDCFC at 800°C.

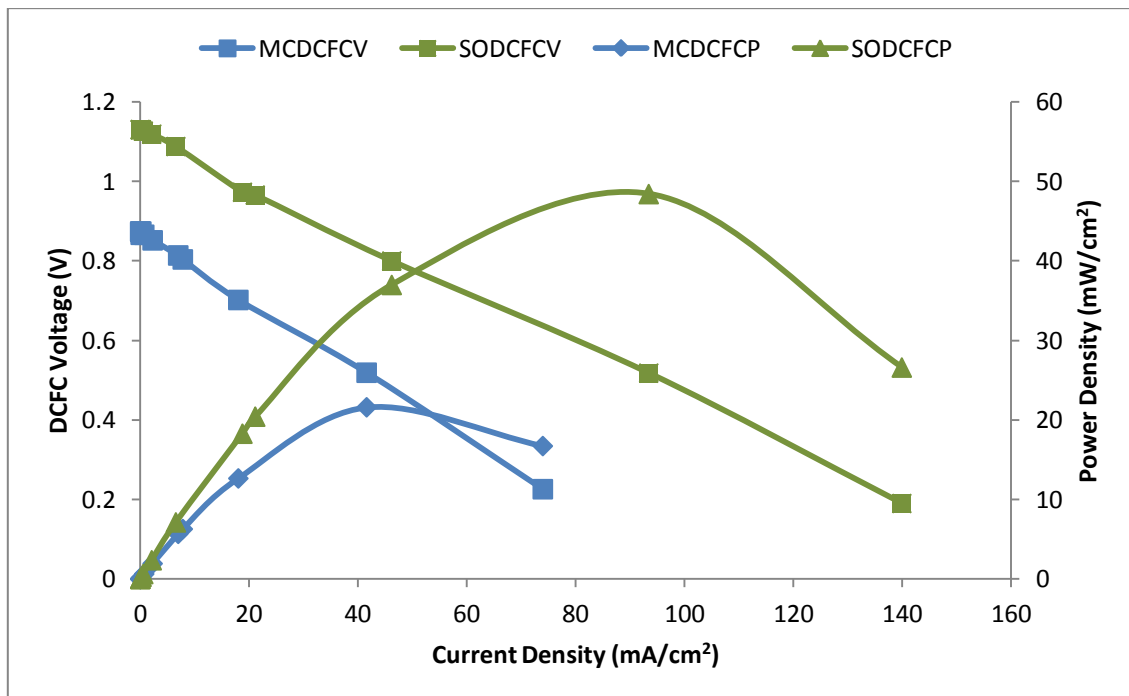


Figure C26: HM Switchgrass performances for SODCFC and MDCFC at 800°C.

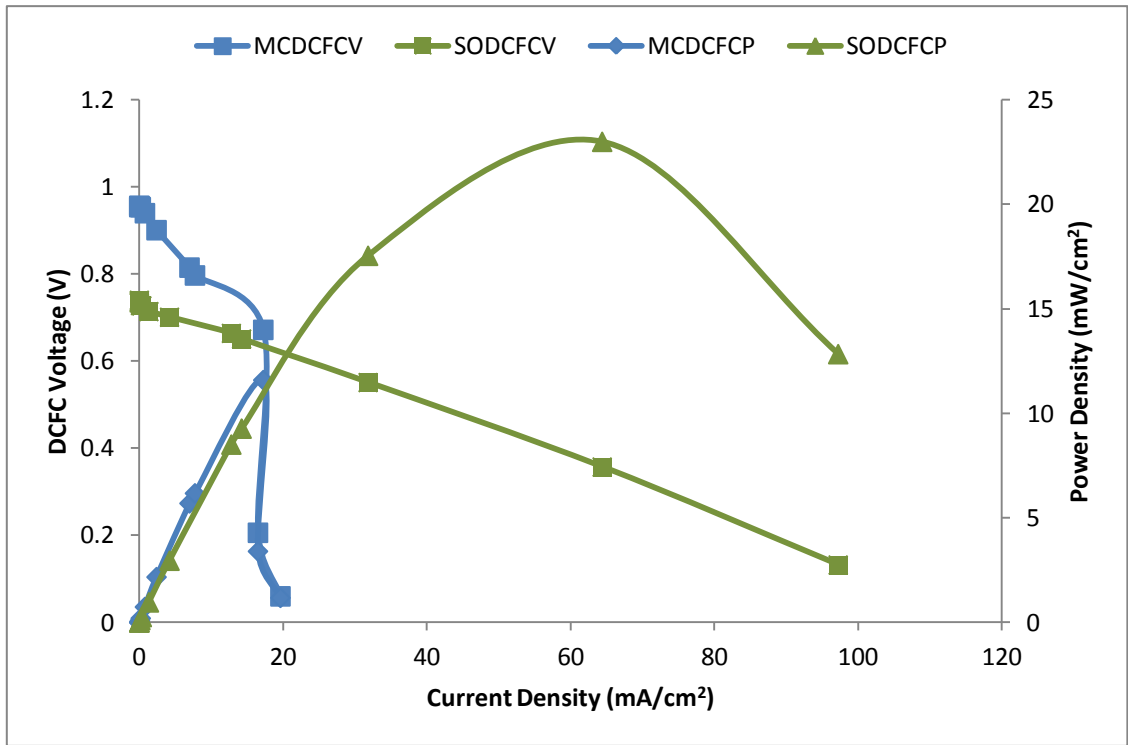


Figure C27: HM Wheat performances for SODFC and MDCFC at 800°C.

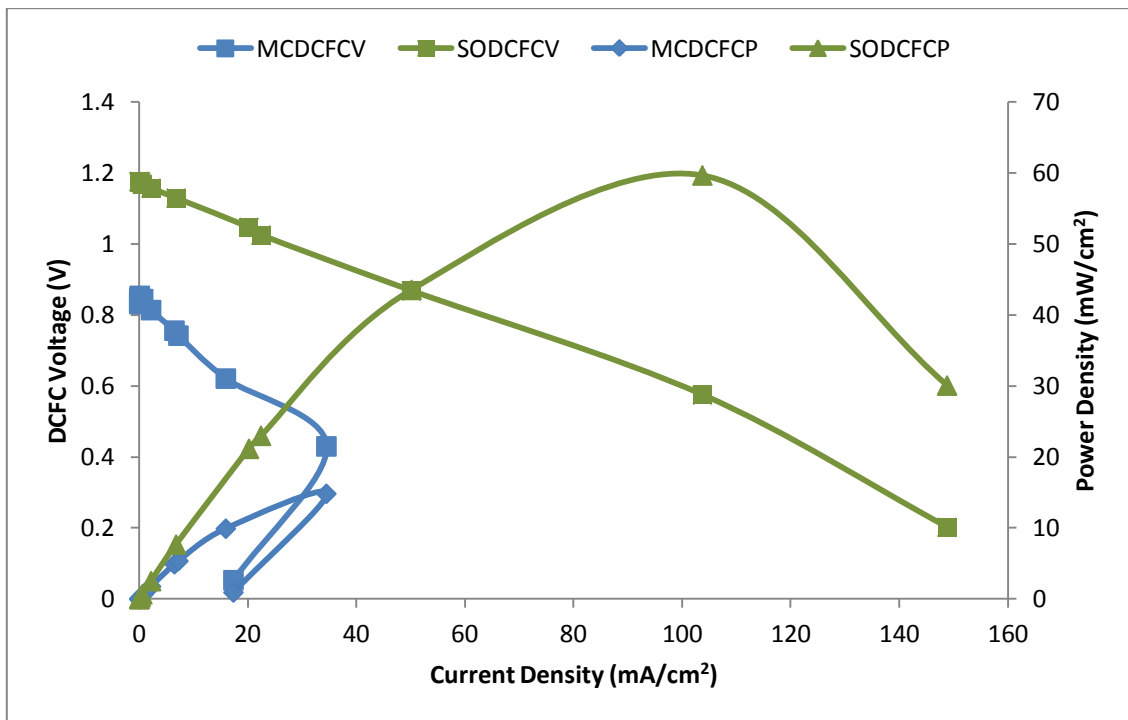


Figure C28: HM Willow performances for SODFC and MDCFC at 800°C.

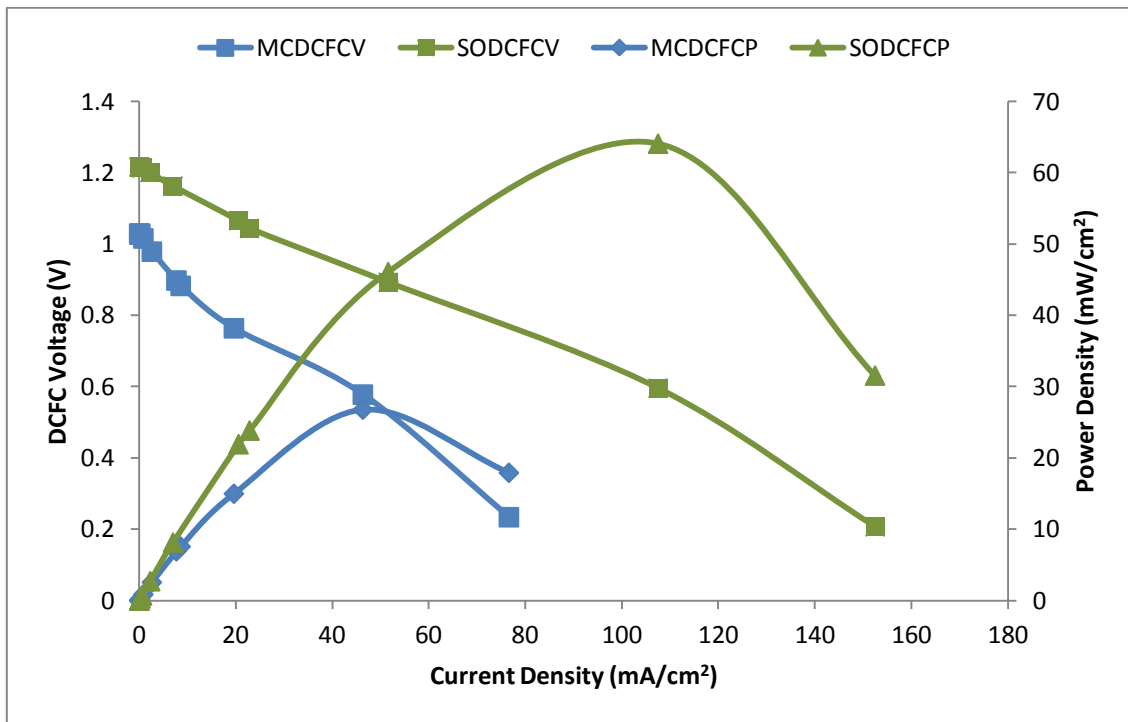


Figure C29: HM Spruce performances for SODFCV and MDCFCV at 800°C.

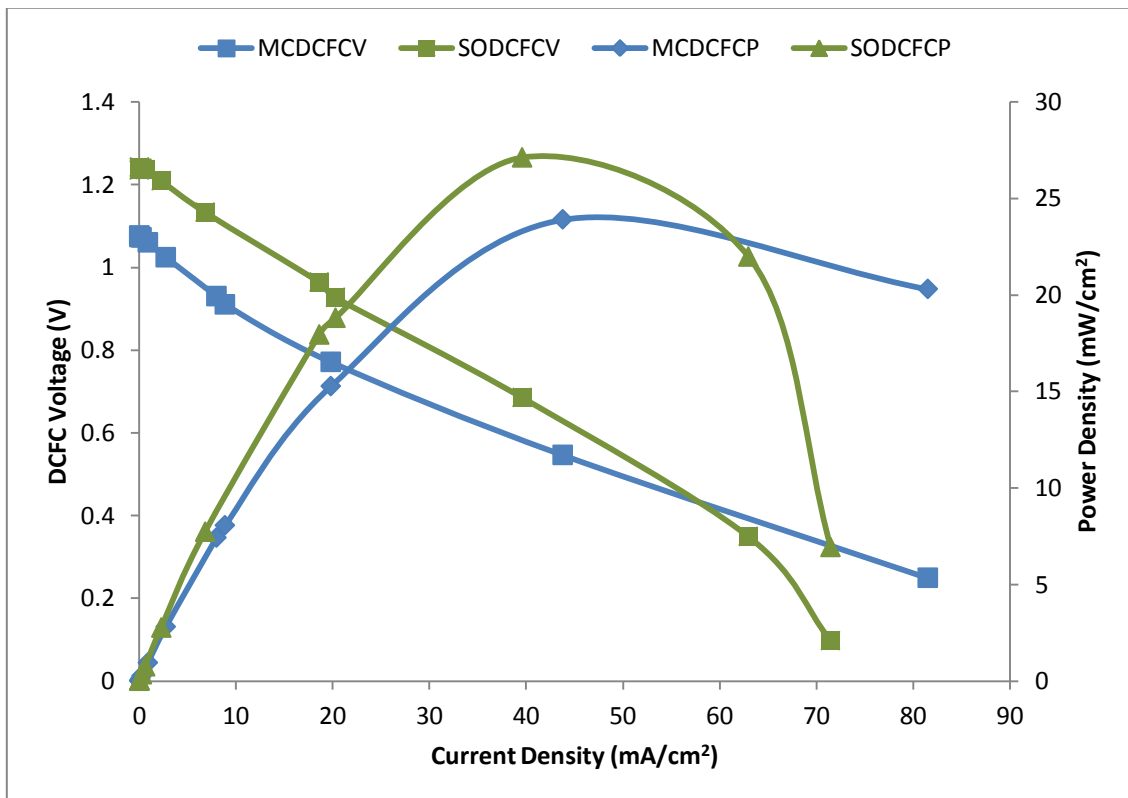


Figure C30: HM Poplar performances for SODFCV and MDCFCV at 800°C.

Appendix D

Tables of DCFC Performances

Table D1: MDCFC Electrochemical data for Switchgrass and Poplar (HM)

Cell Parameter	Switchgrass			Poplar		
	Temperature °C			Temperature °C		
	600	700	800	600	700	800
Open circuit voltage (V)	0.78	0.84	0.87	0.85	0.97	1.08
Peak power density (mW/cm ²)	2.44	10.11	21.60	4.32	13.15	23.91
Maximum current density (mA/cm ²)	16.37	44.86	74.00	24.89	55.34	81.53
Current density at 0.8 V (mA/cm ²)	0.17	0.63	7.82	0.18	6.34	19.80
Voltage at peak power (V)	0.31	0.36	0.52	0.23	0.41	0.55
Area specific resistance (Ω cm ²)	36.73	13.90	9.99	26.22	13.98	12.69
Efficiency at peak power (%)	40.0	43.0	60.0	27.0	42.0	51.0

Table D2: MDCFC Electrochemical data for Wheat and Spruce (HM)

Cell Parameter	Wheat			Spruce		
	Temperature °C			Temperature °C		
	600	700	800	600	700	800
Open circuit voltage (V)	0.72	0.85	0.95	0.80	0.96	1.03
Peak power density (mW/cm ²)	1.87	5.55	11.60	3.64	12.89	26.79
Maximum current density (mA/cm ²)	9.46	19.32	19.65	23.25	51.08	76.62
Current density at 0.8 V (mA/cm ²)	0	0.66	7.75	0.08	2.22	19.62
Voltage at peak power (V)	0.27	0.47	0.67	0.21	0.40	0.58
Area specific resistance (Ω cm ²)	39.53	20.34	13.15	27.22	16.09	10.79
Efficiency at peak power (%)	38.00	55.00	71.00	26.0	42.0	56.0

Table D3: MDCFC Electrochemical data for Switchgrass and Poplar (BM)

Cell Parameter	Switchgrass			Poplar		
	Temperature °C			Temperature °C		
	600	700	800	600	700	800
Open circuit voltage (V)	0.42	0.60	0.77	0.56	0.89	0.59
Peak power density (mW/cm ²)	0.80	3.81	12.32	2.47	7.91	10.22
Maximum current density (mA/cm ²)	5.77	19.97	52.06	16.70	29.80	36.67
Current density at 0.8 V (mA/cm ²)	0	0	0	0	2.10	0
Voltage at peak power (V)	0.18	0.39	0.39	0.31	0.31	0.36
Area specific resistance (Ω cm ²)	36.45	21.68	15.81	26.75	19.64	9.33
Efficiency at peak power (%)	43.00	65.00	51.00	55.00	35.00	61.00

Table D4: MDCFC Electrochemical data for Wheat and Spruce (BM)

Cell Parameter	Wheat			Spruce		
	Temperature °C			Temperature °C		
	600	700	800	600	700	800
Open circuit voltage (V)	0.45	0.63	0.68	0.69	0.88	0.72
Peak power density (mW/cm ²)	0.47	3.50	11.76	2.68	9.11	17.19
Maximum current density (mA/cm ²)	3.53	23.90	42.57	18.34	44.86	73.02
Current density at 0.8 V (mA/cm ²)	0	0	0	0	2.02	0
Voltage at peak power (V)	0.22	0.21	0.38	0.32	0.34	0.46
Area specific resistance (Ω cm ²)	95.18	22.34	10.25	31.08	17.46	6.70
Efficiency at peak power (%)	49.00	33.00	56.00	46.00	35.00	64.00

Table D5: SODCFC Electrochemical performances for Switchgrass and Poplar (BM)

SODCFC Parameter	Switchgrass			Poplar		
	Temperature °C			Temperature °C		
	600	700	800	600	700	800
Open circuit voltage (V)	0.87	0.64	1.13	0.82	0.86	0.78
Peak power density (mW/cm ²)	13.09	10.83	69.81	7.61	12.28	25.24
Maximum current density (mA/cm ²)	55.26	64.10	162.10	31.68	55.26	103.15
Current density at 0.8 V (mA/cm ²)	4.66	0	85.00	1.50	4.57	0
Voltage at peak power (V)	0.48	0.25	0.62	0.36	0.46	0.37
Area specific resistance (Ω cm ²)	11.22	7.88	4.11	25.07	12.55	6.15
Efficiency at peak power (%)	55.00	39.00	55.00	44.00	53.00	47.00

Table D6: SODCFC Electrochemical performances for Wheat and Spruce (BM)

SODCFC Parameter	Wheat			Spruce		
	Temperature °C			Temperature °C		
	600	700	800	600	700	800
Open circuit voltage (V)	0.87	1.11	1.18	0.37	1.01	1.16
Peak power density (mW/cm ²)	2.80	34.35	66.92	1.34	16.60	57.40
Maximum current density (mA/cm ²)	17.68	70.73	138.52	13.26	68.52	156.20
Current density at 0.8 V (mA/cm ²)	1.51	54.00	90.00	0	14.75	60.00
Voltage at peak power (V)	0.38	0.77	0.61	0.15	0.54	0.56
Area specific resistance (Ω cm ²)	40.26	7.24	3.69	21.58	13.28	5.66
Efficiency at peak power (%)	44.00	69.00	52.00	41.00	53.00	48.00

Table E7: SODCFC Electrochemical performances for Switchgrass and Poplar (HM)

SODCFC Parameter	Switchgrass			Poplar		
	Temperature °C			Temperature °C		
	600	700	800	600	700	800
Open circuit voltage (V)	0.76	0.81	1.13	0.77	0.93	1.24
Peak power density (mW/cm ²)	4.69	10.83	48.42	2.95	10.10	27.11
Maximum current density (mA/cm ²)	28.74	56.00	140.00	11.79	44.21	71.47
Current density at 0.8 V (mA/cm ²)	0	0.01	50.00	0	4.70	30.00
Voltage at peak power (V)	0.46	0.43	0.52	0.39	0.42	0.69
Area specific resistance (Ω cm ²)	21.69	11.82	6.62	46.85	11.93	12.54
Efficiency at peak power (%)	61.00	53.00	46.00	51.00	45.00	56.00

Table E8: SODCFC Electrochemical performances for Wheat and Spruce (HM)

SODCFC Parameter	Wheat			Spruce		
	Temperature °C			Temperature °C		
	600	700	800	600	700	800
Open circuit voltage (V)	0.62	0.71	0.74	0.81	0.93	1.22
Peak power density (mW/cm ²)	1.84	9.55	23.00	3.82	12.87	64.10
Maximum current density (mA/cm ²)	12.81	55.26	97.26	25.05	63.37	152.52
Current density at 0.8 V (mA/cm ²)	0	0	0	1.42	8.00	90.00
Voltage at peak power (V)	0.31	0.23	0.36	0.45	0.47	0.60
Area specific resistance (Ω cm ²)	23.61	12.36	5.68	25.39	14.45	5.25
Efficiency at peak power (%)	50.00	32.00	49.00	56.00	51.00	49.00